VOL. 25 NO. 2 APRIL 1970
PUBLISHED MONTHLY

JOURNAL OF ELECTROANALYTICAL CHEMISTRY AND INTERFACIAL ELECTROCHEMISTRY

International Journal devoted to all Aspects of Electroanalytical Chemistry, Double Layer Studies, Electrokinetics, Colloid Stability, and Electrode Kinetics.

ELSEVIER SEQUOIA S.A.
LAUSANNE

GENERAL INFORMATION

Types of contributions

(a) Original research work not previously published in other periodicals.
(b) Reviews on recent developments in various fields.
(c) Short communications.
(d) Preliminary notes.

Languages

Papers will be published in English, French or German.

Submission of papers

Papers should be sent to one of the following Editors:
Professor J. O'M. BOCKRIS, John Harrison Laboratory of Chemistry, University of Pennsylvania, Philadelphia 4, Pa. 19104, U.S.A.
Dr. R. H. OTTEWILL, Department of Chemistry, The University, Bristol 8, England.
Dr. R. PARSONS, Department of Chemistry, The University, Bristol 8, England.
Professor C. N. REILLEY, Department of Chemistry, University of North Carolina, Chapel Hill, N.C. 27515, U.S.A.

Authors should preferably submit two copies in double-spaced typing on pages of uniform size. Legends for figures should be typed on a separate page. The figures should be in a form suitable for reproduction, drawn in Indian ink on drawing paper or tracing paper, with lettering etc. in thin pencil. The sheets of drawing or tracing paper should preferably be of the same dimensions as those on which the article is typed. Photographs should be submitted as clear black and white prints on glossy paper. Standard symbols should be used in line drawings, the following are available to the printers:

All references should be given at the end of the paper. They should be numbered and the numbers should appear in the text at the appropriate places.
A summary of 50 to 200 words should be included.

Reprints

Fifty reprints will be supplied free of charge. Additional reprints (minimum 100) can be ordered at quoted prices. They must be ordered on order forms which are sent together with the proofs.

Publication

The *Journal of Electroanalytical Chemistry and Interfacial Electrochemistry* appears monthly
For 1969, each volume has 3 issues and 4 volumes will appear.
Subscription price: Sfr. 316.— (U.S. $ 74.60) per year incl. postage. Additional cost for copies by air mail available on request. For subscribers in the U.S.A. and Canada, 2nd class postage paid at Jamaica, N.Y. For advertising rates apply to the publishers.

Subscriptions

Subscriptions should be sent to:

ELSEVIER SEQUOIA S.A. P.O. Box 851, 1001 Lausanne 1, Switzerland

If you need to find 10^{-9}M, without spending 10^{4}£, get a Southern A3100

When it comes to determining minute traces (in even the smallest samples), there's nothing like pulse polarography at anywhere near the price. And the Southern A3100 is the most sophisticated pulse polarograph you can buy. It has higher sensitivity, resolution and selectivity than any other electrochemical instrument in analytical work, and its wide range of variable parameters makes it an invaluable tool in electrode reaction studies or reaction kinetics research.

With all adjustments made for maximum sensitivity, it will determine reversibly-reducible ions down to about 10^{-9}M and by the use of hanging drop techniques this can be extended to 10^{-10} to 10^{-11}M. The sensitivity for irreversible reactions is about 10^{-8}M to $5x10^{-8}$M.

For determining impurities in metals and semiconductors, corrosion products, residual monomers and other organic materials, and for electrokinetic research—the A3100 can solve your analytical problems at a down-to-earth price.

And if $5x10^{-8}$M will do, look at the A1660

Southern also makes an advanced differential cathode-ray polarograph that is useful in a wide range of analytical applications including metallurgical analysis, effluent analysis, and determination of trace metals and essential minerals in food and drugs. Based on original work by Davis and Seaborn, the A1660 features high sensitivity plus exceptional versatility. Ask for the descriptive leaflet. For full details, contact Southern Analytical Limited, Camberley, Surrey. Camberley 3401. Telex: 85210.

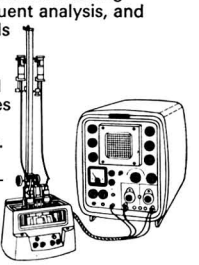

SOUTHERN ANALYTICAL

Detect one part per billion!

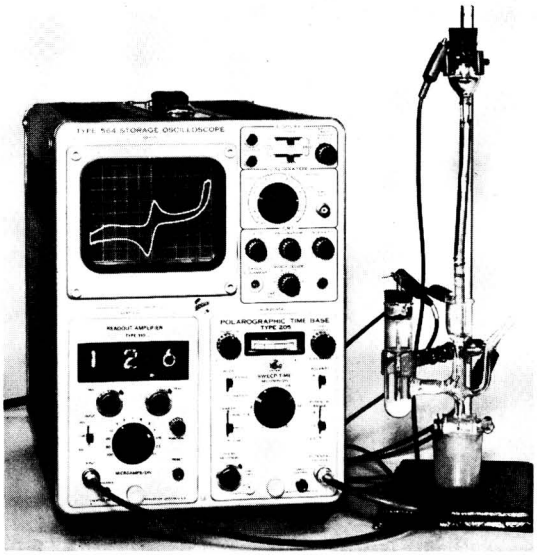

by Anodic

Stripping Polarography

Anodic Stripping Polarography with Chemtrix Single-Sweep Polarographic Analyzers is capable of detecting many elements and compounds in amounts of one ppb and less. This high sensitivity is due to a combination of factors: the concentrating effect of stripping technique, characteristics of the mercury film electrode, and the fast scan capabilities of the Chemtrix Instruments. If you have a detection problem with trace elements or contaminants, anodic stripping may well be the solution.

free-new booklet

The complete story of ANODIC STRIPPING POLAROGRAPHY with detailed experiments and many references.

simple procedure for detection

1. Use wax impregnated graphite electrode coated with a thin layer of mercury.
2. Immerse electrode in cell with electrolyte.
3. Electrolyze at 1.00 volt for 10 minutes with controlled stirring.
4. Stop stirring and scan anodically to zero volts. (Leave peaks stored on oscilloscope screen as blank).
5. Add sample and repeat steps 3 and 4. Note change in peaks and relate to trace metal calibration curves.

rapid simultaneous detections

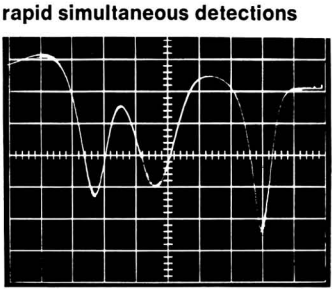

Anodic peaks in illustration are Zinc, Cadmium, and Lead at approximately 50 ppb in 1 molar KC1, stored on screen with single anodic scan.

some typical applications for anodic stripping polarography

- Trace impurities in reagents
- Trace metals in biological systems
- Water pollutants
- Lead in air (tetraethyl)
- Semiconductor trace metals

U.S. SALES PRICES F.O.B. FACTORY

CHEMTRIX polarographic analyzers

for Single-Sweep and Anodic Stripping Polarography

Model SSP-2 Three-Electrode Polarographic Analyzer . . . $3070.00

Model SSP-5 Differential System with Dual DME 3785.00

Illustrated Above:

Model SSP-3 Digital Readout Polarographic Analyzer . . . 3510.00

NEW—TYPE 804—$495 Potentiostatic Waveform Source

This versatile instrument is a waveform source for triangle and square waveforms, single or repetitive, with ±5 volt dc offset and up to 5 volt amplitude. It is also a potentiostat which can accept an external input and combine it with an internal dc level to provide controlled-potential output. It is both a waveform source and a potentiostat, providing controlled-potential output of its internally generated waveforms. In addition, it is

■ A Power Supply, ±5 v dc at 100 ma ■ A Controlled Potential Coulometer ■ An Integrator for Coulometric Titrations ■ An Integrator for External Signals ■ A Supply for Controlled-Current Titrations

CHEMTRIX, INC.

Instrumentation for Science

P.O. Box 725 Beaverton, Oregon 97005 (503) 648 1434

ELECTROANALYTICAL CHEMISTRY AND INTERFACIAL ELECTROCHEMISTRY
Elsevier Sequoia S.A., Lausanne – Printed in The Netherlands

ALTERNATIVE REACTION PATHWAYS IN POTENTIAL-STEP CHRONOCOULOMETRY

JANET OSTERYOUNG* AND JOSEPH H. CHRISTIE**

*Gates and Crellin Laboratories of Chemistry†, California Institute of Technology, Pasadena, California, 91109 (U.S.A.)****

(Received November 17th, 1969)

INTRODUCTION

Recent investigations in these laboratories on the electrochemistry of chromium(II) in the presence of halide[1] presented the interesting situation illustrated by the reaction scheme:

$$R \rightleftarrows O_1 + n_1 e^- \quad (1a)$$

$$R \rightleftarrows O_2 + n_2 e^- \quad (1b)$$

in which the products of the electrochemical reaction, O_1 and O_2, are not in chemical equilibrium with each other [in one of the specific cases studied R was Cr(II), O_1 was $Cr(H_2O)_6^{3+}$, and O_2 was $Cr(H_2O)_5Br^{2+}$]. The product distribution between O_1 and O_2 is almost always potential dependent, so a controlled potential technique is most suitable for the study of reactions of this type. Gileadi and Srinivasan[2] have treated a similar case in which alternative pathways exist following the electron transfer. Presented here are the theoretical coulometric yields to be expected when the potential-step chronocoulometric technique[3] is applied to a system represented by reactions (1a) and (1b).

RESULTS AND DISCUSSION

Reactions (1a) and (1b) are each characterized by the usual kinetic parameters E_i^0, α_i, k_i, and D_i, $i=1,2$; *i.e.*: the standard potential, transfer coefficient, heterogeneous rate constant, and diffusion coefficient, respectively. We wish to find the current and the charge which would flow by each pathway in a potential-step experiment of the following type: the solution initially contains only R and the initial potential, E_0, is adjusted to be sufficiently cathodic that no current flows. At time $t=0$ the potential is stepped to a value E_f at which R is oxidized to both O_1 and O_2.

---

* Present address: Department of Civil Engineering, Colorado State University, Ft. Collins, Colorado 80521 (U.S.A.).

** Present address: Department of Chemistry, Colorado State University, Ft. Collins, Colorado 80521 (U.S.A.).

† Contribution No. 3454.

*** Publication No. CET 69-70 JO-JHC 19 of the Civil Engineering Department, Colorado State University.

The current flowing by each reaction pathway is given by[4]

$$\frac{I_i}{n_i FA} = D_i\left(\frac{\partial C_i}{\partial x}\right)_{x=0} = -\left[C_R(0,t)\kappa_{if} - C_i(0,t)\kappa_{ib}\right], \quad i = 1, 2 \tag{2}$$

where

$$\kappa_{if} = k_i \exp\left[(1-\alpha_i)\frac{n_i F}{RT}(E_f - E_i^0)\right] \tag{3a}$$

$$\kappa_{ib} = k_i \exp\left[-\alpha_i \frac{n_i F}{RT}(E_f - E_i^0)\right] \tag{3b}$$

and C_i is the concentration of O_i. The other symbols have their usual meaning. Note that we are considering an oxidation; the forward rate constants, κ_{if}, are the rate constants for the *anodic* reactions.

Detailed solution to the problem is obtained by solving the diffusion equation:

$$\frac{\partial C}{\partial t} = D\frac{\partial^2 C}{\partial x^2} \tag{4}$$

with the initial conditions

$$C_R(x,0) = C_R^0; \quad C_i(x,0) = 0, \quad i = 1, 2 \tag{5}$$

and the boundary conditions

$$C_R(\infty,t) = C_R^0; \quad C_i(\infty,t) = 0, \quad i = 1, 2 \tag{6a}$$

$$-D_R\left(\frac{\partial C_R}{\partial x}\right)_{x=0} = D_1\left(\frac{\partial C_1}{\partial x}\right)_{x=0} + D_2\left(\frac{\partial C_2}{\partial x}\right)_{x=0} \tag{6b}$$

and the additional boundary conditions given by eqn. (2).

There are two limiting solutions to this problem when the back reactions can be neglected. If both forward reactions are charge-transfer limited (no concentration polarization), then the charge, Q, passing by each reaction pathway is proportional to the rate constant for that pathway, so

$$\frac{Q_i}{Q_1 + Q_2} = \frac{\kappa_{if}}{\kappa_{1f} + \kappa_{2f}} \tag{7}$$

When R is being oxidized at the diffusion-controlled rate (complete concentration polarization) the current must also divide between each pathway in proportion to the rate constant for each pathway, and the coulombic yields are again given by eqn. (7).

To treat the more general case, a solution to the problem presented by eqns. (4)–(6) is required. The solutions to eqn. (4) in Laplace transform space are

$$\bar{C}_i(x,s) = \zeta_i \exp\left(-s^{\frac{1}{2}}x/D_i^{\frac{1}{2}}\right), \quad i = 1, 2 \tag{8a}$$

$$\bar{C}_R(x,s) = \frac{C_R^0}{s} + \zeta_R \exp\left(-s^{\frac{1}{2}}x/D_R^{\frac{1}{2}}\right) \tag{8b}$$

where the conditions in (5) and (6a) have been applied.

Transforming eqn. (2) and combining with the derivatives of eqn. (8a), we find

$$\frac{I_i}{n_i FA} = -D_i^{\frac{1}{2}} s^{\frac{1}{2}} \zeta_i, \quad i = 1, 2 \tag{9}$$

Combining the transform of eqn. (6b) with eqn. (9) and solving for the constants of integration ζ_i, $i = 1, 2$, we obtain

$$\zeta_2 = \frac{C_R^0}{s} \left[\kappa_{2f} D_1^{\frac{1}{2}} s^{\frac{1}{2}} + \kappa_{1b}\kappa_{2f}\right] \Big/ \left\{(D_1 D_2)^{\frac{1}{2}} s + \left[\left(\frac{D_1 D_2}{D_R}\right)^{\frac{1}{2}} (\kappa_{1f} + \kappa_{2f}) + \right.\right.$$

$$\left.\left. + \kappa_{1b} D_2^{\frac{1}{2}} + \kappa_{2b} D_1^{\frac{1}{2}}\right] s^{\frac{1}{2}} + \kappa_{1f}\kappa_{1b}\left(\frac{D_1}{D_R}\right)^{\frac{1}{2}} + \kappa_{1b}\kappa_{2f}\left(\frac{D_2}{D_R}\right)^{\frac{1}{2}} + \kappa_{1b}\kappa_{2b}\right\} \tag{10}$$

The equation for ζ_1 is obtained by permuting all of the numerical subscripts in eqn. (10).

The current is obtained by inverse transformation of eqn. (9). Equation (10) can be written in the form:

$$\zeta_2 = \frac{\lambda s^{\frac{1}{2}} + \mu}{(s^{\frac{1}{2}} + \gamma)(s^{\frac{1}{2}} + \beta)} \tag{11}$$

From this form we find the current by inverse transformation[5];

$$\frac{-I_i}{n_i FA} = \frac{D_i^{\frac{1}{2}} C_R^0}{\gamma - \beta} \left\{(\gamma\lambda_i - \mu_i) \exp(\gamma^2 t) \operatorname{erfc}(\gamma t^{\frac{1}{2}}) - (\beta\lambda_i - \mu_i) \exp(\beta^2 t) \operatorname{erfc}(\beta t^{\frac{1}{2}})\right\}, \quad i = 1,2 \tag{12}$$

and the charge by integration

$$\frac{-Q_i}{n_i FA} = \frac{D_i^{\frac{1}{2}} C_R^0}{\gamma - \beta} \left\{\gamma^{-2}(\gamma\lambda_i - \mu_i)\left(\frac{2\gamma t^{\frac{1}{2}}}{\pi^{\frac{1}{2}}} - 1 + \exp(\gamma^2 t) \operatorname{erfc}(\gamma t^{\frac{1}{2}})\right) - \right.$$

$$\left. - \beta^{-2}(\beta\lambda_i - \mu_i)\left(\frac{2\beta t^{\frac{1}{2}}}{\pi^{\frac{1}{2}}} - 1 + \exp(\beta^2 t) \operatorname{erfc}(\beta t^{\frac{1}{2}})\right)\right\}, \quad i = 1, 2 \tag{13}$$

where

$$\lambda_i = \kappa_{if}/D_i^{\frac{1}{2}}, \qquad i = 1, 2 \tag{14a}$$

$$\mu_i = \frac{\kappa_{if}\kappa_{jb}}{(D_i D_j)^{\frac{1}{2}}}, \qquad i = 1, 2; \quad j = 1, 2; \quad i \neq j \tag{14b}$$

$$\gamma = \tfrac{1}{2}(a - \sqrt{a^2 - 4b}), \qquad \beta = \tfrac{1}{2}(a + \sqrt{a^2 - 4b}) \tag{14c}$$

$$a = (\kappa_{1f} + \kappa_{2f})/D_R^{\frac{1}{2}} + \kappa_{1b}/D_1^{\frac{1}{2}} + \kappa_{2b}/D_2^{\frac{1}{2}} \tag{14d}$$

$$b = \kappa_{1f}\kappa_{2b}/(D_2 D_R)^{\frac{1}{2}} + \kappa_{1b}\kappa_{2f}/(D_1 D_R)^{\frac{1}{2}} + \kappa_{1b}\kappa_{2b}/(D_1 D_2)^{\frac{1}{2}} \tag{14e}$$

DISCUSSION

The solutions for the current and the charge, eqns. (12) and (13), are sufficiently complicated algebraically that their qualitative aspects are obscure. In particular,

the parameters γ and β contain all of the rate parameters for both reaction paths, which means that one cannot single out terms corresponding to a single path. However, eqn. (13) can be simplified when the rate parameters and experimental conditions lie within certain limits.

Totally irreversible reactions

Consider the case where the backward reactions can be ignored at all potentials, $\kappa_{1b}=\kappa_{2b}=0$. Then $\mu_i=0$, and $a=(\kappa_{1f}+\kappa_{2f})/D_R^{\frac{1}{2}}$, $b=0$, so that $\gamma=0$ and $\beta=a$. Referring to eqn. (13),

$$\frac{1}{\gamma^2}\left(\frac{2\gamma t^{\frac{1}{2}}}{\pi^{\frac{1}{2}}} - 1+\exp(\gamma^2 t)\,\mathrm{erfc}\,(\gamma t^{\frac{1}{2}})\right) = t - \frac{4}{3\sqrt{\pi}}\gamma t^{\frac{3}{2}} + \frac{\gamma^2 t^2}{2} - \ldots \tag{15}$$

so clearly the first term of the right-hand side is zero for $\kappa_{1b}=\kappa_{2b}=0$. Therefore eqn. (13) becomes

$$\frac{-Q_i}{n_i FA} = \kappa_{if}\frac{C_R^0}{\beta^2}\left[\exp(\beta^2 t)\,\mathrm{erfc}\,(\beta t^{\frac{1}{2}})-1+\frac{2\beta t^{\frac{1}{2}}}{\sqrt{\pi}}\right] \tag{16}$$

from which it follows directly that

$$\frac{Q_i}{Q_1+Q_2} = \frac{\kappa_{if}}{\kappa_{1f}+\kappa_{2f}} \tag{7}$$

Equation (16) is in exact analogy with the solution for one reaction pathway[3]. The Q–t behavior for two totally irreversible reaction pathways differs only slightly from that for a single reaction path: When $\beta t^{\frac{1}{2}} > 5$

$$\frac{Q_i}{n_i FA} \sim -\kappa_{if}\frac{C_R^0}{\beta^2}\left(\frac{2\beta t^{\frac{1}{2}}}{\pi^{\frac{1}{2}}} - 1\right) \tag{17}$$

or

$$-Q_i \sim \frac{n_i FAD_R^{\frac{1}{2}}\kappa_{if}C_R^0}{\kappa_{1f}+\kappa_{2f}}\left(\frac{2t^{\frac{1}{2}}}{\pi^{\frac{1}{2}}} - \frac{1}{\beta}\right) \tag{18}$$

and if $n_1=n_2=n$

$$Q_1+Q_2 \sim -nFAD_R^{\frac{1}{2}}C_R^0\left(\frac{2t^{\frac{1}{2}}}{\pi^{\frac{1}{2}}} - \frac{1}{\beta}\right) \tag{19}$$

When $1/\beta \ll 2t^{\frac{1}{2}}/\pi^{\frac{1}{2}}$

$$Q_1+Q_2 \sim -\frac{2n}{\pi^{\frac{1}{2}}}FAD_R^{\frac{1}{2}}C_R^0 t^{\frac{1}{2}} \tag{20}$$

which is identical to the result for only one reaction path[3].

Equation (19) differs from the result expected for a single reaction path only in the potential dependence of β. For a single reaction under these conditions α can be determined by plotting Q *vs.* $t^{\frac{1}{2}}$ and determining β from the intercept according to eqn. (20). Then a plot of $\ln\beta$ *vs.* $E_f - E^0$ gives α from the slope. If two alternative reaction pathways are available, a similar plot would be nonlinear and the slope would be

$$\frac{(1-\alpha_1)\frac{n_1F}{RT}\kappa_1+(1-\alpha_2)\frac{n_2F}{RT}\kappa_2}{(\kappa_1+\kappa_2)} \tag{21}$$

Whenever $\alpha_1 \sim \alpha_2$ and $n_1 = n_2$ the plot will be a straight line, or nearly so, with slope

$$(1-\alpha)\frac{nF}{RT} \tag{22}$$

Since many electrochemical reactions have $\alpha \sim 0.5$ it is likely that alternative reaction pathways would not be detected in a chronocoulometric rate determination unless some additional experiments were done to investigate the reactions directly.

Other cases

When the back reactions cannot be ignored at all potentials, the behavior of eqn. (13) can be investigated by making appropriate small or large argument expansions of the exp erfc terms and seeing what limits can be placed on the parameters to give the equation a simple approximate form. It can be shown, for instance, that provided $E_f > E_1^0$ and E_2^0, eqn. (7) follows from eqn. (13) if either $\gamma t^{\frac{1}{2}} < 0.1$ and $\beta t^{\frac{1}{2}}$

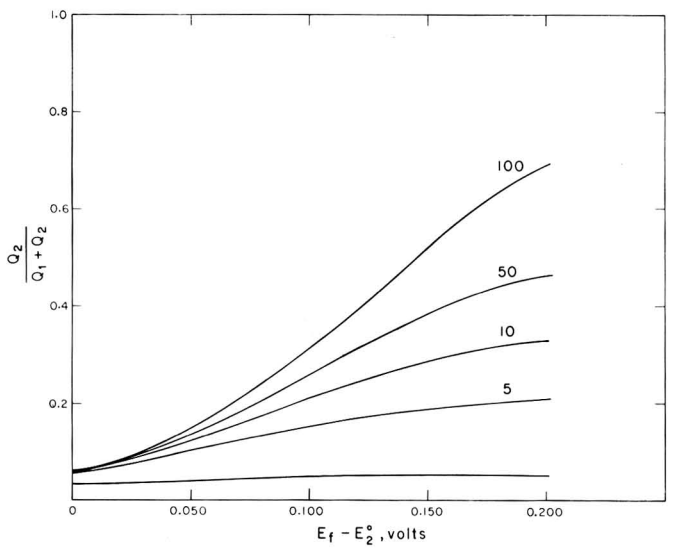

Fig. 1. Dependence of the fraction of the oxidation going *via* pathway two on $E_f - E_2^0$. $E_2^0 - E_1^0 = 0.15$ V, $\alpha_1 = \alpha_2 = 0.5$, $n_1 = n_2 = 1$, $D^{\frac{1}{2}} = 0.00254$ cm s$^{-\frac{1}{2}}$, $t = 0.04$ s, $k_1 = 10^{-2}$ cm s^{-1}. The numbers on the curves are the values of the ratio k_2/k_1. For each curve, the value of $Q_2/(Q_1+Q_2)$ approaches asymptotically the value

$$\frac{1}{1+(k_1/k_2)\exp 0.5\,(nF/RT)(E_2^0-E_1^0)}$$

which equals

$$\frac{1}{1+18.2\,k_1/k_2}$$

for one-electron oxidations at 27°C. For $k_1 = 10^{-2}$ cm s^{-1} these asymptotic values are: for k_2/k_1 = (1) 0.052, (5) 0.275, (10) 0.354, (50) 0.733, (100) 0.846.

< 0.01, or $\gamma t^{\frac{1}{2}} < 0.01$ and $\beta t^{\frac{1}{2}} > 50$. For example, if $t = 0.04$ s these limits correspond roughly to $\kappa_{1f} + \kappa_{2f} < 10^{-5}$, and $\kappa_{1f}\kappa_{2b} + \kappa_{2f}\kappa_{1b} < 10^{-5}$, $\kappa_{1f} + \kappa_{2f} > 0.2$, respectively. These conditions include the two limiting cases given above, namely, charge-transfer control and diffusion control, respectively, but allow for the possibility of significant back reaction.

In Figs. 1 and 2 a and b the charge ratio has been calculated for a variety of conditions to illustrate in more detail the predictions of eqn. (13). Figure 1 shows the

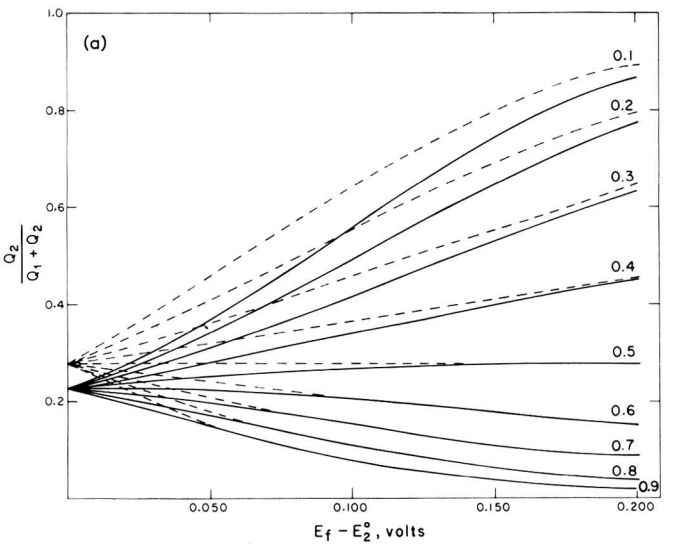

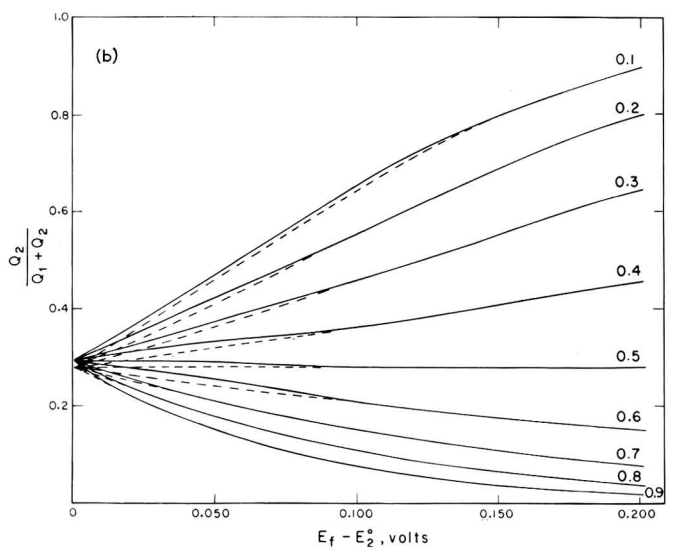

Fig. 2. Dependence of the fraction of charge passing *via* pathway two on $E_f - E_2^0$ for various values of α_2. $E_2^0 - E_1^0 = 0.05$ V, $D^{\frac{1}{2}} = 0.00254$ cm s$^{-\frac{1}{2}}$, $t = 0.04$ s, $T = 27°$C, $\alpha_1 = 0.5$, $n_1 = n_2 = 1$. (a) $k_1 = k_2 = 10^{-2}$ cm s^{-1}, (b) $k_1 = k_2 = 10^{-5}$ cm s^{-1}. Ratio $Q_2/(Q_1 + Q_2)$ calcd. from eqn. (13) (——), from eqn. (7) (– – –).

variation of $Q_2/(Q_1+Q_2)$ as a function of the final potential, E_f, for various values of the ratio of the standard heterogeneous rate constants k_2/k_1. For each choice of k_2/k_1 the ratio $\kappa_{2f}/(\kappa_{1f}+\kappa_{2f})$ is a constant ($\alpha_1=\alpha_2=0.5$) which the value of $Q_2/(Q_1+Q_2)$ calculated from eqn. (13) approaches asymptotically. These cases (with the exception of $k_2/k_1=1$) do not come under the category of faster reactions for which eqn. (7) should apply because the rate constants are sufficiently large ($k_1=10^{-2}$ cm s^{-1}) that $\gamma t^{\frac{1}{2}}>0.1$. If exactly the same calculations are done with $k_1=10^{-5}$ cm s^{-1} the values of $Q_2/(Q_1+Q_2)$ from eqn. (13) are virtually independent of potential for $E_f-E_2^0>0.05$ V and equal to the values given by eqn. (7).

Similar calculations are shown in Figs. 2 a and b in which the variation of $Q_2/(Q_1+Q_2)$ with potential is shown for different choices of α_2. In Fig. 2 a where $k_1=k_2=10^{-2}$ cm s^{-1} the approximation of eqn. (7) breaks down for small values of α_2 because γ increases as $\alpha_1+\alpha_2$ decreases and $\gamma t^{\frac{1}{2}}>0.1$ for $\alpha_1+\alpha_2<1$. For $k_1=k_2=10^{-5}$ cm s^{-1} (Fig. 2b) the ratios $Q_2/(Q_1+Q_2)$ calculated from eqn. (13) are well approximated by eqn. (7). By comparing Figs. 2a and 2b it can be seen that at some intermediate choice $k_1=k_2$ the points at $E_f=E_2^0$ will be identical for the two methods of calculation and eqn. (4) should give the same results as eqn. (13) for $E_f>E_2^0$.

The simple rate constant ratio of eqn. (7) is a convenient approximation to the charge distribution which can serve as a guide to the design and qualitative interpretation of experiments. It is also useful for exact calculations of the charge distribution under the special conditions defined by the criteria given above.

An example

From polarographic measurements, uncorrected for double-layer effects, the kinetic parameters for the oxidation of Cr(II) in the presence and absence of bromide are[6]:

Pathway	k^0/cm s^{-1}	E^0/V *vs. SCE*	α
(1) $Cr^{2+} \rightarrow Cr^{3+}+e^-$	0.69×10^{-5}	−0.650	0.63
(2) $Cr^{2+}+Br^-(1F) \rightarrow CrBr^{2+}+e^-$	0.18×10^{-2}	−0.501	0.21

Using these values, $D^{\frac{1}{2}}=2.54\times10^{-3}$ cm $s^{-\frac{1}{2}}$ for all chromium species, and $t=0.04$ s, we calculate $Q_2/(Q_1+Q_2)=0.999$ for 1 *F* Br^- at $E_f=-0.300$ V *vs.* SCE. The corresponding values for 0.1 and 0.01 *F* Br^- are 0.988 and 0.890, respectively. At more negative potentials, less $CrBr^{2+}$ is formed. For instance, at $E_f=-0.400$ V the corresponding values for 1, 0.1, and 0.01 *F* Br^- are 0.994, 0.942, and 0.623, respectively. In 0.002 *F* Br^- solution the values are 0.618 at −0.300 V and 0.977 at −0.100 V. These examples illustrate the sort of variation in product distribution to be expected as the experimental conditions are varied.

ACKNOWLEDGEMENTS

This work was supported in part by the National Science Foundation. J.O. held a National Science Foundation predoctoral fellowship. J.H.C. held a North American Aviation Graduate Fellowship. We wish to express our appreciation to Fred C. Anson for helpful discussions.

SUMMARY

Equations have been derived which predict the distribution of current and charge between two alternative electrochemical reaction pathways for the oxidation of a single species under the conditions of potential-step chronocoulometry. It is shown that the percentage of the total charge consumed in each reaction is given *exactly* by a simple heterogeneous rate constant ratio for the limiting cases of charge transfer control (no concentration polarization) and diffusion control (complete concentration polarization) under conditions where the backward reactions can be ignored, and for totally irreversible reactions (*i.e.* mixed control with negligible back reactions). The product distribution is approximated by this ratio over a wide range of variation of the kinetic parameters. Examples are given of the dependence of the product distribution on the step potential and the kinetic parameters for the two reaction pathways.

REFERENCES

1 J. J. ULRICH (J. OSTERYOUNG) AND F. C. ANSON, *Inorg. Chem.*, 8 (1969) 195.
2 E. GILEADI AND S. SRINIVASAN, *J. Electroanal. Chem.*, 7 (1964) 452.
3 J. H. CHRISTIE, G. LAUER AND R. A. OSTERYOUNG, *J. Electroanal. Chem.*, 7 (1964) 60.
4 P. DELAHAY, *New Instrumental Methods in Electrochemistry*, Interscience Publishers, Inc., New York, 1954, Chap. 4.
5 A. ERDELYI (Ed.), *Tables of Integral Transforms*, Vol. 1, Bateman Manuscript Project, McGraw-Hill Book Co., Inc., New York, 1964, pp. 132, 229.
6 J. OSTERYOUNG AND F. C. ANSON, unpublished results.

ELECTROANALYTICAL CHEMISTRY AND INTERFACIAL ELECTROCHEMISTRY
Elsevier Sequoia S.A., Lausanne – Printed in The Netherlands

ELECTROCHEMICAL MEASUREMENT OF ADSORPTION BY CURRENT REVERSAL CHRONOPOTENTIOMETRY

HARVEY B. HERMAN* AND HENRY N. BLOUNT**
Department of Chemistry, The University of Georgia, Athens, Georgia 30601 (U.S.A.)
(Received December 11th, 1968; in revised form October 1st, 1969)

INTRODUCTION

For the charge transfer process

$$O + n e^- \rightarrow R \qquad (1)$$

adsorption of reactant and/or product will affect the observed electrochemical behavior. In the case of d.c. polarography, Brdicka[1] has shown that product adsorption should manifest itself as an adsorption controlled prewave while reactant adsorption should appear as a postwave.

The same thermodynamic arguments that are invoked in the case of d.c. polarography are also applicable in the case of chronopotentiometry; hence a prewave is expected in the case of product adsorption and a postwave is expected in the case of reactant adsorption. These arguments are totally valid, however, only if adsorption equilibrium is attained and reversible behavior is observed.

Reactant adsorption further manifests itself in an increase of the chronopotentiometric constant, $i_0\tau^{\frac{1}{2}}/C^0$, with decreasing electrolysis time. Several workers have used this fact as a quantitative measure of the amount of electroactive material adsorbed[2-6]. Product adsorption is amenable to treatment by current reversal chronopotentiometry (CRC) in that the observed transition time ratio is enhanced. This technique has been applied to the quantitative determination of the surface excess of electrolysis product[7-9].

Both in the case of reactant adsorption and in the case of product adsorption, a "model" must be assumed and the chronopotentiometric theory based thereon. That is, the relative order of monolayer electrolysis and electrolysis of diffusing species must be assumed. The case of CRC is complicated by the necessity of choosing a model for the reverse electrolysis also. Certain models for the measurement of product adsorption by CRC have been advanced[8,9]. It is the purpose of this work to propose other adsorption models, demonstrate how to calculate the surface excess of electrolysis product for each, and apply these models to experimental systems.

THEORY

In accord with eqn. (1), the initial electrolysis step will be referred to as a reduc-

* Permanent Address: Department of Chemistry, The University of North Carolina at Greensboro, Greensboro, North Carolina 27412.
** Present Address: Department of Chemistry, Case Western Reserve University, Cleveland, Ohio 44106.

tion process. The reverse (oxidation first) is an equally valid way of considering the problem. Ten different models have been treated. The following treatments are for equal forward and reverse currents.

Case I. On first, off last (Onfol)

During the forward electrolysis, the reduced species will form an adsorbed monolayer first and then diffuse into solution. Upon current reversal, the diffusing species will be oxidized first and then the adsorbed monolayer. The surface excess of the product can be calculated from the solution of the following equations:

$$t_a = nF\Gamma/i_0 \tag{2}$$

where t_a is the time required for formation of the monolayer, Γ is the amount adsorbed, and i_0 is the current density.

$$t_d = \tau_f - nF\Gamma/i_0 \tag{3}$$

where τ_f is the forward transition time and t_d is the remainder of the forward transition time after monolayer formation.

$$t'_d = t_d/3 \tag{4}$$

where t'_d is the time required for the diffusing species to be electrolyzed after current reversal.

$$t'_a = \tau_r - t'_d \tag{5}$$

where t'_a is the time required for the adsorbed species to be electrolyzed after current reversal and τ_r is the reverse transition time.

Solution of the above equations gives rise to

$$\begin{aligned} nF\Gamma = 2i_0[\tau_r/\pi \cdot \arccos\{(t'_d - t'_a)/\tau_r\} - 2/\pi \cdot (t'_d \cdot t'_a)^{\frac{1}{2}}] - \\ i_0[(t_d + \tau_r)/\pi \cdot \arccos\{(t_d + t'_d - t'_a)/(t_d + \tau_r)\} - \\ 2/\pi\{(t_d + t'_d) \cdot t'_a\}^{\frac{1}{2}}] \end{aligned} \tag{6}$$

This model has also been advanced by other workers[8,9].

Case II. On first, off first (Onfof)

As in Case I, the monolayer is formed first during the initial electrolysis. On current reversal, the monolayer is electrolyzed first, then the diffusing species. The following equation was derived using the current response function additivity principle[10].

$$(\tau_f + \tau_r - nF\Gamma/i_0)^{\frac{1}{2}} - (\tau_r)^{\frac{1}{2}} - (\tau_r - nF\Gamma/i_0)^{\frac{1}{2}} = 0 \tag{7}$$

Case III. On first, off constant (Onfoc)

Once again, the reduction product first forms the monolayer and then diffuses into solution. However, on current reversal, the monolayer is electrolyzed under constant flux conditions, namely

$$i_a = nF\Gamma/\tau_r \tag{8}$$

where i_a is the current due to reaction of the adsorbed species. Using the current response function additivity principle[10],

$$i_0(\tau_f+\tau_r-nF\Gamma/i_0)^{\frac{1}{2}}-(2i_0-nF\Gamma/\tau_r)(\tau_r)^{\frac{1}{2}}=0 \tag{9}$$

and

$$\Gamma=\{3i_0\tau_r-[9i_0^2\tau_r^2+4(i_0^2\tau_f\tau_r-3i_0^2\tau_r^2)]^{\frac{1}{2}}\}/2nF\,. \tag{10}$$

Case IV. On constant, off constant (Oncoc)

This model assumes that the monolayer is both formed during reduction and removed during reoxidation at constant flux. The current response function additivity principle[10] gives rise to

$$(i_0-nF\Gamma/\tau_f)(\tau_f+\tau_r)^{\frac{1}{2}}-(2i_0-nF\Gamma/\tau_f-nF\Gamma/\tau_r)(\tau_r)^{\frac{1}{2}}=0 \tag{11}$$

and

$$\Gamma=[-b+(b^2-4ac)^{\frac{1}{2}}]/2anF \tag{12}$$

where

$$a=(\tau_f+\tau_r)/\tau_f^2-(\tau_f+\tau_r)^2/\tau_f^2\tau_r \tag{13}$$

and

$$b=2i_0(\tau_f+\tau_r)/\tau_f \tag{14}$$

and

$$c=i_0^2(\tau_f-3\tau_r) \tag{15}$$

Case V. On constant, off first (Oncof)

In this case, the model assumes that the monolayer is formed at constant flux and is reoxidized first. The current response function additivity principle[10] was again used to show that

$$(i_0-nF\Gamma/\tau_f)(\tau_f+\tau_r)^{\frac{1}{2}}-(i_0-nF\Gamma/\tau_f)(\tau_r)^{\frac{1}{2}}-i_0(\tau_r-nF\Gamma/i_0)^{\frac{1}{2}}=0 \tag{16}$$

Case VI. On constant, off last (Oncol)

This model assumes that the adsorbed layer is formed with a constant flux and is reoxidized last. The following equations were derived using the same procedure as for Case I.

$$i_d=i_0-nF\Gamma/\tau_f \tag{17}$$

$$t'_d=i_d^2\tau_f/[(i_d+i_0)^2-i_d^2] \tag{18}$$

$$t'_a=\tau_r-t'_d \tag{19}$$

and

$$nF\Gamma=(2i_0-nF\Gamma/\tau_f)\{\tau_r/\pi\cdot\arccos[(t'_d-t'_a)/\tau_r]-2(t'_dt'_a)^{\frac{1}{2}}/\pi\}-(i_0-nF\Gamma/\tau_f)\times$$
$$\{(\tau_f+\tau_r)/\pi\cdot\arccos[(\tau_f+t'_d-t'_a)/(\tau_f+\tau_r)-2/\pi(\tau_f+t'_d)t'_a]^{\frac{1}{2}}\} \tag{20}$$

Case VII. On last, off first (Onlof)

Formation of the monolayer is assumed to occur last and removal is assumed to occur first. The current response function additivity principle[10] was used to show that

$$(\tau_f+\tau_r)^{\frac{1}{2}}-(\tau_r+nF\Gamma/i_0)^{\frac{1}{2}}-(\tau_r-nF\Gamma/i_0)^{\frac{1}{2}}=0 \tag{21}$$

Case VIII. On last, off last (Onlol)

This model assumes that the reduced species is adsorbed last and reoxidized last. The following equations were derived using the method described for Case I.

$$t_a=nF\Gamma/i_0 \tag{22}$$

$$t_d=\tau_f-nF\Gamma/i_0 \tag{23}$$

$$(\tau_f+t'_d)^{\frac{1}{2}}-(t_a+t'_d)^{\frac{1}{2}}-(t'_d)^{\frac{1}{2}}=0 \tag{24}$$

where the above equation is solved for t'_d, and

$$\begin{aligned} nF\Gamma = {} & i_0/\pi[\tau_r \arccos\{(t'_d-t'_a)/\tau_r\}]-2i_0/\pi\cdot(t'_a t'_d)^{\frac{1}{2}}+ \\ & i_0/\pi(t_a+\tau_r)\arccos\{(t_a+t'_d-t'_a)/(t_a+\tau_r)\}]- \\ & 2i_0/\pi[(t_a+t'_d)t'_a]^{\frac{1}{2}}-i_0/\pi[(\tau_f+\tau_r)\arccos\{(\tau_f+t'_d-t'_a)/(\tau_f+\tau_r)\}]+ \\ & 2i_0/\pi[(\tau_f+t'_d)t'_a]^{\frac{1}{2}} \end{aligned} \tag{25}$$

Case IX. On last, off constant (Onloc)

In this model, the monolayer is assumed to be formed last and reoxidized at constant flux. The following equation was derived using the current response function additivity principle[10].

$$i_0(\tau_f+\tau_r)^{\frac{1}{2}}-i_0(\tau_r+nF\Gamma/i_0)^{\frac{1}{2}}-(i_0-nF\Gamma/\tau_r)(\tau_r)^{\frac{1}{2}}=0 \tag{26}$$

Case X. Equilibrium case (Eqcase)

This last model assumes that the amount of material adsorbed onto the electrode surface is directly proportional to the concentration of diffusing species at the electrode surface. From the result obtained by Lorenz[2], the following equations can be derived[9].

$$\begin{aligned} & 2a/\sqrt{\pi}\cdot(\tau_f+\tau_r)^{\frac{1}{2}}+e^{a^2(\tau_f+\tau_r)}\cdot\operatorname{erfc}[a(\tau_f+\tau_r)^{\frac{1}{2}}]- \\ & \quad (4a/\sqrt{\pi})(\tau_r)^{\frac{1}{2}}+2e^{a^2\tau_r}\cdot\operatorname{erfc}[a(\tau_r)^{\frac{1}{2}}]-1=0 \end{aligned} \tag{27}$$

where

$$a=C\sqrt{D/\Gamma} \tag{28}$$

and

$$\Gamma=i_0/nFa^2\{2a(\tau_f)^{\frac{1}{2}}/\sqrt{\pi}+e^{a^2\tau_f}\cdot\operatorname{erfc}[a(\tau_f)^{\frac{1}{2}}]-1\} \tag{29}$$

A computer program was written whereby the surface excess was calculated according to each model by an iterative process. The program was executed on both IBM 7094 and IBM System 360/65 computers. The amount of electrolysis product adsorbed as calculated by each model and the standard deviations of these calculated values were obtained directly from these computations.

EXPERIMENTAL

The riboflavin used in this work was obtained from New York Quinine and Chemical Works (U.S.P.) and was used without further purification. The perchlorate

medium used for the riboflavin experiments was the same as that employed by Biegler and Laitinen[11]. Standard sodium hydroxide (Fisher) solution was added to standard perchloric acid (J. T. Baker) solution until the desired stoichiometry was obtained (0.1 *F* $NaClO_4$, 0.9 *F* $HClO_4$). The pH of the resulting solution was measured to be 0.93. Riboflavin solutions were prepared by direct weighing of the compound and dissolution thereof.

Iodide solutions were prepared by direct weighing of reagent grade potassium iodide (Fisher) and subsequent dissolution in a 1.0 *F* H_2SO_4 solution prepared from reagent (J. T. Baker) sulfuric acid. These iodide solutions were freshly prepared just prior to experimental measurement since upon standing, air oxidation of the iodide was observed to occur.

All solutions were thoroughly outgassed with solvent-saturated extra high purity nitrogen prior to electrochemical measurements. A solvent-saturated nitrogen atmosphere was maintained above the solutions during experiments. The temperature was maintained at $25 \pm 1°C$.

The polarographic equipment employed in this work consisted of a Heath EUA-19-2 polarographic module coupled to a Heath EUW-19-A operational amplifier manifold. The DME was located in the chronopotentiometric cell for *in situ* polarographic measurements. Polarograms were recorded on a Houston Instruments model HR-98-T X-Y recorder.

The current reversal chronopotentiometric measurements were made using a switching circuit which has already been described[12]. Experiments were initiated by making connection to the input of the constant current amplifier. Both the auxiliary and reference electrodes were saturated calomel electrodes, the auxiliary being a very low resistance one. In the case of measurements in perchlorate media, both electrodes were equipped with sodium chloride-saturated agar plugs to prevent solution mixing, hence undesired precipitation. A hanging mercury drop electrode (HMDE) was employed as the working electrode in the riboflavin study, this electrode being formed by catching drops of mercury from a DME and "hanging" them with a Sargent transfer apparatus (No. S-29314-40). The area of the HMDE was determined from drop mass measurements, assuming spherical geometry. This electrode was renewed before determination of each chronopotentiogram. The platinum working electrode used in the iodine study was a Beckman platinum inlay electrode (No. 39273), the surface of which was polished smooth. The measured diameter of this electrode was 0.52 cm. This electrode was pre-reduced in a solution of 1.0 *F* H_2SO_4 prior to determination of each chronopotentiogram.

Chronopotentiograms were recorded with a Tektronix model 564 storage oscilloscope and photographed with a Tektronix C-27 oscilloscope camera equipped with a Polaroid back. Transition time measurements were taken directly from the resulting photograph.

All current reversal chronopotentiometric data was corrected for non semi-infinite linear diffusion effects by the techniques of Deron and Laitinen[13] and Lingane[14].

RESULTS AND DISCUSSION

Two chemical systems were investigated in this work.

Riboflavin system

The reduced form of riboflavin, *leuko*-riboflavin, is adsorbed on mercury[8]. The polarographic reduction of riboflavin in perchloric acid medium shows a prewave of the type described by Brdicka[1] as being indicative of product adsorption. Such a polarogram is shown in Fig. 1.

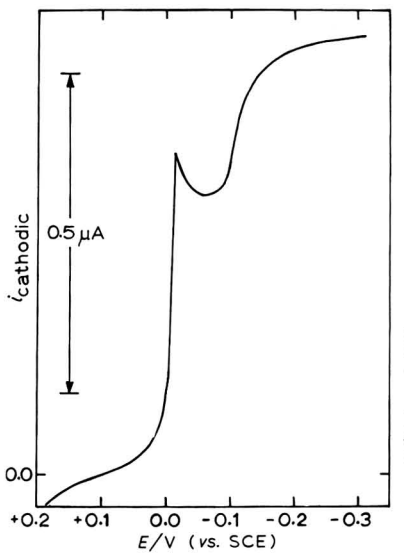

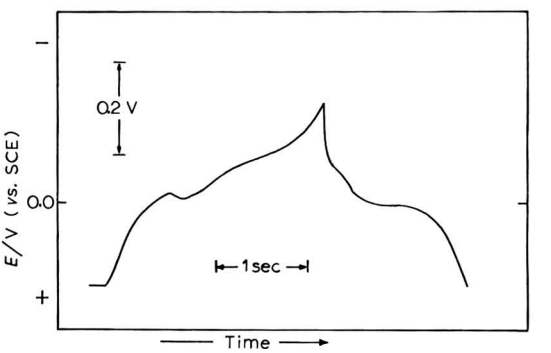

Fig. 1. Polarographic reduction of 0.1 m*M* riboflavin in perchlorate buffer. $T = 25°C$, pH = 0.93, $t = 4.01$ s, $m = 2.02$ mg $s^{-\frac{1}{2}}$, $h = 63.7$ cm. The maximum current profile is shown.

Fig. 2. Current reversal chronopotentiogram for 0.1 m*M* riboflavin in perchlorate buffer. $\tau_f = 2.20$ s, $\tau_r = 1.40$ s, $\tau_{pre} = 0.980$ s, pH = 0.93, $T = 25°C$, $i_0 = 3.76 \times 10^{-2}$ mA cm^{-2}, $A = 5.48 \times 10^{-2}$ cm^2.

Brdicka[1] also suggested that the single drop current–time behavior in the potential region of the prewave was caused by the rate with which the adsorption equilibrium becomes established. Similar single drop current–time behavior was observed in the present study; the current went through a maximum about 0.35 s after beginning of drop life. This observation suggests that the adsorption is probably diffusion controlled since the theoretical time for diffusion controlled monolayer coverage as calculated from[15]

$$t = 1.82 \times 10^6 \Gamma^2 / DC^2 \tag{30}$$

where Γ is assumed to be 2×10^{-10} mol cm^{-2} and D is assumed[11] to be 4.5×10^{-6} cm^2 s^{-1}, is about this value.

The surface excess of the reduction product may be calculated from the height of the polarographic prewave[1] according to

$$\Gamma = [i_\tau \tau^{\frac{1}{2}}] / [(\tfrac{2}{3})(0.85) m^{\frac{2}{3}} nF]$$

where i_τ is the current at the end of the drop life, τ is the drop time, and the flow rate, m, has the units of gm s^{-1}. The results of determinations of the amount of *leuko*-riboflavin adsorbed onto mercury based on this technique are shown in Table 1 for several

TABLE 1

RESULTS OF THE DETERMINATION OF THE SURFACE EXCESS OF *Leuko*-RIBOFLAVIN ON MERCURY IN 0.1 *F* $NaClO_4$/0.9 *F* $HClO_4$ BY POLAROGRAPHIC PREWAVE MEASUREMENTS

$\tau_{pre}=4.0$ s, $m=2.1$ mg s^{-1}, $h=64$ cm

Riboflavin concn./mM	$i_\tau/\mu A$	$10^{10}\ \Gamma/mol\ cm^{-2}$
0.05	0.141	1.26[a]
0.10	0.240	2.12
0.20	0.259	2.24
0.40	0.252	2.15
	Av. $\Gamma = 1.94\ (\pm 0.48) \times 10^{-10}$ mol cm^{-2}	

[a] Considerable uncertainty exists in this measurement owing to the ill-defined i_τ at this low concn.

TABLE 2

RESULTS OF DETERMINATIONS OF THE SURFACE EXCESS OF *Leuco*-RIBOFLAVIN ON MERCURY IN 0.1 *F* $NaClO_4$/0.9 *F* $HClO_4$ BY CHRONOPOTENTIOMETRIC PREWAVE MEASUREMENTS

Mean drop exposure time is *ca.* 100 s.

Riboflavin concn./mM	$Q_{ads}/\mu C$	$10^{10}\ \Gamma/mol\ cm^{-2}$
0.05	2.12	2.00 (±0.11)
0.10	2.15	2.04 (±0.16)
0.20	1.85	1.78 (±0.20)
0.40	1.87	1.79 (±0.08)
	Av. $\Gamma = 1.90\ (\pm 0.14) \times 10^{-10}$ mol cm^{-2}	

concentrations of riboflavin. These values are in agreement with those reported by Brdicka[1].

Current reversal chronopotentiometric results show a prewave for the reduction of riboflavin and a postwave for the subsequent oxidation of *leuko*-riboflavin as is shown in Fig. 2. Because of the pronounced polarographic and chronopotentiometric prewaves, a model which assumes monolayer formation prior to diffusion by the electrolysis product is the most logical choice. This being the case, the surface excess is calculable by

$$\Gamma = Q_{ads}/nF \tag{32}$$

where

$$Q_{ads} = i_0 \tau_{pre} \tag{33}$$

Using a mean drop exposure time of *ca.* 100 s, Γ was calculated from the chronopotentiometric prewave for a series of riboflavin concentrations. These results are shown in Table 2.

It was noted, however, that the value of the $i_0\tau_{pre}$ product was time dependent decreasing slightly with drop exposure time. This behavior is described by Hartley and Wilson in their chronopotentiometric investigation of the adsorption of flavin mononucleotide on mercury[16]. These workers ascribe the time dependence of the prewave to the lack of attainment of adsorption equilibrium, hence some diffusion contri-

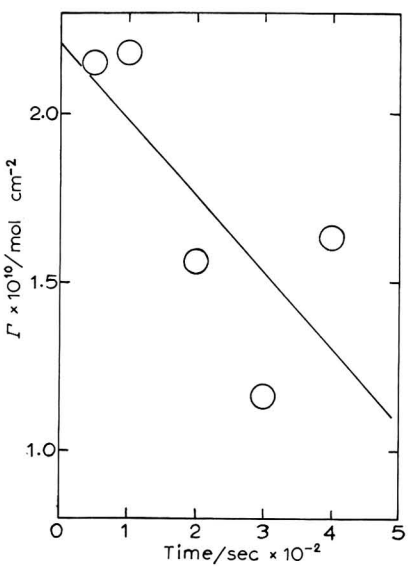

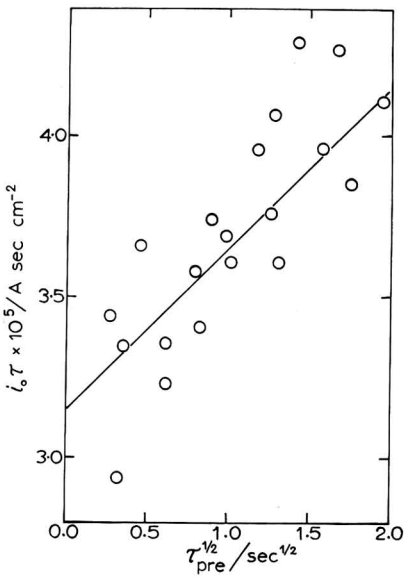

Fig. 3. Effect of electrode exposure time on the surface excess of *leuko*-riboflavin as calculated from the chronopotentiometric prewave. System conditions: 0.2 mM riboflavin in perchlorate buffer, pH = 0.93, $T = 25°C$, $A = 5.45 \times 10^{-2}$ cm^2, $i_0 = 0.137$ mA/cm^{-2}.

Fig. 4. Plot of $i_0\tau_{pre}$ *vs.* $\sqrt{\tau_{pre}}$ for the determination of R in eqn. (36). System conditions: 0.05, 0.10, 0.20, and 0.40 mM riboflavin, pH = 0.93, $T = 25°C$, $A = 5.4 \times 10^{-2}$ cm^2.

bution to the prewave (*i.e.*, formation of the monolayer is a process in which the current efficiency is $< 100\%$). In the present work, the surface excess calculated from eqn. (33) decreased with time only slightly, as is shown in Fig. 3. The extrapolated zero time value of Γ for 0.2 mF riboflavin is $2.2\,(\pm 0.3) \times 10^{-10}$ mol cm^{-2}, not an unreasonable value. The slight change in the value of $i_0\tau_{pre}$ on standing indicates that some reactant-product interaction occurs which the present theory does not treat. However, this time dependent effect is outside the time range of the measurements of this present study and does not perturb the adsorption model advanced here.

The amount of product adsorbed was calculated from transition time ratio measurements for all then models. The results of these calculations are shown in Table 3.

If there is, in fact, a diffusion contribution to the prewave, then the combination of eqns. (32) and (33), namely

$$i_0\tau_{pre} = nF\Gamma \tag{34}$$

is no longer valid. In the event of simultaneous electrolysis of diffusing species, one may write

$$(i_{0\tau} - R/\tau_{pre}^{\frac{1}{2}})(\tau_{pre}) = nF\Gamma \tag{35}$$

where $R/\tau_{pre}^{\frac{1}{2}}$ represents that portion of the current which goes to electrolysis of the diffusing species during formation of the monolayer. By writing eqn. (35) in the form

$$i_0\tau_{pre} - R\tau_{pre}^{\frac{1}{2}} = nF\Gamma \tag{36}$$

TABLE 3

SURFACE EXCESS OF *Leuko*-RIBOFLAVIN ON MERCURY IN 0.9 *F* $NaClO_4$/0.1 *F* $HClO_4$ BY CRC

Transition time measurements taken over range of 150 ms–5 s corresponding to τ_f/τ_r ratios >0.4; τ_{pre} was measured to the inflection in the chronopotentiogram

Conc./mM	$\Gamma \times 10^{10}$/*mol cm*$^{-2}$)											
	Onfol			*Oncoc*			*Onloc*			*Onlof*		
	Γ	*S.D.*	"*t*"	Γ	*S.D.*	"*t*"	Γ	*S.D.*	"*t*"	Γ	*S.D.*	"*t*"
0.05	0.86	0.15	0.18	1.43	0.14	0.10	1.53	0.17	0.11	1.99	0.46	0.23
0.10	0.95	0.26	0.28	1.85	0.28	0.15	2.05	0.30	0.15	3.13	0.78	0.25
0.20	1.06	0.15	0.14	2.09	0.33	0.16	2.33	0.47	0.20	3.66	1.51	0.41
0.40	1.15	0.31	0.27	2.72	0.49	0.18	2.72	0.49	0.18	4.42	1.27	0.29
Concn./mM	*Onfof*			*Onfoc*			*Oncof*			*Oncol*		
	Γ	*S.D.*	"*t*"	Γ	*S.D.*	"*t*"	Γ	*S.D.*	"*t*"	Γ	*S.D.*	"*t*"
0.05	1.91	0.38	0.20	1.33	0.13	0.10	1.96	0.42	0.22	0.98	0.18	0.18
0.10	2.85	0.58	0.20	1.70	0.26	0.15	2.99	0.68	0.23	1.06	0.31	0.29
0.20	3.27	1.08	0.33	1.93	0.26	0.13	3.47	1.29	0.37	1.19	0.19	0.16
0.40	3.92	0.95	0.24	2.21	0.37	0.17	4.18	1.10	0.26	1.29	0.37	0.29
Concn./mM	*Onlol*			*Eqcase*								
	Γ	*S.D.*	"*t*"	Γ	*S.D.*	"*t*"						
0.05	1.56	0.55	0.35	1.66	0.21	0.13						
0.10	2.85	1.11	0.39	2.27	0.35	0.15						
0.20	3.45	2.09	0.60	2.58	0.56	0.22						
0.40	4.26	1.75	0.41	3.02	0.57	0.19						

the value of R may be ascertained from a plot of $i_0\tau_{pre}$ *vs.* $\tau_{pre}^{\frac{1}{2}}$. Such a plot is shown in Fig. 4.

On the basis of these considerations, the Onfol model (Case I) was modified such that the effective current density for the formation of the monolayer was given by

$$(i_0)_{effective} = i_0 - R/\tau_f^{\frac{1}{2}} \tag{37}$$

This is more clearly seen through consideration of the current profile shown in Fig. 5 for the Onfol model before and after modification.

Reconsidering Case I in light of a diffusion contribution to the current during monolayer formation, one obtains the following equations:

$$t_a = nF\Gamma/(i_0 - R/t_a^{\frac{1}{2}}) \tag{38}$$

$$t_d = \tau_f - nF\Gamma/(i_0 - R/t_a^{\frac{1}{2}}) \tag{39}$$

$$(R/t_a^{\frac{1}{2}})(\tau_f + t'_d)^{\frac{1}{2}} + (i_0 - R/t_a^{\frac{1}{2}})(t_d + t'_d)^{\frac{1}{2}} - 2i_0 t_d^{\frac{1}{2}} = 0 \tag{40}$$

and

$$t'_a = \tau_r - t'_d \tag{41}$$

Solution of these equations gives rise to

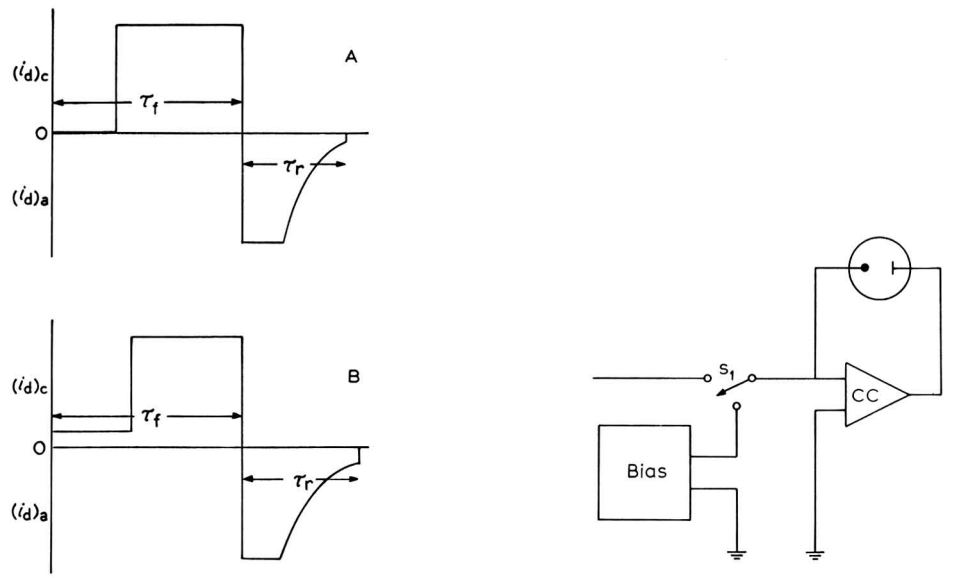

Fig. 5. Current profile of the Onfol adsorption model for CRC. Current to the diffusing species, i_d; c, cathodic; a, anodic. (A) Onfol, (B) modified Onfol assuming some diffusion contribution during monolayer formation.

Fig. 6. Circuit used to "poise" initial potential of working electrode for chronopotentiometric experiments on riboflavin.
(s_1) Switch from bias to amplifier No. 3 in ref. 12; (CC) operational amplifier No. 3 in ref. 12; (Bias) Heath EUW-16-A Voltage reference source.

$$nF\Gamma = 2i_0[\tau_r/\pi \cdot \arccos\{(t'_d - t'_a)/\tau_r\} - 2/\pi \cdot (t'_d t'_a)^{\frac{1}{2}}] - (i_0 - R/t_a^{\frac{1}{2}})[t(t_d + \tau_r)/\pi \cdot \arccos\{(t_d + t'_d - t'_a)/(t_d + \tau_r)\} - 2/\pi \cdot ((t_d + t'_d)t'_a)^{\frac{1}{2}}] - (R/t_a^{\frac{1}{2}})[(\tau_f + \tau_r)/\pi \cdot \arccos\{(\tau_f + t'_d - t'_a)/(\tau_f + \tau_r)\} - 2/\pi \cdot ((\tau_f + t'_d)t'_a)^{\frac{1}{2}}] \quad (42)$$

The results of this treatment indicated, however, that there was essentially no alternation of the value of the surface excess of *leuko*-riboflavin when diffusion contribution to the formation of the monolayer was taken into account. A 2% increase in the value of Γ occurred, and that only in the 0.05 mM case. This slight increase was within the standard deviation of the determination. The perturbation due to this effect, then is negligible.

No effect on transition time ratio measurements or on chronopotentiometric prewave measurements was noted as a result of "poising" the potential of the working electrode prior to onset of experiment through use of the circuit shown in Fig. 6. The poise potential was chosen to be potentially equidistant between the oxidation potential of mercury and the reduction potential of riboflavin. This value was determined from polarographic results.

The values of the surface excess of *leuko*-riboflavin on mercury as determined by the various techniques are summarized in Fig. 7.

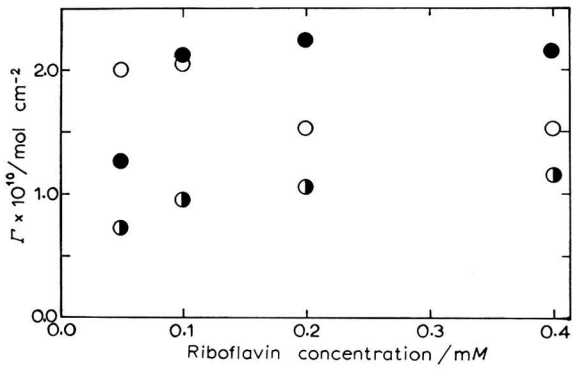

Fig. 7. Adsorption isotherms of *leuko*-riboflavin on mercury. Technique of measurement: (○) chronopotentiometric prewave, (●) polarographic prewave, (◑) CRC Onfol model.

Iodide system

The oxidized form of iodide, iodine, is adsorbed on platinum[6,17-19]. The chronopotentiometric oxidation of iodide at a platinum electrode in 1.0 *F* sulfuric acid showed no evidence of a prewave as had been the case in the reduction of riboflavin. This fact precluded the determination of the surface excess of iodine by the technique of prewave measurement. Moreover, this fact suggested that an adsorption model of the "on constant" variety might be operative.

Current reversal chronopotentiometric experiments were initiated in the same manner as in the case of the riboflavin system. No open circuit potential control was attempted. Current reversal chronopotentiometric data were taken at several levels

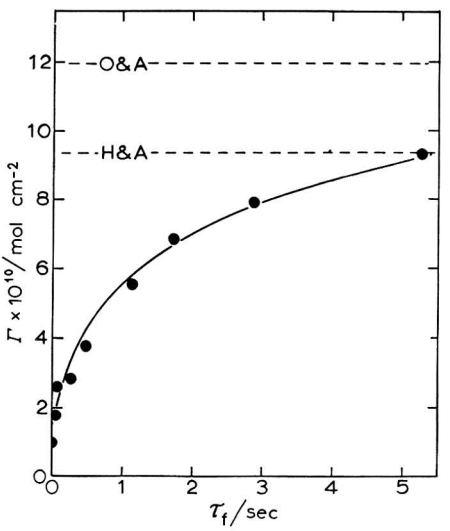

Fig. 8. Variation in surface excess of iodine on platinum with forward transition time as calculated by CRC Oncoc model. (O & A) Value of Γ as determined by Osteryoung and Anson[17], (H and A) value of Γ as determined by Hubbard *et al.*[18].

TABLE 4

SURFACE EXCESS OF IODINE ON PLATINUM IN 1.0 F H_2SO_4 BY CRC

Transition time measurements taken over range of 50 ms–5 s corresponding to τ_f/τ_r ratios >0.4

Concn./mM	$\Gamma \times 10^{10}$/*mol cm*$^{-2}$											
	Onfol			*Oncoc*			*Onloc*			*Onlof*		
	Γ	*S.D.*	"*t*"	Γ	*S.D.*	"*t*"	Γ	*S.D.*	"*t*"	Γ	*S.D.*	"*t*"
0.5	1.16	0.74	0.64	1.86	1.18	0.64	1.97	1.25	0.63	2.42	1.53	0.63
1.0	2.13	1.17	0.55	4.36	2.87	0.66	4.87	3.31	0.68	7.49	5.77	0.76
1.5	2.08	1.10	0.53	3.58	2.13	0.59	3.86	2.37	0.61	5.18	3.59	0.69
2.0	2.87	1.09	0.38	5.50	3.34	0.61	6.08	4.00	0.66	9.22	8.06	0.87
Concn./mM	*Onfof*			*Onfoc*			*Oncof*			*Oncol*		
	Γ	*S.D.*	"*t*"	Γ	*S.D.*	"*t*"	Γ	*S.D.*	"*t*"	Γ	*S.D.*	"*t*"
0.5	2.37	1.50	0.63	1.74	1.11	0.64	2.40	1.52	0.63	1.33	0.84	0.63
1.0	6.87	5.09	0.74	3.98	2.58	0.65	7.21	5.45	0.76	2.38	1.28	0.54
1.5	4.95	3.34	0.67	3.33	1.95	0.59	5.08	3.48	0.68	2.36	1.24	0.53
2.0	8.40	6.70	0.80	5.09	2.97	0.58	8.83	7.39	0.84	3.22	1.17	0.36
Concn./mM	*Onlol*			*Eqcase*								
	Γ	*S.D.*	"*t*"	Γ	*S.D.*	"*t*"						
0.5	1.78	1.12	0.63	2.13	1.35	0.63						
1.0	6.75	5.69	0.84	5.41	3.73	0.69						
1.5	4.15	3.19	0.77	4.22	2.65	0.63						
2.0	8.34	8.87	1.06	6.71	4.57	0.68						

of iodide concentration and these data were treated by all ten adsorption models. The results of these treatments are shown in Table 4. Of all those treated, the Oncol model gave rise to the best results based on the computed "*t*" values.

It was noted that the value of Γ exhibited a time dependent trend. Although Hubbard *et al.*[18], reported that no electroactive iodide was adsorbed on platinum, Bard[20] noted a non-constant chronopotentiometric constant, $i_0\tau_f^{\frac{1}{2}}/C^\circ$, with time in the case of iodide oxidation. This latter result was attributed to non-faradaic charging. With this in mind, the iodide results were examined for non-faradaic effects in light of a constant adsorption model. For diffusion control,

$$i_0\tau_f^{\frac{1}{2}} = \text{constant} \tag{42}$$

Assuming a first order double layer charging correction, we have

$$Q_{dl} = i_{dl}\tau_f \tag{43}$$

hence

$$(i_0 - Q_{dl}/\tau_f)^{\frac{1}{2}}(\tau_f)^{\frac{1}{2}} = CC \tag{44}$$

where CC is the constant in eqn. (42). Equation (43) may be written in two different ways for the evaluation of Q_{dl}, namely

$$i_0\tau_f^{\frac{1}{2}} = Q_{dl}/\tau_f + CC \tag{45}$$

and

$$i_0\tau_f = CC(\tau_f)^{\frac{1}{2}} + Q_{dl} \tag{46}$$

Treatment of the iodide data showed a negligible double layer correction by both techniques of evaluation. Hence the variation in the surface excess of iodine with time shown in Fig. 8 is probably best explained as lack of attainment of adsorption equilibrium. It should be noted, however, that the value of the surface excess calculated by this constant flux model approaches the values of Γ obtained by Osteryoung and Anson[17] and by Hubbard, *et al.*[18].

CONCLUSION

The value of the surface excess of *leuko*-riboflavin on mercury as calculated by the "on first, off last" model is in good agreement with the results of other workers using CRC[8] and other independent methods of measurement[4]. The value of the surface excess of iodine on platinum calculated on the basis of the "on constant" models is in reasonable agreement with other reported values[7,17,18].

While it was hoped that the computed "t" values would provide a criterion for choice between adsorption models, the results of this study are not quite that clear-cut. A set of current reversal chronopotentiometric data spanning a broad range of transition times and corresponding to $\Gamma = 1.035 \times 10^{-10}$ mol cm^{-2} as calculated by the Onfol model was generated. This "exact" data was then used to calculate the surface excess of electrolysis product according to all ten adsorption models. Also, this "exact" data was perturbed to the extent of 1 % by randomly varying the reverse transition time. The resulting data exhibited a normal distribution which ranged to $\pm 3\sigma$. This "perturbed" data was also treated by all ten adsorption models. The results of the calculation of the surface excess from the "exact" and the "perturbed" data are shown in Table 5. Based on consideration of the "t" statistic, all models can be eliminated except Onfol for the "exact" data and Onfol and Oncol in the case of the

TABLE 5

ONFOL TEST DATA

COMPARISON OF THE SURFACE EXCESS AND "t" STATISTIC FOR "EXACT" AND "PERTURBED" SYNTHETIC DATA AS DESCRIBED IN THE TEXT

Model	*"Exact" data*		*"Perturbed" data*	
	$\Gamma \times 10^{10}$/*mol cm*$^{-2}$	"t"	$\Gamma \times 10^{10}$/*mol cm*$^{-2}$	"t"
Onfol	1.035	0.001	1.015	0.053
Oncoc	2.124	0.300	2.103	0.317
Onfof	3.446	0.514	3.430	0.525
Onfoc	1.950	0.276	1.929	0.294
Oncof	3.714	0.565	3.700	0.574
Oncol	1.158	0.028	1.135	0.050
Onlof	3.994	0.616	3.980	0.623
Onlol	4.038	0.819	4.034	0.820
Onloc	2.388	0.359	2.368	0.374
Eqcase	2.604	0.329	2.621	0.394

"perturbed" data. It is, of course, realized that statistical considerations are not the sole basis for drawing inferences[21]. Hence the presence of a chronopotentiometric prewave as was observed in the case of the riboflavin system in this study would indicate an "on first " mechanism.

The above approach was repeated, basing the "exact" data calculations on the Oncoc model. The results of treatment of this "exact" and 1% "perturbed" data by all ten adsorption models are shown in Table 6. Consideration of the "t" statistic serves to eliminate all models except Oncoc for the "exact" data and Oncoc and Onfoc in the case of the "perturbed" data. The absence of a chronopotentiometric prewave as was the case in the iodine system in this study would favor choice of the Oncoc model over the Onfoc model.

TABLE 6

ONCOC TEST DATA

COMPARISON OF THE SURFACE EXCESS AND "t" STATISTIC FOR "EXACT" AND "PERTURBED" SYNTHETIC DATA AS DESCRIBED IN THE TEXT

Model	*"Exact" data*		*"Perturbed" data*	
	$\Gamma \times 10^{10}/mol\ cm^{-2}$	"t"	$\Gamma \times 10^{10}/mol\ cm^{-2}$	"t"
Onfol	0.418	0.394	0.419	0.385
Oncoc	1.035	0.001	1.041	0.059
Onfof	1.891	0.236	1.907	0.259
Onfoc	0.941	0.019	0.946	0.058
Oncof	2.169	0.333	2.189	0.353
Oncol	0.463	0.425	0.463	0.416
Onlof	2.630	0.483	2.648	0.497
Onlol	3.702	0.827	3.705	0.829
Onloc	1.205	0.070	1.213	0.105
Eqcase	1.341	0.079	1.349	0.111

Although the use of chronopotentiometry as a tool for the measurement of adsorption has been seriously questioned[22], it is nevertheless felt to be a valid one when discriminately applied. Chronopotentiometry's most important use has been in the measurement of chemical kinetics. In this case, adsorption corrections are probably best made using the perturbation treatment of Deron and Laitinen[13] employing a constant current model. However, if the only complication to the electrode process is adsorption and the order of formation and electrolysis of the adsorbed layer is known, the equations reported here will be of considerable use. Some of the models treated are more probable than others, but the nature of the electrode process is such that all can be experimentally observed. If an adsorption model is not known, then the Oncoc model (Case IV) can give an order of magnitude value of the surface excess. Better still, another electrochemical method such as chronocoulometry[23] could be used in such cases. The advantages of the latter technique have been documented[24]. Of course, if one is interested in studying the adsorption process in general as opposed to just calculating the amount adsorbed, the method described here may well be more useful.

ACKNOWLEDGEMENT

This work was supported in part by grants from the Petroleum Research Fund (No. 488-G2) and the National Science Foundation (No. 6596).

SUMMARY

Current reversal chronopotentiometry has been applied to the measurement of the surface excess of the product of an electrode process. Ten idealized models of the current distribution are discussed and equations which allow calculation of the amount adsorbed are given. Measurements on riboflavin and iodine systems are reported.

REFERENCES

1 R. BRDICKA, *Collection Czech. Chem. Commun.*, 12 (1947) 522.
2 W. LORENZ, *Z. Elektrochem.*, 59 (1955) 730.
3 W. LORENZ AND H. MUHLBERG, *Z. Elektrochem.*, 59 (1955) 736.
4 S. V. TATWAWADI AND A. J. BARD, *Anal. Chem.*, 36 (1964) 2.
5 R. A. MUNSON, *J. Electroanal. Chem.*, 5 (1963) 292.
6 H. A. LAITINEN AND L. M. CHAMBERS, *Anal. Chem.*, 36 (1964) 5.
7 R. A. OSTERYOUNG, *Anal. Chem.*, 35 (1963) 1100.
8 H. B. HERMAN, S. V. TATWAWADI AND A. J. BARD, *Anal. Chem.*, 35 (1963) 2210.
9 F. MOLLERS AND W. JAENICKE, *J. Electroanal. Chem.*, 18 (1968) 61.
10 R. W. MURRAY AND C. N. REILLEY, *J. Electroanal. Chem.*, 5 (1963) 17.
11 T. BIEGLER AND H. A. LAITINEN, *J. Phys. Chem.*, 68(1964) 2374.
12 H. B. HERMAN AND A. J. BARD, *Anal. Chem.*, 37 (1965) 590.
13 S. DERON AND H. A. LAITINEN, *Anal. Chem.*, 38 (1966) 1290.
14 P. J. LINGANE, *Anal. Chem.*, 36 (1964) 1723.
15 C. N. REILLEY AND W. STUMM in P. ZUMAN (Ed.), *Progress in Polarography*, Vol. I, Interscience Publishers, Inc., New York, 1962, p. 99.
16 A. M. HARTLEY AND G. S. WILSON, *Anal. Chem.*, 38 (1966) 681.
17 R. A. OSTERYOUNG AND F. C. ANSON, *Anal. Chem.*, 36 (1964) 975.
18 A. T. HUBBARD, R. A. OSTERYOUNG AND F. C. ANSON, *Anal. Chem.*, 38 (1966) 692.
19 R. A. OSTERYOUNG, G. LAUER AND F. C. ANSON, *J. Electrochem. Soc.*, 110 (1963) 926.
20 A. J. BARD, *Anal. Chem.*, 35 (1963) 340.
21 A. M. NEVILLE AND J. B. KENNEDY, *Basic Statistical Methods for Scientists and Engineers*, International Textbook Co., Scranton, Pa., 1964, p. 145.
22 P. J. LINGANE, *Anal. Chem.*, 39 (1967) 485.
23 R. W. MURRAY AND D. J. GROSS, *Anal. Chem.*, 38 (1966) 392.
24 W. H. REINMUTH, *Anal. Chem.*, 40 (1968) 185R.

ELECTROANALYTICAL CHEMISTRY AND INTERFACIAL ELECTROCHEMISTRY
Elsevier Sequoia S.A., Lausanne – Printed in The Netherlands

POTENTIEL D'ÉCOULEMENT, COURANT D'ÉCOULEMENT ET CONDUCTANCE DE SURFACE À L'INTERFACE EAU–VERRE

A. WATILLON ET R. DE BACKER
Université Libre de Bruxelles (Belgium)
(Reçu le 7 juin, 1969; en forme revisée le 1ier novembre, 1969)

1. INTRODUCTION

Parmi les méthodes expérimentales susceptibles de fournir des informations sur la structure de la couche double électrique, l'étude des phénomènes électrocinétiques aux interfaces continus a joué un rôle non négligeable.

Ces phénomènes se produisent, par exemple, lors du déplacement relatif d'un liquide par rapport à un solide, séparés par un interface comportant une couche double électrique. Le plan de glissement se situe quelque part dans la partie diffuse de la couche double et est caractérisé par un potentiel ζ, directement accessible par l'étude des phénomènes électrocinétiques.

Dans le cas du verre, ce potentiel ζ ne peut être assimilé, ni au potentiel ψ_0 de la surface, ni directement à ψ_δ, potentiel défini dans le modèle de Stern[1]. Le potentiel ζ présente cependant des analogies avec ψ_δ comme nous le verrons plus loin.

Dans la présente étude, les phénomènes électrocinétiques auxquels nous nous sommes plus spécialement intéressés sont le potentiel et le courant d'écoulement[2].

Lorsque l'écoulement du liquide est laminaire et que le rayon de courbure de la paroi de la cellule de mesure est beaucoup plus grand que l'épaisseur de la couche double, le déplacement du liquide, sous l'action d'une force mécanique au voisinage d'une surface chargée, provoque l'apparition d'un courant de convection I_1, dû à l'entraînement des charges électriques se trouvant dans l'atmosphère ionique existant au voisinage de la paroi. L'accumulation des charges aux extrémités du système va provoquer l'apparition d'une différence de potentiel E qui donnera naissance à un courant de conduction I_2 en sens inverse. A l'équilibre, le courant de convection I_1, proportionnel à la pression P exercée sur le liquide, sera égal et de signe contraire à I_2, courant de conduction proportionnel au potentiel d'écoulement E, ce qui amène la relation:

$$\frac{E}{P} = \frac{\varepsilon\zeta}{4\pi\eta}\,\frac{k_0}{G} \tag{1}$$

ε étant la constante diélectrique, η la viscosité, G la conductance totale et k_0 la constante conductométrique de la cellule exprimée en cm.

Si on empêche la formation du courant de conduction I_2 dans la cellule, en permettant le retour des charges électriques par une voie extérieure à la solution, le courant ainsi mesuré sera directement proportionnel au courant de convection I_1, ce qui nous donnera la relation suivante:

$$\frac{I}{P} = \frac{\varepsilon\zeta}{4\pi\eta} k_0 \tag{2}$$

On constate donc que le calcul de ζ à partir du courant d'écoulement ne fait pas intervenir la valeur de la conductance G de la cellule, contrairement au cas précédent.

Ce point est intéressant car pour expliciter G, on ne peut négliger les effets de la conductance de surface existant à la paroi de la cellule de mesure, qui contribue pour une part importante, dans le cas de solutions diluées, à la valeur de la conductance du système. Cette dernière, figurant dans l'éqn. (1), sera donnée par l'expression:

$$G = k_0\lambda_0\left(1 + \frac{D}{S}\frac{\lambda_s}{\lambda_0}\right) \tag{3}$$

D étant le périmètre, S la section de la cellule de mesure, λ_0 la conductivité au coeur de la solution, et λ_s la conductance de surface. On voit que la constante conductométrique k_0 s'obtient aisément à partir d'une mesure de G en solution concentrée ($D/S \cdot \lambda_s/\lambda_0 \ll 1$).

D'autre part, Bikerman[3] a établi une relation permettant de calculer la conductance de surface de l'atmosphère ionique à partir du potentiel ζ:

$$\lambda_s = \sqrt{\frac{\varepsilon RT}{2\pi F^2}}\, C\left\{\left[l_c(e^{z^+ F\zeta/2RT} - 1) + l_a(e^{-(z^- F\zeta/2RT)} - 1)\right] + \right.$$
$$\left. + \left[\frac{\varepsilon RT}{2\pi\eta z^+}(e^{z^+ F\zeta/2RT} - 1) + \frac{\varepsilon RT}{2\pi\eta z^-}(e^{-(z^- F\zeta/2RT)} - 1)\right]\right\} \tag{4}$$

où R est la constante des gaz parfaits, T la température absolue, F le Faraday, $z^{\pm}$ la valence, C la concentration équivalente, l_c la mobilité du cation et l_a celle de l'anion.

Le premier terme de l'équation correspond à la composante de migration ionique, et le deuxième terme est dû à la contribution du déplacement électroosmotique du liquide.

La comparaison des valeurs de la conductance de surface déterminées expérimentalement à celles calculées par la théorie de Bikerman fait ressortir un désaccord assez important, les valeurs expérimentales étant systématiquement trop élevées. Aussi, différents auteurs[4-7] ont-ils émis l'hypothèse de l'existence d'une conductance de surface supplémentaire, due à la présence d'ions adsorbés qui garderaient une certaine mobilité dans une couche "gelée" ayant par exemple pour origine dans le cas du verre, soit un gonflement de la surface lié à un phénomène d'hydratation[8], soit une porosité superficielle[9].

Tout d'abord, en vue de tester la validité des techniques de mesure, nous avons déterminé sur le même système et dans des conditions expérimentales identiques, les potentiels et les courants d'écoulement, ainsi que la conductance de surface.

De plus, afin d'étudier le rôle joué par l'hydratation superficielle, nous avons utilisé un verre sodo-calcique ordinaire, supposé plus hydratable que le verre Jéna 16^{III} précédemment utilisé dans ce laboratoire pour ce genre d'étude[10,11].

2. METHODES EXPERIMENTALES

Le projet de mesure simultanée du potentiel d'écoulement, du courant d'écoulement et de la conductance de surface sur un même système expérimental nous

a amenés à l'étude d'une cellule permettant de concilier les divers impératifs imposés par les éqns. (1), (2) et (3).

Jusqu'à présent, les mesures valables effectuées dans ce domaine ont été réalisées au moyen de capillaires de géométrie parfaitement connue[12,13].

Examinons le cas d'un capillaire de 150 μ de diamètre et de 10 cm de longueur. Le rapport D/S sera égal à 270 cm^{-1} et la valeur de k_0 sera de $2 \cdot 10^{-5}$ cm.

Dans un tel capillaire, le potentiel d'écoulement correspondant à $\zeta = 100$ mV, $P = 100$ mm H_2O, $\lambda_0 = 10^{-6}\ \Omega^{-1}\ cm^{-1}$ et $\lambda_s = 10^{-9}\ \Omega^{-1}$ sera égal à $E = 0.60$ V pour une résistance de cellule de $4 \cdot 10^{10}\ \Omega$. Le potentiel d'écoulement sera mesurable au moyen d'un montage électrométrique, dont la résistance d'entrée sera nettement supérieure à celle de la cellule de mesure.

De même, la conductance de surface sera obtenue à partir de l'éqn. (3) par la mesure de la conductance totale de la cellule, réalisée au moyen d'un pont de Wheatstone classique à haute résistance et fonctionnant en courant continu.

Par contre, le courant d'écoulement dans les mêmes conditions expérimentales sera égal à $I = 1.5 \times 10^{-11}$ A. La mesure précise d'un tel courant à l'aide d'un appareil possédant une résistance interne faible devant la résistance du capillaire présente un certain nombre de difficultés techniques.

Aussi, s'est-il avéré utile de mettre au point une cellule ayant une valeur de k_0 nettement plus élevée. Cette cellule en forme de parallélépipède rectangle a une constante k_0 de 2.5×10^{-2} cm et son rapport D/S est de 400 cm^{-1}. Une telle cellule a sensiblement le même rapport D/S que le capillaire précité, mais sa constante k_0 est 1000 fois plus élevée. Dans les conditions expérimentales envisagées précédemment, le potentiel d'écoulement mesuré sera toujours le même, mais le courant d'écoulement aura comme valeur : $I = 1.9 \times 10^{-7}$ A, pour une résistance de cellule de $5 \cdot 10^{7}\ \Omega$. La mesure du potentiel d'écoulement et de la conductance de surface ne présentera pas de difficultés et le courant d'écoulement pourra être mesuré à l'aide d'un appareil à condensateur vibrant du type "Philips" GM 6020, d'une sensibilité de 10^{-10} A à fond

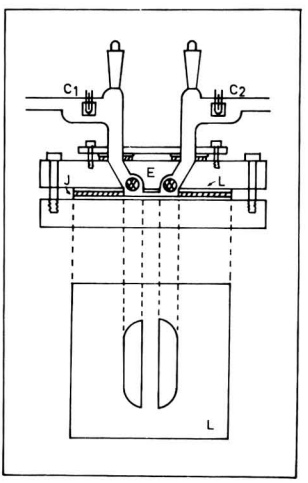

Fig. 1. Cellule de mesure.

d'échelle, en shuntant sa résistance d'entrée par une résistance faible vis-à-vis de celle de la cellule de mesure.

Une telle cellule (Fig. 1) a été réalisée au moyen de deux lames de verre et d'un joint en polyéthylène (J), serrés entre deux montures en polyméthacrylate de méthyle. Dans l'une des lames (L), nous avons découpé par forage aux ultra-sons deux secteurs dont les sections droites, parallèles et longues de 3 cm, sont séparées de 0.6 cm. L'écartement des deux lames correspond à l'épaisseur du joint J dans lequel une ouverture rectangulaire de 2 cm sur 3 cm a été découpée. Ce montage permet de délimiter une cellule de 0.6 cm de longueur, 3 cm de largeur et 48 μ d'épaisseur. Cette dernière valeur a été déterminée par voie conductométrique. Des amenées de liquide ainsi que le logement des deux électrodes de mesure (E) en platine platiné sont prévus dans l'une des montures de fixation. Deux paires d'électrodes en platine (C1 et C2) placées respectivement en amont et en aval de la cellule de mesure permettent de s'assurer de la mise à l'équilibre de concentration, qui est mesurée à l'aide d'un pont Wayne–Kerr B 221 BF. Cette cellule est montée sur un appareil d'écoulement précédemment décrit[10].

3. RESULTATS EXPERIMENTAUX

A. Contrôle du pH

Bien que le présent travail étudie surtout le rôle de la concentration et de la valence du contre-ion, il s'est cependant avéré nécessaire d'estimer l'incidence du pH sur le comportement des systèmes, les protons jouant pour le verre le rôle d'ions déterminant le potentiel. Les points de charge nulle du verre sodo-calcique et du Jena 16^{III} sont tous deux inférieurs à pH = 3, et se situent probablement au voisinage de pH = 2. L'influence du pH sur les divers paramètres électrocinétiques fera l'objet d'une étude ultérieure. Il était cependant important de savoir si notre verre, dans les conditions expérimentales réalisées, pouvait être considéré comme étudié à pH constant. Pour cela, sur l'appareil précédemment décrit[10], nous avons intercalé une cellule Ingold type 435 permettant le contrôle du pH en écoulement continu, entre la cellule de mesures électrocinétiques et le réservoir de récupération de l'eau d'écoulement.

On a tout d'abord réalisé l'écoulement d'eau très pure ($\lambda_0 \sim 0.7 \times 10^{-7}\ \Omega^{-1}\ cm^{-1}$) dont le pH s'est maintenu à 6.8 ± 0.2. Nous avons ensuite réalisé des concentrations croissantes des différents sels utilisés jusqu'à $C = 10^{-3}$ équiv. l^{-1}. Les variations de pH observées pour l'ensemble des solutions sont toujours restées dans les limites de 6.8 ± 0.5 unités de pH. Vu la nécessité de travailler à de très faibles forces ioniques, on peut donc raisonnablement considérer que les expériences ici décrites ont été réalisées à pH constant.

Il faut toutefois remarquer que ces mesures étaient effectuées immédiatement après l'arrêt de l'écoulement car pendant celui-ci un potentiel d'écoulement prenant vraisemblablement naissance entre le capillaire de l'électrode de verre et l'électrode de référence se superposait au potentiel lié au pH du système, cet effet étant d'autant plus important que la solution est diluée.

Nous avons ensuite réalisé un écoulement prolongé d'eau pure, puis confiné le compartiment de mesure électrocinétique et le compartiment de mesure du pH. Dans le premier, en 10 h, la conductivité est passée de $0.7 \times 10^{-7}\ \Omega^{-1}\ cm^{-1}$ à 1.5×10^{-7}

Ω^{-1} cm^{-1}. Dans le second, le pH est passé progressivement de 6.8–10. Nous attribuons cet effet à une solubilité non négligeable du verre de l'électrode de verre. Par contre, l'évacuation de cette eau et son remplacement par l'eau du compartiment électrocinétique ont montré que, dans celui-ci, le pH était resté constant, ce qui montre que notre verre sodo-calcique a un comportement très différent du verre d'électrode de verre. Dans cet ordre d'idées, les points de charge nulle de verres d'électrodes réversibles par rapport aux Na^+ et aux K^+ se situent[19] au voisinage de pH = 6. Notre verre sodo-calcique et le verre Jena 16^{III} ont donc un comportement électrocinétique beaucoup plus voisin de celui de la silice.

B. Effet de temps

On a observé précédemment à l'aide de KNO_3[14] des valeurs différentes de ζ, si l'on part de l'eau pure en concentrant progressivement la solution, ou si l'on procède à des dilutions successives d'une solution plus concentrée. L'écart existant entre ces deux séries de mesures nous a incités à estimer le temps mis par un système pour reprendre son équilibre après une modification de force ionique, et ceci respectivement pour les nitrates de potassium, de baryum et de lanthane.

On a d'abord écoulé pendant 10 h de l'eau pure de conductivité inférieure à 10^{-7} Ω^{-1} cm^{-1} ; ensuite, on a fait s'écouler pendant 10 autres heures des concentrations 10^{-4} équiv. l^{-1} de chaque électrolyte ; finalement, on a rétabli l'écoulement d'eau pure pendant un temps suffisant pour atteindre l'équilibre. Les potentiels d'écoulement et les conductances de surface ont été mesurés simultanément. Pour chaque expérience, les parois de la cellule ayant été préalablement nettoyées dans HNO_3 concentré et lavées à la vapeur, le potentiel ζ de départ a toujours avoisiné -114 mV et est resté stable pendant les 10 h d'écoulement. Comme on le voit sur la Fig. 2, lors

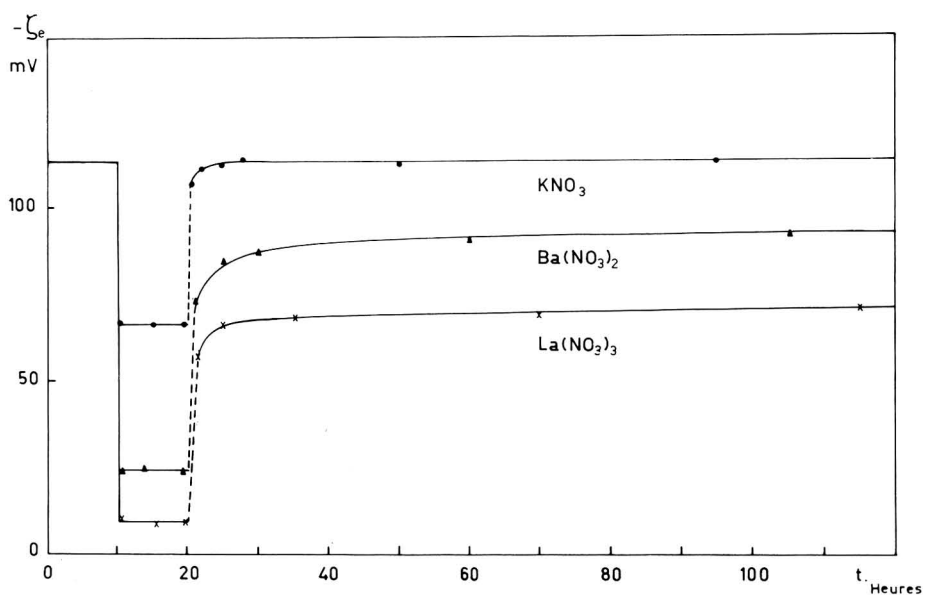

Fig. 2. Effet de temps sur le potentiel ζ lors de l'addition de 10^{-4} équiv. l^{-1} de divers électrolytes, puis de l'écoulement d'eau pure.

de l'addition de 10^{-4} équiv. d'électrolyte, le potentiel ζ tombe à -67, -25 et -10 mV lors de l'emploi de KNO_3, $Ba(NO_3)_2$ et de $La(NO_3)_3$ respectivement. Ces potentiels sont toujours restés remarquablement stables pendant les 10 h d'écoulement à cette concentration.

Lorsqu'on repasse à l'écoulement d'eau pure, pour les trois électrolytes, le potentiel ζ redevient environ 50 mV plus négatif pendant la première heure. Ensuite, en milieu KNO_3, il atteint sa valeur de départ (-114 mV) en une dizaine d'heures. Pour les deux autres électrolytes, il semble se stabiliser après une centaine d'heures, respectivement à une valeur de -93 mV pour $Ba(NO_3)_2$ et -72 mV pour $La(NO_3)_3$.

A la Fig. 3, nous avons représenté les variations de la conductance de surface, dont les valeurs ont été obtenues simultanément à celles des potentiels ζ reportés à la Fig. 2.

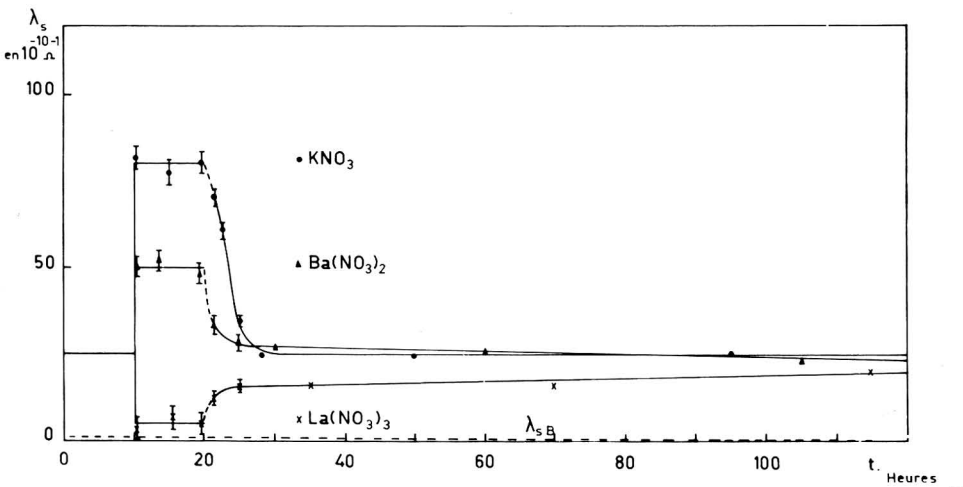

Fig. 3. Effet de temps sur la conductance de surface lors de l'addition de 10^{-4} équiv. l^{-1} de divers électrolytes, puis de l'écoulement d'eau pure.

Dans l'eau pure, la conductance de surface reste sensiblement constante pendant les 10 h d'écoulement préliminaire ($\lambda_s = 25 \cdot 10^{-10}\ \Omega^{-1}$). En solution 10^{-4} équiv. l^{-1} en électrolyte, si les valeurs restent également stables, on observe cependant une augmentation importante pour KNO_3 ($\lambda_s = 80 \cdot 10^{-10}\ \Omega^{-1}$), une augmentation plus faible pour $Ba(NO_3)_2$ ($\lambda_s = 50 \cdot 10^{-10}\ \Omega^{-1}$) et une diminution drastique pour $La(NO_3)_3$ ($\lambda_s = 5 \cdot 10^{-10}\ \Omega^{-1}$).

Cette divergence de comportement pourra être interprétée, nous semble-t-il, en considérant les propriétés d'adsorption spécifique des divers ions étudiés en relation avec leur valence ; nous reviendrons plus loin sur ce point.

Lors du retour à l'écoulement d'eau pure, nous observons, comme dans le cas des potentiels ζ, un effet de temps marqué. Dans le cas de KNO_3, la conductance de surface retombe après quelques heures à sa valeur d'origine. Pour le $La(NO_3)_3$, même après 100 h, $\lambda_{s,exp}$ n'est pas encore remontée à sa valeur initiale. Enfin, en présence de $Ba(NO_3)_2$, $\lambda_{s,exp}$ redescend à une valeur qui est même légèrement inférieure à sa valeur d'origine. Ce point sera également repris plus loin.

C. Effet de la concentration de l'electrolyte

Après cette série d'observations, nous avons résolu d'effectuer les mesures ultérieures en procédant à concentration croissante en électrolyte et de considérer que l'équilibre du système était atteint pendant le temps nécessaire à la préparation de la mesure. Nous avons porté dans les Figs. 4, 5 et 6 les valeurs du potentiel électrocinéti-

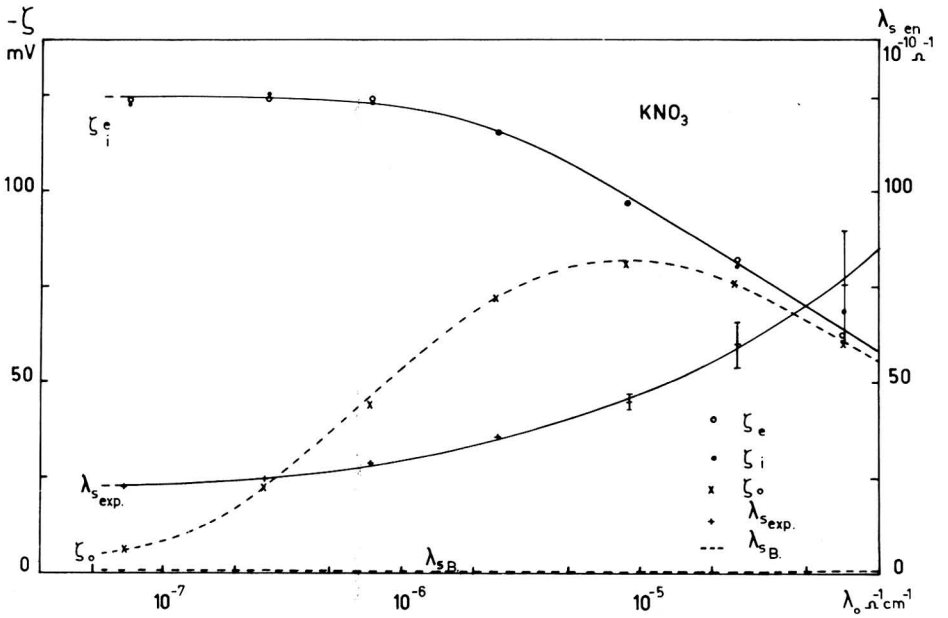

Fig. 4. Potentiels ζ et conductances de surface pour diverses conductivités en KNO_3.

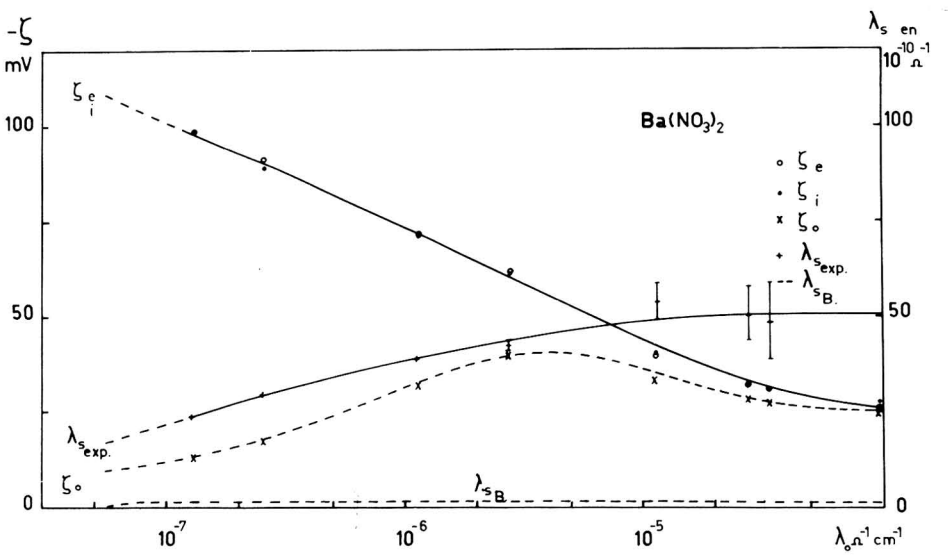

Fig. 5. Potentiels ζ et conductances de surface pour diverses conductivités en $Ba(NO_3)_2$.

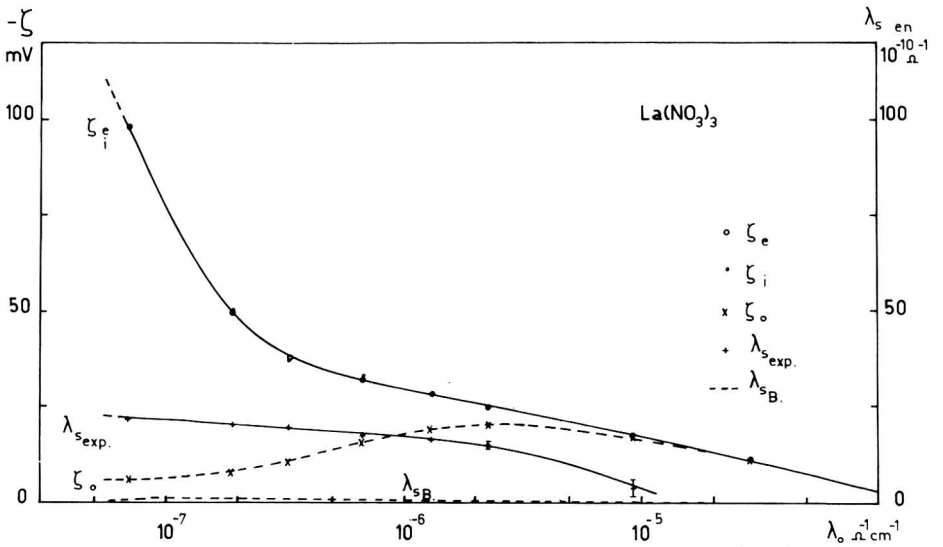

Fig. 6. Potentiels ζ et conductances de surface pour diverses conductivités en $La(NO_3)_3$.

que obtenues respectivement à l'aide des potentiels d'écoulement ζ_e et des courants d'écoulement ζ_i, ainsi que les valeurs des conductances de surface $\lambda_{s,exp}$ mesurées dans les mêmes conditions expérimentales, en fonction de la conductivité des solutions de KNO_3, $Ba(NO_3)_2$ et $La(NO_3)_3$ utilisées. Subsidiairement, nous y montrons les valeurs de ζ_0 qu'on obtiendrait à partir des potentiels d'écoulement sans tenir compte de la conductance de surface, ainsi que la valeur de la conductance de surface $\lambda_{s,B}$ de l'atmosphère ionique, calculée à partir de la théorie de Bikerman.

4. DISCUSSION DES RESULTATS

A. Relation potentiel–courant d'ecoulement

Sur les figures précitées, on remarque la bonne concordance existant entre les valeurs de ζ_e et de ζ_i, déjà signalée précédemment[14]. L'écart est généralement de ± 2 mV, ce qui correspond aux erreurs expérimentales des méthodes utilisées. Il faut cependant signaler que les mesures par courant d'écoulement sont plus commodes à obtenir, car ne nécessitant pas une connaissance précise de la conductance du système ; elles sont donc moins sensibles à une éventuelle fluctuation de concentration.

B. Adsorption ionique à la paroi et conductance de surface

L'observation des diverses courbes ζ–λ_0 des Figs. 4, 5 et 6 montre que les valeurs de ζ obtenues sont nettement inférieures à celles correspondant à un verre Jena 16^{III} précédemment mesurées à l'aide du même appareil[10]. Comme on l'observe généralement[2], pour des concentrations équivalentes indentiques, les potentiels ζ sont d'autant plus faibles que la valence est élevée.

D'autre part, les valeurs des conductances de surface $\lambda_{s,exp}$ déterminées pour les diverses conductivités λ_0 simultanément à la mesure de ζ sont 5–6 fois supérieures à celles mesurées précédemment sur le verre Jena 16^{III}.

La valence du contre-ion a également un effet marqué sur $\lambda_{s,exp}$: si, en solution très diluée, les conductances de surface mesurées pour les divers cations sont du même ordre de grandeur, par contre, lorsqu'on se déplace vers des solutions plus concentrées, on observe une augmentation sensible dans le cas de KNO_3, une augmentation nettement plus faible dans le cas de $Ba(NO_3)_2$ et une diminution importante dans le cas de $La(NO_3)_3$.

On constate enfin que les valeurs expérimentales de la conductance de surface $\lambda_{s,exp}$ sont 10–20 fois supérieures à celles calculées par la théorie de Bikerman $\lambda_{s.B}$, relatives à la conductance de surface de l'atmosphère ionique ; la contribution de celle-ci aux phénomènes que nous avons observés peut donc être considérée comme négligeable.

Vu la complexité du problème, il nous a semblé intéressant de choisir un modèle d'interface eau–verre aussi simple que possible, qui permettrait d'expliquer les divers résultats expérimentaux obtenus. En effet, le comportement des potentiels ζ et des conductances de surface peut être interprété en admettant l'existence d'un gel superficiel dont la limite interne correspond au feuillet de Stern, caractérisé par le potentiel ψ_δ, et dont la limite externe correspond au plan de glissement hydrodynamique caractérisé par le potentiel ζ.

L'épaisseur de cette couche figée pourrait dépendre de la nature du verre utilisé : dans le cas du verre Jena 16^{III} peu hydratable, elle serait plus faible que dans le cas du verre sodo-calcique utilisé ici[11].

En faisant l'hypothèse qu'à l'équilibre, la répartition des ions, tant dans la couche figée que dans le liquide, obéit à la distribution de Maxwell–Boltzmann, nous constatons que le potentiel ζ sera d'autant plus faible que l'épaisseur de gel est importante, les ions présents dans cette couche ne pouvant participer au déplacement hydrodynamique lors des mesures de potentiels et de courants d'écoulement. D'autre part, les ions de la couche figée restant mobiles, ils pourront contribuer pour une part importante à la conductance de surface, le potentiel ψ_δ régissant l'ensemble de l'atmosphère ionique.

C. Effet de la valence

Les valeurs de ζ et de $\lambda_{s,exp}$ représentées dans les Figs. 2–6 permettent une étude comparative entre des ions de diverses valences.

Dans le cas de KNO_3, et suivant le modèle proposé, les ions K^+ se comportent d'une manière réversible et l'ensemble de leur population peut s'échanger librement entre le feuillet figé et la solution. En effet, les Figs. 2 et 3 montrent un retour aux valeurs de départ, ce qui exclut une adsorption, du moins irréversible, dans le feuillet de Stern et dans le gel. De plus, la forte augmentation de $\lambda_{s,exp}$ avec la concentration montre que les ions K^+ sont très nombreux dans la couche figée et y gardent leur mobilité (Fig. 4) ou du moins une partie importante de celle-ci. Dans le cas de $La(NO_3)_3$, si ζ diminue avec la concentration par compression de la couche double, il faut remarquer que $\lambda_{s,exp}$, contrairement au cas de KNO_3, diminue ici d'une manière spectaculaire (Figs. 3 et 6). Les ions La^{3+} ayant une forte tendance à s'adsorber dans le feuillet de Stern et dans le gel en perdant leur mobilité, il en résulte une diminution importante de ψ_δ, de ζ et de $\lambda_{o,exp}$.

Lors du passage ultérieur d'eau pure, l'effet de temps est très marqué, ces ions ne se désorbant que très lentement et d'une manière partielle. ζ et $\lambda_{s,exp}$. restent infé-

rieurs à leur valeur de départ. La faible augmentation dans le temps de $\lambda_{s,exp}$ de la Fig. 3 correspondrait alors à l'augmentation de ψ_δ dû au passage progressif des La^{3+} du feuillet de Stern vers la couche figée, dans laquelle ils retrouvent une certaine mobilité.

Les valeurs de ζ et de $\lambda_{s,exp}$ obtenues dans le cas de $Ba(NO_3)_2$ montrent un comportement intermédiaire entre les deux cas précédents. On observe, à concentration croissante, une augmentation de $\lambda_{s,exp}$, cependant moins marquée que dans le cas de KNO_3 (Figs. 3 et 5). Toutefois, en repassant à l'écoulement d'eau pure, à la Fig. 2, le potentiel ζ ne retrouve pas sa valeur d'origine, et à la Fig. 3, $\lambda_{s,exp}$ repasse en dessous de sa valeur de départ, ce qui s'expliquerait par une adsorption résiduelle de Ba^{2+} à la surface.

Ces observations, fort qualitatives, vont cependant nous permettre à partir du modèle proposé de déduire quelques paramètres de l'interface eau–verre.

D. Evaluation du potentiel ψ_δ

En utilisant un traitement assez analogue à celui proposé par Wijga [5] et par Mossman et Mason[15], nous avons fait l'hypothèse que la répartition des ions, tant dans la couche figée que dans le liquide, obéit à la distribution de Maxwell–Boltzmann. Cette approximation est d'autant plus vraisemblable que la couche figée est épaisse. On pourra alors admettre que la conductance de surface totale obéit à une équation similaire à celle de Bikerman.

Il sera cependant nécessaire de considérer séparément la contribution due à la mobilité ionique de celle due à l'électroosmose. En effet, les ions de la couche gelée apportent une contribution prépondérante au terme de mobilité ionique, qui dépendra de ce fait du potentiel ψ_δ.

D'autre part, le déplacement électroosmotique étant impossible dans la couche gelée, le terme électroosmotique sera fonction du potentiel ζ.

Dans ces conditions, nous pourrons écrire l'éqn. (4) sous la forme :

$$\lambda_s = \sqrt{\frac{\varepsilon RT}{2\pi F^2}}\, C \left\{ \left[l_c (e^{z^+ F\psi_\delta/2RT} - 1) + l_a (e^{-(z^- F\psi_\delta/2RT)} - 1) \right] + \right.$$
$$\left. + \left[\frac{\varepsilon RT}{2\pi\eta z^+} (e^{z^+ F\zeta/2RT} - 1) + \frac{\varepsilon RT}{2\pi\eta z^-} (e^{-(z^- F\zeta/2RT)} - 1) \right] \right\} \qquad (5)$$

Connaissant expérimentalement λ_s et ζ, nous pourrons estimer la valeur de ψ_δ correspondant à l'hypothèse envisagée.

Le résultat de ce traitement, représenté à la Fig. 7, montre les ψ_δ obtenus pour KNO_3, $Ba(NO_3)_2$ et $La(NO_3)_3$.

Il faut cependant remarquer que nous n'avons pas calculé de valeurs de ψ_δ correspondant à des solutions très diluées, car on se trouve alors en présence de mélanges de cations, les protons de l'eau, vu leur grande mobilité, ayant un effet marqué sur $\lambda_{s,exp}$, et le traitement utilisé n'étant pas valable pour les mélanges. Dans la gamme des concentrations utilisées, ψ_δ est compris entre 275 et 200 mV pour KNO_3, entre 150 et 100 mV pour $Ba(NO_3)_2$ et entre 100 et 25 mV pour $La(NO_3)_3$, ce qui montre l'effet très marqué sur le potentiel ψ_δ de la valence des cations en relation avec l'adsorbabilité de ceux-ci dans le feuillet de Stern.

E. Estimation de l'epaisseur de la couche hydrodynamiquement immobile

Nous avons ensuite introduit les valeurs de ψ_δ et de ζ dans l'équation donnant

le profil potentiel–distance de la théorie de la couche double[16,17] écrite en utilisant les notations du modèle de Stern :

$$\kappa x = \ln \tanh(ze\,\psi_\delta/4kT) - \ln \tanh(ze\,\psi/4kT) \qquad (6)$$

κ étant l'inverse de l'épaisseur de la couche double et x la distance au feuillet de Stern.

En choisissant pour ψ la valeur particulière ζ au plan de glissement, il nous sera possible, pour chaque concentration électrolytique étudiée, c'est-à-dire pour chaque groupe de valeurs ψ_δ, ζ, κ, de déterminer une certaine valeur de $\kappa\Delta x$, Δx étant la distance sur laquelle a lieu la chute de potentiel ψ_δ–ζ, correspondant à l'épaisseur de la couche immobilisée en surface. Le terme κ figurant dans l'éqn. (6) correspond en toute rigueur aux conditions de force ionique régnant à l'intérieur du dit feuillet, qui ne sont pas nécessairement identiques à celles de la solution, une rétention d'ions pouvant exister dans la couche gelée. Cet effet sera surtout sensible aux faibles concentrations, pour lesquelles Δx sera surestimé.

Si le modèle proposé est valable, dans le domaine où la couche figée peut être considérée comme étant à l'équilibre ionique avec la solution, en portant les valeurs de $\kappa\Delta x$ obtenues à partir de l'éqn. (6). en fonction des κ correspondant aux concentrations au coeur de la solution, on doit obtenir une relation linéaire dont la pente correspond à l'épaisseur Δx.

Un tel traitement appliqué aux résultats expérimentaux montre qu'on obtient une relation $\kappa\Delta x$–κ raisonnablement linéaire, représentée à la Fig. 8 respectivement pour KNO_3, $Ba(NO_3)_2$ et $La(NO_3)_3$.

Pour ces trois cations, les épaisseurs Δx obtenues valent respectivement 67, 63 et 80 Å.

Comme lors du calcul de ψ_δ, les valeurs de $\kappa\Delta x$ n'ont été déterminées que pour des concentrations cationiques grandes devant la concentration en protons provenant de l'eau.

L'examen de la Fig. 8 nous amène encore à d'autres considérations.

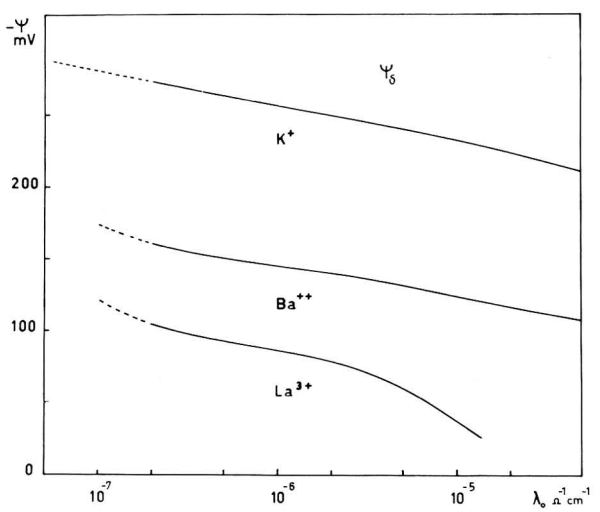

Fig. 7. Potentiels ψ_δ calculés pour diverses conductivités de solutions de KNO_3, $Ba(NO_3)_2$ et $La(NO_3)_3$.

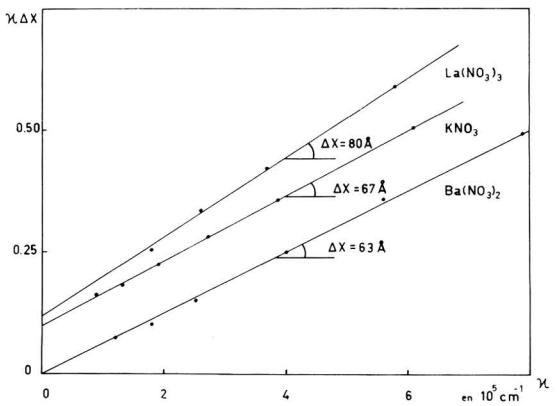

Fig. 8. Estimation de l'épaisseur Δx de la couche figée, en présence de KNO_3, de $Ba(NO_3)_2$ et de $La(NO_3)_3$.

Tout d'abord, la droite correspondant au $Ba(NO_3)_2$ passe par l'origine, ce qui impliquerait qu'au départ, dans l'eau pure, la couche gelée ne contiendrait pratiquement aucun ion excédentaire mobile. Dans le cas de KNO_3 et de $La(NO_3)_3$, on observe également une relation $\kappa\Delta x$–κ linéaire. Cependant, l'extrapolation à κ nul montre que les systèmes se comportent comme s'il existait déjà dans l'eau pure une concentration résiduelle d'ions piégés dans le gel. Nous attribuons ce fait à une certaine contamination de la surface antérieure aux mesures.

Le présent traitement implique la connaissance de ψ_δ. Une erreur dans l'estimation de ce paramètre pourrait provenir d'une inexactitude du profil potentiel – distance choisi, qui aurait par exemple pour origine une saturation diélectrique dans la couche gelée. Cependant, le terme en ψ_δ de l'éqn. (6) ne contribue que pour une part représentant de 3–8% du terme en ζ lors de la détermination de $\kappa\Delta x$. En conséquence, une erreur d'estimation de ψ_δ ne modifiera pas de façon appréciable les épaisseurs obtenues pour la couche gelée.

F. Charges specifiques des divers feuillets

Nous avons calculé les charges spécifiques des contre-ions correspondant respectivement à la couche gelée et à la partie hydrodynamiquement mobile de l'atmosphère ionique.

La charge spécifique du feuillet gelé peut être estimée à partir de l'équation:

$$\sigma_{\Delta x} = \frac{(\lambda_{s,exp} - \lambda_{s.B})F}{\Lambda_+} \tag{7}$$

où $(\lambda_{s.exp} - \lambda_{s.B})$ correspond à la partie de la conductance de surface due à la couche gelée. F est le Faraday et Λ_+ la conductivité équivalente à dilution infinie du contre-ion, considérée comme identique à celle existant au coeur de la solution[18]. La contribution des anions est considérée comme négligeable.

De plus, la charge spécifique de la partie diffuse dans le liquide peut être obtenue à partir du potentiel ζ et de la concentration ionique C en solution par l'équation:

$$\sigma_d = \sqrt{\frac{2C\varepsilon RT}{1000\pi}} \sinh \frac{zF\zeta}{2RT} \tag{8}$$

A titre d'exemple, nous avons porté, à la Fig. 9, pour le cas de KNO_3, les valeurs de $\sigma_{\Delta x}$ et σ_d obtenues aux diverses concentrations étudiées.

On constate que si les charges de chaque feuillet croissent régulièrement avec la concentration, 90% de la charge totale se trouvent toujours dans le feuillet figé et seulement 10% de celle-ci se trouvent dans le liquide mobile.

Ces valeurs peuvent se comparer à celles obtenues par Tadros et Lyklema[19] qui ont estimé la répartition des charges à la surface d'un verre d'électrode de verre au moyen des isothermes d'adsorption ionique. Ils ont observé qu'une partie de la charge pouvant atteindre jusqu'à 99% de la charge totale se trouve localisée dans une couche superficielle gelée, ce qui est compatible avec nos résultats, bien que ce type de verre, susceptible d'une plus grande rétention d'eau[11], ne puisse être directement comparé au nôtre.

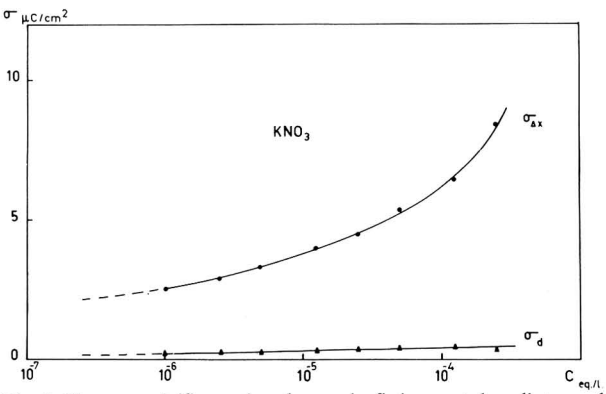

Fig. 9. Charges spécifiques dans la couche figée $\sigma_{\Delta x}$ et dans l'atmosphère diffuse σ_d pour diverses concentrations en KNO_3.

G. Validité du modèle utilisé

Le modèle utilisé ici correspond à l'existence d'un feuillet liquide hydrodynamiquement immobile le long de la paroi de verre, qui peut avoir diverses origines.

—Tout d'abord, une couche aqueuse pourrait être retenue par microrugosité du verre, comme l'avait suggéré Bikerman[20]; dans cet ordre d'idée, des mesures interférométriques réalisées par Koehler et White[21] sur un verre poli montrent une rugosité de 68 Å. Ils obtiennent la même valeur sur des verres étirés à chaud[22]. Schroeder[23] a déterminé que, pour un verre sodo-calcique au voisinage de la neutralité, on avait en surface des pores d'un diamètre de 70–100 Å distants d'environ 100 Å.

—D'autre part, Derjaguin et ses collaborateurs [24–26] ont montré la tendance que présentent les molécules anisotropes des liquides à s'organiser au voisinage de surfaces possédant une affinité pour elles. Ils ont trouvé que des films liquides en contact avec du verre ou du mica pouvaient être rigidifiés sur une épaisseur atteignant dans certains cas 1000–1500 Å. Forslind[27,28] a montré qu'à l'interface eau–argile, la rigidité du film d'eau peut être augmentée jusqu'à une distance de l'ordre de 300 Å.

Dans ces deux hypothèses, l'adsorption serait alors uniquement localisée dans le feuillet de Stern.

—Dans un autre ordre d'idées, on doit aussi envisager la possibilité d'une couche

poreuse qui serait due au gonflement de la surface du verre avec formation d'un gel par hydratation et ionisation en profondeur des groupes silanols. On pourrait alors avoir une distribution des charges superficielles dans toute l'épaisseur de la couche figée. Lyklema[29] a utilisé un tel modèle pour expliquer les charges énormes obtenues en milieu alcalin sur des surfaces de verre[19]. Dans son modèle, les sites ionogènes sont répartis sur une certaine épaisseur suivant une distribution exponentielle décroissante vers l'intérieur du solide. Il est difficile d'appliquer pour le moment cette théorie à nos systèmes. Toutefois, quelques remarques d'ordre général peuvent être faites afin de situer nos grandeurs expérimentales dans le cadre théorique précité.

Sans entrer dans les détails du traitement, disons que la distribution ionique dans l'interface est régie par un terme B qui est fonction de l'apport ionique à l'interface et de la spécificité de l'ion pour la surface. Ce terme influence également dans une large mesure le taux de compensation des charges de surface par les contre-ions dans la couche gelée et de ce fait la variation de potentiel dans celle-ci.

Dans le domaine de concentration où la conductance de surface est expérimentalement mesurable, ce terme est toujours extrêmement faible ($B \leqq 10^{-5}$). Ceci implique d'une part que le profil potentiel–distance dans le solide se réduirait, dans les conditions précitées, à celui d'un modèle de Gouy–Chapman. D'autre part, cela implique également que le taux de compensation dans le gel serait faible.

Il serait intéressant de poursuivre ce calcul pour de faibles valeurs de B afin de voir si ce modèle est capable d'expliquer des taux de compensation de l'ordre de 90% observés même aux concentrations les plus faibles, pour lesquelles la charge contre-ionique totale n'est que de quelques μC cm^{-2}.

Subsidiairement, et dans le même ordre d'idées, il serait intéressant de tenter de réaliser des mesures de conductance de surface en fonction du pH. Vu la nécessité des faibles forces ioniques, il serait peut-être possible de fixer le pH sur quelques unités autour de la neutralité.

5. CONCLUSIONS

Nous avons réalisé, à l'aide d'une cellule de géométrie appropriée, une étude simultanée des potentiels et courants d'écoulement et de la conductance de surface. Les deux méthodes donnent des valeurs identiques pour le potentiel électrocinétique. On a montré tout l'intérêt qu'il y a à utiliser la technique des courants d'écoulement.

Nous avons choisi pour la réalisation de la cellule un verre sodo-calcique supposé plus fortement hydratable que le verre Jena 16^{III} généralement utilisé pour ce genre d'études. Pour des ions de diverses valences, la conductance de surface s'est révélée 5–6 fois supérieure à celle du Jena 16^{III} et 10–20 fois celle de l'atmosphère ionique, calculée à l'aide de la théorie de Bikerman. Nous avons tenté d'interpréter les résultats obtenus en considérant, comme divers auteurs, la présence d'une couche figée superficielle, quelle qu'en soit l'origine. Nous avons fait l'hypothèse que la distribution des ions, tant dans la couche figée que dans le liquide, obéit, à l'équilibre, à la distribution de Maxwell–Boltzmann, ce qui nous permet, à partir d'un raisonnement inspiré de celui de Bikerman, connaissant dans chaque cas la concentration C, le potentiel ζ et la conductance de surface, de déterminer la valeur du potentiel ψ_δ à la limite du feuillet de Stern. Ensuite, à l'aide de la théorie de la couche double, il est possible, connaissant C, ψ_δ et ζ, d'évaluer l'épaisseur du feuillet immobilisé et son

contenu ionique. L'épaisseur de la couche figée a été estimée à 60–80 Å et est indépendante de la valence de l'ion utilisé. Les valeurs obtenues sont à rapprocher des mesures d'eau adsorbée sur le verre: d'après Holland[9] l'épaisseur d'eau adsorbée sur de la laine de verre serait de l'ordre de 105 Å à 23°C. Garbe *et al.*[30], par l'étude de la désorption d'un verre sodo-calcique, ont obtenu une épaisseur d'eau d'environ 35 Å. Enfin, Kuznetsov[31], par des considérations relatives à la conductance de surface d'un verre en équilibre avec une vapeur saturante d'eau, estime l'épaisseur du gel superficiel à environ 50 Å. Ces diverses valeurs sont d'un ordre de grandeur compatible avec l'épaisseur de la couche figée obtenue dans le présent travail.

Nous avons ensuite calculé les charges spécifiques dues aux contre-ions dans le feuillet figé et dans la partie mobile de l'atmosphère ionique. Nous avons constaté que 90% des ions se trouvent piégés dans le gel superficiel et que 10% seulement restent dans le feuillet mobile.

Enfin, il serait souhaitable de tenter de développer une technique permettant des mesures de conductance de surface à divers pH et de comparer les résultants obtenus à l'extension des calculs de Lyklema relatifs à une distribution des sites ionogènes dans la couche gelée.

RÉSUMÉ

Les potentiels électrocinétiques de parois de verre ont été mesurés, par les méthodes des potentiels d'écoulement et des courants d'écoulement. La conductance de surface a également été déterminée. KNO_3, $Ba(NO_3)_2$ et $La(NO_3)_3$ ont été successivement utilisés comme électrolytes. Les résultats obtenus ont été interprétés en considérant l'existence d'une couche gelée superficielle, dont l'épaisseur a été estimée à partir des paramètres expérimentaux. Cette épaisseur a été trouvée raisonnablement constante quelle que soit la valence du contre-ion; elle est en accord avec des valeurs obtenues à partir d'autres techniques expérimentales.

La répartition de la charge spécifique entre le gel et la phase liquide a également été estimée.

SUMMARY

Electrokinetic potentials on glass walls have been measured using the methods of streaming potentials and streaming currents. Surface conductance has also been determined. KNO_3, $Ba(NO_3)_2$ and $La(NO_3)_3$ were used as electrolytes. The results obtained have been interpreted considering a superficial gel layer, the thickness of which was estimated from the experimentally available parameters. This thickness has been found reasonably constant whatever the valency of the counter-ion and in agreement with values obtained from other techniques.

The repartition of the specific charge between the gel and the liquid phase was also investigated.

BIBLIOGRAPHIE

1 O. STERN, *Z. Elektrochem.*, 30 (1924) 508.
2 H. R. KRUYT, *Colloid Science*, Vol. I, Elsevier, Amsterdam, 1952, p. 204.

3 J. J. BIKERMAN, *Z. Physik. Chem.*, A163 (1933) 378.
4 H. R. KRUYT, *Colloid Science*, Vol. I, Elsevier, Amsterdam, 1952, p. 238.
5 P. W. O. WIJGA, Thèse, Utrecht, 1946.
6 N. STREET, *Australian J. Chem.*, 9 (1956) 333.
7 J. J. BIKERMAN, *J. Chem. Phys.*, 9 (1941) 880.
8 R. G. BATES, *Determination of pH*, Wiley, New York, 1964.
9 L. HOLLAND, *The Properties of Glass Surfaces*, Chapman and Hall, London, 1964.
10 A. WATILLON, *J. Chim. Phys.*, 54 (1957) 130.
11 D. HUBBARD, *J. Res. Natl. Bur. Std.*, 36 (1946) 511.
12 J. TH. G. OVERBEEK ET P. W. O. WIJGA, *Rec. Trav. Chim.*, 65 (1946) 556.
13 A. J. RUTGERS ET M. DE SMET, *Trans. Faraday Soc.*, 43 (1947) 102.
14 A. WATILLON ET R. DE BACKER, 5è *Congr. Intern. des Substances Tensioactives, 1968*, Communication B/O 195, sous presse.
15 C. E. MOSSMAN, ET S. G. MASON, *Can. J. Chem.*, 37 (1959) 1153.
16 E. J. W. VERWEY ET J. TH. G. OVERBEEK, *Theory of the Stability of Lyophobic Colloids*, Elsevier, Amsterdam, 1948.
17 J. F. DANIELLI, K. G. A. PANKHURST ET A. C. RIDDIFORD, *Recent Progress in Surface Science*, Vol. I, Academic Press, New York, 1964.
18 J. J. BIKERMAN, *J. Phys. Chem.*, 46 (1942) 724.
19 TH. F. TADROS ET J. LYKLEMA, *J. Electroanal. Chem.*, 22 (1969) 9.
20 J. J. BIKERMAN, *J. Chem. Phys.*, 9 (1941) 880.
11 W. F. KOELER ET W. C. WHITE, *J. Opt. Soc. Am.*, 45 (1955) 940.
22 W. F. KOELER ET W. C. WHITE, *J. Opt. Soc. Am.*, 45 (1955) 1011.
23 H. SCHROEDER, *Z. Naturforsch.*, 4a (1949) 515.
24 B. V. DERJAGUIN, *Nature*, 138 (1936) 330.
25 B. V. DERJAGUIN ET V. V. KARASSEV, *Proc. Intern. Congr. Surface Activity 2nd, London*, 3 (1957) 531.
26 B. V. DERJAGUIN ET A. S. TITJEVSKAYA, *Proc. Intern. Congr. Surface Activity 2nd, London*, 1 (1957) 211, 254.
27 E. FORSLIND, *Acta Polytech.*, 115 (1952) 9.
28 E. FORSLIND, *Proc. Intern. Congr. Rheol. 2nd., Oxford, 1953*, Butterworth, London, 1954.
29 J. LYKLEMA, *Electroanal. Chem.*, 18 (1968) 341.
30 S. GARBE, A. KLOPFER ET W. SCHMIDT, *Vacuum*, 10 (1960) 81.
31 A. YA. KUZNETSOV, *Zh. Fiz. Khim.*, 27 (1953) 657.

ELECTROANALYTICAL CHEMISTRY AND INTERFACIAL ELECTROCHEMISTRY
Elsevier Sequoia S.A., Lausanne – Printed in The Netherlands

IONIC HYDRATION AND THE THERMODYNAMIC CATIONIC SURFACE EXCESS AT THE MERCURY–AQUEOUS ELECTROLYTE INTERFACE

J. A. HARRISON*, J. E. B. RANDLES AND D. J. SCHIFFRIN**
Department of Chemistry, University of Birmingham (England)
(Received October 18th, 1969; in revised form November 5th, 1969)

INTRODUCTION

The thermodynamic ionic excess of cations at a polarized Hg–aqueous electrolyte interface differs from the values calculated from the diffuse double layer theory and this difference has been attributed to the existence of an electrolyte-free region at the metal surface[1-6]***. The purpose of this work was to study the influence of the degree of hydration of the cation on this difference when specific adsorption is absent. Ionic surface excesses were obtained by studying the electrocapillary curves for several electrolytes.

The thermodynamic ionic excess is related to the interfacial tension through the Gibbs adsorption equation, which in the case of a single electrolyte at constant temperature and pressure becomes[7]:

$$-\mathrm{d}\gamma = q^{\mathrm{m}}\,\mathrm{d}E_{\pm} + \Gamma_{\mp}\,\mathrm{d}\mu_{\mathrm{s}} \tag{1}$$

γ is the measured interfacial tension, $E_{\pm}$ is the potential of the Hg with respect to an electrode in the same solution and reversible to either the cation or anion of the salt, μ_{s} is the chemical potential of the salt and q^{m} is the surface charge density. The surface excess of component i with respect to H_2O, $\Gamma_{\mathrm{i(H_2O)}}$, is given by

$$\Gamma_{\mathrm{i(H_2O)}} = \left[m_{\mathrm{i}} - m_{\mathrm{H_2O}} \cdot \frac{n_{\mathrm{i}}}{n_{\mathrm{H_2O}}} \right] \tag{2}$$

where m_{i} and $m_{\mathrm{H_2O}}$ are the amounts of components i and H_2O per unit area and n_{i} and $n_{\mathrm{H_2O}}$ the amounts in the bulk of the solution, respectively.

Ionic excesses were calculated from

$$\Gamma_{\pm\mathrm{(H_2O)}} = -\left(\frac{\partial\gamma}{\partial\mu_{\mathrm{s}}} \right)_{T,P,E_{\mp}} \tag{3}$$

---

* Present address: Electrochemistry Research Laboratory, Department of Physical Chemistry, University of Newcastle upon Tyne, Newcastle upon Tyne, NE1 7RU (England).
** Present address: Chemistry Department, The University, Southampton, SO9 5NH (England).
*** During the preparation of the present paper, the translation of a recent publication[15] came to our notice. Similar results to those presented in this paper for the $NaClO_4$ system were presented and discussed on a similar basis.

EXPERIMENTAL

The capillary electrometer used consisted of a U-tube, one arm of which was a very fine capillary of uniform bore (0.04 mm) and the other a tube some 30 mm in diameter. This large bore size made the capillary depression correction very small[8]. When the system is in mechanical equilibrium, the pressure which is supported by the meniscus is given by:

$$D_{Hg}gh - D_{soln}gl = \frac{2\gamma}{r}\cos\theta \tag{4}$$

where r is the radius of the capillary, θ the contact angle of the Hg surface with the capillary walls, γ is the interfacial tension, g is the acceleration due to gravity, h the difference in height of the mercury column supported by the meniscus, D_{Hg} and D_{soln} the density of the mercury and the solution, respectively, and l is the distance from the surface of the mercury in the capillary to the solution level in the cell. No attempt was made to measure directly the radius of the capillary. Instead, it was calibrated using solutions of known interfacial tension at the ECM. The contact angle was assumed to be zero at all potentials and concentrations.

The use of an "inverted" capillary has some advantages over the method used by Lippman[9]. In his apparatus, a condition necessary for mechanical equilibrium of the Hg column is that the capillary must be tapered, otherwise no stable equilibrium position of the meniscus can be found. If the radius is uniform, any displacement downwards or upwards of its "equilibrium" position would increase or decrease the Hg head and hence tend to move it further down or up the capillary. The opposite effects occur with an inverted capillary and the changes in height of the mercury thread inside it are equal and in the same direction as the corresponding changes in mercury level in the wider tube. This difference in the condition for mechanical equilibrium leads to a slight difference in the sensitivity conditions between the two methods. In the vertically dipped capillary type of electrometer, the variation in the position of the meniscus inside the capillary is determined by the taper of the capillary walls, and in this way, by a careful selection of the capillary used, great sensitivity for a given change in the mercury head can be achieved. The uncertainty in the measurement is determined in this case by errors in the measurement of the total height of Hg. For the capillary electrometer described here, the changes in the position of the mercury inside the capillary equalled the changes in the total head and its position could be determined to ± 0.01 mm, or better, with the microscope employed. Thus, in our case again, the errors arose from uncertainties in the measurement of the total height of the Hg column. In general, the use of an inverted uniform bore capillary will not lead to any loss in accuracy provided the position of the meniscus inside the capillary can be determined with an accuracy comparable to (or better than) that of the total Hg head, with the added convenience of easy replacement by using commercially available capillary tubing.

The apparatus is shown in Fig. 1, where (a) is the tube containing the mercury column and supporting a micrometer and pointer; (b) two glass containers in which the final purification of the solutions with charcoal was effected, (c) the cell with the capillary and (d) a reference electrode and its connecting bridge.

The micrometer was mounted on a 10 cm long screw which allowed for coarse changes in its level. This screw was clamped into position with a lock nut. A 25 cm steel rod was attached to the end of the micrometer screw. The end of this rod was pointed and it had been aligned with a lathe to avoid lateral movements as much as possible. The point and the mercury surface were viewed through a telescope.

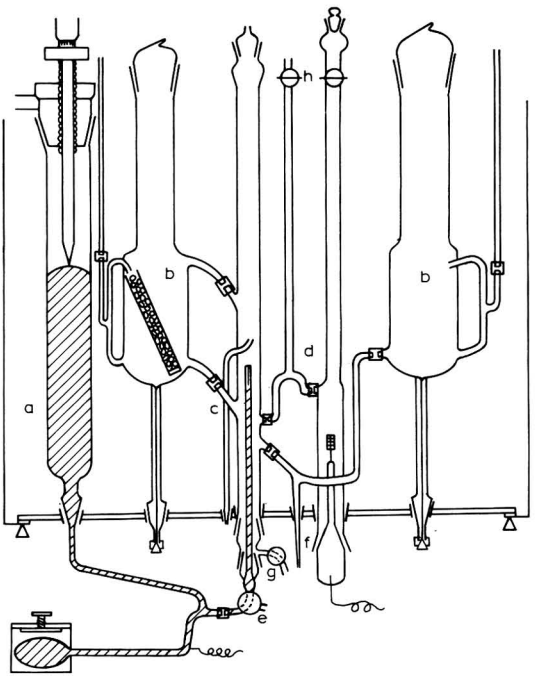

Fig. 1. Capillary electrometer employed. Explanation in the text.

Small charcoal containers were put into both reservoirs (b). These were glass tubes with a sintered glass disc in one end, and they were set in such a position that solution would circulate through them when hydrogen gas bubbled through the lateral tubes. A device for circulating the solution through the cell was included in order to be able to purify its contents. Hydrogen pressure was applied from the top so that the solution would be swept to container (b) *via* the upper tube connecting container (b) to the cell, and fresh portions would fill it *via* the lower connecting tube. The transfer of solution from the containers to the cell was controlled by means of two externally operated mercury cut-offs. One of them consisted of the U-shaped tube connecting the cell with the reservoir to the right. The mercury level in this U-tube was controlled *via* tube (f). The other cut-off was the mercury level inside the cell itself and it was controlled by tap (g). An inverted tube kept the level of the liquid in the cell constant by siphoning out any excess. The capillary was made by joining a piece of regular bore (0.04 mm in diam.) capillary tubing to a piece of tubing connected to a three-way tap. This tap was used to sweep away the remaining air in the tubing connecting the capillary with a rubber reservoir and the mercury column. The level of the mercury in the column could be changed by applying pressure to the rubber bulb.

The mercury level in the capillary was viewed through a microscope. An external reference point, which could be seen at the same time as the capillary, was set up by the cell in order to ensure that the measurements referred to the same point in the capillary.

The reference electrode was filled from the top. The bridge was filled with powdered glass and both ends were closed with sintered glass discs. This bridge was filled by applying suction through tap (h).

Hydrogen gas was purified by passing it through heated Cu gauze and then bubbling it through two saturators containing the same solution as the one under study. The temperature of these saturators was kept the same as that of the cell so that no appreciable change in concentration of the solutions would occur after several hours of bubbling through them. The various parts of the electrometer were mounted in sockets which were set in position on a 3 mm thick bronze plate by means of rubber bungs. This plate was the base of a water bath, the front and back walls of which were made of glass. The temperature was kept at $25 \pm 0.05^{\circ}$C. The water was circulated from a main thermostat which was kept at just below 25° C, through the external envelopes of the gas saturators and then, before entering the water bath containing the apparatus, through an auxiliary heater. This was a 30W bulb operated by a hard valve relay and a mercury contact thermometer. The mercury surface was polarized with respect to the reference electrode by means of a potentiometer.

For the $NaClO_4$ and LiCl systems a Ag/AgCl reference electrode was employed. It was prepared by electrolysis of silver gauze, which had been etched with nitric acid, in dilute hydrochloric acid. For the $MgSO_4$ system, the reference electrode used was Hg/Hg_2SO_4, $MgSO_4$ (1.5 *M*). $NaClO_4$ was prepared from Na_2CO_3 and $HClO_4$; it was purified by recrystallization from ethanol and finally heated to 300°C. LiCl was purified by dissolving pure Li_2CO_3 in an insufficient amount of AnalaR HCl; the solution was filtered, made slightly alkaline with ammonia solution in order to precipitate heavy metal impurities, refiltered and Li_2CO_3 reprecipitated with AnalaR Na_2CO_3. This Li_2CO_3 was thoroughly washed with hot water until there was a negative reaction for Cl^- with $AgNO_3$, and then dissolved in an insufficient amount of pure HCl. AnalaR $MgSO_4$ was twice recrystallized from distilled water. Na_2SO_4 was purified by twice recrystallizing the AnalaR compound.

Mercury was first purified by wet treatment with dilute HNO_3, bubbling air through it for several days and finally by vacuum distillation. The vacuum distillation was replaced later on by distillation under reduced pressure with a stream of air bubbling through the hot mercury through a small capillary. This latter procedure was found to produce somewhat more satisfactory mercury.

The solutions were circulated over charcoal for several hours before measurements were made. The charcoal was purified by refluxing with HCl for several weeks and then with water until no trace of Cl^- could be detected.

The apparatus was cleaned with fresh chromic acid mixture, rinsed thoroughly with distilled water, dried, assembled and then placed in position inside the thermostat tank. The capillary was similarly cleaned, then filled with mercury by suction and placed in position with tap (e) closed to prevent the mercury inside the capillary from falling down. The gap of air between the tap and the connecting glass tubing was eliminated by letting some mercury run through the three-way tap, keeping the section connecting the capillary with the mercury column closed. It was found necessary

to adopt this procedure after some unsuccessful attempts had been made with an empty capillary, without a tap connecting it to the mercury reservoir, to try to fill it from below. In all these attempts the capillary became blocked up since any impurity present floated on the Hg and would be swept up the capillary.

It was then decided to suck up the Hg and let some of it overflow. It was also found that a final cleaning of the capillary with dilute NaOH helped to make the Hg thread move more freely. Mercury was allowed to flow continuously through the capillary when measurements were not being performed. Before each measurement, the Hg was brought down to the wider section and then pushed up to the fixed point in the capillary, and also from time to time Hg drops were squeezed out to ensure that the capillary walls were always wet and a fresh Hg surface was always used.

Imparting small and rapid oscillations to the Hg column when the Hg was near the reference position was found to be of great assistance in ensuring that the system was in true equilibrium, especially when small changes in height were involved. This was used as a test that the Hg was not getting stuck to the walls.

A galvanometer was put in series with the polarizing circuit; the current was in all cases less than 10^{-9} A, so no correction was made for the ohmic potential drop in the cell.

The changes in height of the Hg column were measured with the micrometer by observing the pointer and its reflection on the Hg surface. It is possible in this way to measure changes in height with a precision of the order of 0.02 mm or better. The total height of the Hg column was obtained by adding the distance between the pointer when the reading was zero and the top of the Hg meniscus, to the micrometer reading. Care was taken to ensure that both the Hg column and the cathetometer were vertical. The distance from the Hg in the capillary to the liquid level in the cell was also measured with the cathetometer.

The concentration of electrolyte of the reference electrode was kept constant during the measurements. In order to calculate the ionic excesses, the potentials were corrected to the $E_{\pm}$ potential scale by measuring the potentials of the corresponding cells with transport. The cells studied were:

$$\mathrm{Na(Hg)}\,|\,\mathrm{NaClO_4}\ 4M\,|\,\mathrm{NaClO_4}\ XM\,|\,\mathrm{Na(Hg)}$$

$$\mathrm{Ag}\,|\,\mathrm{AgCl}\,|\,\mathrm{KCl}\ 4M\,|\,\mathrm{LiCl}\ 3M\,|\,\mathrm{LiCl}\ XM\,|\,\mathrm{AgCl}\,|\,\mathrm{Ag}$$

and

$$\mathrm{Hg}\,|\,\mathrm{Hg_2SO_4}\,|\,\mathrm{MgSO_4}\ 1.5\ M\,|\,\mathrm{MgSO_4}\ XM\,|\,\mathrm{Hg_2SO_4}\,|\,\mathrm{Hg}$$

A cell with two similar compartments was used for the $NaClO_4$ solutions. A sodium amalgam flowed from two capillaries in the compartments with the solutions. The solutions were deoxygenated with a stream of hydrogen. The sodium amalgam was kept in a reservoir in an atmosphere of H_2 to prevent any change in the concentration of the amalgam. The potentials measured were reproducible to 0.1 mV and were independent of the rate of amalgam flow.

For the $MgSO_4$ solutions a new electrode was prepared for each concentration. It was prepared by grinding together Hg_2SO_4 with Hg and the $MgSO_4$ solution under study, in order to avoid concentration errors.

The electrometer was calibrated with 0.5 M Na_2SO_4 for the $NaClO_4$ and $MgSO_4$ solutions. The interfacial tension of the Na_2SO_4 solution at the ECM was

taken as 426.0 dyn cm^{-1}. This value was calculated from Gouy's work at 18° C[10] and from the temperature coefficient of the interfacial tension[11]. For the LiCl solutions, 1 *M* LiCl was used for the calibration. The interfacial tension at the ECM was taken as 423.2 dyn cm^{-1} for this solution.

RESULTS

Six different concentrations were studied for the $NaClO_4$ system and seven for the LiCl and $MgSO_4$ solutions.

Measurements on the cathodic branch were easier to make and more reproducible than those at anodic potentials, where the Hg tended to stick to the capillary walls.

Purification with charcoal was found to be necessary and effective for the $NaClO_4$ and LiCl systems. For example, for the LiCl solutions, two hours of circulation were enough to render the interfacial tension reading constant. A good test for the absence of surface active materials was to see whether the mercury would stay in the same position in the capillary at a given potential near the ECM for several hours.

Complete sets of experimental results are reported elsewhere[2,4]. The interfacial tension was plotted for each value of the potential E_+ or E_-, against log $a_\pm$, and graphically differentiated to obtain the surface excesses. The values of the surface charge density at various potentials for the $NaClO_4$ and LiCl solutions were obtained by graphical differentiation of the electrocapillary curves with respect to the potential at constant concentration. For the $MgSO_4$ solutions the charge was obtained by integration of capacitance data[4].

The graphs in Figs. 2, 3 and 4 show the cationic surface excess for the systems studied. The results for $MgSO_4$ were confirmed by capacitance measurements[4]. These were twice integrated with respect to the potential, made to fit the electrometer data at negative potentials and then differentiated with respect to the chemical po-

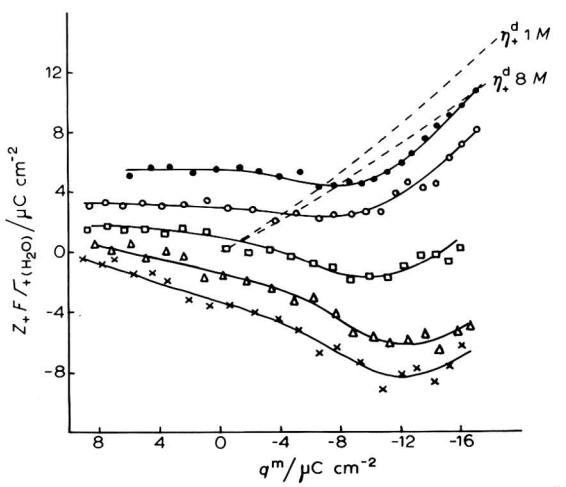

Fig. 2. Cationic surface excess for $NaClO_4$ solns. of different concns.: (●) 1, (○) 2, (□) 4, (△) 6, (×) 8 *M*. (--------) η_+^d from diffuse layer theory for two concns. (M = mol l^{-1}).

tential of the salt. Both sets of results coincided satisfactorily. The maximum deviation in the interfacial tension was less than 1 dyn cm^{-1} over all the potential range.

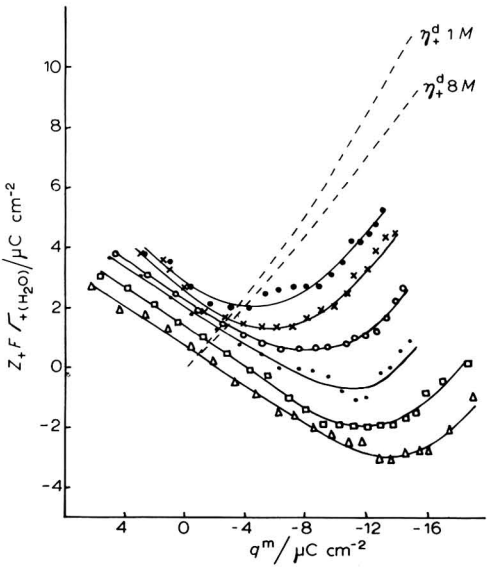

Fig. 3. Cationic surface excess for LiCl solns. of different concns.: (●) 1, (×) 2, (○) 3, (•) 4, (□) 6, (△) 8 *M*. (--------) η_+^d from diffuse layer theory for two concns. (*M* = molality).

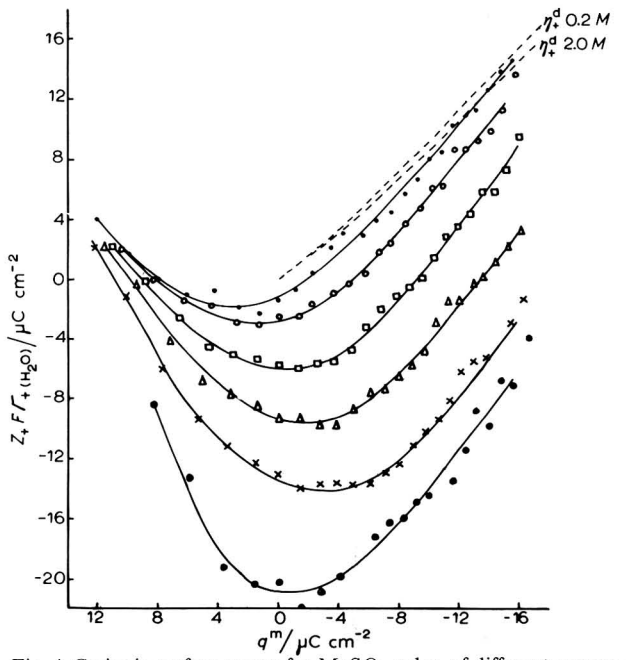

Fig. 4. Cationic surface excess for $MgSO_4$ solns. of different concns.: (•) 0.2, (○) 0.5, (□) 1.0, (△) 1.5, (×) 2.0, (●) 2.5 *M*. (-------) η_+^d from diffuse layer theory for two concns. ($M = \text{mol}\ l^{-1}$).

DISCUSSION

As can be seen in Figs. 2, 3 and 4, the cationic surface excess $\Gamma_{+(H_2O)}$ differs from η_+^d calculated from the theory of the diffuse double layer in potential regions where specific adsorption is absent. The reason for this difference is that η_+^d gives ionic surface excesses in the diffuse layer region only, whereas $\Gamma_{+(H_2O)}$ refers to the interface as a whole, including water which may be present in a region inaccessible to cations.

η_+^d is obtained by an integration of the ionic excess per unit volume from the outer Helmholtz plane (O.H.P.) into the solution[12].

$$\eta_+^d = Z_+ F \int_a^\infty (c_+(x) - c_+^{bulk}) dx = Z_+ F \left[m_+ - m_{H_2O}^d \frac{m_+}{m_{H_2O}} \right] \quad (5)$$

where a is the distance from the electrode to the O.H.P., $c_+(x)$ is the concentration of cations at a distance x from the electrode and $m_{H_2O}^d$ is the amount of water present in the diffuse layer only. It is convenient to divide the total amount of water present in the interface into a part present in the diffuse region and another $m_{H_2O}^{inner}$ present in the electrolyte free layer. From (2) and (5)

$$\frac{1}{Z_+ F} [\eta_+^d - Z_+ F \Gamma_{+(H_2O)}] = m_{H_2O}^{inner} \frac{m_+}{m_{H_2O}} \quad (6)$$

and

$$m_{H_2O}^{inner} = \frac{m_{H_2O}}{m_+} \frac{1}{Z_+ F} (\eta_+^d - Z_+ F \Gamma_{+(H_2O)}) \quad (7)$$

Figure 5 shows the concentration dependence of the difference $(Z_+ F)^{-1}[\eta_+^d - Z_+ F \Gamma_{+(H_2O)}]$ at a surface charge density on the metal sufficiently negative to prevent specific adsorption of the anion*. As can be seen from Fig. 6, the amount of water in the ion-free layer at a given charge on the Hg, seems to be constant up to solution concentrations of $\sim 2\ M$. Similarly, the inner layer capacitance of a non-adsorbed electrolyte, seems to be constant in a wide concentration range[13], indicating that the properties of the inner layer are independent of the concentration in the bulk of the solution in the absence of specific adsorption. A similar line of reasoning has been employed by Damaskin *et al.*[15] in the analysis of electrocapillary data for concentrated $NaClO_4$ solutions.

In accordance with the results presented here, these authors found that the difference $(Z_- F)^{-1}[Z_- F \Gamma_{-(H_2O)} - \eta_-^D]$, at charges sufficiently negative to ensure absence of specific adsorption, depended on the total solution concentration, and also the apparent ion-free layer thickness decreased at higher concentrations. The value of $m_{H_2O}^{inner}$ calculated from their results is $\sim 1.4 \times 10^{-9}$ equiv. cm^{-2} in the concentration range, 0–2 M, in excellent agreement with the results presented here.

$m_{H_2O}^{inner}$ increases in the order $Li^+ \simeq Na^+ < Mg^{2+}$, although in solution concen-

* For the $MgSO_4$ solutions, η_+^d was calculated assuming incomplete dissociation of the electrolyte. The difference $[\eta_+^d - Z_+ F \Gamma_{+(H_2O)}]$ would be ~25% smaller for a 1 M solution if complete dissociation was assumed in the calculation. The possible differences due to incomplete ion pairing in the diffuse region are too small to affect in any way the argument presented here.

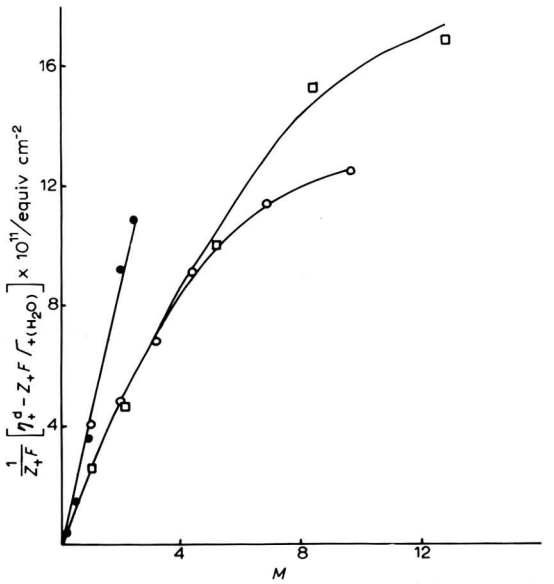

Fig. 5. Cationic surface deficit for $NaClO_4$, LiCl and $MgSO_4$ solns. at several concns.: (□) $NaClO_4$, (○) LiCl, (●) $MgSO_4$.

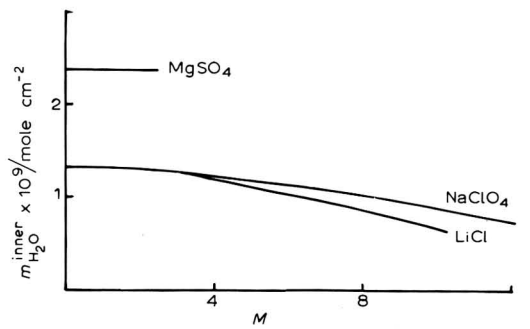

Fig. 6. Amount of water in the ion-free layer for the solns. studied at several concns. (M = molality).

trations greater than 2 M, $m_{H_2O}^{inner}$ for LiCl solutions seems to be less than that for $NaClO_4$ solutions, but the possibility of some Cl^- adsorption cannot be ignored.

If the density of the water in the inner region is assumed to be similar to that of bulk water, the thickness of this ion-free layer is of the order of 2.5 Å for Li^+, Na^+ and K^+ [2,3] ions and 4.4 Å for Mg^{2+} *. A naive view of the physical significance of $m_{H_2O}^{inner}$ might lead to the expectation of the double layer capacitance being smaller when $m_{H_2O}^{inner}$ is large, but the experimental capacitance results do not bear this out. It is difficult to ascertain the charge dependence of $m_{H_2O}^{inner}$; for the $NaClO_4$ and LiCl systems,

* Frumkin *et al.*[6] calculated a distance of closest approach of ~3.3 Å for Mg^{2+}, from electrocapillary data for $MgSO_4$ at the ECM. Since SO_4^{2-} ion is specifically adsorbed at this potential (see Fig. 4) the value they quote is bound to be lower than the one reported in this work.

the range of potentials where specific adsorption is absent is too small; for the $MgSO_4$ solutions there seems to be a fairly good degree of parallelism between $\Gamma_{+(H_2O)}$ and η_+^d (except for the 2.5 M solution), indicating that the changes in the ion-free layer thickness are probably small. An analysis similar to that of Parsons and Zobel[5] leads to an apparent decrease of $m_{H_2O}^{inner}$ of $\sim 10\%$ between -8 and -16 $\mu C\ cm^{-2}$, but the uncertainties in the diffuse layer theory calculations make it difficult to attempt a more quantitative study of the charge dependence of $m_{H_2O}^{inner}$.

As can be seen in Fig. 6, there is a decrease in the apparent ion-free layer thickness for very concentrated solutions, which obviously may result from a decrease in the hydration of ions due to the lack of water.

It is of interest to compare the air–solution with the Hg–solution interface. At the air–solution interface there is an ion-free layer corresponding to 1.6, 1.8, and 4.2×10^{-9} mol of water per cm^2 for LiCl, NaCl and $MgSO_4$ solutions, respectively (a monolayer of water at normal density contains 1.7×10^{-9} mol cm^{-2}). The values for the same cations at the interface between mercury (with a charge of between -12 to -15 $\mu C\ cm^{-2}$) and aqueous solution at 2 M concentration are 1.3, 1.3 and 2.4×10^{-9} mol cm^{-2}, respectively. The comparison should be made at the point of zero charge on the mercury, but then the specific adsorption of anions interferes. Nevertheless, the cation attraction by the large negative charge on the mercury would certainly tend to diminish the ion-free layer thickness below what it would be at the air–solution interface as, in fact, is found. There is, however, the same dependence on ionic charge, which seems to imply that the degree of hydration of the ions determines the thickness of the ion-free layer at both interfaces.

ACKNOWLEDGEMENT

One of us (D.J.S.) wishes to thank the Consejo Nacional de Investigaciones Científicas y Técnicas (Argentina) for a fellowship during the course of this work.

SUMMARY

Interfacial tension measurements of several concentrated aqueous electrolytes have been made using a modified form of a capillary electrometer which is described. The measurements indicate the presence of an ion-free layer adjacent to the mercury surface, the thickness of which appears to depend on the degree of hydration of the ions concerned.

REFERENCES

1 J. E. B. RANDLES AND J. A. HARRISON, informal meeting, Newcastle, 1959.
2 J. A. HARRISON, Thesis, University of Birmingham, 1960.
3 D. C. GRAHAME AND R. PARSONS, *J. Am. Chem. Soc.*, 83 (1961) 1291.
4 D. J. SCHIFFRIN, Thesis, University of Birmingham, 1965.
5 R. PARSONS AND F. G. R. ZOBEL, *J. Electroanal. Chem.*, 9 (1965) 333.
6 A. N. FRUMKIN, R. V. IVANOVA AND B. B. DAMASKIN, *Dokl. Akad. Nauk SSSR*, 157 (1964) 1202.
7 R. PARSONS, *Can. J. Chem.*, 37 (1959) 308.
8 LORD RAYLEIGH, *Proc. Roy. Soc., London*, A92 (1915) 184.
9 M. LIPPMAN, *Ann. chim. et phys.*, 5 (1875) 494.
10 G. GOUY, *Ann. phys. (Paris)*, 6 (1916) 5.

11 G. GOUY, *Ann. chim. et phys.*, 29 (1903) 145.
12 D. C. GRAHAME, *Chem. Rev.*, 41 (1947) 441.
13 D. C. GRAHAME, *J. Am. Chem. Soc.*, 76 (1954) 4819.
14 J. E. B. RANDLES in P. DELAHAY AND C. W. TOBIAS (Eds.), *Advances in Electrochemistry and Electrochemical Engineering*, Vol. 3, Interscience Publishers, New York–London, 1963, Chap. 1.
15 B. B. DAMASKIN, A. N. FRUMKIN, V. F. IVANOV, N. I. MELEKHOVA AND V. F. KHONINA, *Elektrokhimiya*, 4 (1968) 1336.

ELECTROANALYTICAL CHEMISTRY AND INTERFACIAL ELECTROCHEMISTRY
Elsevier Sequoia S.A., Lausanne – Printed in The Netherlands

KINETICS OF ADSORPTION OF CAMPHOR, CAMPHENE, PINENE AND NONYLIC ACID AT THE MERCURY–SOLUTION INTERFACE

S. SATHYANARAYANA AND K. G. BAIKERIKAR
Department of Chemistry, Indian Institute of Technology, Bombay-76 (India)
(Received September 12th, 1969)

The effect of adsorption of surface active molecules at a mercury–solution interface on the structure of the electrical double layer and on the rate of electrochemical reactions is well known. The adsorption process may not be at equilibrium if the concentration of the surfactant in solution is small or if the surfactant is strongly surface active. The kinetics of adsorption will then influence the double layer structure and the rates of electrode processes.

The kinetics of adsorption of neutral molecules at the mercury–solution interface has been studied experimentally mainly by two methods: the frequency-dependence[1–4] or the time-dependence[5–9,18,19] of the adsorption pseudo-capacitance. However, it has been demonstrated[10] that surfactants such as camphor and certain other compounds provide mostly 'peakless' differential capacitance curves even when measurements are carried out with a low frequency (45 Hz) impedance bridge. In the virtual absence of adsorption pseudo-capacitance peaks at low frequencies, the kinetics of adsorption cannot be studied by measuring capacitance as a function of frequency.

In the present work, the time-dependence of differential capacitance has been obtained experimentally during the adsorption of camphor, camphene, α-pinene and nonylic acid at an ideally polarised mercury–solution interface. The results have been correlated theoretically with the way capacitance changes with time when the adsorption process is controlled by diffusion and satisfies any arbitrary adsorption isotherm. For the special case of the Frumkin isotherm, explicit equations have been derived relating the non-equilibrium capacitance with the time of adsorption. The interaction parameter for the adsorption of camphor at the mercury–solution interface has been evaluated by comparing theory with experimental data.

THEORETICAL

The variation of the differential capacitance with time during adsorption of a surfactant may be due, in principle, to either a slow diffusion step or a slow adsorption step. It has been demonstrated[11] that the adsorption step is generally fast when adsorption occurs from solution on a mercury surface. Since in the present work the time intervals in which capacitance variations are found to occur are of the order of minutes, it is reasonable to assume that diffusion of the surfactant to the electrode surface is the rate-determining step during adsorption.

Diffusion-controlled adsorption of organic molecules on an initially clean

mercury electrode has been investigated by several workers[5-9,11]. A few reviews are also available[12-14]. In general, the coverage by the adsorbate at a given time is determined by the nature of the adsorption isotherm. Thus, the time-dependence of adsorbate coverage has been theoretically evaluated for the case of the linear isotherm[5], the Langmuir isotherm[6,17] and, with a reasonable approximation, for any arbitrary isotherm[11].

Frequently, the experimentally accessible parameter is the capacitance of the electrode. Hence, a more directly useful relation between the differential capacitance of the electrode and the time of adsorption (which determines the instantaneous coverage) is deduced below.

According to Frumkin and Damaskin[13], if adsorption of neutral molecules on mercury occurs with a fixed orientation, does not give rise to multilayers, and satisfies the arbitrary isotherm $f(\theta)=Kc_0$, the equilibrium capacitance is given, to a fair degree of approximation, by the following equation:

$$C = C_0 - 2A\alpha\theta + 4A\alpha^2(E-E_m)^2 \frac{\partial\theta}{\partial \ln f(\theta)} \tag{1}$$

where $\alpha=(C_0-C_1)/2RT\Gamma_s$, $A=RT\Gamma_s$, C is the differential capacitance at the coverage θ and the rational potential E, E_m is a constant and corresponds to the potential of maximum adsorption, C_0 and C_1 are the capacitance values corresponding to $\theta=0$ and $\theta=1$, respectively, K is the equilibrium constant for the adsorption process, Γ_s is the saturation surface excess of the adsorbate and c_0 is the concentration of the surfactant in solution.

We now assume that the form of eqn. (1) is valid at any time, t, during adsorption. Hence,

$$C_t = C_0 - 2A\alpha\theta_t + 4A\alpha^2(E-E_m)^2 \frac{\partial\theta_t}{\partial \ln f(\theta_t)} \tag{2}$$

Here, the time-dependent parameters are shown with the subscript, t. Let the adsorption process obey the arbitrary isotherm of the form, $f(\theta_e)=Kc_0$ at equilibrium where θ_e is the equilibrium coverage at a given potential. With diffusion as the rate-determining step,

$$f(\theta_t)=Kc_t \quad \text{and} \quad f(\theta_e)=Kc_0 \tag{3}$$

Expanding the function $[\partial\theta_t/\partial \ln f(\theta_t)]$ in eqn. (2) by the Taylor series around θ_e, we get,

$$\frac{\partial\theta_t}{\partial \ln f(\theta_t)} = \frac{f(\theta_t)}{f'(\theta)_t} = \frac{f(\theta_e)}{f'(\theta_e)} + (\theta_t-\theta_e)\left[1 - \frac{f(\theta_e)f''(\theta_e)}{\{f'(\theta_e)\}^2}\right] + \ldots \tag{4}$$

Here, $f'(\theta)$ denotes $[\partial f(\theta)/\partial\theta]$ and $f''(\theta)$ denotes $[\partial^2 f(\theta)/\partial\theta^2]$. For diffusion-controlled adsorption satisfying the general isotherm (3), it has been shown[11] that at $t \gg 0$,

$$\theta_t \simeq \theta_e\left[1 - \frac{f(\theta_e)}{f'(\theta_e)}\frac{\Gamma_s}{2c_0}\left(\frac{\pi}{Dt}\right)^{\frac{1}{2}}\right] \tag{5}$$

Substituting (4) and (5) in (2), and simplifying,

$$C_t = C_e + \frac{A\alpha\Gamma_s}{c_0}\frac{\theta_e f(\theta_e)}{f'(\theta_e)}\left[1-2\alpha(E-E_m)^2+2\alpha(E-E_m)^2\frac{f(\theta_e)f''(\theta_e)}{\{f'(\theta_e)\}^2}\right]\left(\frac{\pi}{Dt}\right)^{\frac{1}{2}} \quad (6)$$

where C_e is the value of C_t as $t \to \infty$, *i.e.* the equilibrium capacitance, given by eqn. (1) when $\theta = \theta_e$.

Equation (6) is a general expression, being valid for any adsorption isotherm. For evaluating the parameters of a given adsorption isotherm, it is necessary at this stage to introduce the particular form of $f(\theta)$. We shall evaluate the result for the case of the Frumkin isotherm which is generally obeyed during the adsorption of neutral molecules on mercury. The Frumkin isotherm is $f(\theta_e) = Kc_0$ where,

$$f(\theta_e) = \frac{\theta_e \exp(-2\alpha\theta_e)}{(1-\theta_e)} \quad (7)$$

It can be easily shown that,

$$f'(\theta_e) = f(\theta_e)\frac{1-2\alpha\theta_e(1-\theta_e)}{\theta_e(1-\theta_e)} \quad (8)$$

and

$$f''(\theta_e) = f'(\theta_e)\frac{1-2\alpha\theta_e(1-\theta_e)}{\theta_e(1-\theta_e)} + f(\theta_e)\frac{(2\theta_e-1)}{\theta_e^2(1-\theta_e)^2} \quad (9)$$

Substituting (7)–(9) in (6), and simplifying,

$$C_t = C_e + \frac{A\alpha\Gamma_s}{c_0}\frac{\theta_e^2(1-\theta_e)}{1-2a\theta_e(1-\theta_e)}\left[1+\frac{2\alpha(E-E_m)^2(2\theta_e-1)}{\{1-2a\theta_e(1-\theta_e)\}^2}\right]\left(\frac{\pi}{Dt}\right)^{\frac{1}{2}} \quad (10)$$

It should be emphasised that the calculations are valid for $t \gg 0$ (or $\theta_t \approx \theta_e$) under conditions of pure diffusion control. The following conclusions may be drawn from eqn. (10).

1. Capacitance will vary linearly with $t^{-\frac{1}{2}}$ for any value of concentration of the surfactant, degree of coverage, and electrode potential.

2. A decrease in capacitance with time will be observed at (and near) the potentials of maximum adsorption, *i.e.* at $E \simeq E_m$, because at these potentials, $\theta_e \simeq 1$ and $2a\theta_e(1-\theta_e) \ll 1$ and from (10)

$$C_t \simeq C_e + \frac{A\alpha\Gamma_s\theta_e^2(1-\theta_e)}{c_0[1-2a\theta_e(1-\theta_e)]}\left(\frac{\pi}{Dt}\right)^{\frac{1}{2}} \quad (11)$$

It follows that the slope of the curve C_t *vs.* $t^{-\frac{1}{2}}$ will be positive if $\theta_e \approx 1$.

3. An increase in capacitance with time will be observed at the desorption potentials ($\theta_e \simeq 0.5$) under the condition $a > 2$ since the slope of the curve C_t *vs.* $t^{-\frac{1}{2}}$, again given by eqn. (11), will be negative. In other words, surfactants with strong, attractive interaction ($a \gtrsim 2$) will show this unusual behaviour.

4. At a given electrode potential, the product $c_0\sqrt{t}$ is a constant when the capacitance at time t differs from the equilibrium value, C_e, by a constant value, provided θ_e and E_m do not change appreciably with c_0 at this potential.

5. The slope of the line C_t *vs.* $t^{-\frac{1}{2}}$ is equal to,

$$\left[\frac{dC_t}{d(t^{-\frac{1}{2}})}\right]_{E=E_m} = \frac{A\alpha\Gamma_s\theta_e^2(1-\theta_e)}{c_0[1-2a\theta_e(1-\theta_e)]}\left(\frac{\pi}{D}\right)^{\frac{1}{2}} \quad (12)$$

and

$$\left[\frac{dC_t}{dt^{-\frac{1}{2}}}\right]_{\theta_e=0.5} = \frac{A\alpha\Gamma_s}{4c_0(2-a)}\left(\frac{\pi}{D}\right)^{\frac{1}{2}} \quad (13)$$

at the potentials corresponding to the middle region of adsorption [eqn. (12)] and at the desorption potentials [eqn. (13)], respectively. Equations (12) and (13) thus provide a method of evaluating the isotherm parameters, Γ_s and a, from experimental data on the change of capacitance with time at different electrode potentials.

EXPERIMENTAL

The experimental set-up has been described elsewhere[10]. In brief, the capacitance of a hanging mercury drop electrode (HMDE) in deoxygenated solutions was measured as a function of time using a low frequency (45 Hz) impedance bridge. Special precautions were taken to (i) keep the area of HMDE constant ($\pm 1\%$) by careful thermostatting, (ii) maintain the electrode potential constant (± 0.5 mV) by polarising the HMDE against a large, non-polarisable counter electrode and (iii) minimise hysteresis effects by taking a fresh mercury drop for each electrode potential.

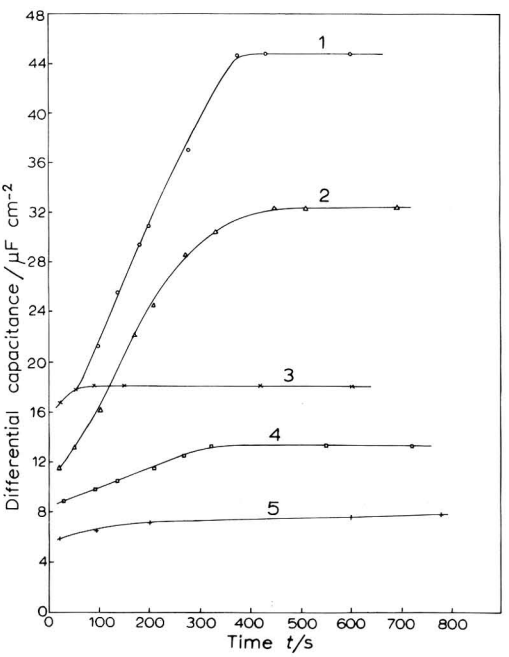

Fig. 1. Time-dependence of capacitance of HMDE in a soln. of 0.5 M Na_2SO_4 satd. with camphor in the region of cathodic desorption potentials. (1) -1.7743, (2) -1.7755, (3) -1.7762, (4) -1.7730, (5) -1.7712 V. All potentials refer to the sulphate reference electrode in the same solution (Hg/Hg_2SO_4(s), Na_2SO_4 (0.5 M)).

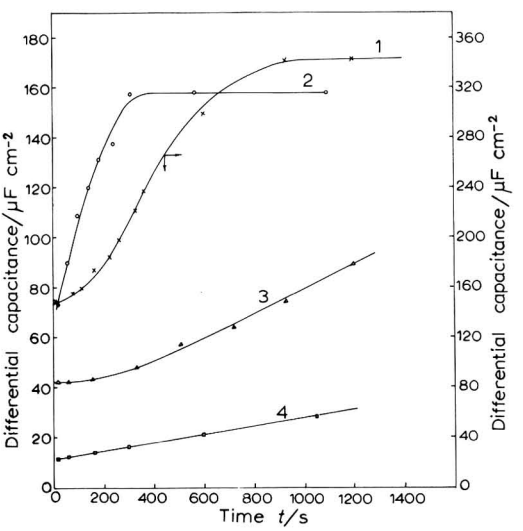

Fig. 2. Time-dependence of capacitance of HMDE in a soln. of 0.5 M Na_2SO_4 satd. with camphor in the region of anodic desorption potentials. (1) -0.3870 (the ordinate scale on the left refers to this curve), (2) -0.3886, (3) -0.3840, (4) -0.3953. All potentials refer to the sulphate reference electrode in the same soln.

RESULTS

Figures 1 and 2 represent the change of capacitance with time for solutions saturated with camphor at potentials corresponding to the region of cathodic and anodic desorption potentials, respectively (*cf.* Fig. 2 of ref. 10). The conspicuous features of these curves are that (i) the capacitance *increases* with time during adsorption, (ii) a change in the electrode potential of *one or two millivolts* causes a large change in the rate of approach of capacitance to the equilibrium value, (iii) the equilibrium values of the capacitance are much larger than the value in the supporting electrolyte. Such *equilibrium values* in the region of the desorption potentials give rise to the usual peaks of adsorption pseudo-capacitance as shown in Fig. 2 of ref. 10. In contrast to the slow approach to equilibrium at the desorption potentials, the equilibrium capacitance is attained well within a second at potentials in the region of maximum adsorption when the solution is saturated with camphor (Fig. 3).

The effect of concentration of camphor in solution on the capacitance–time curves is shown in Fig. 3. All the curves were obtained at a potential in the region of maximum adsorption, *viz.* -1.0 V *vs.* 0.5 *M* sulphate reference electrode (*cf.* Fig. 1 of ref. 10). It can be seen that the capacitance invariably *decreases* with time to the equilibrium value. With increasing concentration of camphor in solution, the adsorption equilibrium is reached in shorter times. Also, the equilibrium capacitance is equal to the monolayer value for all concentrations of camphor in solution.

Figures 4–6 show the capacitance as a function of time when the solutions are saturated with camphene, α-pinene and nonylic acid, respectively. In all the cases, the

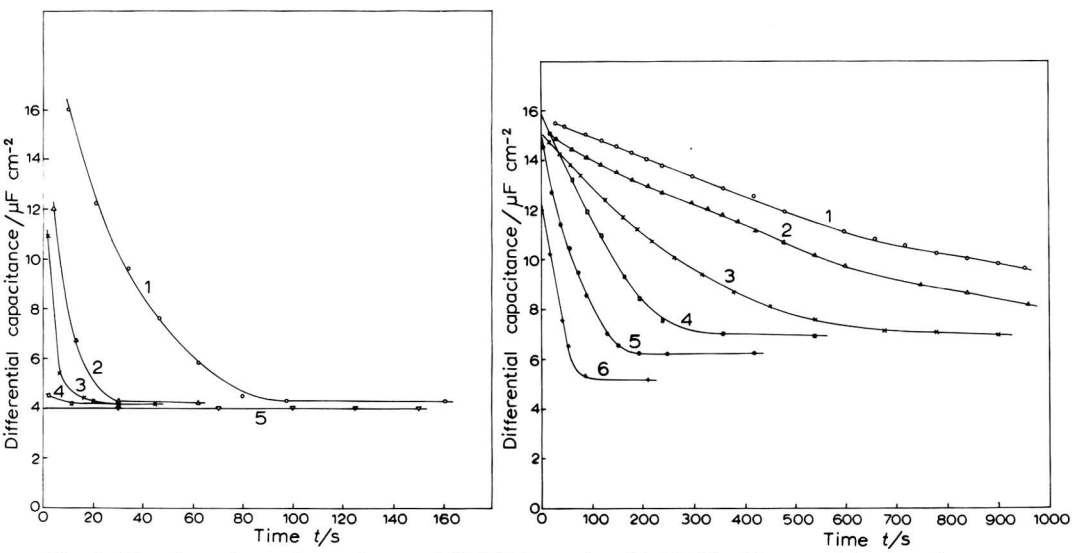

Fig. 3. Time-dependence of capacitance of HMDE in a soln. of 0.5 *M* Na_2SO_4 containing camphor at concns: (1) 5.46×10^{-5}, (2) 6.83×10^{-5}, (3) 8.20×10^{-5}, (4) 10.92×10^{-5} *M*, (5) satd. The electrode potential is -1.0 V *vs.* sulphate reference electrode in the same soln.

Fig. 4. Time-dependence of capacitance of HMDE in a soln. of 0.5 *M* Na_2SO_4 satd. with camphene in the region of cathodic desorption potentials. (1) -1.3015, (2) -1.2730, (3) -1.2514, (4) -1.2364, (5) -1.2245, (6) -1.2050 V. All potentials refer to the sulphate reference electrode in the same soln.

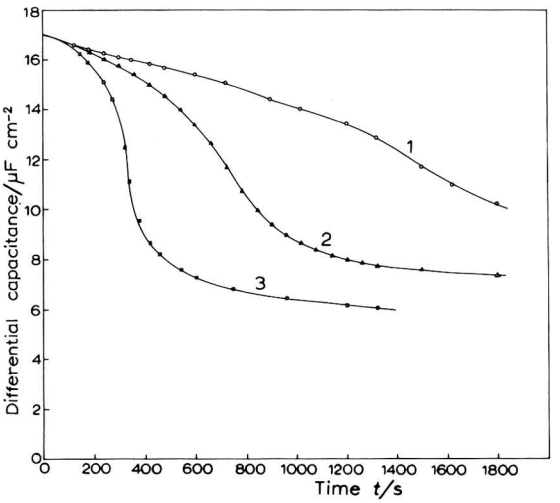

Fig. 5. Time-dependence of capacitance of HMDE in a soln. of 0.5 M Na_2SO_4 satd. with α-pinene in the region of cathodic desorption potentials. (1) −1.7520, (2) −1.7020, (3) −1.6508 V. All potentials refer to the sulphate reference electrode in the same solution.

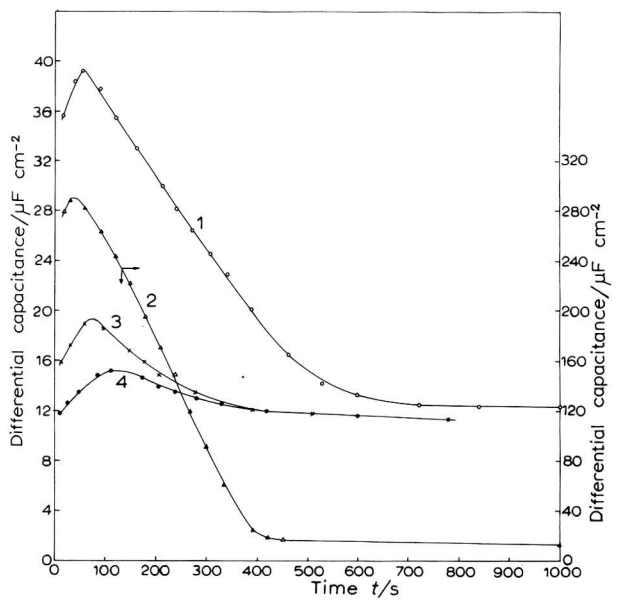

Fig. 6. Time-dependence of capacitance of HMDE in a soln. of 0.5 M Na_2SO_4 satd. with nonylic acid in the region of cathodic desorption potentials. (1) −1.5375, (2) −1.5485 (the ordinate scale on the left refers to this curve), (3) −1.5211, (4) −1.5104 V. All potentials refer to the sulphate reference electrode in the same soln.

capacitance decreases with time. However, with nonylic acid as the surfactant (Fig. 6) there is an *initial rise* in capacitance with time. The potentials indicated in the Figures correspond to the region of the cathodic desorption potentials of the corresponding surfactants (Fig. 4 of ref. 10). The trend is similar at the anodic desorption potentials (not shown in Figures). At potentials in the middle region of adsorption, however, the equilibrium capacitance is attained much faster (within a few seconds) in each case.

DISCUSSION

It has been shown above that the capacitance should vary linearly with $t^{-\frac{1}{2}}$, when t is near the region where capacitances reach their equilibrium values. This, as well as the other theoretical conclusions described above, are in fair agreement with the experimental data, plotted in Fig. 7. In particular, with camphor as the adsorbate, the rising trend of capacitance with time, in the region of desorption potentials, (Figs. 1 and 2) permits the application of eqn. (13) to obtain the value of the interaction parameter a in the Frumkin isotherm. For this purpose, the slope factor (13) may be identified with the experimentally obtained slope corresponding to the C_t–$t^{-\frac{1}{2}}$ curve with the highest *equilibrium* pseudo-capacitance (Curve 1, Fig. 1), since this value of capacitance very nearly corresponds to $\theta_e = 0.5$. Hence, from (13) and Fig. 1,

$$\frac{A\alpha\Gamma_s}{4c_0(2-a)}\left(\frac{\pi}{D}\right)^{\frac{1}{2}} \approx -300\ \mu\mathrm{F\,cm^{-2}\,s^{-\frac{1}{2}}}$$

Substituting the values for $\Gamma_s (= 5.6 \times 10^{-10}$ mol cm^{-2}), $C_0 (= 16.5\ \mu$F cm^{-2}) and $C_1 (= 4.0\ \mu$F cm^{-2}) from ref. 10, and assuming that $D = 5 \times 10^{-6}$ cm^2 s^{-1} and $c_0 = 1.1 \times 10^{-5}$ mol ml^{-1} [15] we get $a \approx 2.01$ for camphor. This value for the interaction parameter corresponds to a strong attractive interaction leading to a two-dimensional condensation in the double layer, and is consistent with other data[10] for the adsorption of camphor at the mercury–solution interface.

Similar calculations for the interaction parameter could not be carried out for the other compounds studied in this work, since ascending C_t–t curves characteristic of the region $\theta_e = 0.5$ were not realised. This is probably a result of the extremely low solubility of these compounds in aqueous media (compared to that of camphor) as a result of which the desorption peaks will be too narrow to be experimentally realised when adsorption leads to a two-dimensional association.

If adsorbate coverages less than a monolayer (*i.e.* $\theta_e < 1$) are experimentally accessible at potentials in the middle region of adsorption (unlike the situation with camphor, *cf.* Fig. 1 of ref. 10), the use of eqn. (10) along with the well-known relation, $\theta_e = [(C_0 - C_e)/(C_0 - C_1)]_{E \approx E_m}$ will provide a general method for evaluating the interaction parameter from data on adsorption kinetics.

The above conclusions are based on the theoretical relations for diffusion-controlled adsorption. An alternative mechanism for slow adsorption has recently been suggested[16] according to which fractional coverages at equilibrium are obtained by a slow, two-dimensional nucleation of the adsorbate with strong attractive interaction. It is not clear, however, whether such an interfacial slow step will account for the large times of adsorption observed in the present work.

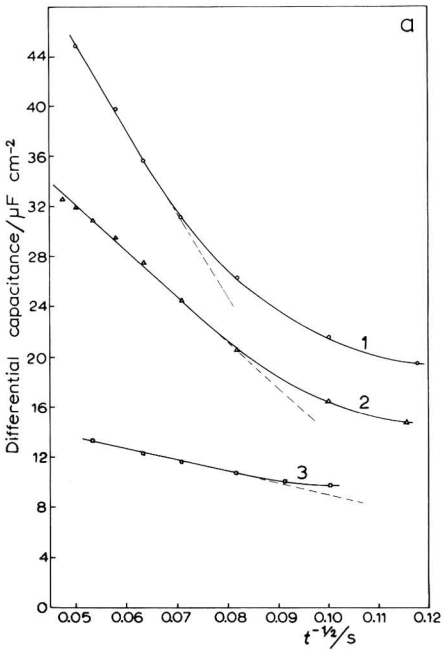
a
Differential capacitance/μF cm⁻²
t^-½/s
1
2
3

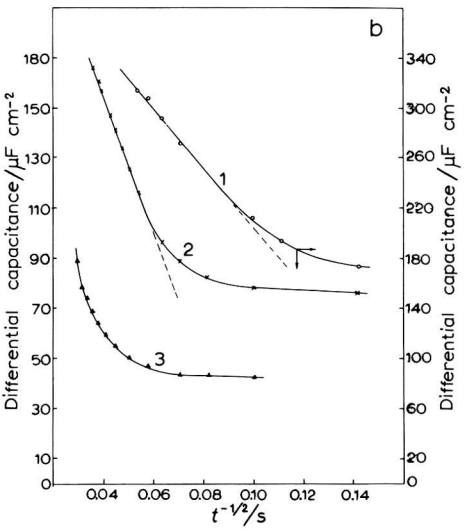
b
Differential capacitance/μF cm⁻²
t^-½/s
1
2
3

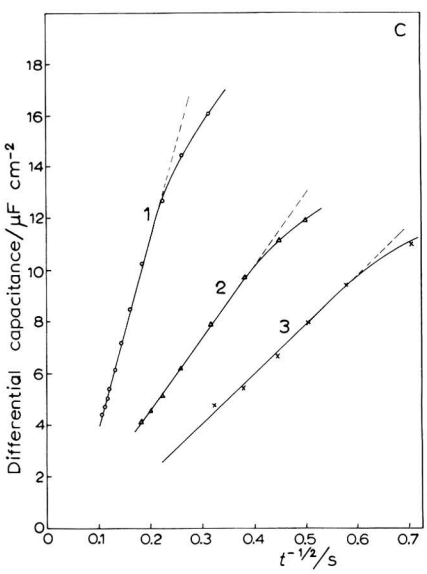
c
Differential capacitance/μF cm⁻²
t^-½/s
1
2
3

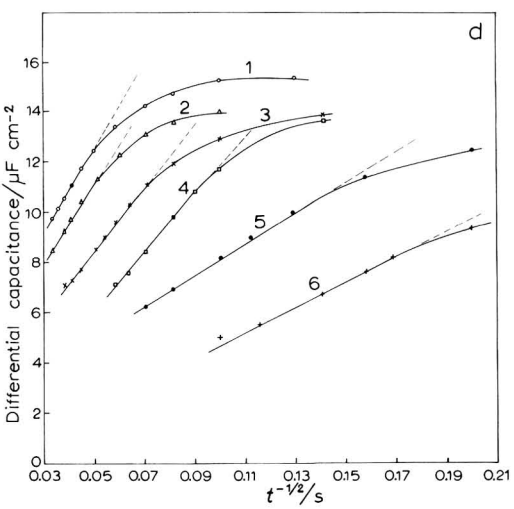
d
Differential capacitance/μF cm⁻²
t^-½/s
1
2
3
4
5
6

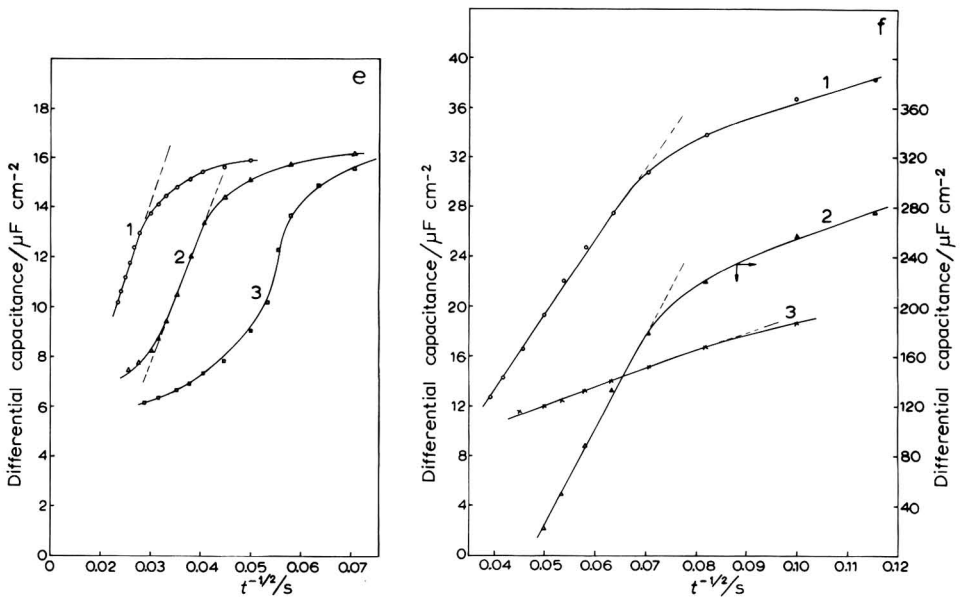

Fig. 7. Capacitance *vs.* $t^{-\frac{1}{2}}$ plots for the curves represented in: (a) Fig. 1, (b) Fig. 2, (c) Fig. 3, (d) Fig. 4, (e) Fig. 5, (f) Fig. 6.

ACKNOWLEDGEMENT

K. G. Baikerikar thanks the Council of Scientific and Industrial Research (India) for financial support.

SUMMARY

Adsorption kinetic measurements have been made for substances such as camphor, camphene, α-pinene and nonylic acid which undergo a two-dimensional condensation at an ideally polarised mercury–solution interface. The results have been correlated theoretically with the way capacitance changes with time when the adsorption process is controlled by diffusion and satisfies any arbitrary adsorption isotherm. For the special case of Frumkin's isotherm, explicit equations have been derived relating the non-equilibrium capacitance with the time of adsorption. The interaction parameter for the adsorption of camphor at the mercury–solution interface has been evaluated by comparing theory with experimental data.

REFERENCES

1 A. N. Frumkin and V. I. Melik-Gaikazyan, *Dokl. Akad. Nauk SSSR*, 78 (1951) 855.
2 W. Lorenz and F. Möckel, *Z. Elektrochem.*, 60 (1956) 507.
3 R. D. Armstrong, W. P. Race and H. R. Thirsk, *J. Electroanal. Chem.*, 16 (1968) 517.
4 V. I. Melik-Gaikazyan, *Zh. Fiz. Khim.*, 26 (1952) 560.
5 P. Delahay and I. Trachtenberg, *J. Am. Chem. Soc.*, 79 (1957) 2355.
6 P. Delahay and C. T. Fike, *J. Am. Chem. Soc.*, 80 (1958) 2628.
7 J. H. M. Rek, M. D. Wijnen and J. H. Sluyters, *Rec. Trav. Chim.*, 84 (1965) 1071.

8 D. W. IMHOFF AND J. W. COLLAT, *J. Phys. Chem.*, 71 (1967) 3048.
9 W. LORENZ AND F. MÖCKEL, *Z. Elektrochem.*, 60 (1956) 939.
10 K. G. BAIKERIKAR AND S. SATHYANARAYANA, *J. Electroanal. Chem.*, 24 (1970) 333.
11 V. G. LEVICH, B. I. KHAIKIN AND E. D. BELOKOLOS, *Elektrokhimiya*, 1 (1965) 1273.
12 R. PARSONS in P. DELAHAY AND C. W. TOBIAS (Eds.), *Advances in Electrochemistry and Electrochemical Engineering*, Vol. I, Interscience, New York, 1961, Chap. 1.
13 A. N. FRUMKIN AND B. B. DAMASKIN in J. O'M. BOCKRIS AND B. E. CONWAY (Eds.), *Sovremennye aspekty elektrokhimii*, Russian Translation edited by YA. M. KOLOTYRKIN, 'Mir' Moscow, 1967, Chap. 3.
14 A. K. N. REDDY in E. GILEADI (Ed.), *Electrosorption*, Plenum Press, New York, 1967, p. 53.
15 A. SIEDELL, *Solubilities of Organic Compounds*, Vol. II, D. Van Nostrand Co. Inc., New York, 1941, p. 678.
16 R. D. ARMSTRONG, *J. Electroanal. Chem.*, 20 (1969) 168.
17 W. H. REINMUTH, *J. Phys. Chem.*, 65 (1961) 473.
18 L. NEMEC, *Collection Czech. Chem. Commun.*, 31 (1966) 1162.
19 S. VAVRICKA, L. NEMEC AND J. KORYTA, *Collection Czech. Chem. Commun.*, 31 (1966) 947.

ELECTROANALYTICAL CHEMISTRY AND INTERFACIAL ELECTROCHEMISTRY
Elsevier Sequoia S.A., Lausanne – Printed in The Netherlands

DIE BESTIMMUNG DER STANDARDGALVANISPANNUNG DER Hg/Hg_2Br_2-ELEKTRODE MIT DER KETTE

$$Hg\left|Hg_2Cl_2(s)\right|\begin{matrix}KCl\ xm\\KNO_3(1-x)m\end{matrix}\Big\|\begin{matrix}KBr\ xm\\KNO_3(1-x)m\end{matrix}\left|Hg_2Br_2(s)\right|Hg$$

W. LEUSCHKE UND K. SCHWABE
Institut für Elektrochemie und physikalische Chemie, Technische Universität, Dresden (D.D.R.)
(Eingegangen am 31. Juli 1969)

Die Standardgalvanispannung der $Hg|Hg_2Br_2$-Elektrode ist bisher meistens mit Hilfe der Kette

$$Hg|Hg_2Br_2(s)HBr|(Pt)H_2 \qquad (I)$$

bestimmt worden. Bei sauerstoffhaltigen Lösungen wurden Werte von 0.1396 abs. V bei 25°C (bezogen auf die Standardwasserstoffelektrode) erhalten[1], während bei Ausschluss von Sauerstoff Werte von 0.1392 abs. V gefunden wurden[2]. Gupta und Mitarbeiter[3] erhielten bei sehr sorgfältigen Messungen 0.1392[3] abs. V. Wir hatten in Zusammenhang mit Untersuchungen der Kette (I) in organischen Lösungsmitteln den Wert 0.1394 abs. V gefunden[4]. Owen und Brinkley[5] haben mit Hilfe der Kette

$$Ag\left|AgCl(s)\right|\begin{matrix}KCl\ xm\\KNO_3(1-x)m\end{matrix}\Big\|\begin{matrix}KBr\ xm\\KNO_3(1-x)m\end{matrix}\left|AgBr(s)\right|Ag \qquad (II)$$

die Differenz der Standardgalvanispannungen der beiden Silberelektroden bestimmt. Wir haben mit der Kette

$$Hg\left|Hg_2Cl_2(s)\right|\begin{matrix}KCl\ xm\\KNO_3(1-x)m\end{matrix}\Big\|\begin{matrix}KBr\ xm\\KNO_3(1-x)m\end{matrix}\left|Hg_2Br_2(s)\right|Hg \qquad (III)$$

die Differenz der Standardgalvanispannungen der beiden Quecksilberelektroden in analoger Weise und, da die Standardgalvanispannung der Kalomelektrode sehr genau bekannt ist[6], die der $Hg|Hg_2Br_2$-Elektrode gewonnen. Wenn man für verschiedene Werte von x die gemessene Spannung gegen x aufträgt, so erhält man bei konstanter Molalität m im Bereich von 0.05–0.01 Mol/kg Geraden, die man auf $x=0$ extrapolieren kann, wobei das Diffusionspotential verschwindet. Wenn man die so erhaltenen Werte gegen verschiedene Werte von m aufträgt, so erhält man wieder eine Gerade, deren Extrapolation auf 0 die Differenz der Standardgalvanispannungen liefert. Dass der lineare Zusammenhang zwischen Kettenspannung und Konzentration, der eine bequeme Extrapolation auf den Standardzustand ermöglicht, theoretisch begründet ist, haben einerseits Spiro[7] und andererseits Covington[8] neuerdings nachgewiesen. Damit ist das Auswertungsverfahren nach Owen als theoretisch gerechtfertigt anzusehen.

MESSANORDNUNG UND VERSUCHSDURCHFÜHRUNG

Die Meszelle ist in Abb. 1 dargestellt, sie besteht aus 4 Gefässen, wobei die Elektroden paarweise angeordnet sind und damit 4 Kombinationen sowie ein Vergleich gleichartiger Elektroden möglich ist. Durch die Zuleitungen C und E werden die Gefässe gefüllt, die Anschlüsse A, B, F und G dienen zum Entlüften bzw. Einsaugen der entlüfteten Lösungen. Durch den Stutzen D an dem Hahn X, der zur Herstellung der Grenzfläche zwischen den beiden Lösungen dient und der in Abb. 2

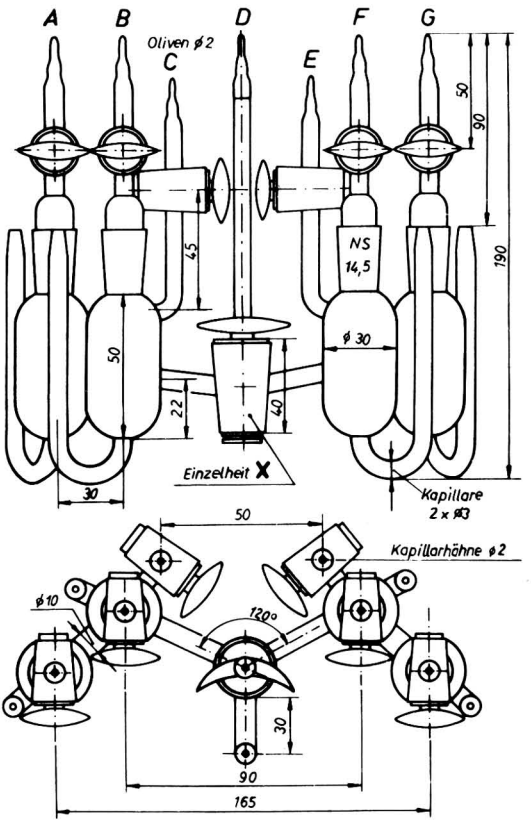

Abb. 1. Meszelle.

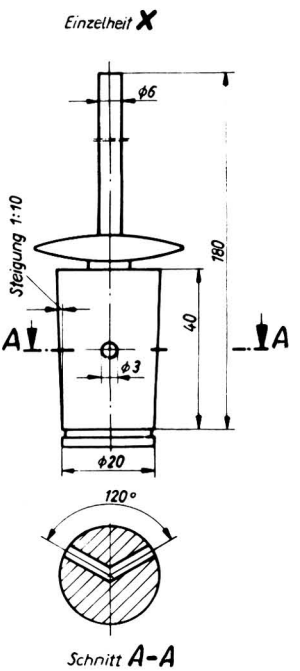

Abb. 2. Hahnstopfen zur Meszelle (Einzelheit X).

genauer dargestellt ist, kann die Zelle entleert bzw. die Grenzfläche erneuert werden. Eine Verlängerung des Griffes an diesem Hahn gestattete, ihn auch mühelos zu betätigen, wenn sich die ganze Messzelle in einem mit Wasser gefüllten Thermostaten befand, dessen Temperatur auf $\pm 0.01°C$ konstant gehalten werden konnte. Die Stromzuführung zum Quecksilber erfolgte durch Pt-Drähte, die in die Kapillarrohre die unten an die Gefässe angesetzt waren, eingeführt wurden.

Die Kettenspannungen wurden mit einem Präzisionskompensator (VEB Messtechnik Mellenbach) und einem Spiegelgalvanometer (Forschungsinstitut Meinsberg G 6, Empfindlichkeit $1 \cdot 10^{-9}$ A/Skt) gemessen, die Messgenauigkeit betrug 0.01 mV.

Für die Herstellung der Elektroden, die nach der Vorschrift von Hills und Ives[6] erfolgte, wurde bidestilliertes Hg verwendet, die Elektrodengefässe waren mit Silikonöl hydrophobiert, Hg_2Cl_2 und Hg_2Br_2 wurden elektrolytisch hergestellt[6]. Nachdem die Gefässe mit Hg, das mit einer dünnen Schicht Hg_2Cl_2 bzw. Hg_2Br_2 bedeckt war, gefüllt waren, wurden sie eine Stunde lang mit reinstem N_2 gespült und dann die in direkt angeschlossenen Vorratsgefässen befindliche, sorgfältig entlüftete Lösung eingesaugt. KBr und KCl waren Spektroskopiestandards der Firma Merck, Darmstadt, KNO_3 (p.A. Merck). Die Lösungen wurden aus den bei 115°C getrockneten und im P_2O_5-Exsikkator aufbewahrten Salzen mit bidestilliertem Wasser hergestellt. Ausgehend von Stammlösungen der Konzentration $m=0.05$ Mol kg^{-1} mit den x-Werten 0.2, 0.4, 0.6, 0.8 und 1.0 wurden durch Verdünnen die Konzentrationen 0.04, 0.03, 0.02 und 0.01 Mol kg^{-1} mit den entsprechenden x-Werten eingestellt[9].

Nachdem die Entlüftung abgeschlossen und die Lösungen mit Hilfe von Injektionsspritzen aus den bei C und E angeschlossenen Vorratsgefässen (100 ml Waschflaschen) eingesaugt sind, so dass die Gefässe völlig mit Lösung gefüllt sind, werden die Hähne A, B, F und G geschlossen und der Hahn X gefüllt, indem man wechselweise die Lösungen durch D abzieht. Bei geschlossenem Hahn X und offenen Hähnen C und E wird die Gleichgewichtseinstellung abgewartet, die nach etwa 60 Minuten erfolgt ist. Man erkennt sie daran, dass die Potentialdifferenz zwischen den Hg_2Cl_2- bez. den Hg_2Br_2-Elektroden nicht mehr als 0.02–0.03 mV beträgt. Dann werden alle Hähne geschlossen und nun Hahn X langsam geöffnet, womit die Grenzfläche hergestellt ist. Die Kettenspannung wird zwischen den vier möglichen Elektrodenkombinationen bestimmt und die Messung eventuell nach Auswechseln der Messlösungen wiederholt. Die Werte wurden als konstant angesehen, wenn sie sich innerhalb von 2 Stunden nicht mehr messbar veränderten.

MESSERGEBNISSE

In Tabelle 1 sind die Galvanispannungen ($-E$), die Mittelwerte aus 4–12 Messungen an Messreihen in Lösungen mit konstantem x bei veränderter Gesamtkonzentration m bei 25° C in abs. V, bezogen auf Mol/kg, zusammengestellt. Daraus

TABELLE 1

DIE E.M.K.-WERTE

$m/mol\ kg^{-1}$	0.05	0.04	0.03	0.02	0.01
x	$-E/V$	$-E/V$	$-E/V$	$-E/V$	$-E/V$
1.0	0.12925	0.12918	0.12913	0.12910	0.12903
0.8	0.12933	0.12927	0.12918	0.12913	0.12905
0.6	0.12940	0.12931	0.12926	0.12915	0.12909
0.4	0.12944	0.12936	0.12927	0.12918	0.12907
0.2	0.12953	0.12941	0.12933	0.12920	0.12910
0	0.12960	0.12947	0.12938	0.12922	0.12912
x	1.0	0.8	0.6	0.4	0.2
$m=0$	0.12898	0.12898	0.12900	0.12899	0.12899

folgt für die Standardgalvanispannung der Kette bei 25° C durch Extrapolation auf $m=0$ und $x=0$

$$-E^0 = (0.12899 \pm 0.00003) \text{ abs. V bei } 25° \text{ C.}$$

Wie die Extrapolationsgeraden zeigen (Abb. 3–5), erhält man bei der Extrapolation auf $m=0$ bei $x=$konst. das gleiche Ergebnis wie bei der vollständigen, von Owen vorgeschlagenen Extrapolation ($x=0$ und $m=0$). Bei $m\to 0$ und $x=$konst. verschwinden, wie zu erwarten, ebenfalls die Diffusionspotentiale. Eine ausführliche Fehlerdiskussion zeigt, dass die angegebene Fehlergrenze ± 0.03 mV nicht überschritten wird. Die Hg_2Cl_2-Elektroden unterschieden sich maximal um 0.02, die Hg_2Br_2-Elektroden um maximal 0.03 mV.

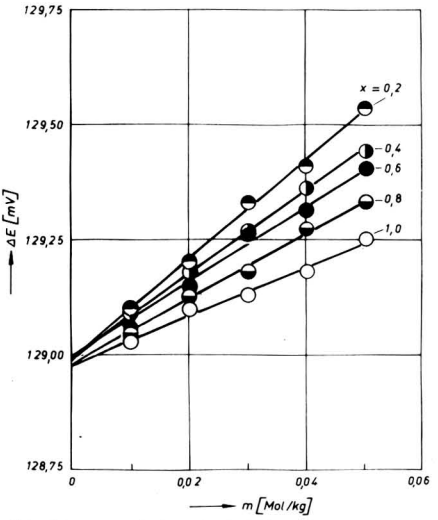

Abb. 3. Extrapolation der E.M.K.-Werte von Lösungen mit konstantem x auf $m=0$, Radien der Meszpunkte 0.015 mV.

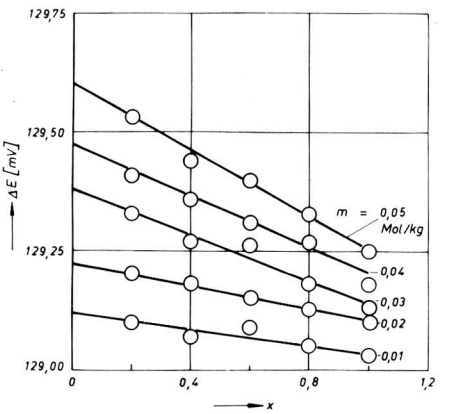

Abb. 4. Erste Stufe der Extrapolation nach Owen und Brinkley. Extrapolation bei konstanter Gesamtionenkonzentration m auf $x=0$. Radien der Meszpunkte 0.015 mV.

Wenn man für die Standardgalvanispannung der Kalomelelektrode den Wert +0.26820 V zugrunde legt[3,6], so ergibt sich für die Standardgalvanispannung der Hg_2Br_2-Elektrode

$$E^\circ_{Hg/Hg_2Br_2} = +(0.13921 \pm 0.00004) \text{ abs. V bei } 25°C$$

in guter Übereinstimmung mit dem Wert, den Gupta und Mitarbeiter[3] mit der Kette (I) erhielten: (0.13923 ± 0.00003) abs. V. Daraus folgt, dass das Extrapolationsverfahren nach Owen aus den Ketten mit Überführung genaue Standardgalvanispannungen zu ermitteln gestattet.

Nach demselben Verfahren wurden auch die Kettenspannungen bei 20, 30 und 35° C bestimmt und daraus durch Extrapolation $-E^0$ berechnet (Tabelle 2). Nach Lagrange wurde daraus eine Temperaturfunktion für $-E^0$ aufgestellt:

$$-E^0(t) = 0.12899 - 1.56 \times 10^{-4}(t-25) + 6.2 \times 10^{-6}(t-25)^2 - 5.1 \times 10^{-7}(t-25)^3$$

Daraus ergeben sich nach:

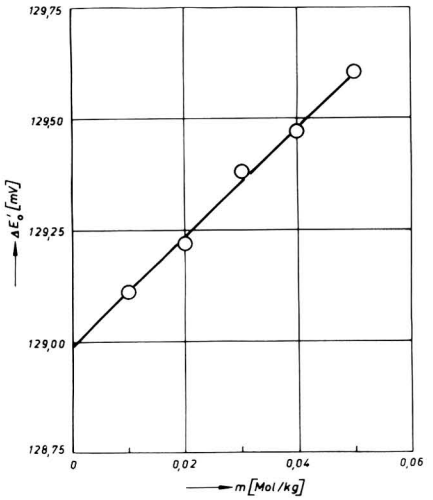

Abb. 5. Zweite Stufe der Extrapolation nach Owen und Brinkley. Extrapolation der aus der ersten Stufe erhaltenen E_0'-Werte für $x=0$ auf die Gesamtionenkonzentration $m=0$. Radien der Meszpunkte 0.02 mV.

TABELLE 2

ANGABEN VON $-E$ IN ABS. mV

$m/mol\ kg^{-1}$ / $t/°C$	0.05	0.04	0.03	0.02	0.01	$0_{Ex.}$
20	130.16	130.15	130.10	130.08	130.01	129.98
25	129.25	129.18	129.13	129.10	129.03	128.98
30	128.63	128.57	128.47	128.45	128.35	128.29
35	127.94	127.79	127.72	127.63	127.63	127.53

$$\Delta S^0 = -nF\frac{\partial E^0}{\partial T}$$

die Änderungen der Standardentropien. Aus $\Delta G^0 = nFE^0$ lassen sich nach $\Delta G^0 = \Delta H^0 - T\Delta S^0$ die Standardenthalpieänderungen für die Kettenreaktion berechnen. Die Werte für die drei thermodynamischen Grössen sind in Tabelle 3 zusammengestellt. Gupta und Mitarbeiter[3,6] haben an Ketten vom Typ (I) die Temperaturkoeffizienten der Hg_2Cl_2- und der Hg_2Br_2-Elektrode bestimmt und daraus ΔG^0, ΔS^0, ΔH^0 für diese Ketten bei 25 °C berechnet. Aus den Differenzen lassen sich ΔG^0, ΔS^0

TABELLE 3

$t/°C$	$-\Delta G^0/kcal\ mol^{-1}$	$-\Delta H^0/kcal\ mol^{-1}$	$-\Delta S^0/cal\ mol^{-1}K^{-1}$
20	5.998	9.46	11.81
25	5.949	8.09	7.19
30	5.917	7.71	6.08
35	5.882	8.51	8.53[a]

[a] Der Wert bei 35 °C ist wegen der grösseren Streuung der Kettenspannung unsicher.

und ΔH^0 für die Kette (III) gewinnen. Die so ermittelten Werte stimmen mit den von uns in dieser Kette selbst bei 25° C erhaltenen Werten befriedigend überein ($\Delta G^0 = -5.946$ kcal, $-\Delta S^0 = 6.5$ cal mol^{-1} K^{-1}, $-\Delta H^0 = 7.952$ kcal)*, wenn man bedenkt, dass ein Fehler von 0.03 mV sich in ΔS^0 schon beträchtlich auswirkt.

Auch daraus folgt, dass man mit Ketten vom Typ (III) durch Extrapolation auf $m=0$ (und $x=0$) genaue Werte von Standardgalvanispannungen bestimmen kann. Natürlich muss zur Berechnung des Standardwertes einer Elektrode der der anderen genau bekannt sein.

Nach Covington[8] setzt sich das Diffusionspotential an der Flüssigkeitsgrenze einer Kette vom Typ (II) aus einem idealen Anteil ε'_D und einem Anteil ε''_D, der durch die interionische Wechselwirkung hervorgerufen wird, zusammen. Für ε'_D gilt nach Henderson

$$\varepsilon'_D = -\frac{x(l_{Cl}-l_{Br})}{(l_{NO_3}+l_K)} \cdot f_N \tag{1}$$

worin $f_N = RT/F$ und l die Beweglichkeiten der entsprechenden Ionen sind. Für ε''_D erhält man unter Verwendung der Koeffizienten von Guggenheim[10] für die Aktivitätskoeffizienten von Elektrolytmischungen

$$\varepsilon''_D = +f_N \ln \frac{f_a^{II}}{f_a^{I}} - \frac{2m \cdot x(\beta_{KBr}-\beta_{KCl}) l_{NO_3} \cdot f_N}{(l_{NO_3}+l_K)} \tag{2}$$

Dabei sind f_a^{II} der Aktivitätskoeffizient des K^+ im Bromid, f_a^{I} im Chlorid.
Für das gesamte Diffusionspotential ε_D erhält man daher:

$$\varepsilon_D = f_N \ln \frac{f_a^{II}}{f_a^{I}} - \frac{f_N(l_{Cl}-l_{Br})x}{(l_{NO_3}+l_K)} - \frac{2mx(\beta_{KBr}-\beta_{KCl}) \cdot l_{NO_3} \cdot f_N}{(l_K+l_{NO_3})} \tag{3}$$

Wenn man den Quotienten f_a^{II}/f_a^{I} als konzentrationsunabhängig ansieht, erhält man für die Änderung des Diffusionspotentials mit x

$$\left(\frac{\partial \varepsilon_D}{\partial x}\right)_m = -\frac{f_N[l_{Cl}-l_{Br}+2m(\beta_{KBr}-\beta_{KCl})l_{NO_3}]}{l_K+l_{NO_3}} \tag{4}$$

und für die Änderung mit m

$$\left(\frac{\partial \varepsilon_D}{\partial m}\right)_x = -\frac{2x(\beta_{KBr}-\beta_{KCl})l_{NO_3} \cdot f_N}{l_K+l_{NO_3}} \tag{5}$$

Für die gesamte Galvanispannung der Kette (III) ist

$$\left(\frac{\partial E}{\partial m}\right)_x = f_N\left(\frac{\partial \ln(f_{Cl}/f_{Br})}{\partial m}\right)_x + \left(\frac{\partial \varepsilon_D}{\partial x}\right)_m \tag{6}$$

f_{Cl}, f_{Br}-Aktivitätskoeffizienten von Cl^- bzw. Br^-.

Wenn für $x=0$ nur das Diffusionspotential verschwindet[5], so muss sein

$$\left(\frac{\partial E}{\partial m}\right)_{x=0} = f_N\left(\frac{\partial \ln(f_{Cl}/f_{Br})}{\partial m}\right)_{x=0} \tag{7}$$

und die Differenz aus beiden Steigungen müsste die Steigung der Diffusionspotentiale

* 1 cal = 4.1840 J.

mit m, wie sie sich aus (5) errechnete, ergeben.

Aus den Ionenbeweglichkeiten[11] und den spezifischen Wechselwirkungskoeffizienten β (nach[10]) wurde $(\partial\varepsilon\,\mathrm{Diff}/\partial m)$ für verschiedene Werte von x berechnet und mit den Werten, die aus $(\partial E/\partial m)_x - (\partial E/\partial m)_{x=0}$ experimentell erhalten wurden, verglichen. Wie Tabelle 4 zeigt, stimmen die Steigungen nur dem Vorzeichen nach überein, die

TABELLE 4

x		0.2	0.4	0.6	0.8	1.0
$\left(\frac{\partial\varepsilon\,\mathrm{Diff}}{\partial m}\right)_{x(\mathrm{gem.})}$	$\frac{\mathrm{mV\ kg}}{\mathrm{mol}}$	−1.6	−2.2	−4.2	−5.6	−7.2
$\left(\frac{\partial\varepsilon\,\mathrm{Diff}}{\partial m}\right)_{x(\mathrm{ber.})}$	$\frac{\mathrm{mV\ kg}}{\mathrm{mol}}$	−0.5	−1.0	−1.5	−2.0	−2.5

berechneten Werte sind erheblich kleiner. Es ist kaum anzunehmen, dass die Vernachlässigung der Konzentrationsabhängigkeit des 1. Terms in (3) die Ursache für die grosse Differenz zwischen den Werten ist, da ja die Gesamtionenstärke auf beiden Seiten immer gleich war. Natürlich ist auch hier der Einfluss einer Streuung von 0.02–0.03 mV erheblich. Immerhin scheint auch unter Berücksichtigung der interionischen Wechselwirkung nach Covington eine exakte Berechnung der Diffusionspotentiale noch nicht möglich zu sein.

ZUSAMMENFASSUNG

Die Standardgalvanispannung der im Titel genannten Kette wird zu

$$-E^0 = (0.12899 \pm 0.00003)\text{abs. V bei } 25^\circ\text{ C}$$

bestimmt. Im Bereich von 20°–35° C folgt die Standardkettenspannung der Gleichung

$$U = 0.12899 - 1.56 \times 10^{-4}(t-25) + 6.2 \times 10^{-6}(t-25)^2 - 5.1 \times 10^{-7}(t-25)^3$$

Mit dem Wert $E^0 = 0.26820$ abs. V bei 25°C für die Kalomelelektrode erhält man für die Standardgalvanispannung der Hg_2Br_2-Elektrode den Wert

$$E^0_{Hg/Hg_2Br_2} = (0.13921 \pm 0.00004)\text{abs. V bei } 25^\circ\text{ C}$$

in sehr guter Übereinstimmung mit dem von Gupta und Mitarbeiter mittels der Kette (I) bestimmten Wert von (0.13923 ± 0.00003) abs. V.

SUMMARY

The standard potential of the cell given in the title was determined to be:

$$-E^0 = 0.12899 \pm 0.00003 \text{ abs. V at } 25^\circ\text{C}\,.$$

In the range 20°–35° C the standard cell potential follows the equation:

$$U = 0.12899 - 1.56 \times 10^{-4}(t-25) + 6.2 \times 10^{-6}(t-25)^2 - 5.1 \times 10^{-7}(t-25)^3$$

With the value $E^0 = 0.26820$ abs. V at 25° C for the calomel electrode, the standard

electrode potential of the $Hg|Hg_2Br_2$ electrode is found to be:

$$E^0_{HgHg_2Br_2} = 0.13921 \pm 0.00004 \text{ abs. V at } 25^\circ C$$

in very good agreement with the value of 0.13923 ± 0.00003 abs. V obtained by Gupta *et al.* using cell (I).

LITERATUR

1 R. H. GERKE UND J. R. GEDDES, *J. Phys. Chem.*, 31 (1927) 886, C 1927, II, 674; F. ISHIKAWA UND U. UEDA, *J. Chem. Soc. (Japan)*, 2 (1930) 59; W. D. LARSON, *J. Am. Chem. Soc.*, 62 (1940) 765.
2 F. ISHIKAWA, J. FERUI UND T. TAKAI, *Bull. Inst. Phys. Chem. Research (Tokio)*, 15 (1936) 339; H. N. PARTON UND J. W. MITCHELL, *Trans. Faraday Soc.*, 35 (1939) 758.
3 K. K. GUPTA, G. J. HILLS UND D. J. G. IVES, *Trans. Faraday Soc.*, 59 (1963) 1875.
4 K. SCHWABE UND R. URLASS, *Z. Elektrochem.*, 68 (1964) 46.
5 B. B. OWEN UND S. R. BRINKLEY, *J. Am. Chem. Soc.*, 63 (1941) 1711; 64 (1942) 2671.
6 vergl. z.B. G. J. HILLS UND D. J. G. IVES, *J. Chem. Soc. (London)*, (1951) 305; C 1951, II, 1394; K. SCHWABE UND W. SCHWENKE, *Z. Elektrochem.*, 63 (1959) 441.
7 M. SPIRO, *Electrochim. Acta*, 11 (1966) 569.
8 A. K. COVINGTON, *Electrochim. Acta*, 11 (1966) 959.
9 Genaue Angaben über die Herstellung und das Einfüllen der Lösungen siehe Diplomarbeit W. LEUSCHKE, TU Dresden, Institut für Elektrochemie und physikalische Chemie, 1967.
10 E. A. GUGGENHEIM UND J. C. TURGEON, *Trans. Faraday Soc.*, 51 (1955) 747; *Phil. Mag.*, 21 (1935) 588.
11 Entnommen aus H. S. HARNED UND B. B. OWEN, *The Physical Chemistry of Electrolytic Solutions*, Reinhold Publ. Corp., New York, 1958.

ELECTROANALYTICAL CHEMISTRY AND INTERFACIAL ELECTROCHEMISTRY
Elsevier Sequoia S.A., Lausanne – Printed in The Netherlands

DIE COULOMETRISCHE BESTIMMUNG GERINGER PLATINMENGEN

G. SCHEIDHAUER UND K. SCHWABE

Technische Universität Dresden, Sektion Chemie, Lehrbereich Elektrochemie u. physikal. Chemie, Dresden (D.D.R.)

(Eingegangen am 31. Juli 1969)

1. EINLEITUNG

Die Bestimmung kleiner Mengen von Platinmetallen, die z.B. in der Glasindustrie von Bedeutung ist, lässt sich mit modernen Grossgeräten (Atomabsorptionsspektroskopie, Massenspektrometrie, Neutronenaktivierung) durchführen[1], während man bei einfacheren Analysenverfahren auf Schwierigkeiten stösst. Es wurde versucht, Mengen unter 10^{-4} *M* Pt auf galvanostatisch-coulometrischem Wege mit möglichst einfachen Mitteln zu bestimmen[2].

2. AUFBAU DER APPARATUR

Zur Konstanthaltung des Stromes wurde eine einfache handgeregelte Einrichtung, die auf der Verwendung eines Ballastwiderstandes beruht, verwendet. Die Schaltung der Apparatur zeigt Abb. 1. Zur Strommessung wurde ein Präzisions-Mikroamperemeter und zur Zeitmessung eine Stoppuhr benutzt. Als Arbeitselektrode dienten verschiedene Materialien. Das Potential der Arbeitselektrode wurde mit

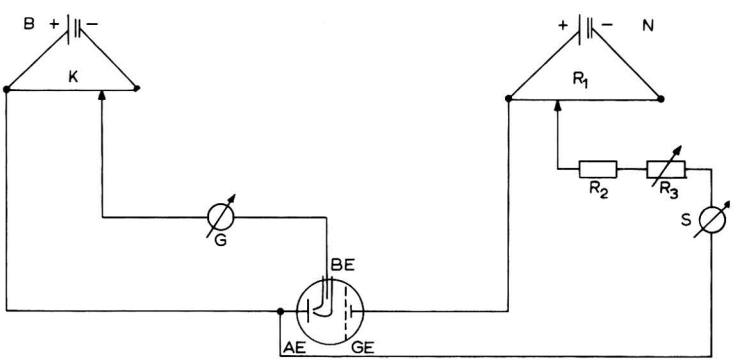

Abb. 1. Schaltung der Apparatur: (B) 4 V Akkumulator, (K) Kompensator mit Normalelement, (G) Galvanometer, (N) Netzgerät mit 70 V Ausgang, (R_1) Spannungsteiler 50 kΩ, (R_2) Festwiderstand 50 kΩ, (R_3) Regelwiderstand 1 MΩ, (S) μA-Meter, (AE) Arbeitselektrode, (GE) Gegenelektrode, (BE) Bezugselektrode.

Hilfe eines Kompensators gegen eine gesättigte Kalomelektrode gemessen. Die Potentialmessung erfolgte über eine Sonde vom Typ einer Le-Blanc-Kapillare. Diese war mit dem jeweils verwendeten Leitelektrolyten gefüllt. Als Gegenelektrode diente in allen Fällen ein quadratisches Platinblech von etwa 1 cm Seitenlänge. Die Gegenelektrode stand über einen Stromschlüssel mit der coulometrischen Zelle in leitender Verbindung. Anodisch eventuell in Lösung gehendes Platin konnte somit nicht in die zu messende Lösung gelangen. Stromschlüssel und Elektrodengefäss waren ebenfalls mit dem jeweils verwendeten Leitelektrolyten gefüllt.

3. COULOMETRISCHE ZELLEN

Für die meisten Versuche wurde ein 25 ml-Becherglas (niedere Form) verwendet. Es war mit einem 5-fach durchbohrten Gummistopfen verschlossen. Dieser diente Aufnahme von Rührer, Stickstoffeinleitungsrohr, Sonde mit Bezugselektrode, Arbeitselektrode und Stromschlüssel von der Gegenelektrode. Diese Zelle konnte sowohl für feste Elektroden als auch für Quecksilber (als Bodenelektrode) verwendet werden. Das Elektrolytvolumen betrug 10–20 ml. Für Messungen mit kleineren Flüssigkeitsmengen (untere Grenze 1 ml) diente ein kleines Gläschen von 3.5 cm Höhe und 2.5 cm Durchmesser. Durch einen Gummistopfen wurden Arbeitselektrode (als Bodenblech ausgeführt), Stromschlüssel, Stickstoffeinleitungsrohr und Bezugselektrode eingeführt. Die Analysenlösung wurde hier durch den Stickstoffstrom gerührt. Die Potentialmessung erfolgte ohne Sonde, da die Bezugselektrode direkt auf der Arbeitselektrode aufsass.

Ausschliesslich für die Verwendung von Quecksilber als Arbeitselektrode wurden zwei spezielle Zellen entwickelt, die hier nicht näher beschrieben werden sollen[3].

4. SAUERSTOFFENTFERNUNG

Sauerstoff wird kathodisch zu H_2O_2 bzw. H_2O reduziert. Da Sauerstoff in allen wässrigen Lösungen gelöst ist, werden deshalb die Stromdichte–Potential- und Potential–Zeit-Kurven bei der kathodischen Metallabscheidung verfälscht, oder die Abscheidung wird überhaupt unmöglich. Wegen der Gefahr einer Reduktion der Platinlösungen kam nur eine Sauerstoffentfernung durch Einleiten von Stickstoff in Frage. Der Stickstoff wurde nach dem Verfahren von Meyer und Ronge[4] von Sauerstoffresten befreit.

5. MESSMETHODIK

Durch Auflösen von physikalisch reinem Platindraht in Königswasser[5] wurde eine 10^{-3} *M* Lösung der Hexachloroplatinsäure hergestellt. Aus dieser wurden durch Verdünnen mit Leitelektrolytlösung die gewünschten Konzentrationen bereitet. Die Untersuchungen erstreckten sich hauptsächlich auf das Auffinden der geeignetsten Arbeitselektrode und des günstigsten Leitelektrolyten. Zur Untersuchung des Abscheidungsverhaltens wurden Stromdichte–Potential- und Potential–Zeit-Kurven aufgenommen. Vor jeder Kurvenaufnahme wurde die Messlösung in der Zelle entlüftet, bis sich ein konstantes Potential einstellte. Auch während der Messung wurde ein

mässiger Stickstoffstrom durch die Lösung geleitet. Die Entlüftung dauerte im Durchschnitt 40 Minuten, liess sich aber durch Auskochen beträchtlich verkürzen. Ein Restgehalt an Sauerstoff in der Messlösung täuschte bei der coulometrischen Abscheidung zu hohe Platingehalte vor.

Nach der Aufnahme von Stromdichte–Potential-Kurven zur Ermittlung des Abscheidungspotentials under den betreffenden Elektrolysebedingungen wurde das Potential der Arbeitselektrode bei der eigentlichen coulometrischen Abscheidung in der Nähe des durch orientierende Vorversuche ermittelten Potentialsprunges in kurzen Zeitintervallen bestimmt.

6. VERSUCHE

Bei Verwendung von 0.1 *M* KCl-Lösung als Leitelektrolyt wurde ein Abscheidungspotential des Pt von -0.5 V (gemessen gegen ges. Kalomelektrode) gefunden, während sich für die Reaktion

$$PtCl_6^{2-} + 4\,e \rightarrow Pt + 6\,Cl^-$$

ein Wert von $+0.44$ V errechnet[6-8].

Wegen der sehr niedrigen Pt-Konzentration und des hohen Überschusses von Cl^--Ionen ist das Potential allein schon stark nach negativen Werten verschoben. Dazu kommt wahrscheinlich eine erhebliche Überspannung, so dass man leicht in den Bereich der Wasserstoffabscheidung gelangt und zu kleine Pt-Mengen findet.

Eine Verbesserung trat durch Verwendung von Kaliumsulfat in 0.1 *M* Lösung ein. Nach Grube[9] finden bei der Elektrolyse von H_2PtCl_6 folgende Vorgänge statt:

$$PtCl_6^{2-} + 4\,e \rightarrow Pt + 6\,Cl^- \quad (1)$$

$$PtCl_6^{2-} + 2\,e \rightarrow PtCl_4^{2-} + 2\,Cl^- \quad (2)$$

$$PtCl_4^{2-} + 2\,e \rightarrow Pt + 4\,Cl^- \quad (3)$$

$$2\,H^{\bullet} + 2\,e \rightarrow H_2 \quad (4)$$

Ferner ist noch das Gleichgewicht

$$2\,PtCl_4^{2-} \rightleftharpoons PtCl_6^{2-} + Pt + 2\,Cl^- \quad (5)$$

zu berücksichtigen.

In einer chloridfreien Grundlösung soll die Reduktion nach (1) den Hauptanteil des Stromes verbrauchen, während die Reduktion nach (2) wegen des Gleichgewichtes (5) nur eine untergeordnete Rolle spielt. Die Stromausbeuten, bezogen auf Platinabscheidung, gibt Grube mit 70–90 % an. Die Differenz zu 100 % entfällt auf die Reduktion Pt^{4+} zu Pt^{2+} und die Wasserstoffabscheidung. Beide Prozesse werden durch erhöhte Wasserstoffionenkonzentration verstärkt.

Auch mit Kaliumsulfat als Leitelektrolyt gelang es nicht, geringere Platinkonzentrationen als 10^{-4} *M* coulometrisch zu bestimmen.

Nachdem die Verwendung anderer Elektrodenmaterialien als Arbeitselektrode (Glaskohle, Quecksilber u.a.) keine Verbesserung der Ergebnisse gebracht hatte, wurde zwecks weiterer Verminderung der Komplexbildung und der Negativierung des Pt-Abscheidungspotentials Natriumperchlorat als Leitelektrolyt geprüft.

Die günstigste Konzentration wurde zu 0.5 *M* ermittelt. Dadurch erhielt man einen ausgeprägteren Potentialabfall (Abb. 2). Für die Platinelektrode musste die

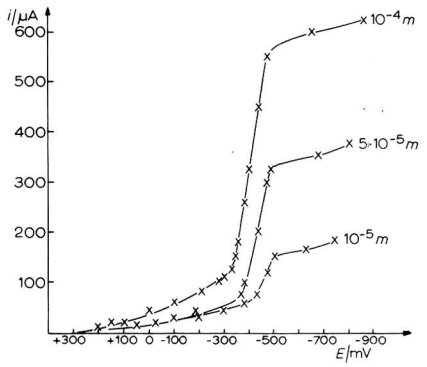

Abb. 2. Stromdichte–Potentialkurve von H_2PtCl_6-Lösungen verschiedener Konzentration in 0.5 *M* $NaClO_4$-Lösungen.

optimale Fläche und die günstigste Art der Oberflächenbehandlung gefunden werden. Die optimale Fläche wurde zu 1.5 cm^2 ermittelt. Die glatten Elektroden wurden in Königswasser kalt geätzt und in destilliertem Wasser ausgekocht.

Platinierte Elektroden schieden wegen der Gefahr einer Mitabscheidung von Wasserstoff aus. Bei der Verwendung heiss geätzter Platinelektroden entstanden grössere Plusfehler.

Das Abscheidungspotential wurde (in Übereinstimmung mit dem aus den Stromdichte–Potential-Kurven ermittelten Wert) schneller erreicht und blieb dann bis zur Beendigung der Abscheidung nahezu konstant (Abb. 3). Die Stromausbeuten

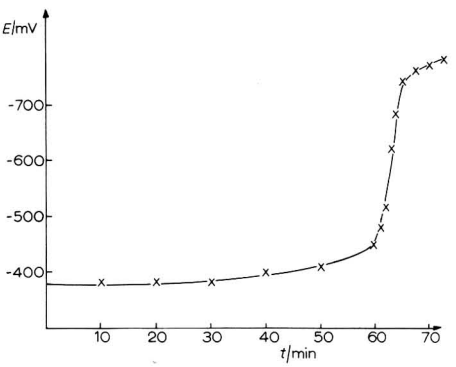

Abb. 3. Potential–Zeit-Kurve einer coulometrischen Pt-Bestimmung bei 100 μA in 10 ml 10^{-4} *M* H_2PtCl_6.

lagen hierbei zwischen 94 und 100%, bezogen auf die Pt-Abscheidung des vierelektronigen Prozesses nach Reaktion (1). Der erfasste Konzentrationsbereich reichte von 10^{-4}–10^{-6} *M* bei Elektrolyseströmen zwischen 100 und 5 μA. Da mit zunehmender Verdünnung der Elektrolysestrom gesenkt werden muss, kommt man unterhalb einer Konzentration von 10^{-6} *M* in einen Bereich, wo sich der Grundstrom störend bemerkbar macht. Die Aufnahme von Potential–Zeit-Kurven des Leitelek-

trolyten bei der kleinsten verwendeten Stromdichte dient dem Nachweis von etwaigen Verunreinigungen (Blindwert) und eines eventuell auftretenden Grundstromes (Abb. 4).

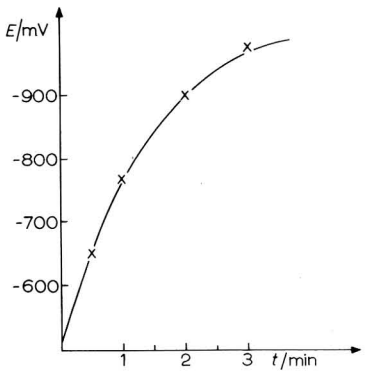

Abb. 4. Potential–Zeit-Kurve einer 0.5 *M* $NaClO_4$-Lösung bei 5 μA.

7. Pt-BESTIMMUNG DURCH SENKUNG DER WASSERSTOFFÜBERSPANNUNG

Nachdem die Erfassungsgrenze der coulometrischen Platinbestimmung ermittelt worden war, interessierte es, ob durch den bekannten Effekt der Herabsetzung der Wasserstoffüberspannung am Quecksilber durch geringe Platinmengen die Möglichkeit besteht, noch geringere Pt-Mengen als durch die Coulometrie zu bestimmen. Obwohl die kathodische Abscheidung elementaren Wasserstoffs eine der am häufigsten untersuchten elektrochemischen Reaktionen darstellt[10], ist die analytische Anwendung des Effektes der katalytischen Herabsetzung der Wasserstoffüberspannung noch immer unvollkommen[11].

Zur Durchführung der Versuche wurde die beschriebene Versuchseinrichtung benutzt. Als Leitelektrolyt diente 1 *N* Schwefelsäure, als Arbeitselektrode Quecksilber. Es wurden auch spezielle Messzellen erprobt, um geringere Flüssigkeitsmengen untersuchen zu können.

Bei einer konstanten Stromdichte (400 μA) wurden die Potentiale der Arbeits-

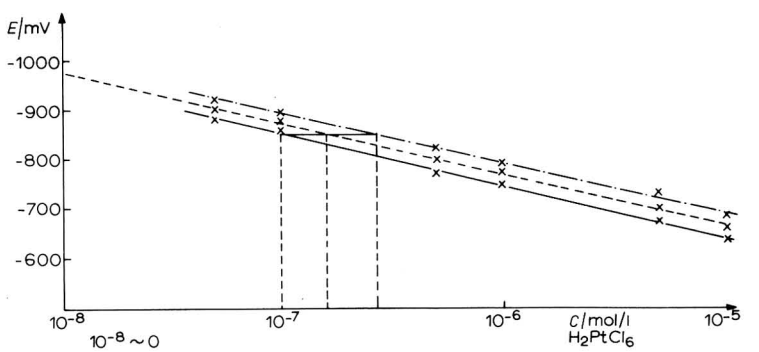

Abb. 5. Erniedrigung der Wasserstoffüberspannung an Quecksilber durch Platin. (–·–·–) Maximalwerte; (– – –) Durchschnittswerte; (——) Minimalwerte.

elektrode in verschiedenen Platinkonzentrationen gemessen. Trägt man die Potentialwerte als Funktion der Pt-Konzentration halblogarithmisch auf, so erhält man eine Gerade (Abb. 5). Die Potentiale konnten bei Wiederholungsmessungen mit einer Schwankung von etwa 50 mV reproduziert werden. Daraus resultiert eine wesentlich grössere Fehlerbreite als bei der coulometrischen Bestimmung. Wegen der grösseren Empfindlichkeit ist aber diese Methode zur Abschätzung kleinster Platingehalte zu gebrauchen. Die Erfassungsgrenze lag bei einer Konzentration von $5 \cdot 10^{-8}$ *M*. Da die geringste Flüssigkeitsmenge 0.25 ml betrug, konnten somit noch 0.002 μg Pt bestimmt werden.

8. ANWENDUNG DER AUSGEARBEITETEN METHODEN

Die Anwendung erstreckte sich auf die Bestimmung geringer Pt-Gehalte in bestimmten Gläsern. In diesen Gläsern waren folgende Komponenten enthalten: B_2O_3, SiO_2, BaO, Al_2O_3, Na_2O, K_2O, CaO, ZnO, TiO_2, La_2O_3, ThO_2, CdO, As_2O_3 und F. Der zweckmässigste Aufschluss der gemörserten Proben ist das Abrauchen mit Flusssäure in Korundschalen unter Berücksichtigung der für die Herstellung von H_2PtCl_6 geltenden Bedingungen. Nach entsprechenden Untersuchungen konnte ein Einfluss der Glaskomponenten auf die Pt-Bestimmung nicht festgestellt werden. Lediglich beim Titan ist zu beachten, dass es in der vierwertigen Form vorliegt, da es sonst zur Reduktion der H_2PtCl_6 kommt. Weiterhin wurde noch untersucht, ob der Aufschluss einen Einfluss auf die Pt-Bestimmung hat. Diese Untersuchungen wurden an einer Modellsubstanz sowie an absolut Pt-freien Glasproben durch Dotierungen mit bekannten Pt-Mengen durchgeführt.

9. ERGEBNISSE

Es ist möglich, mit Hilfe der galvanostatischen Coulometrie Platin zu bestimmen. Bei konstantem Strom wird das Platin, welches als Hexachloroplatinsäure vorliegt, an einer kalt geätzten Pt-Elektrode aus einer 0.5 *M* $NaClO_4$-Leitelektrolytlösung quantitativ abgeschieden. Aus der Strommenge $i \cdot t$ wird der Platingehalt

TABELLE 1

Pt-Konzentr./ Mol/l	*Elektrolytvol./ ml*	*vorgeg. Pt-Menge/ µg*	*Zahl der Bestimmungen*	*gefund. Pt-Menge (Mittelwert)/µg*	*Syst. Fehler/%*	*Standardabweichg./ %*
10^{-4}	10	198	10	194.57	−1.73	±2.41
$5 \cdot 10^{-5}$	10	99	10	97.6	−1.41	±2.33
10^{-5}	10	19.8	10	19.37	−2.17	±3.51
$5 \cdot 10^{-6}$	10	9.9	10	10.03	+1.33	±3.29
10^{-6}	10	1.98	10	1.95	−1.54	±6.15
10^{-6}	5	0.99	10	0.93	−6.67	±6.45
Modellsubst.	20	40	10	38.89	−2.77	±3.93
Pt vor Glas Aufschluss	10	20	5	19.16	−4.20	±4.75
Pt nach Glas Aufschluss	10	20	5	19.32	−3.40	±3.47

berechnet. Die Grenzkonzentration beträgt 10^{-6} *M* Pt. Bei einem Minimum des Arbeitsvolumens von 1 ml können somit noch 0.2 μg Pt bestimmt werden. Für verschiedene Konzentrationsbereiche wurde eine Fehlerermittlung durchgeführt (Tabelle 1).

Das Verfahren wurde auf die Bestimmung geringer Platingehalte in bestimmten Gläsern angewendet.

Orientierende Versuche ergaben, dass man den Effekt der Herabsetzung der Wasserstoffüberspannung am Quecksilber durch geringe Pt-Mengen ausnutzen kann, um sehr geringe Konzentrationen grössenordnungsmässig abzuschätzen. Bei einer Grenzkonzentration von $5 \cdot 10^{-8}$ *M* und einem Minimum des Arbeitsvolumens von 0.25 ml können hierbei noch 0.002 μg Pt erfasst werden.

ZUSAMMENFASSUNG

Durch galvanostatische Coulometrie lassen sich 0.2 μg Pt in 1 ml 10^{-6} molarer Lösung mit einer Standardabweichung von 6.5% bestimmen. Durch Bestimmung der Abnahme der Wasserstoffüberspannung an Quecksilber lassen sich noch Gehalte von 5×10^{-8} Mol l^{-1} Pt abschätzen.

SUMMARY

By galvanostatic coulometry it is possible to determine 0.2 μg of Pt in 1 ml of 10^{-6}-molar solution with a standard deviation of 6.5%. From the lowering of the hydrogen overpotential of mercury it is possible to estimate the content of 5×10^{-8} mol l^{-1} Pt.

LITERATUR

1 F. E. BEAMISH, *The Analytical Chemistry of the Noble Metals*, 1st edn., Pergamon Press, Oxford, 1966, S. 1, 10, 363, 454, 460, 464, 466, 488, 537.
2 K. ABRESCH UND I. CLAASSEN, *Die coulometrische Analyse*, Verlag Chemie, Berlin, 1961.
3 Näheres siehe Diplomarbeit G. SCHEIDHAUER, TU Dresden, Institut für Elektrochemie und physikalische Chemie, 1968.
4 F. R. MEYER UND G. RONGE, *Z. Angew. Chem.*, 52 (1939) 637.
5 *Gmelins Handbuch der anorg. Chem.*, 68, Teil C, S. 78.
6 *Gmelins Handbuch der anorg. Chem.*, 68, Teil B, S. 263.
7 W. M. LATIMER, *The Oxidation States of the Elements and their Potentials in Aqueous Solutions*, Prentice-Hall, New York, 1952, S. 206.
8 G. CHARLOT, J. BADOZ-LAMBLING UND B. TRÉMILLON, *Electrochemical Reactions*, Elsevier, Amsterdam–New York, 1962, S. 370.
9 G. GRUBE UND H. REINHARDT, *Z. Elektrochem.*, 37 (1931) 307.
10 W. FORKER, *Elektrochemische Kinetik*, Akad.-Verlag, Berlin, 1966, S. 61, 129, 130.
11 T. A. KRJUKOWA, S. I. SINJAKOWA UND T. W. AREFJEWA, *Polarographische Analyse*, Leipzig, 1964, S. 362.

ELECTROANALYTICAL CHEMISTRY AND INTERFACIAL ELECTROCHEMISTRY
Elsevier Sequoia S.A., Lausanne – Printed in The Netherlands

A NEW DEVICE FOR ANODIC STRIPPING VOLTAMMETRY

M. G. TAMBA AND N. VANTINI
Centro Sperimentale Metallurgico S.p.A., 00129, Roma (Italy)
(Received November 5th, 1969)

1. INTRODUCTION

The method of anodic stripping voltammetry, in its classical form, has hitherto attained limited practical acceptance because of the lack of commercial type electrodes of easy and rapid application. The essential features of such electrodes are, besides the constancy of their surface, the reproducibility at each stage of the method and their renewability. Among the several types of stationary mercury electrodes (except for film electrodes[1-5]) almost exclusive use has been made of hanging drop electrodes[6-8], which are still difficult in practical applications in spite of the various modifications which they have undergone[8-12].

Our attention has been focused on pool type electrodes[13-16] consisting essentially of the exposed area of mercury emerging from a cup support. Such electrodes are characterized by a remarkable ease of renewal, which we consider to be a fundamental feature for a wider practical development of anodic stripping voltammetry. The main purpose of the present work is the development of a particular cell and of a working method suitable for the determination of traces of amalgam-forming elements directly from the solution used to dissolve the sample, so avoiding the complex preliminary separations which make the polarographic method somewhat difficult to apply especially in metallurgical analysis. The technique investigated represents an improvement of classical anodic stripping voltammetry. Besides the two fundamental operations of the classic technique, electrodeposition and deamalgamation, it allows for some intermediate operations which improve the selectivity of the method.

The operations allowed are:

(a) Electrodeposition at controlled potential on a special mercury pool electrode flushed by a thoroughly deaerated stream of the appropriate solution used to dissolve the sample.
(b) Full replacement of the solution by the injection of a suitable differentiating standard electrolyte.
(c) Deamalgamation by a potential linearly increasing toward anodic values, while recording the dissolution current curve.

The latter stage may be preceded by an appropriate selective electrodissolution of interfering elements. This is possible owing to the peculiar design of the cell employed here, which allows either the electrodeposition or the replacement of solutions under such conditions that the working electrode is continuously flushed by a solution stream flowing from a capillary tube.

2. EXPERIMENTAL

2.1. *Apparatus and general procedure*

The cell* is outlined in Fig. 1. It is essentially constructed of a cylinder (1), having three side holes (2, 3 and 4) which, respectively, maintain a constant level of solution, evacuate the cell, and allow for the electrolytic connection with a large saturated calomel electrode through a particular salt bridge. From the slanted bottom (5) rises the support (6) for the mercury pool electrode (7) consisting of mercury coming from the reservoir (8) *via* the pipes (9) and (10) through the capillary tube (11). The shape and the dimensions of the working electrode are therefore determined by the cavity obtained within the cylindrical upper end of the support.

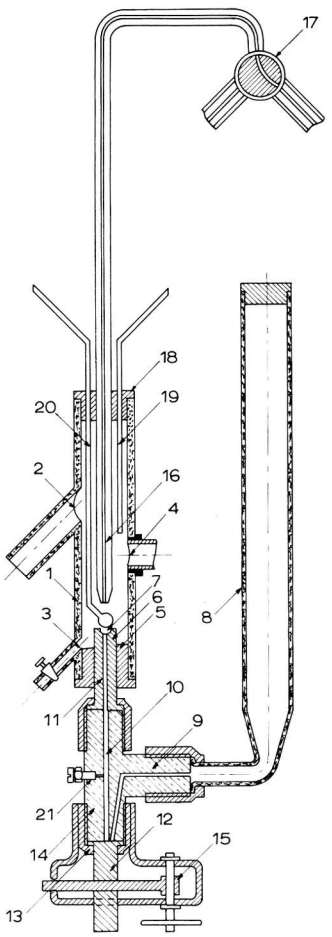

Fig. 1. Electrode and cell assembly.

* A Patent is pending on the device described in this paper.

The mercury supply is controlled through a special Teflon membrane valve, formed by a cylindrical stem (12), ending with a thin head of larger diameter, inserted in the joint (14). The valve is operated through the shaft (15), which produces small vertical displacements of the stem. The test solutions, as well as the differentiating solutions, conveniently deaerated, are fed through the calibrated tube (16) facing the working electrode and communicating with the solution reservoirs, through a two-way stop-cock with a Teflon plug (17). The cell cover (18) has three holes: the first one at the center lets the solution in through the capillary tube; the second allows the deaeration of the cell through the small pipe (19); the third is used as a guide for a glass rod (20) ending with a knob for the levelling of mercury and the preparation of the electrode before the experiments proper. The electrical contact is secured by a platinum wire (21).

For correct performance of the electrode, air bubbles must be avoided, and this is attained, in the first filling of both the reservoir and the portion below the valve, with the aid of vacuum pump. The electrode is so arranged, that it will work without interruption by the successive additions of mercury to the reservoir. In order to avoid a possible exchange between the test solution and the saturated calomel electrode, the salt bridge end of the reference electrode connected with the cell is shielded by a cellulose membrane.

For the measurements carried out with a potentiostat, the cell is also provided with a platinum wire counter electrode. In this work the available instruments were an Amel model 451 cathode ray polarograph with a scanning rate of 15 V/min and an Amel model 561 potentiostat.

The solution were always prepared with bidistilled water and reagent grade chemicals. The stream of solution was obtained by means of a calibrated capillary tube, 50 cm long and 1 mm diam, while the solution reservoir was kept at such a height that the solution level was about 75 cm. The capillary tip was about 5 mm away from the electrode surface.

2.2. *Results*

To study the behaviour of the proposed working electrode both Teflon and glass were tested as materials for the electrode support owing to their distinctly different properties. Pool electrodes with a Teflon support (2 and 3 mm diam.), were used to investigate the following factors affecting electrode reactions: potential scanning rate, temperature and time of electrolysis.

Measurements were carried out by means of the potentiostat on relatively concentrated solutions of Cd^{2+} and $Cd^{2+} + Pb^{2+}$ ($\geqq 10^{-4}$ *M*) in 2*M* KCl. For times up to 2 min the peak current *vs.* time of electrolysis followed a linear trend (Fig. 2). For a time of electrolysis of 5 min the values obtained were lower than the extrapolated values.

The effect of the scanning rate is shown in Fig. 3, together with the results obtained by the cathode ray polarograph with a scanning rate of 15V/min, which are reported in broken lines with a contracted current scale. In accordance with other workers[17], for rates in the range 0.1–1V/min, the validity of the equation for direct voltammetry giving a linear dependence of the peak current on the square root of the scanning rate is confirmed. In this range, no appreciable variation of the potential for different electrolysis times was detected. The value of the peak current for 15V/min

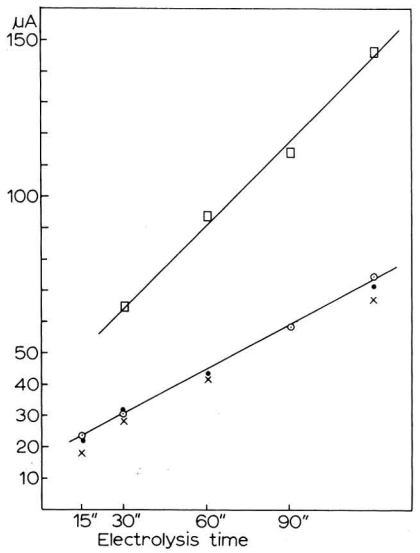

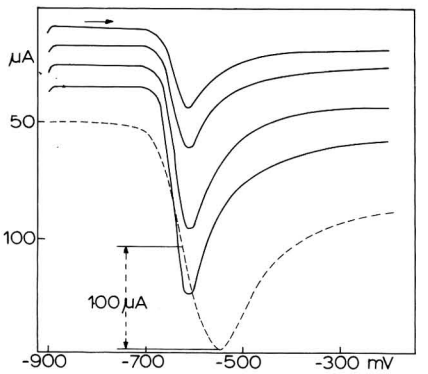

Fig. 2. Plot of peak height *vs.* electrolysis time. Teflon support 3 mm diam., scan rate 500 mV/min. (■) Cd^{2+} 10^{-3} *M*, (⊙) Cd^{2+} 5×10^{-4} *M*, (×) Cd^{2+} 5×10^{-4} *M* in presence of Pb^{2+} 5×10^{-4} *M*, (●) Pb^{2+} 5×10^{-4} *M* in presence of Cd^{2+} 5×10^{-4} *M*. The peak height for Cd^{2+} 5×10^{-4} *M* after 5 min electrolysis is 132 μA, waiting time 30 s, supporting electrolyte 2 *M*, KCl.

Fig. 3. Influence of the scanning rate on height and shape of peaks. Scanning rate from top: 0.1, 0.2, 0.5, 1, 15 V/min. Teflon support 3 mm diam., 5×10^{-4} *M* Cd^{2+} in 2 *N* KCl; electrolysis time 2 min, waiting time 30 s.

was lower than the value extrapolated by the results with lower scanning rates.

Typical anodic stripping curves carried out with the potentiostat for 5×10^{-4} *M* $Cd^{2+} + Pb^{2+}$ in 2*M* KCl are shown in Fig. 4. In such curves, beyond the Cd and Pb peaks, a current maximum appears which grows with increasing deposition time and prevents carrying out the electrolysis at a potential of −600 mV *vs.* SCE.

It is interesting to observe that such a noise disappeared also in the case of simultaneous separation of the two species by flushing with a 2*M* KCl solution after the electrodeposition and before the anodic stripping operations. Under such conditions, curves of better quality were obtained, as shown in Fig. 5a. It must be emphasized that this possibility presents a definite advantage of the method under investigation, which allows for one or more washing operations.

The curves shown in Fig. 5b were obtained by operating with 10^{-3} *M* solutions of Cd^{2+} in 2*M* KCl with the same electrode and with various times of electrolysis.

The reproducibility of the method may be derived from the data of Tables 1 and 2 obtained by operating with different solutions and under different electrolysis conditions.

The oscillograms shown in Fig. 6 relate to experiments with a 10^{-6} *M* solution. The influence of room temperature (*ca.* 25° C) variations upon peak currents was 2–3%° C.

Considerable shifts in peak potential were found at the upper scanning rate (15V/min) mainly as a function of the time of electrolysis rather than to concentration effects[18,19].

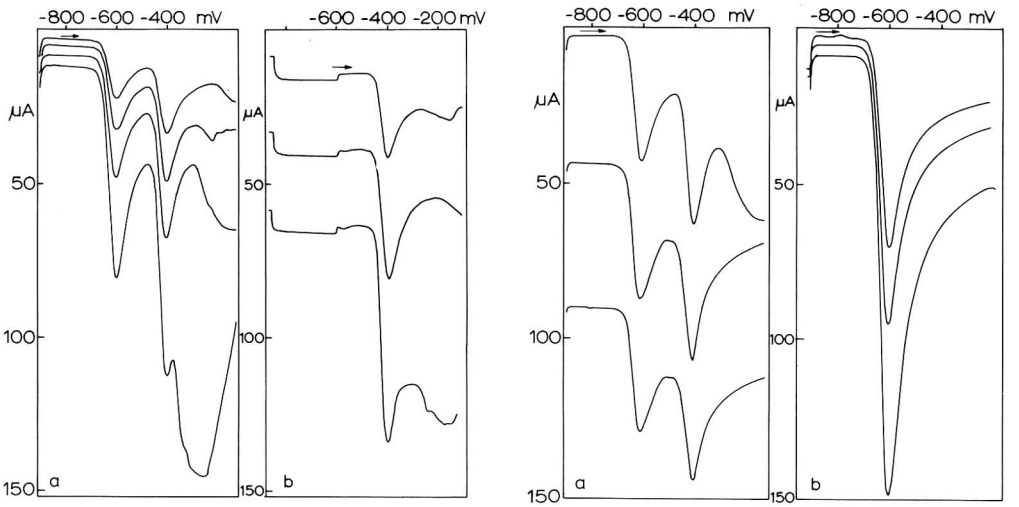

Fig. 4. Anodic curves for 5×10^{-4} *M* $Cd^{2+} + 5 \times 10^{-4}$ *M* Pb^{2+} in 2 *M* KCl. Teflon support 3 mm diam. (a) Electrolysis potential −900 mV; electrolysis time from the top: 15 s, 30 s, 60 s, 120 s. (b) Electrolysis potential −600 mV; electrolysis time from the top: 30 s, 60 s, 120 s.

Fig. 5. (a) 5×10^{-4} *M* $Cd^{2+} + 5 \times 10^{-4}$ *M* Pb^{2+} in 2 *M* KCl, electrolysis time 1 min, electrolysis potential −900 mV. The second and the third curve from the top were obtained after the electrode was flushed for 3 min and 1 min with 2 *M* KCl. (b) 10^{-3} *M* Cd^{2+} in 2 *M* KCl, electrolysis time from the top: 30 s, 60 s, 120 s.

With the Teflon support it was not possible to reactivate the electrode by carrying out an electrolysis at the dissolution potential of the formerly discharged element. By performing a subsequent experiment, according to the usual procedure using the same electrode so renewed, a reduced current peak (about 10%) was obtained. This suggests that during the anodic dissolution stage, rather insoluble compounds are formed at the surface, or the electrode undergoes an "ageing" through polarization or other phenomena which may be due to insufficient purity of mercury, to impurities coming from the solution, the salt bridge or the cell, or to traces of oxygen[20-25]. The best results were obtained by means of a glass support.

A series of measurements was performed, using an electrode support of the type

TABLE 1

REPRODUCIBILITY EXPERIMENTS CARRIED OUT WITH THE POTENTIOSTAT (500 mV min^{-1})

Cd^{2+} 5×10^{-4} *M* + Pb^{2} 5×10^{-4} *M*, 2 *M* KCl, Teflon support 3 mm diam., electrolysis potential −900 mV, waiting time 30 s.

Time of electrolysis/s	*No. of experiments (n)*	*Cd*		*Pb*	
		$\bar{h}_p/\mu A$	s^a	$\bar{h}_p/\mu A$	s^a
30	8	29.28	2.10	32.50	2.50
60	22	42.05	3.42	46.50	4.30
120	6	68.33	3.38	—	—

[a] s = standard deviation

TABLE 2

REPRODUCIBILITY EXPERIMENTS CARRIED OUT WITH POTENTIOSTAT (500 mV min^{-1}) AND WITH CATHODE RAY POLAROGRAPH (15 mV min^{-1})
Teflon support 3 mm in diam., electrolysis potential −900 mV, waiting time 30 s.

Concn. Cd^{2+} in 2 M KCl	*Time of electrolysis/s*	*No. of experiments (n)*	$\bar{h}_p/\mu A$	s^a
10^{-3} (potentiostat)	30	9	65.14	4.81
10^{-3} (potentiostat)	60	17	94.30	4.86
10^{-6} (cathode ray-polarograph)	120	19	0.39	0.014

[a] s = standard deviation.

which we had previously and successfully investigated in direct voltammetry, applied to an ion–ion process[26]. By using a glass pipe 3 mm diam. as support in the device shown in Fig. 1, the variation of the peak potential with increase in the time of electrolysis was considerably reduced. Peak height appeared to be a linear function of the ion concentration in the solution in a larger range of electrolysis times (see Fig. 7). Moreover, only with such a support, could peaks of the same height be obtained either by renewing the electrode mechanically in the usual way, or electro-

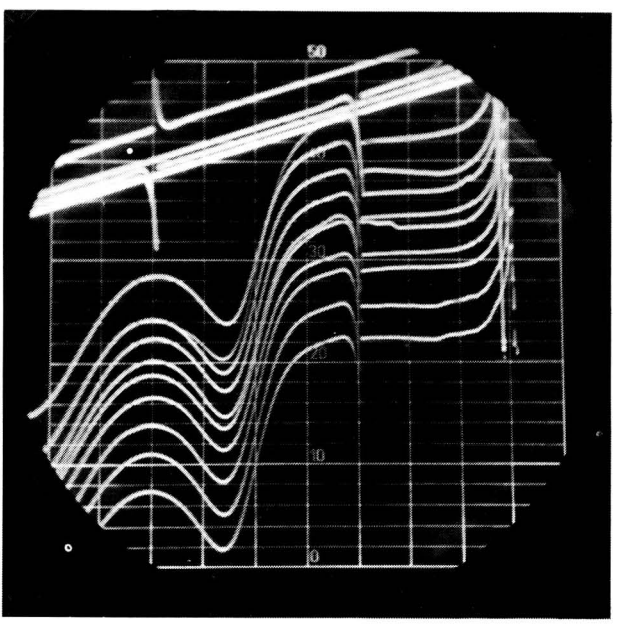

Fig. 6. Voltammetric curves for $CdCl_2$ 10^{-6} *M* in 2 *M* KCl obtained with the Teflon support 3 mm diam., electrolysis time 2 min, waiting time 30 s, voltage range −900–400 mV, sensibility 0.02 μA/div., marker position −760 and −560 mV, electrode mechanically renewed before each measurement.

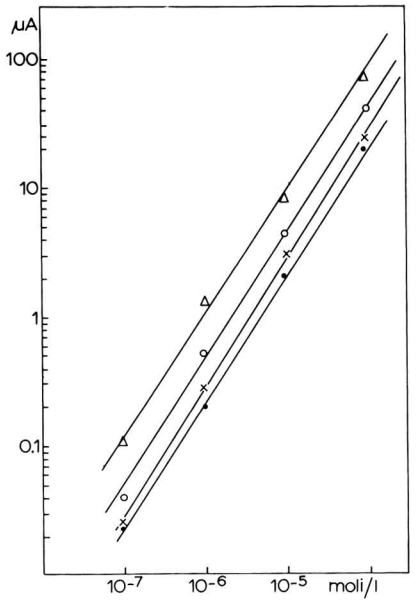

Fig. 7. Peak height *vs.* Cd^{2+} concn. for various electrolysis times. Supporting electrolyte 2 *M* KCl, glass support 3 mm in diam., electrolysis time (●) 15 s, (×) 30 s, (○) 2 min, (▲) 5 min.

lytically as previously described. A considerable improvement in the operating conditions was also obtained and it became possible and easy to deal with concentrations of the order of 10^{-8} moles l^{-1}. A series of typical oscillograms obtained with several electrolysis times is shown in Fig. 8.

3. DISCUSSION AND CONCLUSIONS

From the experiments performed it appears that in any case the essential feature of the electrode is the good reproducibility. An interesting result obtained while investigating the most favourable test conditions was the elimination of interferences (especially evident when using the Teflon support) by replacing the electrolyte by means of a stream of solution. In this connection it should be noted that, while it is possible to limit the sensitivity loss due to the diffusion of the relevant element toward the inner part of the electrode, this intermediate flushing operation can produce a considerable improvement in the quality of the curves. The elimination of the said interference through "flushing" is suggested as the means of solving several problems connected with precipitation phenomena at the surface or with the "ageing" of the electrode. These phenomena, in spite of much published work, are still not sufficiently clear. As to the "ageing" process characteristic of the Teflon support, we may formulate essentially three hypotheses:

(a) the effective electrode surface is reduced, independently of eventual chemical or electrochemical processes, by coverage with impurities coming from the mercury, the support, or the solutions;

(b) the electrode is altered as a consequence of chemical reactions;

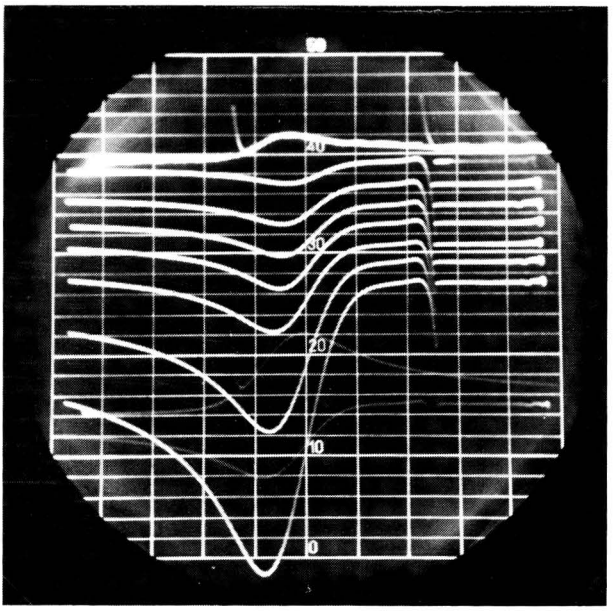

Fig. 8. Voltammetric curves for Cd^{2+} 10^{-5} *M* in 2 *M* KCl obtained with glass support 3 mm diam. Range of potential −900–400 mV, electrolysis time: 0, 15 s, 30 s, 1 min, 2 min, 5 min, 10 min, sensibility 0.5 μA/div., marker position −800 and −600 mV, electrode mechanically renewed before each measurement.

(c) the electrode, owing to the applied potential, undergoes polarization in contact with the electrolyte.

The three hypotheses seem to be reasonable and could explain the observed effects: the impossibility of renewing the electrode through the electrodissolution of the species under test at the required potentials; the potential shift during the electrolysis; the irregular trend of the calibration curve within a large concentration interval (4 orders of magnitude).

The first and second hypotheses might be supported by the electrode reactions suggested by Meites[27]:

$$4\,Hg + O_2 + 4\,H^+ = 2\,Hg_2^{2+} + 2\,H_2O$$

$$2\,Hg + Pb^{2+} + 2\,Cl^- + \tfrac{1}{2}O_2 + H_2O = Hg_2Cl_2 + Pb(OH)_2$$

and by Kolthoff[28], concerning the reaction of mercury with oxygen and chloride ions in non-buffered media:

$$O_2 + 2\,Hg + 2\,Cl^- + 2\,H_2O \rightleftarrows H_2O_2 + Hg_2Cl_2 + 2\,OH^-$$

However, our observations did not support such hypotheses because no variation of the peak heights and of the respective potentials appeared in direct voltammetric measurements, even if prior to each run the waiting times with the cell switched off were prolonged.

The trend of the curves, peak current *vs.* concentration, depends upon the particular type of electrode support. This fact further substantiates the third hypo-

thesis and moreover indicates that oxygen probably has considerable influence upon electrode polarization.

In fact, it is clear that at the interface mercury–support, the elimination of oxygen appears the more difficult the coarser and the more hydrophobic the cup surface, as is the case with Teflon supports.

Consequently, we suggest that the electrode "ageing" is mainly caused by electrode reactions, suggested by Dahms[25]:

$$O_2 + 2\,H_2O + 4\,e^- = 4\,OH^-$$

$$2\,OH^- + Me^{2+} = Me(OH)_2$$

or by the series of reactions suggested by Vetter[14]:

$$O_2 + 2\,H^+ + 2\,e^- \rightleftarrows H_2O_2$$

$$H_2O_2 + Me^{2+} + 2\,e^- = Me(OH)_2$$

or by those reported by Kemula[24]:

$$Me^{\bullet\bullet}\,(Hg) + \tfrac{1}{2}O_2 + H_2O = Hg + Me^{2+} + 2\,OH^-$$

$$Me^{\bullet\bullet}\,(Hg) + Hg^{2+} = Hg + Me^{2+}$$

The better results obtained with the glass support for the mercury pool electrode are probably due therefore to the surface properties of the glass.

The reproducibility of the electrode and its easy handling are the main advantages of the method. These features encourage a wider practical application of anodic stripping voltammetry. Moreover, the full replacement of the solution by the injection of a suitable differentiating electrolyte allows some electrode interferences to be eliminated, thus increasing the selectivity of the method. The possiblity of operating intermediate flushing substantially improves the quality of the voltammetric curves.

The continuous renewal of the solution avoids troublesome vibrations produced by mechanical stirring and makes it possible to operate directly on the solutions used to dissolve the samples. Owing to the ease of constructing identical electrodes of this type, such electrodes could be suitable for differential polarography.

SUMMARY

A technique for the determination of amalgam-forming elements based on a new device allowing the continuous replacement of the solution was developed. Such a method makes it possible to increase the selectivity, to eliminate completely troublesome vibrations due to mechanical agitation and to operate directly on solutions used for dissolution. Two different types of materials: Teflon and glass, were tested as electrode support. The glass support gave the better results. Electrodes made with this support are easily reproducible and allow the analysis of solutions as dilute as 10^{-8} mol l^{-1}. A linear calibration curve for Cd^{2+} as wide as four order of magnitude was obtained.

Some interesting electrode phenomena occurring with the Teflon supports are discussed.

REFERENCES

1 S. A. MOROS, *Anal. Chem.*, 34 (1962) 1584.
2 W. T. DE VRIES, *J. Electroanal. Chem.*, 9 (1965) 448.
3 M. S. ZAKHAROV AND L. F. TRUSHINA, *J. Anal. Chem. USSR, English Transl.*, 21 (1966) 129.
4 A. I. KAMENEV AND E. N. VINOGRADOVA, *J. Anal. Chem. USSR, English Transl.*, 21 (1966) 282.
5 V. A. IGOLINSKII, *Ind. Lab. USSR, English Transl.*, 32 (1966) 1301.
6 H. GERISCHER, *Z. Physik. Chem. Leipzig*, 202 (1953) 302.
7 T. BERZINS AND P. DELAHAY, *J. Am. Chem. Soc.*, 77 (1955) 6448.
8 W. KEMULA AND Z. KUBLIK, *Anal. Chim. Acta*, 18 (1958) 104.
9 R. KALVODA, *Zavodsk. Lab.*, 24 (1958) 1319.
10 V. CERMAK, *Collection Czech. Chem. Commun.*, 24 (1959) 831.
11 J. RIHA, *Progress in Polarography*, Vol. II, Interscience, New York, 1962, p. 386.
12 Z. KOWALSKI, *J. Electroanal. Chem.*, 21 (1969) 9.
13 P. ARTHUR, J. C. KOMYATHY, R. F. MANESS AND H. W. VAUGHAN, *Anal. Chem.*, 27 (1955) 895.
14 D. J. ROSIE AND W. D. COOKE, *Anal. Chem.*, 27 (1955) 1360.
15 J. W. ROSS, R. D. DE MARS AND J. SHAIN, *Anal. Chem.*, 28 (1956) 1768.
16 P. V. PEURIFOY AND W. G. SCHRENK, *Anal. Chem.*, 29 (1957) 410.
17 J. G. NIKELLY AND W. D. COOKE, *Anal. Chem.*, 29 (1957) 933.
18 A. HICKLING, J. MAXWELL AND J. V. SHENNAN, *Anal. Chim. Acta*, 14 (1956) 287.
19 I. M. KOLTHOFF AND Y. OKINAKA, *Progress in Polarography*, Vol. II, Interscience, New York, 1962, p. 373.
20 E. N. VINOGRADOVA AND G. V. PROKHOROVA, *Ind. Lab. USSR, English Transl.*, 26 (1960) 40.
21 A. G. STROMBERG AND V. E. GORODOVYKH, *Ind. Lab. USSR, English Transl.*, 26 (1960) 44.
22 C. H. YARNITSKY AND M. ARIEL, *J. Electroanal. Chem.*, 10 (1965) 110.
23 T. KUWANA AND R. N. ADAMS, *Anal. Chim. Acta*, 20 (1959) 51.
24 W. KEMULA AND J. W. STROJEK, *J. Electroanal. Chem.*, 12 (1966) 1.
25 M. DAHMS, *J. Electroanal. Chem.*, 8 (1964) 5.
26 S. MANESCHI AND N. VANTINI, *J. Polarog. Soc.*, 12 (1966) 44.
27 L. MEITES, *Polarographic Techniques*, Vol. II, Interscience, New York, 1965, p. 65.
28 I. M. KOLTHOFF AND J. J. LINGANE, *Polarography*, Vol. II, Interscience, New York, 1952, p. 554.

ELECTROANALYTICAL CHEMISTRY AND INTERFACIAL ELECTROCHEMISTRY
Elsevier Sequoia S.A., Lausanne – Printed in The Netherlands

THIOCYANATE ELECTROCATALYSIS OF THE REDUCTION OF In(III)

LUBOMÍR POSPÍŠIL* AND ROBERT DE LEVIE
Department of Chemistry, Georgetown University, Washington, D.C. 20007 (U.S.A.)
(Received October 21st, 1969)

INTRODUCTION

The polarographic reduction of In(III) from aqueous thiocyanate solutions exhibits curious behavior. In concentrated thiocyanate solutions, a pronounced polarographic minimum is observed, and the corresponding a.c. polarogram features negative resistive and capacitive components. We have already given the formal description of these phenomena[1,2], but the underlying molecular mechanism was not quite understood at the time. We will discuss the latter in the present communication.

It is useful first to review the available evidence in a qualitative manner. In solutions containing only perchlorate, nitrate or sulfate ions, the reduction of aquoindium ions is extremely slow, and at pH $\gtrsim 2$ proceeds almost exclusively *via* hydrolysis products, most probably[3,4] $In(H_2O)_4(OH)_2^+$. Millimolar additions of thiocyanate ions, as well as of halides or several organic anions, strongly catalyze the reduction[5,6]. Apparently, this catalysis proceeds *via* anions adsorbed on the electrode, because the currents decrease as the potential is made progressively more negative. With increasing catalyst concentration, *e.g.* in 0.01–0.1 *M* NaSCN, the polarographic reduction current becomes diffusion-limited. At still higher thiocyanate concentrations, the current first reaches a diffusion-limited plateau, but subsequently exhibits a minimum. The latter can again be ascribed to catalyst desorption at negative electrode charge densities. The fact that the reduction rate decreases at high thiocyanate concentrations suggests that the electrocatalytic reduction proceeds *via* In^{3+} and/or $InSCN^{2+}$.

An additional clue can be found in our observation[1], that the a.c. and d.c. polarograms in 1 *M* NaSCN lead to the same rate constants. This can only mean that the wave exhibiting the d.c. polarographic minimum is not superimposed on a regular d.c. polarographic limiting current. In other words, one and the same reduction process is involved in both a.c. and d.c. polarograms.

EXPERIMENTAL

In concentrated ($\geqq 0.5$ *M*) solutions, rate constants for the reduction of In(III) from acidified solutions (pH $\leqq 3$) were obtained from d.c. polarograms, using the approximate eqn. (34) of ref. 1, and from a.c. polarograms using eqn. (33) of the same

* On leave from the J. Heyrovský Polarographic Institute of the Czechloslovak Academy of Sciences in Prague.

paper. For the diffusion coefficient D we have assumed a value of 6×10^{-6} cm^2 s^{-1}. This choice is inconsequential as long as the value of D does not vary markedly with the thiocyanate concentration, *i.e.* as long as all thiocyanato-indium(III) complexes in solution have about the same diffusion coefficients.

In more dilute solutions, in which the d.c. polarogram features a diffusion-limited current, the rate constants can be obtained only from the a.c. polarogram, see Fig. 1. At still lower thiocyanate concentrations, the d.c. polarographic currents are

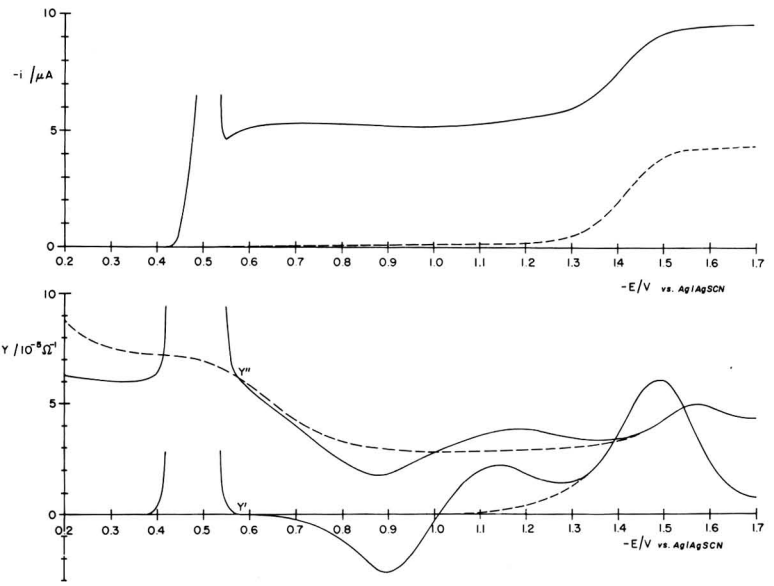

Fig. 1. Polarogram (top) of 1 mM $In(SCN)_3$ in 0.1 M NaSCN acidified with HSCN to pH 3.22, and the inphase and quadrature components (bottom) of the electrode admittance of the same soln., measured with a 16.4 Hz sine wave of 10 mV amplitude. The dashed lines indicate the response of the same soln. in the absence of $In(SCN)_3$. Note that there is virtually no minimum in the polarogram, but that the negative faradaic admittance still allows quantitative evaluation of the reduction rate constant.

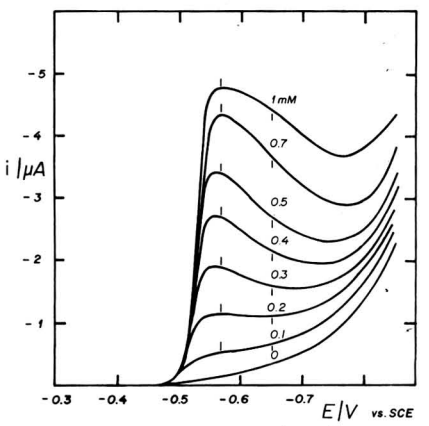

Fig. 2. Polarograms of 1 mM $In(ClO_4)_3$ in 0.1 M $NaClO_4$, 0.05 M $HClO_4$ with varying amounts of NaSCN; NaSCN concn. indicated in mM. The diffusion-limited current, observed with 0.1 M NaSCN, was -5.88 μA. Short vertical lines indicate data used for Fig. 9.

again controlled by the slow electrode reaction, and can be used for the evaluation of rate constants, see Fig. 2. In the more dilute solutions, the pH was lowered to about 1.3 in order to suppress hydrolysis. The resulting hydrogen reduction wave restricted the range of potentials over which rate constants could be measured with sufficient accuracy. All d.c. and a.c. polarograms were obtained on an instrument described earlier[7].

RESULTS

The measured rate constants reflect the combined effect of two variables: an electrical parameter governing the reduction rate itself; and a chemical one, regulating the reacting species. Since adsorbed thiocyanate is apparently involved in the reduction process, an obvious plot is that of log k *vs.* log Γ, where Γ is the surface excess of SCN^- at the potentials E at which the reduction rate constants k were measured. At these potentials, the oxidation rate is negligibly small[1]. Values of Γ were taken from Minc and Andrzejczak[8].

As can be seen in Fig. 3, no simple correlation[9] between k and Γ is evident. If

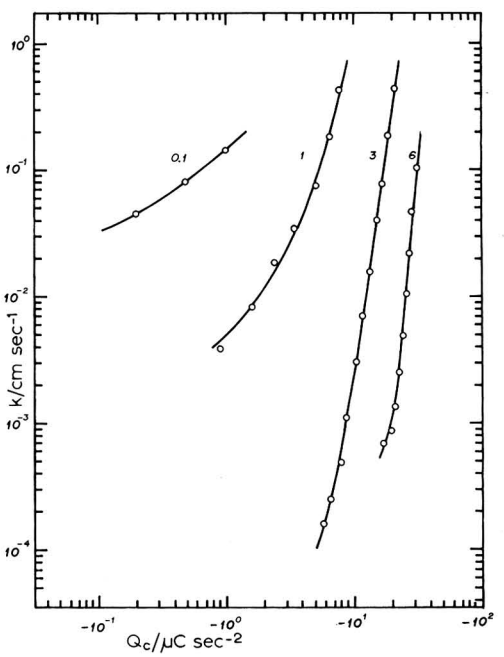

Fig. 3. The measured reduction rate constant k as a function of the charge density Q_c of specifically adsorbed thiocyanate ions, for different NaSCN concns. as indicated (in M).

we try to describe the data of Fig. 3 *via* an equation of the type $k = k_0\Gamma^n$, then values of n range all the way from 0.7 in 0.1 M NaSCN to 12 in 6 M NaSCN. An exponential relationship[10] of the type $\log k = \log k_0 + aF\Gamma$ fares somewhat better, see Fig. 4, but still shows a distinct variation of a-values, *viz.* ~0.6, 0.27, 0.21 and 0.18 $cm^2\ \mu C^{-1}$ for 0.1, 1, 3 and 6 M, respectively.

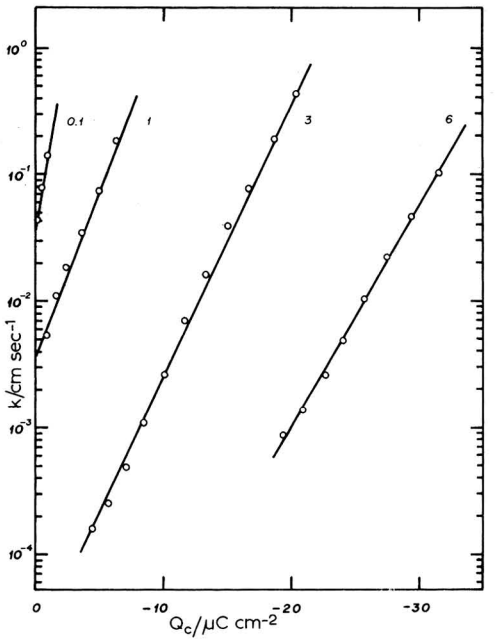

Fig. 4. The same parameters, k and Q_c, as in Fig. 3, but now in a semi-logarithmic representation.

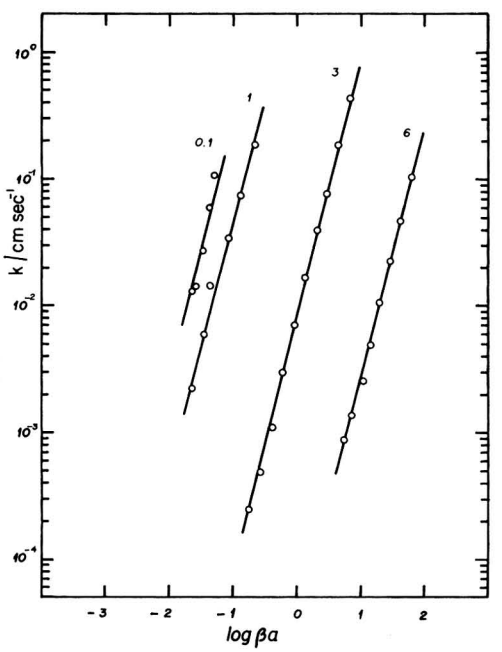

Fig. 5. The measured reduction rate constant k as a function of the surface activity βa of adsorbed thiocyanate ions, for different NaSCN concns. (indicated in M). All lines are drawn with slope 2.

Since the rate-limiting step in the reduction mechanism obviously is a slow reaction involving adsorbed thiocyanate ions, the pertinent parameter to use is the activity rather than the surface excess of the adsorbed thiocyanate. Fortunately, the surface activity βa of adsorbed thiocyanate was determined by Minc and Andrzejczak[8]. These authors showed that the adsorption of thiocyanate ions can be described quantitatively by the Frumkin adsorption isotherm[11], and that β is a linear function of the electrode charge density Q_e. The latter property is especially useful because it allows us to extrapolate the data to more negative charge densities Q_e where direct measurements are inaccurate or impossible.

In Fig. 5 we have plotted log k *vs.* log βa as calculated from Minc's data[8]. As can be seen, all data can be represented accurately by lines of slope 2, indicating that two adsorbed thiocyanate ions are involved in the rate-limiting step.

So far, we have not considered any double layer correction[12]. In order to verify whether such a correction would modify our conclusion, we have calculated the "outer Helmholtz" potential ϕ for 3 M and 6 M NaSCN from Minc's data[8], using[13]

$$\phi = 0.0514 \operatorname{arc\,sinh} \frac{Q_d}{11.72 c^{\frac{1}{2}}} \tag{1}$$

to relate the potential ϕ (in V) to the charge density Q_d (in μC cm^{-2}) in the diffuse double layer for a given thiocyanate concentration c (M). The value of Q_d was obtained from the electroneutrality condition

$$Q_c + Q_d + Q_e = 0 \tag{2}$$

where Q_c is the specifically adsorbed charge density (in the compact double layer) and Q_e the (electronic) charge density on the metal. For 0.1 M and 1 M NaSCN, ϕ potentials obtained in a similar fashion were kindly made available by Dr. Parsons. In Fig. 6, the resulting values of ϕ are seen to be essentially constant and, indeed, rate

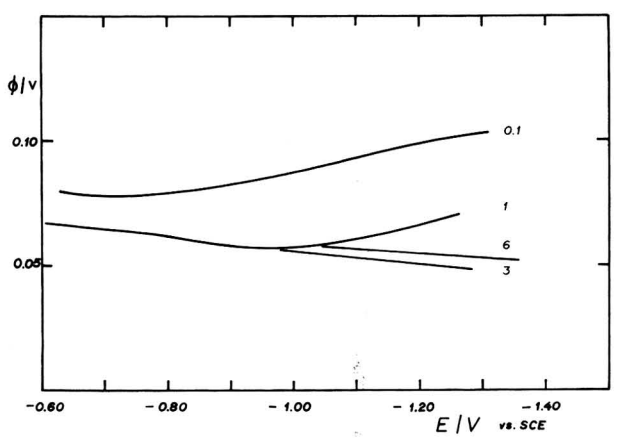

Fig. 6. Double layer potentials ϕ for solutions of different NaSCN concns. (indicated in M) vary little with potential in the range of potentials in which the rate constants were obtained: from about -0.9 to -1.1 V *vs.* SCE for 0.1 M NaSCN, from -0.95 to -1.2 V for 1 M NaSCN, and for the ranges shown in the more concentrated NaSCN solns.

constants corrected for the double layer potential using

$$k_{corr} = k \exp\left[\frac{zF\phi}{RT}\right] \tag{3}$$

yield plots of log k_{corr} *vs.* βa of slope 2 for all reasonable values of z, *i.e.* for $z = +3, +2, +1, 0, -1$ and -2. Comparison of Fig. 5 (corresponding to $z = 0$) and Fig. 7 ($z = +3$)

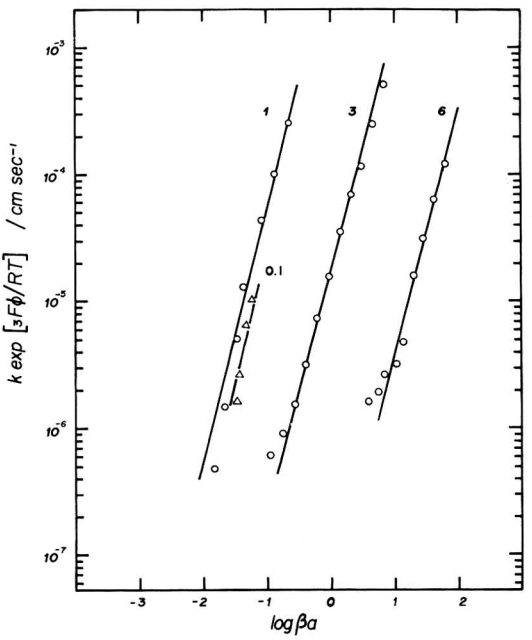

Fig. 7. Rate constants corrected for $z = +3$ yield essentially the same functional dependence on thiocyanate surface activity βa as the uncorrected data of Fig. 5, with the exception of the 0.1 *M* data. Lines are drawn with slope 2.

shows that the double layer correction greatly affects the numerical values of the rate constants, but not their functional dependence on either βa (slope of the curves) or bulk thiocyanate concentration (distance between curves). As the latter two are the parameters of importance in the elucidation of the reaction mechanism, and also since it is not self-evident anyway what value(s) of z should be used in the double layer correction, we will use the uncorrected, directly measured rate constants.

Now that we have established the dependence of the rate constant on the catalyst activity βa, we can compare rate data at constant βa in order to find the identity of the reacting indium species. The vertical distances between the lines of Fig. 5 yield the four points of Fig. 8, with a limiting slope (at low $pSCN^-$) of about 5. These data can be compared with logarithmic concentration diagrams[14-16] based on published equilibrium constants. Sundén[17] reports evidence for complexes $In(SCN)_n^{(3-n)+}$ where $n = 0, 1, 2$ and 3, with $pK_3 = 1.03$, so that Fig. 8 should yield a limiting slope of 3 when In^{3+} is the reacting species, slope 2 for $InSCN^{2+}$, etc. Golub and Samoilenko[18] reported evidence for complexes up to $n = 4$, with $pK_4 = 0.06$, yielding a limiting slope

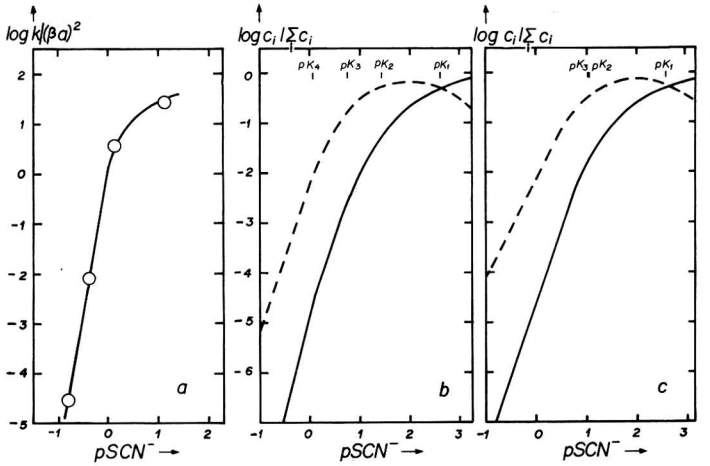

Fig. 8. Reduction rate constants at constant thiocyanate activity βa, as a function of bulk thiocyanate concn. (a), and logarithmic concn. diagrams for In^{3+} (straight line) and $InSCN^{2+}$ (broken line) according to the data of Golub and Samoilenko[18] (b) and Sundén[17] (c).

of 4 for In^{3+}, 3 for $InSCN^{2+}$, etc. Equilibrium constants for complexes up to $n=6$ have been reported by Radhakrishnan and Sundaram[19], but we do not consider their polarographic data to be as reliable as those obtained from potentiometric titrations. At any rate, the reliability of pK_n values obtained by either technique is always poor for large values of n and, moreover, activity corrections may be quite appreciable in 3 *M* and 6 *M* NaSCN. We therefore conclude that the *most likely* reacting species is In^{3+}.

Equilibrium data are much more reliable in very dilute thiocyanate solutions. For low thiocyanate concentrations, the hexaquo indium ion, In^{3+}, is the predominant one. Unfortunately, a non-complexing acid like $HClO_4$ or HNO_3 must be added in order to suppress hydrolysis, and the specific adsorption of perchlorate or nitrate

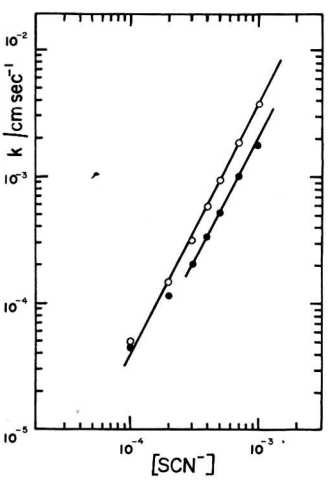

Fig. 9. Reduction rate constants obtained at -0.565 (○) and -0.650 (●) V *vs.* SCE from the polarograms shown in Fig. 2, as a function of thiocyanate concn. The lines are drawn with slope 2.

anions from the necessarily fairly concentrated solutions of their acids is not at all negligible compared to that of sub-millimolar concentrations of NaSCN. In view of these difficulties, the following rather crude experiment was performed (*cf.* ref. 6).

To a 0.05 *M* $HClO_4$, 0.1 *M* $NaClO_4$, 1 m*M* $In(ClO_4)_3$ solution, small amounts of 0.1 *M* NaSCN were added, varying the thiocyanate concentration between 0.1 and 1 m*M*. From the resulting d.c. polarograms, Fig. 2, the rate constants were obtained, using the diffusion-limited current as observed in the same solution with $[SCN^-] = 0.1$ *M*, and eqn. (34) of ref. 1. The resulting rate constants at $E = -0.565$ and -0.650 V *vs.* SCE are shown in Fig. 9. Clearly, the rate constants are proportional to $[SCN^-]^2$.

In the above, very dilute thiocyanate solutions, the surface activity is proportional to the surface excess, which again is proportional to the bulk concentration $[SCN^-]$. Consequently, the observation that the reduction rate at very low concentrations is proportional to $[SCN^-]^2$ reinforces our conclusion that In^{3+}, not $InSCN^{2+}$ or $In(SCN)_2^+$, is the reacting species. Had $InSCN^{2+}$ been the (only) reacting species, then k would have been proportional to $[SCN^-]^3$ in this experiment.

DISCUSSION

1. The experiments described above are consistent with the following reduction mechanism:

$$In^{3+} + 2\ SCN^-_{ads} \xrightarrow[\text{slow}]{} In(SCN)^+_{2\ ads} \qquad (4)$$

$$In(SCN)^+_{2\ ads} + 3e^- \xrightarrow[\text{fast}]{} In^0 + 2\ SCN^- \qquad (5)$$

Since the thiocyanate ions released in reaction (5) are generated right at the electrode surface, it is most probable that they are readsorbed immediately. The resulting reaction sequence is thus truly electrocatalytic in that both the bulk and interfacial concentrations of thiocyanate remain unchanged during the reaction, and only hexaquoindium ions are converted into indium atoms in the amalgam. Since the electron transfer step, reaction (5), is so much faster than reaction (4), it is not surprising that no experimental evidence was found[1] for the adsorption of any In(III) species at potentials negative of the polarographic wave.

2. From the strong dependence of the reduction rate on the thiocyanate concentration, at constant βa, we have concluded that it is unlikely that $InSCN^{2+}$ is reduced, see Figs. 5 and 8. Certainly we can rule out the possibility that $In(SCN)_2^+$ is reduced. This brings up the interesting question why a transient $In(SCN)_2^+$ species, formed at the electrode interface, is readily reduced, whereas the bulk species $In(SCN)_2^+$ appears to be electrochemically inert.

It would be tempting to ascribe this peculiar behavior to possible differences between sulfur- and nitrogen-bonded thiocyanate ions. Most likely, SCN^- is sulfur-bonded to the mercury surface, so that reaction (4) would produce the nitrogen-bonded dithiocyanato indium(III) complex. If the bulk species were the sulfur-bonded isomer, the differences in behavior could be readily explained.

Although such an explanation would appear quite plausible for the isolated case of thiocyanate catalysis, it is difficult to reconcile it with the observation that hali-

de ions catalyze the reduction of In(III) in what appears to be a very similar way. Measurements on halide catalysis, especially with Br^- and I^- where the catalytic effect is quite marked, are now under way in this laboratory, in order to clarify this point.

3. Electrocatalysis appears to be a fairly common mechanism, even on a mercury electrode. Heyrovsky[20] noticed the rate-enhancing effect of the presence of chloride ions in many polarographic reductions. Aikens and Ross[21] showed conclusively that halides catalyze the oxidation of Cr(II). The marked effect of halides on the reduction of Zn(II) has been studied quantitatively by Sluyters *et al.*[10,22]. In the latter two cases, the electrocatalyzed reaction appears to proceed in parallel with the uncatalyzed one, which makes the analysis more complicated. In the present case of the thiocyanate-catalyzed reduction of indium, there is only one reaction pathway. This has enabled us to elucidate the mechanism and to demonstrate also the importance of surface activity, βa, rather than of surface excess Γ. Of course, βa differs much more from Γ for SCN^- than for Cl^-, which also was a fortunate circumstance.

4. Electrocatalytic reduction of In(III) has been observed with a number of anions. Similar anion electrocatalysis has been observed in this laboratory[23] with other cations, *e.g.* Ni(II), Sn(IV), V(V) and Mo(VI), and with a variety of catalyzing anions. Unfortunately, it is thermodynamically impossible[24] to obtain surface excesses and the corresponding surface activities for anions of weak acids like oxalate (which appears to be a quite effective electrocatalyst for most of the above cations).

5. The interpretation given above for the reduction of In(III) from thiocyanate solutions differs in a number of aspects from those of other investigators. The correlation of reaction rate with surface activity βa (rather than[9] with surface excess Γ), which we believe to have established firmly in the present case, appears to be a novel one.

Our interpretation differs even more from that given recently by Sluyters *et al.*[25]. The occurrence of a minimum, *i.e.* a decreasing reduction rate with increasingly negative potentials, is not usually expected within the framework of the Volmer-Erdey Grúz formalism. Since, in that formalism, the potential-dependence of electrode reactions is expressed in terms of a transfer coefficient α, one could formally describe[26] the peculiar behavior of In(III) in NaSCN as resulting from a negative value of α. Alternatively, one can postulate[25] that the standard rate constant k_{sh} is potential-dependent but that the transfer coefficient is not. There seems to be little justification for such a postulate and, moreover, the values obtained in this way for the potential-dependent standard rate constant depend on the arbitrarily assumed values of the transfer coefficient[27].

Our interpretation does not require such postulates, and provides a simple mechanism consistent with all observations reported. The decrease in rate constant, at increasingly negative electrode potentials, is simply due to increasing coulombic repulsion between the electrode and the adsorbed anions[28].

6. We have only investigated the region of negative charge transfer resistance, since in that region the electrocatalytic reduction can be studied most conveniently. At still more negative potentials, the reduction rate increases again. This always coincides with the reduction of H^+ (*cf.* ref. 1, Fig. 4) and is therefore simply due to the formation of hydrolyzed, and hence reducible, indium species near the electrode interface. In the region of the polarographic wave, around $E_{\frac{1}{2}}$, the normal increase in net reduction rate with increasingly negative potential is superimposed upon the

simultaneously decreasing catalyst activity.

7. The sequence of heterogeneous reactions given in eqns. (4) and (5) is analogous to homogeneous electron transfer *via* double ligand bridging. Such bridging has been reported[29,30] with azide, which is isoelectronic with SCN^-. Unfortunately, at the low pH necessary to avoid indium hydrolysis, azide is converted into hydrazoic acid, which is not catalyzing the indium reduction[5]. Double ligand bridging seems to be the exception rather than the rule in homogeneous electron transfer reactions, and this may hold for electrocatalysis as well.

ACKNOWLEDGEMENTS

This research was supported by the Air Force Office of Scientific Research (OAR, USAF) under grant 68-1344, by the National Science Foundation under grant GP 8575, and by the Office of Naval Research under contract N00014-69-A-0220-0002. This manuscript is submitted for publication with the understanding that the United States Government is authorized to reproduce and distribute reprints for governmental purposes.

SUMMARY

The slow step in the thiocyanate-catalyzed electro-reduction of In(III) on Hg has been identified as the surface reaction of In^{3+} with two adsorbed thiocyanate ions. This appears to be the only reaction pathway available in thiocyanate solutions when the pH is sufficiently low to prevent hydrolysis. The reaction rate is proportional to the square of the surface activity βa of adsorbed SCN^-.

REFERENCES

1 R. DE LEVIE AND A. A. HUSOVSKY, *J. Electroanal. Chem.*, 22 (1969) 29.
2 R. DE LEVIE AND L. POSPÍŠIL, *J. Electroanal. Chem.*, 22 (1969) 277.
3 A. I. MOLODOV AND V. V. LOSEV, *Elektrokhimiya*, 1 (1965) 651.
4 J. G. LAWSON AND D. A. AIKENS, *J. Electroanal. Chem.*, 15 (1967) 193.
5 A. J. ENGEL, J. G. LAWSON AND D. A. AIKENS, *Anal. Chem.*, 37 (1965) 203.
6 M. A. LOSHKAREV AND A. A. KAZAROV, *Elektrokhimiya*, 3 (1967) 39.
7 R. DE LEVIE AND A. A. HUSOVSKY, *J. Electroanal. Chem.*, 20 (1969) 181.
8 S. MINC AND J. ANDRZEJCZAK, *J. Electroanal. Chem.*, 17 (1968) 101.
9 N. TANAKA, T. TAKEUCHI AND R. TAMAMUSHI, *Bull. Chem. Soc. Japan*, 37 (1964) 1435.
10 P. TEPPEMA, M. SLUYTERS-REHBACH AND J. H. SLUYTERS, *J. Electroanal. Chem.*, 16 (1968) 165.
11 A. N. FRUMKIN, *Z. Physik*, 35 (1926) 792.
12 A. N. FRUMKIN, *Z. Physik. Chem.*, 164A (1933) 121.
13 D. C. GRAHAME, *Chem. Rev.*, 41 (1947) 441.
14 L. G. SILLÉN, *Treatise Anal. Chem.*, I, 1 (1959) 277.
15 J. N. BUTLER, *Ionic Equilibrium*, Addison-Wesley, Reading (Mass.), 1964.
16 R. DE LEVIE, *J. Chem. Educ.*, in press.
17 N. SUNDÉN, *Svensk Kem. Tidskr.*, 66 (1954) 50.
18 A. M. GOLUB AND V. M. SAMOILENKO, *Ukr. Khim. Zh.*, 29 (1963) 472.
19 T. P. RADHAKRISHNAN AND A. K. SUNDARAM, *J. Electroanal. Chem.*, 5 (1963) 124.
20 J. HEYROVSKÝ, *Discussions Faraday Soc.*, 1 (1947) 212.
21 D. A. AIKENS AND J. W. ROSS, *J. Phys. Chem.*, 65 (1961) 1213.
22 M. SLUYTERS-REHBACH, J. S. M. C. BREUKEL AND J. H. SLUYTERS, *J. Electroanal. Chem.*, 19 (1968) 85.

23 J. C. KREUSER AND R. DE LEVIE, in preparation.
24 E. BLOMGREN AND J. O'M. BOCKRIS, *J. Phys. Chem.*, 63 (1959) 1475.
25 M. SLUYTERS-REHBACH, B. TIMMER AND J. H. SLUYTERS, *Z. Physik. Chem. Frankfurt*, 52 (1967) 89.
26 R. TAMAMUSHI, Paper presented at 19th CITCE meeting, Detroit, Sept. 1968; extended abstracts p. 106.
27 B. TIMMER, M. SLUYTERS-REHBACH AND J. H. SLUYTERS, *J. Electroanal. Chem.*, 19 (1968) 73.
28 D. COZZI AND S. VIVARELLI, *Z. Elektrochem.*, 57 (1953) 408; 58 (1954) 907.
29 R. SNELLGROVE AND E. L. KING, *J. Am. Chem. Soc.*, 84 (1962) 4609.
30 A. HAIM, *J. Am. Chem. Soc.*, 88 (1966) 2324.

ELECTROANALYTICAL CHEMISTRY AND INTERFACIAL ELECTROCHEMISTRY
Elsevier Sequoia S.A., Lausanne – Printed in The Netherlands

ON THE ELECTROCHEMICAL OSCILLATOR

R. DE LEVIE
Department of Chemistry, Georgetown University, Washington, D.C. 20007 (U.S.A.)
(Received September 29th, 1969)

INTRODUCTION

In a recent series of papers[1-3] we have elucidated both the mathematical formalism and the molecular mechanism of the ligand-catalyzed electroreduction of indium(III). In short, we have found[1] that there is a range of potentials in which this reaction exhibits a negative charge transfer resistance R_{ct}, and we have shown, both experimentally and theoretically, that a negative charge transfer resistance results in a negative diffusion impedance[1,2], which contributes an additional negative resistance and negative capacitance to the equivalent circuit. Finally, we have demonstrated[3] that these phenomena are caused by a rather simple reaction mechanism, whereby the reduction of indium ions proceeds only through ligand electrocatalysis, the ligand being adsorbed on the electrode interface and the slow step being the combination reaction of the indium species with the adsorbed ligand.

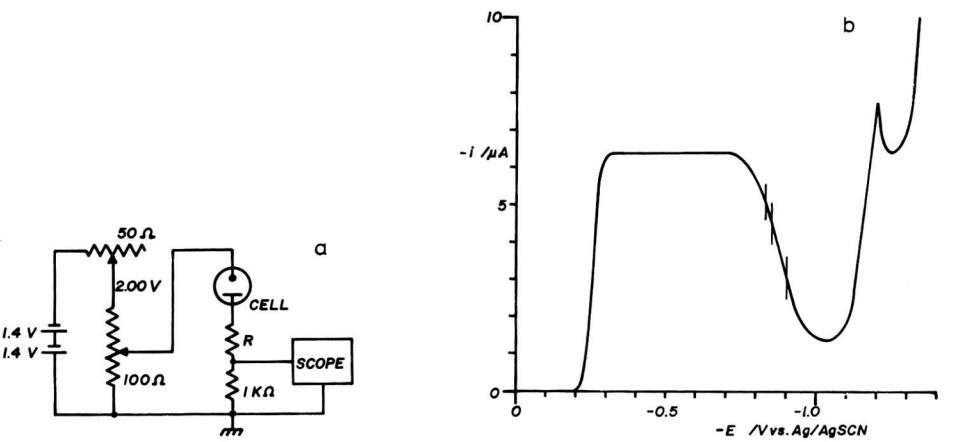

Fig. 1. (a) The circuit used for the observations reported in Figs. 2, 3, 4 and 9. The voltage source consists of two D-size mercury batteries. The potential across a precision wirewound ten-turn potentiometer (Bourns 500 S-1-101) is adjusted to 2.00_0 V with the aid of a 50 Ω carbon potentiometer (Clarostat 53 C 1). R is an adjustable decade resistor bank (General Radio 1434 G); the current is monitored across a 1-KΩ 1% metal-film resistor. Cell solution: 1.2 m*M* $In(NO_3)_3$ in 5 *M* NaSCN, pH adjusted to 3.6 with HNO_3. Negative electrode: dropping mercury electrode (for Figs. 2–4) or hanging mercury drop (Metrohm E 410). Positive electrode: Ag/AgSCN. Oscilloscope: Hewlett Packard 1200 B, scope trace photographed with Hewlett Packard 197 A camera on Polaroid 107 film. (b) Polarogram of the solution used, showing the potentials at which the pictures of Figs. 2–4 were taken.

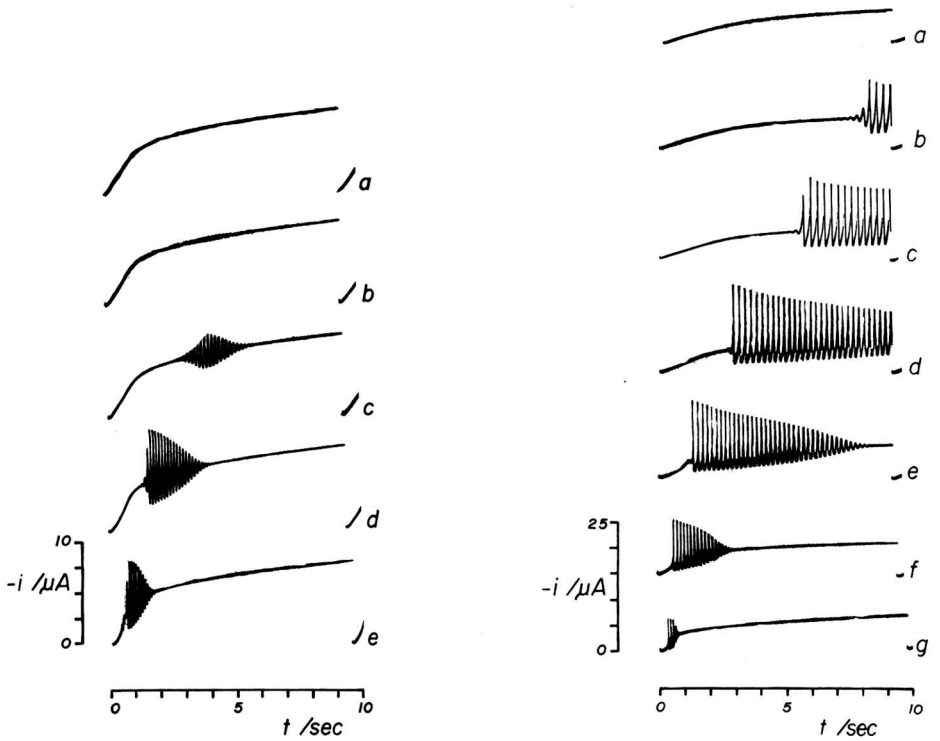

Fig. 2. Current–time curves observed on a dropping mercury electrode at −0.830 V *vs.* Ag/AgSCN in 1.2 m*M* $In(NO_3)_3$, 5 *M* NaSCN at pH 3.6. External resistance (apart from the 1-KΩ measuring resistor and the output impedance of less than 50 Ω of the voltage source) 15, 15.5, 16, 20 and 30 KΩ, respectively, in (a)–(e). With decade box resistances of less than 15 KΩ, the curves obtained are identical with that of (a).

Fig. 3. Current–time curves like those of Fig. 2, but observed at −0.850 V and with decade box resistance values of 10.5, 11, 12, 15, 20, 30 and 50 KΩ, respectively, in (a)–(g).

It is clear that a system which exhibits both a negative resistance and a negative capacitance, in combination with positive (solution) resistance and (double layer) capacitance, is capable of spontaneous oscillations, without any additional, external reactive (capacitive or inductive) components. Indeed, such spontaneous oscillations are easily observable in the circuit of Fig. 1a, and Figs. 2–4 depict several of the observed wave shapes. For reference, the corresponding d.c. polarogram is given in Fig. 1b.

THE NATURE OF A NEGATIVE IMMITTANCE*

On the basis of the relationship between current and voltage, one can distinguish between linear and non-linear devices. A linear device exhibits a strict proportionality between applied potential and resulting current. Examples of such devices are resistors, for which the proportionality is quite obvious, or capacitors and induc-

* Following Bode[4], we will use the term immittance to denote either an impedance or an admittance, whenever the discussion is applicable to either one.

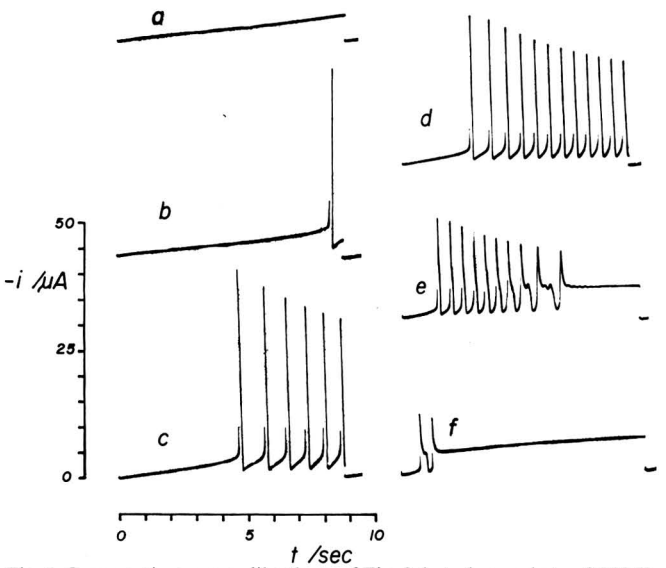

Fig. 4. Current–time curves like those of Fig. 2, but observed at −0.900 V and with decade box resistances of 10, 11.3, 15, 20, 30 and 50 KΩ, respectively, in (a)–(f).

tors, whose responses are linear but time-dependent. Almost all other electronic devices, like vacuum tubes and semiconductor junctions (diodes, transistors) exhibit non-linear behavior. For these devices, a current–voltage curve is usually recorded, and the admittance Y or impedance Z are defined at any specified potential or current as

$$Y = \frac{\mathrm{d}i}{\mathrm{d}E} \qquad Z = \frac{\mathrm{d}E}{\mathrm{d}i} = \frac{1}{Y} \tag{1}$$

For instance, a tunnel diode or a spark discharge have current–voltage curves of the general shape of Fig. 5a, and consequently exhibit a negative immittance* in the interval between E_1 and E_2, see Figs. 5b and 5c. Note that a negative immittance does not imply that a positive voltage would drive a negative current or *vice versa*, since eqn. (1) only defines the *slope* of the current–voltage curve. This distinction can be made more explicit by defining the integral immittances

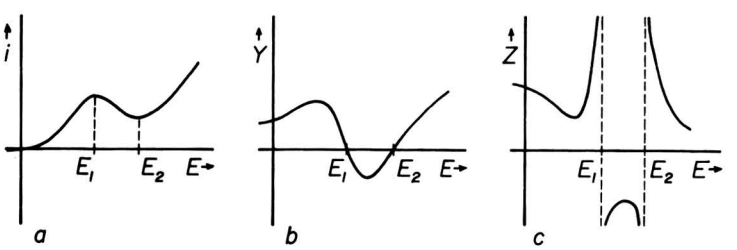

Fig. 5. An N-shaped current–voltage curve (a) exhibiting a region of negative slope between E_1 and E_2. The corresponding admittance Y and impedance Z are indicated schematically in (b) and (c).

* Following Bode[4], we will use the term immittance to denote either an impedance or an admittance, whenever the discussion is applicable to either one.

$$Y_{\text{int}} = \frac{i}{E} \qquad Z_{\text{int}} = \frac{E}{i} = \frac{1}{Y_{\text{int}}} \tag{2}$$

by analogy with the differential and integral double layer capacitance[5]. A negative integral immittance would bring us in conflict with thermodynamics, but not so a negative (differential) immittance. The electrode immittance certainly behaves like a non-linear device, and current–voltage curves of the general shape of Fig. 5a are not at all uncommon.

Of course, stability and instability are dynamic rather than static concepts, which require a discussion of the transient, time-dependent behavior, *e.g.*, *via* the impedance function. The above discussion is intended only to illustrate the meaning of negative resistances or conductances. For a more detailed understanding, steady-state curves like those of Fig. 5a, even when adorned with load lines, do not appear to be overly useful.

CONDITIONS FOR OSCILLATION

It appears that systems which generate spontaneous oscillations always contain negative immittance elements. However, although the presence of a negative immittance seems to be a necessary requirement for oscillatory behavior, it certainly is not a sufficient one. In a general, physical sense, an undamped oscillation requires an element of negative resistance in order to compensate for energy dissipation in unavoidable positive resistances in the circuit. Also, at least two "containers" in which energy can be stored, out of phase with one another, appear to be necessary, so that the energy can be shifted back and forth between them, giving rise to the oscillation[5,9]. For example, in an LC oscillator, the energy is stored alternately in the electric field of the capacitor C and in the magnetic field of the inductor L, while an electronic device (vacuum tube or transistor) provides the negative resistance. No oscillation results when either the capacitance or the inductance is left out, illustrating that a negative resistance *per se* is insufficient to sustain an undamped oscillation. In an RC feedback oscillator, the positive feedback generates the equivalents of both a negative resistance and a negative capacitance, whence the possibility of oscillation.

The electrochemical system discussed in this paper, *viz.* the electrocatalyzed reduction of In(III), exhibits a negative charge transfer resistance R_{ct} over a considerable range of electrode potentials[1]. As a consequence of the coupling between interfacial and diffusional immittances[2], the (Warburg) diffusion immittance is also negative. The 45° phase shift of the diffusion immittance (for semi-infinite, plane diffusion) thus results in an additional negative resistance and negative capacitance. Together with the usual, positive solution resistance and double layer capacitance, the combination of a negative charge transfer resistance and a negative diffusion immittance contains all the elements necessary for an undamped oscillation.

Now that we have indicated the conceptual, physical conditions for oscillatory behavior, we will proceed to a strict, mathematical formulation. The criterion for oscillation can be taken immediately from general electrical circuit theory[6]. Let us write the impedance function $Z(s)$ by substituting s for $j\omega$ in the usual expression for the circuit impedance. Then the circuit will oscillate when, at a zero of $Z(s)$, s has a zero or positive real part as well as a non-zero imaginary component. In terms of the admittance function $Y(s)$, the same criterion applies to the poles of $Y(s)$. In a physical

sense, the above criterion can be understood by noting that the zeros of $Z(s)$ or the poles of $Y(s)$ correspond to solutions of the differential equation governing the potentials and currents in the circuit. These solutions can be written in terms of factors $\exp[st] = \exp[(\sigma \pm j\omega)t]$, where σ is the real and ω the imaginary part of s, t is time and $j=(-1)^{\frac{1}{2}}$. Thus, an undamped oscillation, initially of frequency ω, will result when $\sigma \geqslant 0$ and $\omega > 0$.

In view of the fact that graphical representations of the cell impedance[7] are now quite commonly used in electrochemical investigations, a graphical criterion is sometimes more convenient. Such a criterion, which follows from the above properties of zeros of $Z(s)$ and poles of $Y(s)$ in the complex s plane, was derived by Llewellyn[8,9], and can be formulated as follows: the system will be stable if the locus of $Z(j\omega)$ encircles the origin of the complex cell impedance plane in a counter-clockwise direction as the frequency is continuously varied from $-\infty$ to $+\infty$. In electrochemical impedance representations, which usually deal with positive resistances and capacitances, it is customary to plot the *negative* imaginary impedance axis (capacitive axis) as the positive ordinate, *i.e.* pointing upwards. In such a representation, the Llewellyn criterion of course corresponds to stability when the origin is encircled in a clockwise direction. The requirement that ω be varied from $-\infty$ to $+\infty$ need not worry us, since the value of $Z(-j\omega)$ is simply the conjugate complex of the corresponding value of $Z(+j\omega)$, and consequently $Z(-j\omega)$ can be drawn immediately (see dashed curves in Fig. 6) when $Z(j\omega)$ has been determined experimentally.

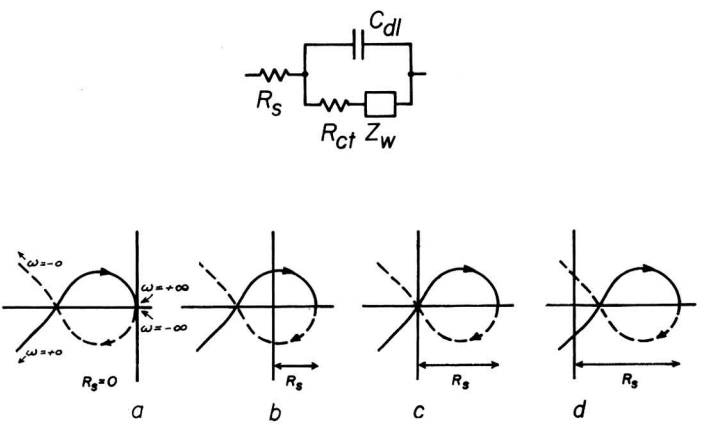

Fig. 6. The equivalent circuit (top) of an electrochemical (half-) cell with series resistance R_s, double layer capacitance C_{dl}, charge transfer resistance R_{ct} and Warburg (diffusion) impedance Z_w. The complex impedance plane representation of this circuit, for negative R_{ct} and consequently negative Z_w, and for different values of R_s, is depicted in (a)–(d). The circuit is stable in (a) and (b), but unstable in (c) and (d).

It might be emphasized here that the Llewellyn criterion indicates stability, but that the lack of stability does not necessarily imply oscillatory behavior. In fact, the Llewellyn criterion is equivalent to the condition that s has a negative real part, $\sigma < 0$. For oscillatory behavior it is not only necessary that $\sigma \geqslant 0$, but also that $\omega \neq 0$, *i.e.* that s has a non-zero imaginary part. If $\sigma \geqslant 0$ and $\omega = 0$, instability without oscillation will occur, resulting in a unidirectional shift of potential and/or current until limited by non-linearity of the circuit.

The following mechanical analogue may illustrate the difference between instability and oscillatory behavior. An unsuspended weight is unstable, and will fall down, converting potential energy into kinetic energy, until it hits the floor. A weight suspended from an off-balance, frictionless pendulum will also be unstable, but its downward motion will be oscillatory since it can convert potential energy back and forth into kinetic energy.

The extreme simplicity of the application of Llewellyn's criterion is illustrated in the following example. We have previously reported[2] the electrode impedance $Z(j\omega)$ of indium in thiocyanate solutions in the region of potentials in which this system exhibits a negative charge transfer resistance, see Fig. 6a. Upon addition of a sufficiently large positive resistance R_s in series with the electrode, the system moves from stable (Figs. 6a, 6b) to unstable (Figs. 6c, 6d) behavior. In the two latter cases, oscillations may or may not occur; they are impossible under the conditions of Figs. 6a and 6b. Additional illustrations of the usefulness of the Llewellyn criterion in electrochemical circuit analysis are given in the Appendix.

MATHEMATICAL ANALYSIS

We will now analyze the real and imaginary components of s at the zeros of $Z(s)$. We have shown[1] that the combination of plane diffusion and a first-order electrode reaction, $R \rightleftharpoons O + ne$, results in a cell impedance which can be represented accurately by the equivalent circuit of Fig. 6 as long as the impedance of the auxiliary electrode is so small as to be negligible. Here, R_s is the series resistance of solution, electrode and external circuit, C_{dl} is the double layer capacitance, and R_{ct} is the charge transfer resistance. The latter can be positive, negative or zero, and is given by

$$R_{ct} = (nFA)^{-1} \left\{ c'_R \frac{\partial \vec{k}}{\partial E} - c'_O \frac{\partial \overleftarrow{k}}{\partial E} \right\}^{-1} \tag{3}$$

where $\vec{k}$ and $\overleftarrow{k}$ are the rate constants for oxidation and reduction, respectively, whereas c'_R and c'_O are the average surface concentrations of R and O respectively, F is the Faraday and A the electrode area. The (Warburg) diffusion impedance Z_w is given[2] by*

$$Z_w = R_{ct} z (j\omega)^{-\frac{1}{2}} \tag{4}$$

$$z = \vec{k} D_R^{-\frac{1}{2}} + \overleftarrow{k} D_O^{-\frac{1}{2}} \tag{5}$$

Thus, the impedance of the circuit of Fig. 6 is

$$Z(j\omega) = R_s + \frac{R_{ct}[(j\omega)^{\frac{1}{2}} + z]}{j\omega R_{ct} C_{dl}[(j\omega)^{\frac{1}{2}} + z)] + (j\omega)^{\frac{1}{2}}} \tag{6}$$

and the impedance function $Z(s)$ is obtained from eqn. (6) by substituting s for $j\omega$:

$$\begin{aligned} Z(s) &= R_s + \frac{R_{ct}(s^{\frac{1}{2}} + z)}{sR_{ct}C_{dl}(s^{\frac{1}{2}} + z) + s^{\frac{1}{2}}} \\ &= \frac{R_s R_{ct} C_{dl} s^{\frac{3}{2}} + R_s R_{ct} C_{dl} zs + (R_s + R_{ct}) s^{\frac{1}{2}} + R_{ct} z}{R_{ct} C_{dl} s^{\frac{3}{2}} + R_{ct} C_{dl} zs + s^{\frac{1}{2}}} \end{aligned} \tag{7}$$

* In the notation of ref. 2, $z = \zeta(2\omega)^{\frac{1}{2}}$.

Apart from the trivial solution $R_s=0, s\rightarrow\infty$ (see Fig. 6a), the zeros of $Z(s)$ follow from the cubic equation in $s^{\frac{1}{2}}$

$$s^{\frac{3}{2}}+zs+\frac{R_s+R_{ct}}{R_sR_{ct}C_{dl}}s^{\frac{1}{2}}+\frac{z}{R_sC_{dl}}=0 \tag{8}$$

the roots of which are given by:

$$\begin{aligned}&\{-b+(a^3+b^2)^{\frac{1}{2}}\}^{\frac{1}{3}}+\{-b-(a^3+b^2)^{\frac{1}{2}}\}^{\frac{1}{3}}-\frac{z}{3}\\&-\tfrac{1}{2}(1-j\sqrt{3})\{-b+(a^3+b^2)^{\frac{1}{2}}\}^{\frac{1}{3}}-\tfrac{1}{2}(1+j\sqrt{3})\{-b-(a^3+b^2)^{\frac{1}{2}}\}^{\frac{1}{3}}-\frac{z}{3}\\&-\tfrac{1}{2}(1+j\sqrt{3})\{-b+(a^3+b^2)^{\frac{1}{2}}\}^{\frac{1}{3}}-\tfrac{1}{2}(1-j\sqrt{3})\{-b-(a^3+b^2)^{\frac{1}{2}}\}^{\frac{1}{3}}-\frac{z}{3}\end{aligned} \tag{9}$$

with

$$\begin{aligned}a&=\frac{R_s+R_{ct}}{3R_sR_{ct}C_{dl}}-\frac{z^2}{9}\\b&=\frac{z^3}{27}-\frac{z(R_s+R_{ct})}{6R_sR_{ct}C_{dl}}+\frac{z}{2R_{ct}C_{dl}}\end{aligned} \tag{10}$$

The necessary and sufficient condition for instability is that the magnitudes (absolute values) of the real parts of the complex roots in eqn. (9) are equal to, or larger than the magnitudes of their imaginary parts, in which case the corresponding values of $s^{\frac{1}{2}}$ lie

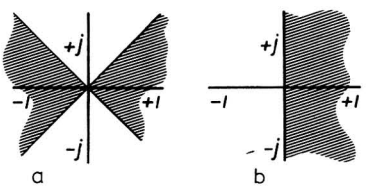

Fig. 7. The roots of eqn. (8) plotted in the complex plane (left), and the corresponding values of s (right), fall in the shaded half-space if the system is unstable.

in the shaded area in the complex plane of Fig. 7a, and consequently s lies in the shaded area in Fig. 7b, which corresponds with the condition $\sigma\geqslant 0$. The special case in which the real and imaginary components of the roots of eqn. (8) have equal magnitudes is that of a small-amplitude, perfectly harmonic oscillation ($\sigma=0$), and the special case in which the roots have no imaginary part corresponds to non-oscillatory instability. On a dropping mercury electrode, the diffusion impedance Z_w need only be considered when it contributes measurably to the electrode admittance at frequencies higher than $1/\tau$, where τ is the droptime. If this is not the case, then the equivalent circuit can be simplified to that of Fig. 8, again assuming a sufficiently large auxiliary electrode. The corresponding impedance is

$$Z(j\omega)=R_s+\frac{R_{ct}}{1+j\omega R_{ct}C_{dl}} \tag{11}$$

$$Z(s)=R_s+\frac{R_{ct}}{1+sR_{ct}C_{dl}}=\frac{R_sR_{ct}C_{dl}s+R_s+R_{ct}}{1+sR_{ct}C_{dl}} \tag{12}$$

which has zeros for $R_s = 0$, $s \rightarrow \infty$ and for

$$s = -\frac{R_s + R_{ct}}{R_s R_{ct} C_{dl}} \tag{13}$$

For positive values of R_s and C_{dl}, instability will occur when

$$R_s \geqq -R_{ct} \tag{14}$$

Since R_s, R_{ct} and C_{dl} are all real, s has no imaginary part. Consequently, a non-oscillatory instability will result, which drives the electrode potential to a region of even more negative R_{ct}. As the potential changes, the approximation $z \approx 0$ embodied

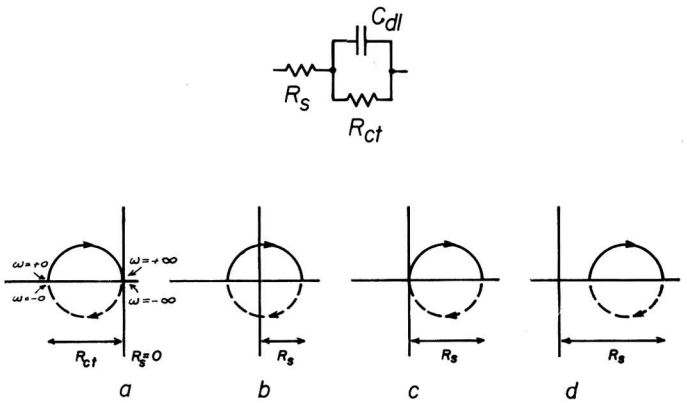

Fig. 8. The equivalent circuit of Fig. 6, and the corresponding complex impedance plane representations, when diffusion can be neglected ($z \ll 1$ hence $Z_w \ll R_{ct}$).

in eqn. (11) may no longer be valid, in which case oscillatory behavior will still be observed. However, the initial unidirectional variation of potential is quite evident in the sharp spikes of Fig. 4. The graphical representation of the impedance, eqn. (12), and the stability condition, eqn. (14), are shown in Fig. 8.

RELATED OBSERVATIONS

Electrochemical oscillations in passivating electrodes like Fe in HNO_3 were reported by Fechner[10] as early as 1828, and were studied subsequently by Herschel, Schönbein and Faraday in the early eighteen thirties. For early reviews and references, see Heathcote[11] and Hedges and Myers[62].

Renewed interest in electrochemical oscillators and related stability problems followed Ostwald's suggestion[11,12] that signal transmission in nerves is in many aspects analogous to that along passivating metal wires, an analogy further demonstrated by Lillie[13-15]. The electrochemical aspects of the problem were taken up again by Bonhoeffer[16-19] and Franck[20-22], who established general criteria for instability. Recently, Degn[23] has also contributed to this problem, although even his fairly general approach is restricted to passivating electrodes exhibiting "active" and "passive" states.

Although it was obvious to these workers that the instability leading to oscil-

latory behavior was connected both with a descending branch in the current–voltage curve and with some time-dependent phenomenon like diffusion, it is only rather recently that such time-dependence has been studied experimentally by Epelboin *et al.*[24,25], albeit in a somewhat different context.

Electrochemical oscillations are by no means restricted to passivating electrodes. They were also observed and studied in the oxidation of H_2 on Pt[26–31]. Here, as with the passivating electrodes, the electrode reaction rate is decreased by the formation of an oxygen or oxide film on the electrode. Similar oscillations have been reported with the oxidations of, *e.g.*, formaldehyde[32–35], carbon monoxide[48] and formic acid[49].

That film formation is no prerequisite for the generation of electrochemical oscillations was demonstrated by Frumkin *et al.*[36–38] with the reduction of anions such as $S_2O_8^{2-}$, $Fe(CN)_6^{3-}$, $PtCl_4^{2-}$, $PtCl_6^{2-}$ and $HCrO_4^-$ on mercury. In all these cases, the current–voltage curves exhibit a region of negative resistance due to double layer repulsion*, and the oscillations occur precisely in that region. The observations with $S_2O_8^{2-}$ were subsequently extended to a rotating copper electrode[40], indicating that earlier associations of the oscillations with tangential movement of the electrode surface (as in polarographic maxima) were incorrect. The oscillations occurred only when a sufficiently large series resistance was inserted into the circuit, unless the solution resistance itself was already very high[36,37]. In a series of papers, Gokhsthein[38,41,42] has attempted to formulate a theory for these oscillations.

The oscillatory behavior of $S_2O_8^{2-}$ in dilute solutions resembles that of indium in concentrated thiocyanate solution. Preliminary results obtained in this laboratory[43] indicate, however, that the simple mathematical formalism of the indium reduction[1] is not quite applicable to that of $S_2O_8^{2-}$, but that migration and/or ion pairing in the double layer must be taken into account for a quantitative description of the electrode impedance.

The oscillatory behavior of In(III) in thiocyanate solutions, illustrated in Figs. 2–4, can also be observed on a hanging mercury electrode. In this case, only the charge transfer resistance R_{ct} is time-dependent *via* the interfacial concentrations c'_R and c'_O, compare eqn. (3). If the external resistance is appropriately chosen, a continuous oscillation can be observed, see Fig. 9. When a less negative potential is applied, the repetition rate (frequency) increases and the amplitude decreases, making the oscillations somewhat less anharmonic. The highly non-linear, large amplitude oscillations like those of Fig. 9 appear to be maintained virtually indefinitely**. This is not unexpected since the currents are small and kinetically controlled except for the short-duration spikes, when the electrode potential moves momentarily into the region of diffusion-controlled currents.

Qualitatively, the formation of repetitive spikes can be understood as follows. The current, and hence the consumption of In(III) at the electrode, is low when the potential is near that of the lowest point in the minimum. Hence the interfacial concentration c'_O of indium ions increases, through diffusion and natural convection. As c'_O increases, $|R_{ct}|$ decreases, until the system becomes unstable, compare eqns. (3) and

* These systems often *also* exhibit polarographic maxima[39].

** After one or several hours, electrical contact is usually lost because the mercury drop falls off or the mercury thread breaks, due to solution creeping up the capillary and formation of an amalgam of continuously increasing indium concentration.

(14)*. Then the potential rapidly moves into the potential region of even more negative R_{ct}. The electrode potential can become more positive since the accompanying reduction current increases, so that the increased iR drop across R_s compensates for the decreased cell potential. This clearly shows the necessary interplay between the series resistance R_s and a negative branch on the (instantaneous) i–E-curve.

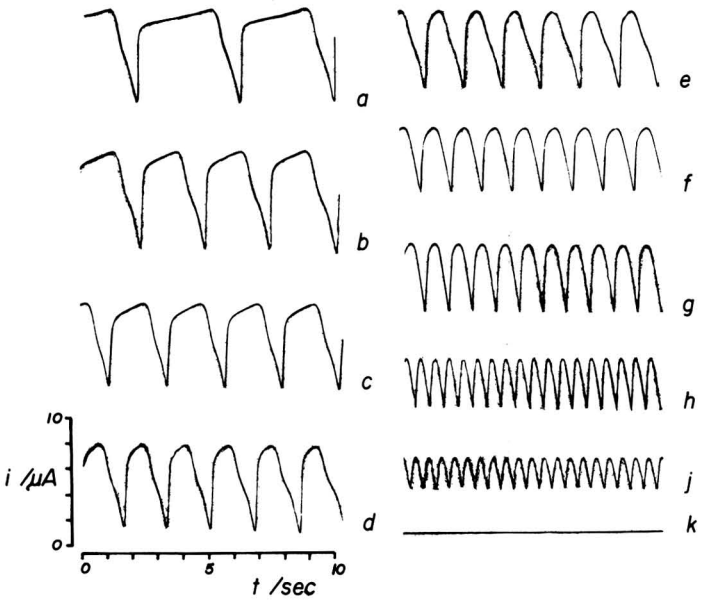

Fig. 9. Steady-state oscillations observed on a single hanging mercury droplet, with the circuit of Fig. 1a (R = 50 KΩ) at various potentials: (a) −0.99, (b) −0.98, (c) −0.97, (d) −0.95, (e) −0.93, (f) −0.89, (g) −0.85, (h) −0.74, (j) −0.72, (k) −0.71 V *vs.* Ag/AgSCN. Current and time sensitivities indicated in bottom left-hand corner, the same for all traces. The oscillations are established immediately after a change of potential, and appear to be perfectly stationary.

As the cell potential drops and the current increases, the interfacial concentration c'_O of indium ions rapidly decreases. This in turn reduces the reduction current, and hence the iR_s drop, driving the cell potential back up to its original value. After a while, as c'_O has increased again, the cycle will repeat itself, etc. Note that this explanation does not require any concepts like those of "active" and "passive" states, specific adsorption sites, competing reactions, etc.

There are many more systems which show unstable behavior. For example, in the reduction of phenylglyoxylic acid[44,45], the double layer field causes a slight minimum on the kinetically-limited current of the first wave at pH values of about 7–8. Indeed, a.c. measurements[46] reveal a negative charge transfer resistance in the descending branch of the minimum. With a sufficiently large external series resistance, this system again becomes unstable, but over most of the pH range the capacitive component of the negative diffusion admittance is negligibly small, so that the system will not oscillate[46].

In the reduction of an aqueous oxalate solution of ammonium metavanadate, which also exhibits a minimum[47], the reduction current in neutral solutions reaches a

* In the present example, the term $c'_R(\partial\vec{k}/\partial E)$ is negligible at the potentials considered[1].

diffusion-limited current before it drops to a low value in the minimum. The system shows oscillatory behavior[46] much like that of In(III) or Ni(II) in halide or pseudo-halide solutions. However, the half-wave potential of the first wave becomes more negative, and the minimum occurs at more positive potentials, when the pH is increased. Consequently, in a bicarbonate–carbonic acid buffer, the diffusion-limited current is no longer reached before the minimum appears, and the system becomes unstable but non-oscillatory[46].

Of course, not every decrease in reduction current (upon making the potential more negative) is accompanied by a negative charge transfer resistance. For instance, the very pronounced minimum observed in the reduction of chlorite ions from concentrated sodium hydroxide solutions is due[50] to the decrease of the interfacial concentration of the catalyst impurity, Fe(II), and not to any decrease of reduction rate constant with increasingly negative potential. Indeed, this system does not exhibit a negative charge transfer resistance and is stable with any series resistance.

On the other hand, the absence of a minimum on a current–voltage curve does not automatically imply the absence of a negative charge transfer resistance. We have already reported[1,3] that, with In(III) in 0.1 *M* NaSCN solutions, the reduction rate constant in the region of the minimum does not fall below 10^{-2} cm s^{-1}. Consequently, no polarographic minimum is observed in this case since this lowest reduction rate constant still exceeds the polarographic diffusion "rate constant", $(7D/12t)^{\frac{1}{2}}$, but oscillations can readily be generated on a dropping mercury electrode by the insertion of a sufficiently large series resistance into the polarographic circuit.

DISCUSSION

1. We have seen that electrochemical systems can become unstable when they incorporate a negative charge transfer resistance. Because of the coupling[2] between interfacial and diffusional impedances, a negative charge transfer resistance results in a negative diffusion impedance, so that the instability can result in oscillatory behavior unless the rate constants of the electrode reactions involved are very much smaller than diffusion rate constants over the entire region of negative charge transfer resistance. A second requirement for the instability, at least in the cases studied in the present paper, is that of a sufficiently large series resistance R_s[60]. Of course, the insertion of inductors into the external circuit[51,52] enhances the circuit instability (see the Appendix). Consequently, in systems containing negative charge transfer resistances, measurements on a.c. bridges containing transformers[61] are less accurate than those on direct-reading instruments which do not contain any inductive circuit elements and compensate for almost all of the series (solution) resistance[53].

2. The present discussion has started from the potential-dependence of the rate constants, since, in general, it is more useful to start with potential and associated driving forces rather than with resulting fluxes, the currents. However, this is largely a matter of conceptual and mathematical convenience and, at least in principle, the treatment could be transposed into one in terms of currents. In the literature on oscillatory behavior, however, some confusion appears to exist in this connection. As a typical example, Osterwald and Feller[32] reported that no instability is encountered with Ni in H_2SO_4 when the system is controlled potentiostatically, whereas oscillations are observed under galvanostatic conditions. The proper explanation[60] for this

observation is that galvanostats have a high output impedance, in contrast to potentiostats, and it is this output resistance, rather than the control of either current or potential, which causes the system to oscillate in the region of negative electrode immittance. The paper quoted[32] and the concordant impedance measurements of Epelboin *et al.*[24,25] also show that oscillatory behavior is associated with a measurable negative electrode immittance but not necessarily with a negative slope of the steady-state current–voltage curves, since the oscillatory behavior is observed at potentials positive of those at which the *i–E* curve exhibits a negative slope. Incidentally, the molecular mechanism responsible for the oscillatory behavior of Ni in H_2SO_4 is clearly different from that discussed in the present paper, as can be seen from the reported electrode impedance data[24,25].

3. Of the criteria for stability used in the present paper, the graphical test appears to be the more useful one since it does not require any mechanistic understanding, or even formal description of the electrochemical processes, but is based entirely on experimentally accessible impedance measurements. In the Appendix we have indicated that it can also be a useful tool in the understanding of electrochemical instrumentation, as in the example given there of *iR* compensation by positive feedback.

4. Although we have established the criteria for unstable and oscillatory behavior, we have not attempted to calculate the resulting wave shapes. This problem is a highly complicated one, since it necessarily involves the non-linearity of the charge transfer resistance. Since R_{ct} is a function of both potential and time (through the interfacial concentrations), the resulting equations can be expected to be most suitable for computer calculation. On a dropping mercury electrode, the problem would be further complicated by the changing surface area and solution resistance.

5. Qualitatively, we can note that the oscillations are fairly harmonic when the electrode potential is in a region of considerable negative diffusion admittance, whereas distinctly non-linear, relaxation-like oscillations result at potentials where the negative charge transfer conductance predominates, compare Figs. 2–4. Both pulse shape and pulse frequency can be varied by changing the applied potential, see Fig. 9.

6. This brings us to the possible biophysical implications. Many biological transducers generate electrical pulse trains from non-oscillatory excitations ("electrogenesis"). It is the pulse frequency, not their amplitude or shape, which carries the information about the excitation along the nerve. For instance, the sequence of processes in a sensory transducer might be visualized as follows. An external signal excites a molecular process. The resulting chemical response is amplified, *e.g.* by catalysis, and finally the signal is converted into a sequence of pulses. It is this last-mentioned stage which might utilize a mechanism similar to that of an electrochemical oscillator. From a neurophysical point of view, it is interesting to note that an electrochemical oscillator can be turned on and off, and that its frequency can be varied, by changing a (redox) potential. That the observed wave shapes often bear a striking resemblance to those of the nervous system of course reflects the high degree of non-linearity in both systems.

7. In the vertebrate eye, for example, the initial excitation step has been identified as the photo-isomerization of 11-*cis*-retinene. Wald has suggested[54] that a molecular amplification might be initiated when 11-*cis*-retinene is isomerized to *trans*-retinene, thereby possibly exposing an enzymatic group in the initially attached

opsin. Carrying this hypothesis one step further, if such catalysis causes a shift in the potential of a redox couple, then this potential might be shifted into the region of negative charge transfer resistance of this or possibly a second redox couple, and so generate a sequence of pulses until the 11-*cis*-retinene is isomerized back and blocks off the enzymatic group. The localized generation of the redox potential would give the system the essential features of a heterogeneous reaction, apparently needed for the occurrence of a negative (charge transfer) resistance. Several striking features of optical transducers, *e.g.* their efficient enhancement of contrast in space or time, would follow readily from the properties of R_{ct}, which depends on the time-dependent interfacial concentrations c'_R and c'_O.

Although such a sequence of events is quite conceivable, and seems to offer a relatively simple chemical explanation of electrogenesis, it should be emphasized that it must be considered as entirely hypothetical as long as no chemical species have been identified with such processes. Also, it should be noted that the computer calculations of Cole *et al.*[55] suggest that the well-established formalism of nervous pulse transmission[56] might also be capable of pulse generation (see also the direct observations reported by Huxley[57]), in which case no additional, hypothetical oscillatory mechanism would be required to explain electrogenesis. Moreover, the Hodgkin–Huxley formalism[56] results in an interfacial impedance which, in series with a sufficiently large resistance, leads to unstable behavior[63]. The way in which this problem was solved by Chandler *et al.*[63] shows an interesting alternative to our present approach.

8. All electrically excitable membranes seem to exhibit N-shaped current–voltage curves like those of Fig. 5a, and are therefore likely to have a region of negative resistance. Again, the coupling of interfacial and diffusional impedances can generate the corresponding negative diffusion capacitance, and, indeed, negative capacitances have been measured at low frequencies on squid nerve membranes[58]. Thus it appears that oscillatory instability of the type discussed in the present paper is a rather general neurobiological phenomenon. In the electrochemical oscillators on Hg discussed before, the negative charge transfer resistance is essentially the result of coulombic repulsion. In the case of the reduction of anions like $S_2O_8^{2-}$ (or the oxidation of cations like Eu^{2+}), it is the repulsion between the charged electrode and the electroactive particle. In the case of the reduction of cations like In(III), it is the repulsion between the negatively charged electrode and the catalyst anion SCN^-. Other processes appear to be involved in most electrochemical oscillators on solid electrodes. The interesting question remains as to the origin of the negative interfacial resistance in excitable biological membranes.

ACKNOWLEDGEMENT

The author gratefully acknowledges support of his research by the National Science Foundation under grant NSF GP 8575 and by the Air Force Office of Scientific Research (OAR-USAF) under grant 68-1344. This manuscript is submitted for publication with the understanding that the United States Government is authorized to reproduce and distribute reprints for governmental purposes.

SUMMARY

Spontaneous oscillations have been observed in a circuit composed of a source of direct voltage, a resistor and an electrochemical cell containing In(III) in aqueous

NaSCN solution. The physical and mathematical requirements for the occurrence of such oscillations have been investigated. The oscillations result from a negative charge transfer resistance in combination with diffusional mass transport, and are a direct consequence of the recently reported coupling between interfacial and diffusional impedances. The oscillations also require a sufficiently large series resistance. Similar spontaneous oscillations have also been observed with several other systems, indicating the general nature of the phenomenon.

A simple graphical test of circuit stability has been illustrated. This test is especially useful since it does not require any detailed understanding of the electrode process, but is based exclusively on experimental impedance measurements. Finally, some possible biophysical implications are discussed.

APPENDIX

SOME SIMPLE ELECTROCHEMICAL APPLICATIONS OF THE LLEWELLYN CRITERION

The simplest cell impedance encountered in electrochemical measurements is that of a double layer capacitance C_{dl} in series with a solution resistance R_s. The corresponding complex impedance plane representation is a vertical line intersecting the abcissa in the point R_s, see Fig. 10. Electronic compensation *via* positive feedback,

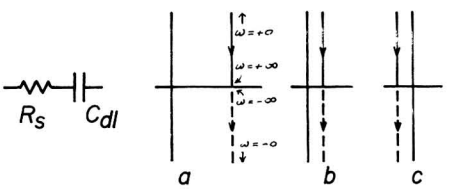

Fig. 10. The equivalent circuit of an electrochemical (half-) cell in the absence of an electrode reaction. In (a), (b) and (c) the effect of compensation (*e.g. via* positive feedback) of R_s by the amount R'_s is indicated. In (a) $R'_s = 0$, in (b) $R'_s < R_s$, in (c) $R'_s > R_s$. In the latter case, the circuit is unstable according to the Llewellyn criterion.

by the amount R'_s, will move the intercept with the abcissa towards the origin by the same amount R'_s. We immediately conclude from Figs. 10b and 10c that stable behavior requires that $R_s - R'_s > 0$, so that one can approach, but not achieve perfect compensation. In practice, the presence of additional capacitances and inductances in any physically realizable circuit makes it impossible even to approach $R_s - R'_s = 0$ too closely. The situation is essentially the same in the presence of a "normal" faradaic reaction, represented in Fig. 11 by a positive charge transfer resistance and (Warburg) diffusion impedance.

Tamamushi[51,52] has recently discussed an electrochemical oscillator composed of a cell containing systems like In(III) in NaSCN solution in series with a resistor and an *external inductor*. The inductance forces the oscillations to higher frequencies, so that the Warburg impedance becomes smaller and can be neglected as a first approximation. The equivalent circuit of the electrochemical cell then reduces to that of Fig. 8 and is similar to that of a tunnel diode oscillator. In terms of zeros of $Z(s)$, we have

$$Z(s) = R_s + sL + \frac{R_{ct}}{sR_{ct}C_{dl}+1} = \frac{R_{ct}LC_{dl}s^2 + (L + R_sR_{ct}C_{dl})s + R_s + R_{ct}}{sR_{ct}C_{dl}+1} \quad (15)$$

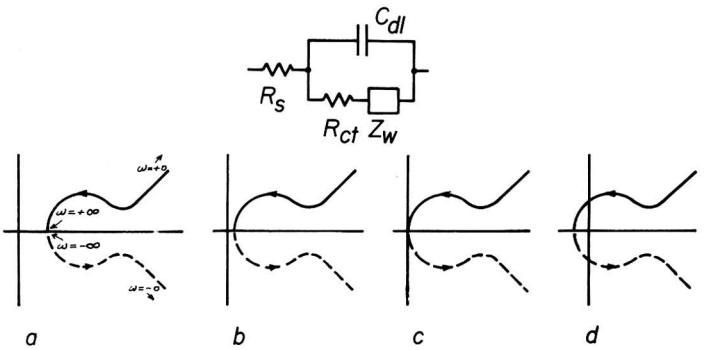

Fig. 11. The equivalent circuit of an electrochemical (half-) cell in the presence of an electrode reaction, represented here by a positive charge transfer resistance and Warburg impedance. The effect of iR compensation is depicted in the complex impedance plane for no (a), insufficient (b), correct (c) and over-compensation (d). The circuit is stable in (a) and (b) only.

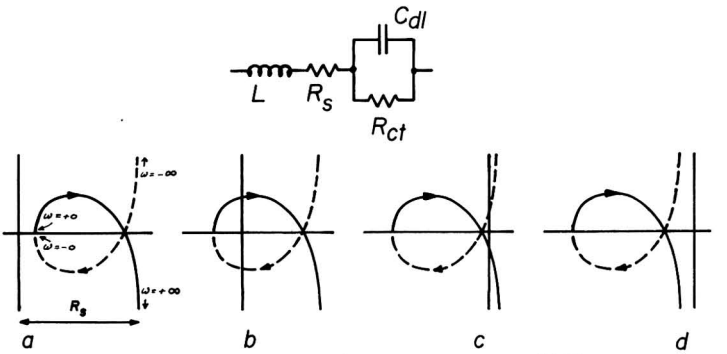

Fig. 12. The equivalent circuit discussed by Tamamushi *et al.* [51,52], containing an external inductance L and a negative charge transfer resistance R_{ct}, and the corresponding complex impedance plane representations. The system is stable only with a sufficiently large series resistance R_s (as in (a) and (b)).

so that

$$s = -\frac{L + R_s R_{ct} C_{dl} \mp \{(L + R_s R_{ct} C_{dl})^2 - 4(R_s + R_{ct}) R_{ct} LC\}^{\frac{1}{2}}}{2R_{ct} LC} \tag{16}$$

$$= -\tfrac{1}{2}\left(\frac{1}{R_{ct}C} + \frac{R_s}{L}\right) \pm \left\{\tfrac{1}{4}\left(\frac{1}{R_{ct}C} + \frac{R_s}{L}\right)^2 - \frac{R_s + R_{ct}}{R_{ct} LC}\right\}^{\frac{1}{2}}$$

and oscillations will result when[51,52]

$$\sigma \geqq 0 \quad \text{or} \quad \frac{1}{R_{ct}C} + \frac{R_s}{L} \leqq 0 \tag{17}$$

and

$$\omega > 0 \quad \text{or} \quad \frac{R_s + R_{ct}}{R_{ct} LC} - \tfrac{1}{4}\left(\frac{1}{R_{ct}C} + \frac{R_s}{L}\right)^2 > 0 \quad \text{or} \quad \left(\frac{1}{R_{ct}\,C} - \frac{R_s}{L}\right)^2 < \frac{4}{LC} \tag{18}$$

The criterion for instability, eqn. (17), is illustrated in Fig. 12.

REFERENCES

1 R. DE LEVIE AND A. A. HUSOVSKY, *J. Electroanal. Chem.*, 22 (1969) 29.
2 R. DE LEVIE AND L. POSPÍŠIL, *J. Electroanal. Chem.*, 22 (1969) 277.
3 L. POSPÍŠIL AND R. DE LEVIE, *J. Electroanal. Chem.*, 25 (1970) 245.
4 H. W. BODE, *Network Analysis and Feedback Amplifier Design*, Van Nostrand, New York, 1945, p. 15.
5 D. C. GRAHAME, *J. Am. Chem. Soc.*, 63 (1941) 1207.
6 A. HURWITZ, *Math. Ann.*, 46 (1895) 273.
7 J. H. SLUYTERS, *Rec. Trav. Chim.*, 79 (1960) 1092.
8 F. B. LLEWELLYN, *Proc. IRE*, 21 (1933) 1532, especially pp. 1562–1563.
9 EN-LUNG CHU, *Proc. IRE*, 32 (1944) 630.
10 M. G. TH. FECHNER, *Schweigger's J. Chemie und Physik*, 53 (1828) 129.
11 H. L. HEATHCOTE, *J. Soc. Chem. Ind. (London)*, 26 (1907) 899.
12 H. L. HEATHCOTE, *Z. Physik. Chem.*, 37 (1901) 368.
13 R. S. LILLIE, *Science*, 48 (1918) 51.
14 R. S. LILLIE, *J. Gen. Physiol.*, 3 (1920) 107, 129; 7 (1925) 473; 13 (1929) 1; 14 (1931) 349; 19 (1935) 109.
15 R. S. LILLIE, *Biol. Rev. Cambridge Phil. Soc.*, 16 (1936) 216.
16 K. F. BONHOEFFER, *Naturwiss.*, 31 (1943) 270; 40 (1953) 301.
17 K. F. BONHOEFFER *et al.*, *Z. Elektrochem.*, 47 (1941) 441, 536; 51 (1948) 24, 29, 60, 67, 149.
18 K. F. BONHOEFFER, *J. Gen. Physiol.*, 32 (1948) 69.
19 K. F. BONHOEFFER, *Angew. Chem.*, 61 (1949) 324; 67 (1955) 1.
20 U. F. FRANCK, *Z. Elektrochem.*, 55 (1951) 535; 57 (1953) 883; 62 (1958) 649.
21 U. F. FRANCK, *Z. Physik. Chem. N.F.*, 3 (1955) 183.
22 U. F. FRANCK, *Progr. Biophys. Biophys. Chem.*, 6 (1956) 173.
23 H. DEGN, *Trans. Faraday Soc.*, 64 (1968) 1348.
24 M. BOYER, I. EPELBOIN AND M. KEDDAM, *Electrochim. Acta*, 11 (1966) 221.
25 D. SCHUHMANN, *J. Electroanal. Chem.*, 17 (1968) 45.
26 S. SEKINE, *Z. Elektrochem.*, 34 (1928) 250.
27 M. THALINGER AND M. VOLMER, *Z. Physik. Chem.*, 150 (1930) 401.
28 J. A. V. BUTLER AND G. ARMSTRONG, *Nature*, 129 (1932) 613.
29 G. ARMSTRONG AND J. A. V. BUTLER, *Discussions Faraday Soc.*, 1 (1947) 122.
30 M. J. JONCICH AND N. HACKERMAN, *J. Phys. Chem.*, 57 (1953) 674.
31 D. T. SAWYER AND E. T. SEO, *J. Electroanal. Chem.*, 5 (1963) 23.
32 J. OSTERWALD AND H. G. FELLER, *J. Electrochem. Soc.*, 107 (1960) 473.
33 R. P. BUCK AND L. P. GRIFFITH, *J. Electrochem. Soc.*, 109 (1962) 1005.
34 H. F. HUNGER, *J. Electrochem. Soc.*, 115 (1968) 492.
35 D. F. A. KOCH, *Proc. 1st Austral. Conf. on Electrochem., 1963*, Pergamon, Oxford, 1965, p. 657.
36 A. YA. GOKHSTHEIN AND A. N. FRUMKIN, *Dokl. Akad. Nauk SSSR*, 132 (1960) 388.
37 A. N. FRUMKIN, O. A. PETRII AND N. V. NIKOLAEVA-FEDOROVICH, *Dokl. Akad. Nauk SSSR*, 136 (1961) 1158.
38 A. YA. GOKHSTHEIN, *Dokl. Akad. Nauk SSSR*, 140 (1961) 1114.
39 N. V. NIKOLAEVA-FEDOROVICH, G. E. TITOVA AND NGUYEN ZUNG, *Elektrokhimiya*, 4 (1968) 392.
40 A. YA. GOKHSTHEIN AND A. N. FRUMKIN, *Dokl. Akad. Nauk SSSR*, 144 (1962) 821.
41 A. YA. GOKHSTHEIN, *Dokl. Akad. Nauk SSSR*, 148 (1963) 136.
42 A. YA. GOKHSTHEIN, *Dokl. Akad. Nauk SSSR*, 149 (1963) 880.
43 J. C. KREUSER, L. POSPÍŠIL AND R. DE LEVIE, unpublished investigation.
44 R. BRDIČKA AND K. WIESNER, *Naturwiss.*, 31 (1943) 247.
45 R. BRDIČKA *et al.*, *Collection Czech. Chem. Commun.*, 12 (1947) 39, 138, 212.
46 J. C. KREUSER AND R. DE LEVIE, in preparation.
47 J. J. LINGANE AND L. MEITES, *J. Am. Chem. Soc.*, 69 (1947) 1021.
48 M. C. DEIBERT AND D. L. WILLIAMS, *J. Electrochem. Soc.*, 116 (1969) 1290.
49 O. A. PETRII AND N. LOKHANYAI, *Elektrokhimiya*, 4 (1968) 656.
50 L. GIERST, L. VANDENBERGHEN AND E. NICHOLAS, *J. Electroanal. Chem.*, 12 (1966) 462.
51 R. TAMAMUSHI, *J. Electroanal. Chem.*, 11 (1966) 65.
52 R. TAMAMUSHI AND K. MATSUDA, *J. Electroanal. Chem.*, 12 (1966) 436.
53 R. DE LEVIE AND A. A. HUSOVSKY, *J. Electroanal. Chem.*, 20 (1969) 181.

54 G. WALD in W. D. MCELROY AND B. GLASS (Eds.), *Light and Life*, Johns Hopkins Press, Baltimore, 1961, p. 724.
55 K. S. COLE, H. A. ANTOSIEWICZ AND P. RABINOWITZ, *J. Soc. Ind. Appl. Math.*, 3 (1955) 153.
56 A. L. HODGKIN AND A. F. HUXLEY, *J. Physiol. (London)*, 117 (1952) 500.
57 A. F. HUXLEY, *Ann. N. Y. Acad. Sci.*, 81 (1959) 221.
58 K. S. COLE AND R. F. BAKER, *J. Gen. Physiol.*, 24 (1941) 771.
59 W. SCHWENK, *Electrochim. Acta*, 5 (1961) 301.
60 J. OSTERWALD, *Electrochim. Acta*, 7 (1962) 523.
61 M. SLUYTERS-REHBACH, B. TIMMER AND J. H. SLUYTERS, *Z. Physik. Chem. Frankfurt*, 52 (1967) 89.
62 E. S. HEDGES AND J. E. MYERS, *The Problem of Physico-chemical Periodicity*, Arnold, London, 1926, Chap. 7.
63 W. K. CHANDLER, F. FITZHUGH AND K. S. COLE, *Biophys. J.*, 2 (1962) 105.

ELECTROANALYTICAL CHEMISTRY AND INTERFACIAL ELECTROCHEMISTRY
Elsevier Sequoia S.A., Lausanne – Printed in The Netherlands

DETERMINATION DES CONSTANTES DE VITESSE HETEROGENES PAR LA METHODE DE DOUBLE SAUT POTENTIOSTATIQUE

J. CHEVALET ET
Laboratoire d'Electrochimie, Faculté des Sciences, 9, Quai Saint-Bernard, Paris, 5e (France)
F. M. KIMMERLE
Département de Chimie, Université de Sherbrooke, Sherbrooke, Québec (Canada)
(Reçu le 30 octobre, 1969)

Ce travail a pour but la vérification expérimentale des résultats théoriques publiés dans un précédent article[1]. L'appareillage de chronocoulométrie réalisé a été spécialement adapté aux conditions proposées dans la théorie, pour le cas de l'électrode à goutte de mercure renouvelée.

Deux modes de programmation distincts sont analysés sur la base de l'étude de deux systèmes électrochimiques. Les constantes cinétiques ainsi mesurées sont comparées à celles obtenues par polarographie classique.

La liste des symboles utilisés a été publiée dans l'article de réf. 1.

RAPPEL DES RELATIONS ÉTABLIES DANS LE PRÉCÉDENT ARTICLE

On considère le cas particulier de l'électrode à goutte de mercure renouvelée, en se limitant au cas où la programmation a pour effet d'inverser le sens du courant d'électrolyse. Le système électrochimique envisagé subit deux réactions successives, soit :

1. $n_1 e + O \underset{k_1}{\longrightarrow} R$ pendant la période de "prépolarisation" τ, suivie de
2. $R \underset{k_2}{\longrightarrow} O' + n_2 e$ pendant la période dite de "polarisation" t'.

Le plus fréquemment il y a régénération de O ($O' \equiv O$ et $n_1 \equiv n_2$). Au point de vue mathématique cette situation est formellement équivalente au cas inverse où la réaction (2) précède (1).

Deux types de programmation ont été mis en oeuvre : le mode D–R dans lequel la réaction (1) est exclusivement contrôlée par la diffusion et (2) est en régime de contrôle mixte (diffusion et réaction), et le mode R–D dans lequel la situation est inversée.

La vérification de la théorie proposée se base nécessairement sur l'analyse de systèmes tels que $O' \equiv O$ (ou $R' \equiv R$), pour lesquels les valeurs de constantes de vitesse peuvent être obtenues simultanément par voie chronocoulométrique et par polarographie directe.

Si $O' \neq O$ on peut s'attendre à observer des comportements totalement différents dont la mise en évidence ne met cependant pas nécessairement la théorie en

question puisque sa vérification devient dès lors impossible.

Il a été établi[1] que:

$$Q'(\text{D–D}) = n_2 F A (D_O)^{\frac{1}{2}} C_O^* (2/\pi^{\frac{1}{2}})[1 + \theta^{-1} - (1+\theta^2)^{\frac{1}{2}}/\theta] \tag{1}$$

avec pour électrode plane

$$\theta = \left(\frac{t}{\tau}\right)^{\frac{1}{2}} \tag{2}$$

et pour l'électrode à goutte

$$\theta = \left(\frac{3}{7}\frac{t'}{\tau}\right)^{\frac{1}{2}} \tag{3}$$

En tenant compte du temps Δt pendant lequel s'écoule le courant de charge de la couche double et après lequel l'intégration commence, nous avons pour l'électrode à goutte:

$$[\cdot Q'(\text{D–D})]_{\Delta t}^{t'} = n_2 F A (D_O)^{\frac{1}{2}} C_O^* (2/\pi^{\frac{1}{2}})[t'^{\frac{1}{2}}(1 + \theta^{-1} - \{1+\theta^2\}^{\frac{1}{2}}/\theta) - \Delta t^{\frac{1}{2}}(1 + \Delta\theta^{-1} - \{1+\Delta\theta^2\}^{\frac{1}{2}}/\Delta\theta)] \tag{4}$$

avec:

$$\theta = \left(\tfrac{3}{7} \cdot \frac{t'}{\tau}\right)^{\frac{1}{2}} \tag{5}$$

et

$$\Delta\theta = \left(\tfrac{3}{7} \cdot \frac{\Delta t}{\tau}\right)^{\frac{1}{2}} \tag{6}$$

Cette relation donne la valeur absolue de la charge récupérée pendant la polarisation lorsque la diffusion règle la réaction. Cette grandeur est directement accessible par l'expérience. D'autre part, si nous établissons le rapport de la relation (1) et de la relation (7) donnant le courant de diffusion pendant la polarisation:

$$\cdot i(\text{D–D}) = -n_1 F (D_O)^{\frac{1}{2}} C_O^* \, 0.85 \, m^{\frac{2}{3}} t^{\frac{1}{6}} (\tfrac{3}{7}\pi)^{-\frac{1}{2}} \tag{7}$$

nous obtenons un rapport homogène au temps, qu'il est facile de vérifier expérimentalement par la comparaison d'une courbe R–D et d'un polarogramme classique (effectué avec un temps t_1)

$$\frac{[\cdot Q'(\text{D–D})]_{\Delta t}^{t'}}{\cdot i(\text{D–D})_{t_1}} = -\frac{n_2}{n_1} 2\tau \left(\frac{\tau}{t_1}\right)^{\frac{1}{6}} [\theta - \Delta\theta - (1+\theta^2)^{\frac{1}{2}} + (1+\Delta\theta^2)^{\frac{1}{2}}] \tag{8}$$

Aucun paramètre (D, C_O, m, etc.) autre que les différents temps expérimentaux n'intervient, ce qui permet une vérification plus aisée.

D'autre part, dans les cas R–D et D–R, il a été montré que

$$\lim_{\theta \to 0} \frac{Q'(\text{R–D})}{Q'(\text{D–D})} = 1 - \exp \chi_1^2 \operatorname{erfc} \chi_1 \tag{9}$$

et que

$$\lim_{\theta \to 0} \frac{Q'(\text{D–R})}{Q'(\text{D–D})} = 1 - (\pi^{\frac{1}{2}}/2 \, \chi_2)(1 - \exp \chi_2^2 \operatorname{erfc} \chi_2) \tag{10}$$

où χ représente un paramètre sans dimensions proportionnel à la constante de vitesse, dont l'expression est

$$\chi = k\left(\frac{t'}{D}\right)^{\frac{1}{2}} \quad \text{pour le mode D–R}$$

et

$$\chi = k\left(\frac{12}{7}\frac{\tau}{D}\right)^{\frac{1}{2}} \quad \text{pour le mode R–D}$$

Les rapports

$$\frac{\cdot Q'(\text{R–D})}{\cdot Q'(\text{D–D})} \quad \text{et} \quad \frac{\cdot Q'(\text{D–R})}{\cdot Q'(\text{D–D})}$$

ont été calculés pour différentes valeurs de χ et de θ en Tableaux 1 et 2. En particulier pour le cas considéré (électrode à goutte), ils ont été calculés pour les différentes valeurs de χ et nous avons tracé les abaques correspondantes donnant log χ en fonction de Q/Q_D pour les deux modes.

CHOIX DU SYSTÈME ÉLECTROCHIMIQUE

Pour la vérification expérimentale, il importe de recourir à un système simple dont les deux réactions $ne + O \rightarrow R$, $R \rightarrow O + ne$ soient accessibles par polarographie classique.

Notre choix s'est porté sur les deux couples oxydo–réducteurs uranylcarbonate (VI)/(V) et chrome (III)/(II). Ils se caractérisent par des ondes irréversibles bien définies, les deux formes oxydantes sont stables, les formes réductrices, bien qu'instables à l'air, sont assez facilement préparées par réduction électrochimique et ne se réoxydent pas en présence d'azote ou d'argon pendant la durée d'une expérience.

Six opérations sont alors possibles sur chaque couple:

(*a*) *à partir d'une solution de la forme oxydée*

1. La polarographie classique conduit à l'onde de réduction de O en R.
2. Le mode R–D conduit à la même information puisque R est formé à des potentiels variables et réoxydé à un potentiel correspondant au régime de diffusion pure.
3. Le mode D–R conduit à l'onde d'oxydation de R en O car R, formé pendant la prépolarisation à potentiel fixe (au palier de diffusion) est réoxydé à des potentiels variables.

(*b*) *à partir d'une solution de la forme réduite les mêmes considérations nous indiquent que*:

4. La polarographie donne l'onde d'oxydation de R.
5. Le mode R–D fournit aussi cette onde d'oxydation de R.
6. Le mode D–R fournit l'onde de réduction de O en R.

Nous vérifions expérimentalement l'exactitude des méthodes proposées en établissant l'identité des fonctions log $\chi = f(E)$ obtenues par polarographie classique d'une part, et par les modes R–D et D–R d'autre part.

CHOIX DES PARAMÈTRES DE TEMPS

$\tau = 5$ s (temps de prépolarisation); $t' = 50$ ms (temps de polarisation); $\Delta t = 1$ ms (temps d'attente); $\theta = (t'/\tau)^{\frac{1}{2}}$ vaut donc 0.01; $t_1 = 4$ s (temps d'enregistrement des polarogrammes classiques). τ a été limité à 5 s car il est à craindre que les phénomènes de convection ne viennent troubler l'apport par diffusion de la première réaction pour des temps supérieurs. t' a été fixé à 50 ms pour que l'approximation de constance de la surface de la goutte reste valable (avec $\tau = 5$ s et $t' = 0.1$ l'augmentation de surface est voisine de 1%). $\Delta t = 1$ ms semble une valeur très correcte expérimentalement, assez courte car la charge récupérée pendant la seconde réaction n'est que peu diminuée, mais suffisamment longue puisque le pic capacitif est complètement éliminé.

$t_1 = 4$ s remplit la condition que t_1 soit $< \tau$ de sorte qu'il convienne pour l'enregistrement simultané du courant de la polarographie classique et de la charge $\cdot Q'$.

APPAREILLAGE

L'ensemble du montage chronocoulométrique peut se schématiser de la manière suivante:

—une cellule polarographique classique est asservie à un potentiostat à réponse rapide. Ce potentiostat est commandé extérieurement par un ensemble générateur d'impulsions dont les durées et les amplitudes sont programmées de façon à satisfaire les conditions exposées dans la partie théorique. L'intensité du courant dans la cellule est amplifiée puis intégrée par un ensemble d'amplificateurs opérationnels commandés eux aussi par diverses impulsions programmées. On recueille ainsi deux tensions, l'une proportionnelle à l'intensité, l'autre proportionnelle à la charge, qui sont alternativement sélectionnées et envoyées en Y sur un enregistreur XY, attaqué d'autre part en X par la rampe de tension qui programme l'amplitude des impulsions du potentiostat.

—description de l'ensemble (la Fig. 1 schématise le montage).

Les générateurs G_1 et G_3 (Tektronix type 161 et 162) fournissent les principaux signaux nécessaires à l'opération. G_1 fournit une onde carrée de durée τ à partir d'une impulsion provenant du marteau électromagnétique. Ce signal est alors transformé par un module et dont l'amplitude est réglée par un potentiomètre "10 tours" accouplé à un moteur synchrone (Mot_1), pour le mode de fonctionnement R–D, assurant ainsi une variation lente (de quelques dizaines de mV min^{-1} à 1 V min^{-1}) de la tension E_1.

Après le temps τ une impulsion provenant de G_1 déclenche d'une part—le générateur G_4 fournissant la seconde valeur du potentiel appliqué, soit E_2, par l'intermédiaire d'un module semblable à celui décrit ci-dessus (le potentiel E_2, dans le cas D–R varie lentement à l'aide du moteur Mot_2)

—les générateurs G_2 et G_3 d'autre part. G_2 fournit une dent de scie et le trigger d'entrée de G_3 se déclenche en un point réglable de cette dent de scie, produisant ainsi l'impulsion t' retardée d'un Δt réglable. Cette impulsion commande le relais d'enclenchement de l'intégrateur.

Les deux signaux E_1 et E_2 arrivent sur un sommateur–décaleur (ampli. opér. Philbrick P 85 A) permettant d'explorer tout le domaine des tensions utilisées en

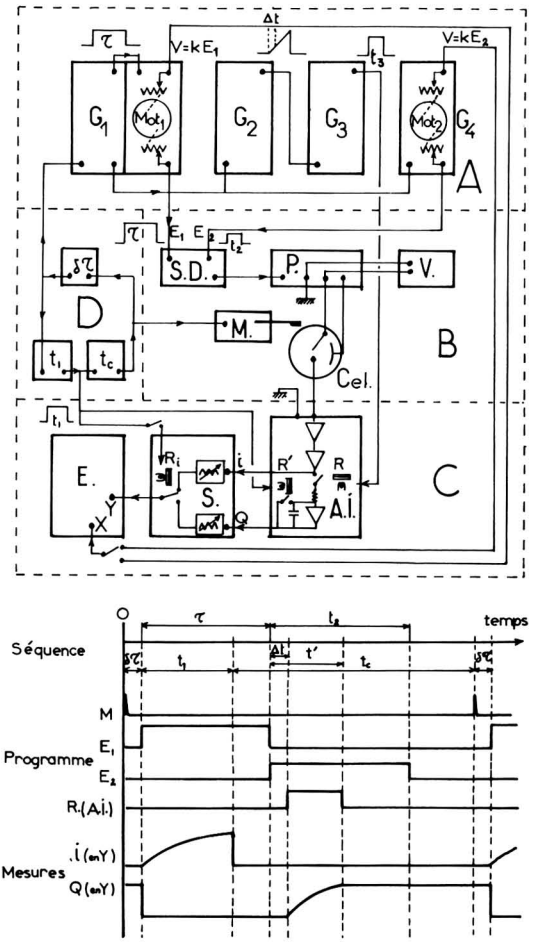

Fig. 1. A, B, C, D représentent les quatre blocs d'appareils: les générateurs, la cellule et ses commandes, les dispositifs de mesure, la programmation des temps. (S.D.) sommateur–décaleur, (P.) potentiostat, (V.) millivoltmètre digital, (M.) marteau électromagnétique, (E.) enregistreur XY, (S.) sélecteur–atténuateur, (A.I.) amplificateur–intégrateur.

électrochimie classique .

Ce module pilote un potentiostat Tacussel type PRT 2000 (quelque peu modifié pour obtenir un temps de réponse minimal (1 μs)) qui commande une cellule de conception classique, offrant de faibles résistances en particulier pour l'électrode de référence, afin d'éviter une constante de temps gênante. L'électrode contrôlée (goutte de mercure) est connectée à l'amplificateur intégrateur. L'entrée, munie d'un dispositif de protection, se comporte comme une impédance nulle (masse virtuelle).

Ce bloc (de conception voisine des montages de Anson, Payne, Osteryoung, etc.[2-4]) est composé de trois amplificateurs opérationnels (Philbrick P25A): le le premier transforme le courant en tension, le deuxième amplifie éventuellement cette tension et le dernier commandé par deux relais (enclenchement et remise à zéro)

intègre avec une constante de temps ajustable.

Les deux tensions, proportionnelles à i et à Q sont alors envoyées sur un atténuateur calibré sélecteur qui permet d'enregistrer soit Q, soit i et Q, soit i seul (polarographie). Un relais connecte le circuit "i" pendant les quatre premières secondes, puis le circuit "Q" (voir carte des signaux Fig. 1). Ce sélecteur commande l'entrée Y de l'enregistreur XY. L'entrée X est connectée, suivant le mode utilisé, à une sortie spéciale des générateurs G_1 et G_4 qui donne une tension proportionnelle à l'amplitude des signaux E_1 et E_2.

Un ensemble synchronisateur constitué de multivibrateurs monostables fournit les autres temps nécessaires à l'opération : $t_1 = 4$ s, déclenché en même temps que τ donne le signal de remise à zéro de l'intégrateur et détermine le temps de mesure polarographique ; t_c déclenché par la fin de t_1 détermine la durée d'un cycle. L'élément $\delta\tau$ introduit un léger retard (quelques 10 ms) entre l'impulsion électrique envoyée au marteau et le début de l'opération, de manière à tenir compte du temps nécessaire pour le décrochement réel de la goutte.

Un millivoltmètre digital Tacussel "Ariès 1000" affiche le potentiel de la goutte dans les différentes étapes. Un oscilloscope de contrôle permet de suivre la forme des différents signaux, le pic capacitif de charge de la couche double, etc....

La stabilité des différents temps est appréciée à l'aide d'un chronomètre électronique.

PERFORMANCES

(*a*) *Temporisateurs*

Les temps τ, t', t_1 sont fixés aux valeurs indiquées antérieurement avec une précision supérieure à 0.2%, 1%, et 0.4%, respectivement. Δt peut varier jusqu'à 3% autour de 1.0 ms mais comme nous verrons ultérieurement (*cf. Interprétation des écarts observés*) cette précision relative apparemment faible n'influence guère les mesures.

(*b*) *L'ensemble potentiostat–cellule*

Les manipulations faites avec l'électrolyte support seul à des sensibilités correspondant aux valeurs courantes montrent l'absence pratiquement totale de charge capacitive récupérée pendant la polarisation dans tout le domaine où l'électrode est idéalement polarisable. Nous avons vérifié ce fait à l'oscilloscope en constatant que le pic capacitif du courant de charge de la double couche pour des sauts de potentiels de plus en plus grands (jusqu'à 1800 mV) et pour des conditions usuelles (support 0.1 ou 1 M), est largement contenu dans les 200 ou 500 premières μs.

(*c*) *Module de mesure*

Limiteurs d'intensité. Le courant polarographique qui passe pendant le temps de prépolarisation se chiffre en μA, l'équation de Cottrel indique qu'il peut facilement atteindre une valeur 10^2 fois supérieure après le temps Δt pendant la polarisation, et lors de la charge de la couche double au saut du potentiel, il atteint des valeurs très supérieures. On a donc prévu un circuit écrêteur d'entrée dont l'effet est extrêmement efficace. Il n'entre en action que pour des courants au moins égaux à ≈ 750 μA, beaucoup plus faibles que le courant correspondant à la saturation de

l'amplificateur d'une part, et beaucoup plus élevé que les valeurs du courant faradaique d'autre part. La linéarité des amplificateurs est parfaite en deçà du seuil d'écrêtage, et au delà on peut faire passer une intensité considérable sans risquer de saturer l'amplificateur et de l'affecter d'une constante de temps de recouvrement prohibitive.

Intensité. Les bruits de fond, et les dérives de toute origine portant sur une durée de l'ordre de l'heure, ne dépassant pas 1% de la déviation totale de l'enregistreur sur sa gamme la plus sensible: (soit: 0.2 μA pleine échelle) qui correspond néanmoins à une très forte sensibilité dans les conditions polarographiques.

Charge. L'intégration des divers bruits et des dérives de l'intégrateur et des amplificateurs le précédant, représentent dans les conditions expérimentales ($t' = 50$ ms) et pour la durée de quelques manipulations, 1% de la lecture sur l'échelle la plus sensible (soit: 0.5×10^{-2} μC à déviation totale).

Remarquons que ces sensibilités élevées ne sont pratiquement pas utilisées, les mesures courantes nécessitent généralement des sensibilités de 1 à 5 μA en pleine déviation pour la polarographie, et 0.1 à 1 μC en pleine déviation pour les courbes D–R et R–D. La précision de l'appareillage est dès lors limitée par le maillon final de la chaîne: l'enregistreur XY et ses atténuateurs, qui permettent une précision de lecture de l'ordre de 0.2 à 0.5% suivant les échelles. (C'est aussi l'ordre de grandeur (0.1 à 0.25%) de la linéarité des amplificateurs et intégrateurs, réglés et étalonnés à l'aide d'un voltmètre digital très précis.)

PARTIE EXPÉRIMENTALE

(*a*) *Choix des conditions*

1. *Système U(V)–U(VI) en milieu carbonate.* Le complexe carbonaté d'uranium(VI) ne pose aucun problème de stabilité dans les domaines de concentration que nous utilisons (constante de complexion[6] avec CO_3^{2-} $K_c = 6.10^{22}$), la structure $UO_2(CO_3)_3^{4-}$ étant généralement admise. Le cas du complexe U(V) est différent: en effet une réaction de dismutation limite l'existence de ce complexe aux forces ioniques et aux concentrations en CO_3^{2-} élevées. De plus la présence des particules de U(IV) précipitées catalysent la dismutation ce qui diminue la stabilité de U(V) lorsque U(IV) produit par cette réaction est insoluble. En fait le domaine d'existence du complexe d'U(V) (vraisemblablement $UO_2(CO_3)_3^{5-}$) est assez restreint. A pH > 12 il précipite par hydrolyse et en milieu acide la dismutation est très rapide. En pratique, le complexe est stable à l'échelle de l'heure[5] pour des concentrations en $CO_3^{2-} > 0.2$ *M* et une force ionique au moins voisine de 1.

Nous avons opéré en milieu carbonate de sodium. Les solutions de U(VI) sont préparées par pesée à partir de sulfate ou de nitrate d'uranyle pur. La concentration 10^{-3} *M* a été adoptée pour presque toutes les manipulations. Le carbonate de sodium est de pureté analytique Carlo Erba. Les solutions de U(V) pour des opérations 4,5,6 sont obtenues par électrolyse des solutions de U(VI) à potentiel contrôlé (−1.4 V/ECS). Cette opération est menée dans une cellule annexe: réduction sur large cathode de mercure, séparation du compartiment anodique par verre fritté, et maintien permanent sous atmosphère d'argon, U(V) se réoxydant assez facilement à l'air.

2. *Système Cr(II)–Cr(III).* En milieu non complexant, il semble admis[7–9] que le chrome (III) se trouve sous la forme d'ions hexaquochromiques stables (forme

violette) mais susceptibles de vieillissement en présence d'anions complexants (forme verte). Nous opérons en milieu $NaClO_4$ 0.3 *M* $HClO_4$ 10^{-3} à 5×10^{-3} *M*, et le chrome 10^{-3} *M* est introduit sous forme d'alun $CrK(SO_4)_2 \cdot 12\,H_2O$. L'onde de réduction est typiquement irréversible pour la concentration du support utilisée. Les solutions de Cr(II) qui serait différemment hydraté[9,10] sont obtenues par réduction à potentiel contrôlé de la forme Cr(III) ($E = -1150$ mV/ECS). On observe que la courbe obtenue par le mode D–R avec Cr(III) (opération 6, Table 1) est totalement différente de l'onde de réduction de Cr(III) obtenue par les autres méthodes, (pour cette raison la Fig. 3f ne fait pas mention de la courbe D–R). Ce comportement est actuellement étudié avec plus de détails. Il est clair dès à présent que l'on n'est pas dans les conditions de validité définies au début de l'article : l'espèce formée pendant la première réaction est différente de la forme "vieillie" puisque sa réduction dans la seconde étape se traduit par une onde différente.

(*b*) *Choix de la programmation*

Les six opérations précédemment ont été exécutées avec chaque couple oxydo–réducteur en imposant les programmes de tensions consignés dans le Tableau 1

TABLEAU 1

Opération	*Paramètre*	*Système U(V)–U(VI)*		*Système Cr(II)–Cr(III)*	
		E_1/*mV vs. ECS*	E_2/*mV vs. ECS*	E_1/*mV vs. ECS*	E_2/*mV vs. ECS*
oxydant en solution					
1	$\chi \rightarrow k_1$	-700 à -1200		-600 à -1000	
2	$\chi_{RD} \rightarrow k_1$	-700 à -1200	-300	-600 à -1000	$+100$
3	$\chi_{DR} \rightarrow k_2$	-1400	-300 à -700	-1000	$+100$ à -600
réducteur en solution					
4	$\chi \rightarrow k_2$	-300 à -700		$+100$ à -600	
5	$\chi_{RD} \rightarrow k_2$	-300 à -700	-1400	$+100$ à -600	-1000
6	$\chi_{DR} \rightarrow k_1$	-300	-700 à -1200	$+100$	-600 à -1000

RÉSULTATS

Vérification de l'expression de $\cdot Q'$*(D–D)*

Les expressions de $[\cdot Q(\text{D–D})]_{\Delta t}^{t}$ et de $\cdot i(\text{D–D})$ ont été rappelées dans le premier paragraphe.

Les différents paramètres ont les valeurs suivantes : $\tau = 5$ s ; $t' = 51 \cdot 10^{-3}$ s ; $\Delta t = 10^{-3}$ s ; $C_O^* = 1$ mmol ; $m = 0.601$ mg s^{-1} *d'où* : $A = 0.0176$ cm^2 ; $\Delta\theta = 0.00926$; $\theta = 0.06590$.

Dans le cas du chrome, nous prenons pour D_O la valeur moyenne 5.6×10^{-6} cm^2 s^{-1} proposée par Cornelissen[10], ce qui nous conduit à : $\cdot Q'(\text{D–D}) = 0.843$ μC ; $\cdot i(\text{D–D})_{t_1} = 1.500$ μA.

Les résultats expérimentaux correspondant à une dizaine d'expériences semblables nous donnent une valeur moyenne : $[\cdot Q'(\text{D–D})]_{\Delta t}^{t'} = 0.815$ μC avec une

reproductibilité de ± 0.015 μC et $\cdot i(\mathrm{D–D})_{t_1} = 1.49$ μA ± 0.02 μA.

La valeur expérimentale de la charge est toujours un peu trop faible, ce qui recevra une tentative d'explication dans les paragraphes suivants. Par contre la valeur de i obtenue est jugée satisfaisante compte tenu de la validité de l'équation d'Ilkovic.

L'utilisation du rapport :

$$\frac{[\cdot Q'(\mathrm{D–D})]_{\Delta t}^{t'}}{\cdot i(\mathrm{D–D})_{t_1}}$$

mentionné dans le premier paragraphe nous permet une vérification indirecte et théoriquement plus précise puisque seuls les paramètres temps interviennent. Avec les valeurs déjà citées de τ, t_1 et t' nous obtenons le rapport théorique :

$$\frac{[\cdot Q'(\mathrm{D–D})]_{\Delta t}^{t'}}{\cdot i(\mathrm{D–D})_{t_1}} = 0.565$$

Sur l'ensemble d'une vingtaine de courbes expérimentales réalisées soit avec le chrome, soit avec l'uranium, à des concentratons variables de dépolarisant et de support, nous obtenons la valeur bien reproductible : 0.545 ± 0.01.

Interprétation des écarts observés

Notons que la valeur systématiquement trop faible (de $\approx 3.5\%$) du rapport $\cdot Q' \cdot i$ s'accorde bien avec la valeur absolue de $\cdot Q'$ trop faible et la valeur de $\cdot i$ correcte. Notons aussi que d'autres systèmes accusent la même erreur ; par exemple Lingane et Christie[11] ont trouvé avec une électrode à goutte de mercure pendante, un rapport Q'/Q_{exp} trop faible de 1.7%. (Un léger désaccord qui ne semble pas être fonction du temps t', leur θ étant fixé à 1.00).

Les causes d'erreurs dues à l'appareillage peuvent être multiples, mais l'étalonnage de l'intégrateur et des amplificateurs est fait à 0.1 et à 0.2%. La précision sur τ et θ qui est déterminante pour le rapport est de l'ordre de 0.1 et 0.2% respectivement. Et nous avons calculé qu'une erreur sur Δt jusqu'à 10% n'entraînerait qu'un écart de 0.7%.

Il s'ensuit que les différentes erreurs liées à l'appareillage paraissent insuffisantes à expliquer l'écart assez reproductible observé. C'est sur le plan de l'applicabilité de la théorie qu'il convient donc de se ramener. En effet le traitement théorique présuppose que la sphéricité du champ de diffusion est négligeable dans le cas de l'électrode de mercure à goutte renouvelée. Or cette approximation (surtout pendant le temps τ) n'est pas entièrement justifiée. En plus, la théorie ne tient pas compte de la convection locale de la solution induite par les mouvements de la goutte dûs d'une part (pendant τ) à son décrochement mécanique et d'autre part (pendant t') à la variation brutale de tension superficielle causée par le saut de potentiel[12].

On peut d'ailleurs se rendre compte qualitativement que la diffusion sphérique et la convection agissent bien dans le sens observé, c'est à dire d'une diminution de la charge récupérée.

Vérification des paramètres cinétiques

Les diverses courbes de polarisation (polarogrammes, chronocoulogrammes) sont converties en diagrammes $\log (k/D^{\frac{1}{2}}) = f(E)$. Compte tenu des différents temps

d'observation t_1 (pol.) = 4 s, $\tau_{(R-D)} = 5$ s et $t'_{(D-R)} = 50$ ms nous obtenons les expressions suivantes :

Méthode	*Expression pour* χ	*Valeurs de log* $(k/D^{\frac{1}{2}})$
R–D	$\chi_{R-D} = k(12\tau/7D)^{\frac{1}{2}}$	$\log \chi_{R-D} - 0.47$
D–R	$\chi_{D-R} = k(t'/D)^{\frac{1}{2}}$	$\log \chi_{D-R} + 0.64$
Polarographie	$\chi = k(12t_1/7D)^{\frac{1}{2}}$	$\log \chi - 0.42$

La Table 2 et la Fig. 2 représentent à titre d'exemple les courbes $\log \chi = f(E)$ obtenues à l'aide des trois méthodes ainsi que leur correspondances en $\log (k/D^{\frac{1}{2}})$.

Les écarts observés entre les courbes $\log (k/D^{\frac{1}{2}})$ étant faibles, nous présenterons les résultats sous forme d'écarts :

$$\log [k/D^{\frac{1}{2}}(\text{RD ou DR})] - \log (k/D^{\frac{1}{2}} \text{ pol}) \text{ en fonction de } \log (k/D^{\frac{1}{2}} \text{ pol})$$

(ou du potentiel, qui lui est lié).

Les barres tracées sur la Fig. 3(a–f) représentent la dispersion des valeurs observées sur 4 à 5 (ou plus) expériences semblables, elles sont à peine plus grandes que les barres d'erreur qui représenteraient l'incertitude sur la détermination graphique des $\log \chi$ pour une expérience donnée (ordre de grandeur : ± 0.03 unités de $\log \chi$ dans la zone précise).

La Fig. 3(a–f) nous montrent que, compte tenu des incertitudes, les écarts observés restent approximativement limités à ± 0.1 unité sur $\log \chi$ (et donc sur $\log V$). Cette précision sur la détermination des vitesses nous paraît satisfaisante.

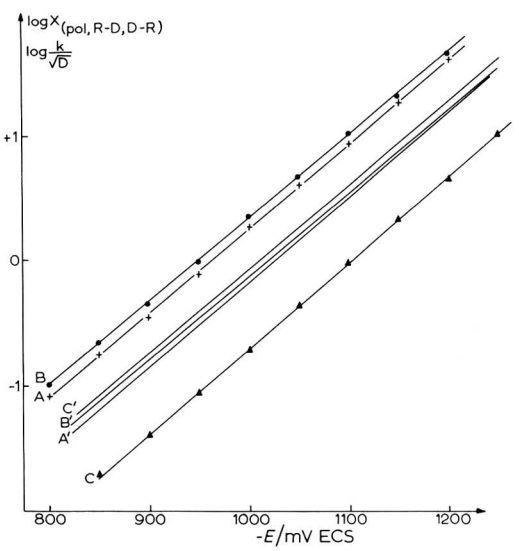

Fig. 2. Onde de réduction du complexe carbonaté de U(VI) 10^{-3} *M* milieu Na_2CO_3 0.5 *M*. (A) polarographie, $\log \chi = f(E)$; (B) mode R–D, $\log k(12\tau/7D)^{\frac{1}{2}} = f(E)$; (C) mode D–R, $\log k(t'/D)^{\frac{1}{2}} = f(E)$. (A'), (B'), (C') courbes correspondantes sous la forme $\log (k/D^{\frac{1}{2}}) = f(E)$.

TABLEAU 2

Polarographie

$U(VI)$	E/mV vs. ECS	i/i_D	$\log \chi$	$\log(k/D^{\frac{1}{2}})$
	−800	0.067	−1.08	−1.50
	−850	0.138	−0.76	−1.18
	−900	0.252	−0.45	−0.87
	−950	0.436	−0.11	−0.53
	−1000	0.658	+0.26	−0.16
	−1050	0.820	+0.60	+0.18
	−1100	0.915	+0.93	+0.51
	−1150	0.960	+1.26	+0.84
	−1200	0.981	+1.60	+1.18

Mode R–D

$U(VI)$	E/mV vs. ECS	Q'/Q'_D	$\log \chi_{RD} = \log k(12\tau/7D)^{\frac{1}{2}}$	$\log(k/D^{\frac{1}{2}})$
	−800	0.068	−0.98	−1.45
	−850	0.147	−0.65	−1.12
	−900	0.250	−0.34	−0.81
	−950	0.430	0.0	−0.47
	−1000	0.639	+0.35	−0.12
	−1050	0.797	+0.67	+0.20
	−1100	0.898	+1.01	+0.54
	−1150	0.946	+1.32	+0.85
	−1200	0.976	+1.66	+1.19

Mode D–R

$U(V)$	E/mV vs. ECS	Q'/Q'_D	$\log \chi_{DR} = \log k(t'/D)^{\frac{1}{2}}$	$\log(k/D^{\frac{1}{2}})$
	−850	0.020	−1.70	−1.06
	−900	0.041	−1.40	−0.76
	−950	0.081	−1.07	−0.43
	−1000	0.172	−0.72	−0.08
	−1050	0.333	−0.37	0.27
	−1100	0.551	−0.03	0.61
	−1150	0.768	+0.31	+0.95
	−1200	0.908	+0.65	+1.29
	−1250	0.976	+1.00	+1.64

Interprétation des écarts observés

Nos courbes polarographiques ne sont pas des polarogrammes classiques, puisque'elles sont affectées en quelque sorte de l'effet de "première goutte"; le potentiel E n'étant appliqué que pendant τ. Cependant, nous avons dans de très nombreux cas enregistré des polarogrammes classiques et leur similitude est très poussée; les écarts en terme de $\log \chi$ sont toujours inférieurs à 0.02 à 0.03 unités, les pentes restant absolument identiques.

Il est notable que les écarts se manifestent surtout dans le cas D–R. La pré-

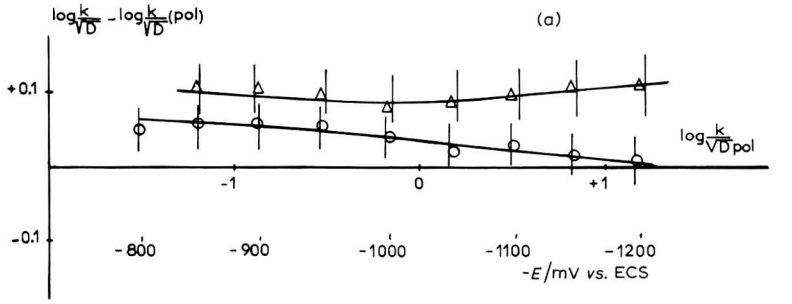
(a)
+0.1
-0.1
-1
0
+1
-800
-900
-1000
-1100
-1200
-E/mV vs. ECS

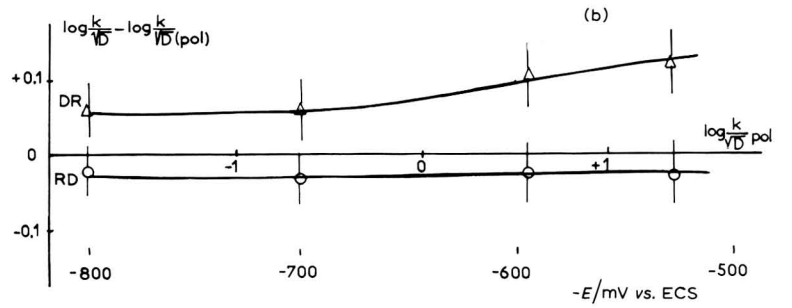
(b)
+0.1
0
-0.1
DR
RD
-1
0
+1
-800
-700
-600
-500
-E/mV vs. ECS

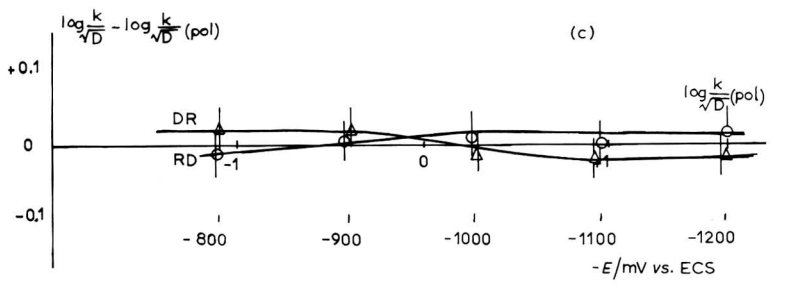
(c)
+0.1
0
-0.1
DR
RD
-1
0
+1
-800
-900
-1000
-1100
-1200
-E/mV vs. ECS

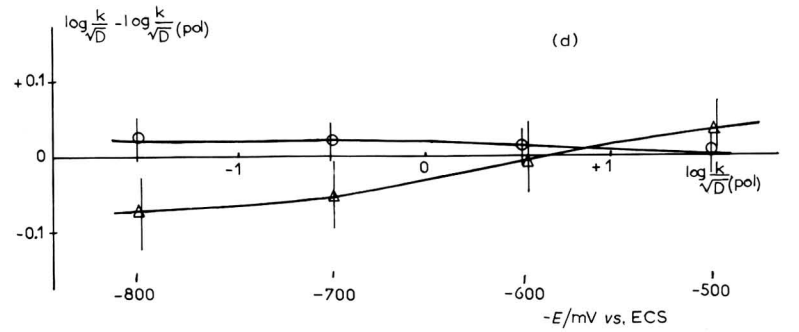
(d)
+0.1
0
-0.1
-1
0
+1
-800
-700
-600
-500
-E/mV vs. ECS

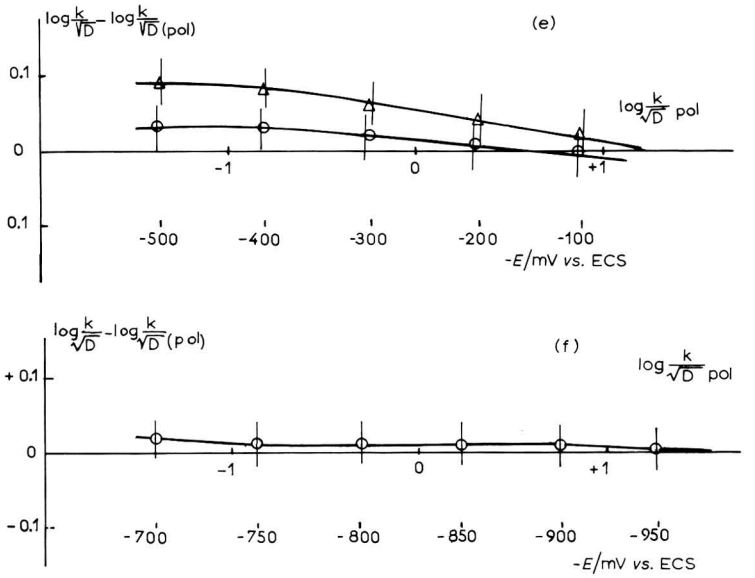

Fig. 3. (○) R–D, (△) D–R. (a) Onde U(VI)→U(V), $[U] = 10^{-3}$ *M*, $[Na_2CO_3] = 0.5$ *M*; (b) onde U(V)→U(VI), $[U] = 10^{-3}$ *M*, $[Na_2CO_3] = 0.5$ *M*; (c) onde U(VI)→U(V), $[U] = 10^{-3}$ *M*, $[Na_2CO_3] = 1$ *M*; (d) onde U(V)→U(VI), $[U] = 10^{-3}$ *M*, $[Na_2CO_3] = 1$ *M*; (e) onde Cr(II)→Cr(III), $[Cr] = 10^{-3}$ *M*, $[NaClO_4] = 0.3$ *M*, $HClO_4 = 10^{-3}$ *M*; (f) onde Cr(III)→Cr(II), mêmes conditions.

cision sur la détermination graphique de log χ à partir des courbes est la même pour les trois cas; d'autre part les différents paramètres τ, t_1, t', etc. sont connus avec une bonne précision et n'interviennent que par le logarithme de leur racine carrée. L'erreur qu'ils apportent est négligeable, mais l'enregistrement de E_2 peut être moins précis que celui de E_1. La pente des droites de la Fig. 2 indique qu'une variation $\Delta\log\chi$ de 0.05 unité correspond à un ΔE de 3 mV environ. Même si une telle non linéarité existait dans nos enregistrements et si les pointages de potentiel faits à partir d'un voltmètre digital (repères pris "au vol" dans le cas D–R où le temps t' d'observation est court) étaient erronnés, ceci n'expliquerait guère les écarts toujours positifs.

Comme l'indique la Table 2 de l'article précédent[1] $\log\chi_{D-R}$ est fonction de Δt et donc du moment exact d'application de potentiel E_2, tandis que $\log\chi_{R-D}$ est insensible aux variations de Δt. Or, même si notre système potentiostat–cellule a un temps de réponse extrêmement rapide, il n'est pas infiniment court et le système prend quelques fractions de ms avant de se stabiliser. Si 200 à 300 μs sont nécessaires pour établir le potentiel E_2, le traitement théorique indique une valeur de χ_{D-R} légèrement plus élevée.

Les expériences de vérification relativement précises que nous avons entreprises semblent donc montrer que les écarts observés entre χ_{D-R} et χ_{pol} s'expliquent principalement par le temps de réponse du système potentiostat–cellule et par l'effet de sphéricité tandis que les écarts entre χ_{R-D} et χ_{pol} sont négligeables. En plus, la technique permet de distinguer aisément les espèces d'un même état de valence produit "*in situ*" ou en équilibre avec l'environment.

REMERCIEMENTS

Les auteurs tiennent à exprimer leur très grande reconnaissance à Monsieur le Professeur L. Gierst de l'Université Libre de Bruxelles pour les conseils qu'il leur a prodigués et le vif intérêt qu'il a porté à ce travail.

RÉSUMÉ

La validité de la théorie établie pour la méthode potentiostatique à double saut avec enregistrement chronocoulométrique a été vérifiée expérimentalement. A cet effet un appareillage a été construit et ses performances ont été analysées de manière systématique.

L'étude cinétique du système U(V)/U(VI) en milieu carbonate conduit à des résultats expérimentaux en bon accord avec la théorie. Les faibles écarts observés sont interprétés en tenant compte de facteurs de second ordre agissant sur le transfert massique.

Comme on peut s'y attendre les courbes de polarisation obtenues par polarographie directe et par les méthodes proposées sont totalement divergentes lorsque le dépolarisant engendré in situ diffère de l'espèce en équilibre avec la solution : il en est ainsi pour le système Cr(II)/Cr(III).

SUMMARY

The validity of the theoretical development established for the double-step potentiostatic method with chronocoulometric recording has been tested experimentally. The performance of an apparatus has been systematically studied.

Experimental results are in good agreement with theory for the U(VI–U(V) system in carbonate media. The small deviations observed between theory and experiment are explained by second-order factors acting on the mass transfer.

As can be expected, the polarization curves obtained by direct polarography and by the chronocoulometric method diverge completely when the depolarizer generated "*in situ*" is different from the species in equilibrium with the solution. Such a case is illustrated by the Cr(III)–Cr(II) system.

REFERENCES

1 F. KIMMERLE ET J. CHEVALET, *J. Electroanal. Chem.*, 21 (1969) 237.
2 F. C. ANSON ET D. A. PAYNE, *J. Electroanal. Chem.*, 13 (1967) 35.
3 J. M. CHRISTIE, G. LAUER ET R. OSTERYOUNG, *J. Electroanal. Chem.*, 7 (1964) 60.
4 P. J. LINGANE ET J. H. CHRISTIE, *J. Electroanal. Chem.*, 13 (1967) 227.
5 J. LEMAIRE, Thèse de Doctorat, Université Libre de Bruxelles, 1965.
6 A. E. KLYGIN ET I. D. SMIRNOVA, *Russ. J. Inorg. Chem. English Transl.*, 4 (1959) 16.
7 H. TAUBE ET M. MYERS, *J. Am. Chem. Soc.*, 76 (1954) 2103.
8 P. J. ELVING ET B. ZEMEL, *Can. J. Chem.*, 37 (1959) 247.
9 C. S. BARRET, *J. Am. Chem. Soc.*, 803 (1961) 1433.
10 R. CORNELISSEN, Thèse de Doctorat, Université Libre de Bruxelles, (1962).
11 P. J. LINGANE ET J. H. CHRISTIE, *J. Electroanal. Chem.*, 13 (1967) 227.
12 I. SLAIN ET K. J. MARTIN, *J. Phys. Chem.*, 65 (1961) 254.

ELECTROANALYTICAL CHEMISTRY AND INTERFACIAL ELECTROCHEMISTRY
Elsevier Sequoia S.A., Lausanne – Printed in The Netherlands

POLAROGRAPHY OF BENZIL MONOSEMICARBAZONE AND RELATED COMPOUNDS

B. FLEET AND R. D. JEE
Chemistry Department, Imperial College of Science and Technology, London, S.W.7. (England)
(Received October 11th, 1969; in revised form November 6th, 1969)

The reduction mechanism for a wide range of azomethine derivatives, RR'C=NYR'' (anils, azines, ketimines, oximes, phenylhydrazones and semicarbazones) has been studied fully by Lund[1]. A detailed study of the reduction of semicarbazones was carried out by Fleet and Zuman[2]. The reduction occurs in acid solution *via* the protonated species, the unprotonated form being electroinactive.

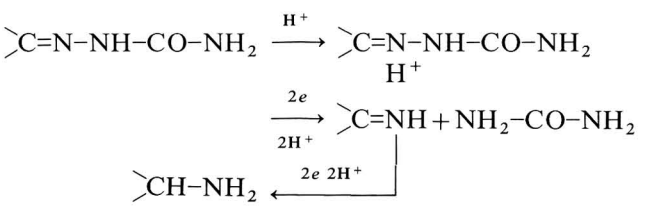

As the pH is raised the wave height decreases and becomes kinetically controlled; in alkaline solution no wave is obtained. The intermediate electroactive product (imine) is generally so reactive that it is reduced immediately, thus giving a single 4-electron wave. In acid solution the wave height reaches its maximum; however, this does not necessarily correspond to a simple 4-electron reduction due to hydrolysis of the semicarbazone.

While the polarography of benzil itself has been widely studied[3-13], no work appears to have been carried out on its monosemicarbazone. A preliminary investigation of the polarographic behaviour of benzil monosemicarbazone showed, surprisingly, that this compound was reduced in a single 2-electron step. Benzoin semicarbazone on the other hand showed a 4-electron wave typical of semicarbazones.

The preparation and chemical properties of benzil monosemicarbazone and related compounds have been studied by Posner[14] and Biltz[15,16]. The semicarbazone was found to undergo easy cyclisation to give 1,2-diphenyloxytriazine. This cyclic compound could then be reduced with zinc–acetic acid to a dihydro compound. None of these compounds has previously been studied polarographically.

EXPERIMENTAL

Apparatus

A Radelkis polarograph type OH-102 (Metrimpex, Hungary) and a Kalousek cell with a saturated calomel electrode (SCE) as reference was used for recording the

polarograms. The capillary constants measured at the potential of the SCE in 0.1 *M* potassium chloride solution were $m = 2.29$ mg s^{-1}, $t = 3.62$ s, at $h = 65$ cm.

Cyclic voltammograms were measured on a 'Chemtrix' polarograph (Beaverton, Oregon,U.S.A.). The instrument was used in its three-electrode mode; the working electrode was a hanging mercury drop electrode type E410 (Metrohm Ltd., Switzerland). The counter electrode was a silver wire while a SCE was used as the reference.

Controlled potential microcoulometry for *n*-value (number of electrons consumed per molecule) determinations, etc., were carried out in a H-type cell[2] using a fairly fast DME (drop time 1.5–2 s). The cell had a capacity of 0.5 ml and the electrolysis of 10^{-3} *M* solutions was carried out over 3–5 h periods, the course of the electrolysis being followed by recording a polarogram at hourly intervals. Preparative scale controlled potential electrolysis was carried out at a mercury pool electrode (area = 10 cm^2) using a solid state potentiostat.

The infrared (i.r.) spectra were obtained on a Perkin Elmer Infracord using a nujol mull and sodium chloride plates. Ultraviolet spectra were measured on a Unicam SP 800, using 2 mm silica cells. The n.m.r. spectra of the dihydro compound were recorded on a Varian A60.

Materials

Reagents were obtained from British Drug Houses Ltd. and were of AnalaR grade where possible. The buffers used had the following compositions; at pH $\leqq$ 2 sulphuric acid; between pH 4 and 7 acetic acid–sodium acetate; pH 8–11 phosphate-based; pH $\geqq$ 12 sodium hydroxide.

Preparation of derivatives

1. *Benzil monosemicarbazone.* The method used was that described by Biltz[16]. The product obtained had a melting point of 174–5° C (lit. 174–5° C); also the i.r. spectrum agreed with that obtained by Awad *et al.*[17]. U.v. spectrum in pH 4.5 medium: 206 nm ($E = 2.9 \times 10^4$), 262 nm ($E = 3.1 \times 10^4$), and shoulder at 280 nm.

2. *1,2-Diphenyloxytriazine.* Method as described by Biltz[16]. The melting point of the product obtained after several recrystallisations from ethanol was found to be 217–9° C, this disagreeing with the value given by Biltz (225–6° C). U.v. spectrum in pH 13 medium: 220 nm ($E = 1.6 \times 10^4$), 262 nm ($E = 1.6 \times 10^4$) and 348 nm ($E = 6 \times 10^3$).

3. *Diphenyldihydro-oxytriazine.* According to Biltz[16] zinc–acetic acid reduction of 1,2-diphenyloxytriazine gives a dihydro compound melting at approx. 200° C; no further information is given. The method of preparation used is as follows.

1 g diphenyloxytriazine, 10 ml ethanol, 10 ml glacial acetic acid, 2 ml water plus zinc turnings were refluxed for approximately 1 h. On cooling a white solid crystallised out. This was recrystallised twice from ethanol. Melting point 262–4° C. (Found: C 71.40% (71.69); H 5.19% (5.22); N 17.61% (16.72); theoretical values in brackets.) U.v. spectrum in pH 13 medium: 220 nm ($E = 1.8 \times 10^4$) and 287 nm ($E = 1.0 \times 10^4$).

Note

The structure of the dihydro compound was not confirmed by Biltz but only assumed from the known reducing properties of zinc–acetic acid. Infrared and n.m.r spectra of this compound were of little use in confirming its structure. The reduction of the cyclic compound could be expected to produce three possible compounds.

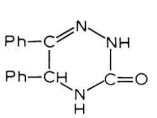

I

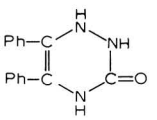

II

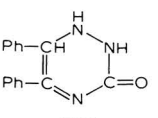

III

The n.m.r spectrum rules out II (no Ph–C–H), but there is little evidence to make a choice between I and III. It will be seen later, however, that structure I and not III fits the polarographic behaviour of this compound.

4. *Benzoin semicarbazone.* Method as described by Biltz[16]. Melting point 202–3° C (lit. 206° C).

Stock solutions 10^{-2} *M*, (10^{-3} *M* in the case of diphenyldihydro-oxytriazine) in ethanol were prepared and used for the polarographic investigations. In the case of benzil monosemicarbazone, fresh solutions must be prepared daily due to the slow cyclisation of this compound. All the polarograms were measured in a 50% ethanol medium and depolariser concentration 2×10^{-4} *M*. The supporting electrolyte was deoxygenated for 5 min and then the depolariser sample added; after a further 15 s of deoxygenation the polarogram was recorded.

RESULTS AND DISCUSSION

Benzil monosemicarbazone

The pH dependence is given in Table 1. Comparison of the wave height with that of 4-chlorobenzaldehyde semicarbazone ($n=4$) and benzil ($n=2$) indicated a 2-electron reduction. The wave shape indicates irreversibility and the dependence of the half-wave potential on pH gives $dE_{\frac{1}{2}}/dpH = 84$ mV. Above pH 8 the wave splits

TABLE 1

pH	*Benzil monosemicarbazone*		*1,2-Diphenyloxytriazine*		*Diphenyldihydro-oxytriazine*		*Benzoin semicarbazone*	
	$E_{\frac{1}{2}}/V$	$i/\mu A$	$E_{\frac{1}{2}}/V$	$i/\mu A$	$E_{\frac{1}{2}}/V$	$i/\mu A$	$E_{\frac{1}{2}}/V$	$i/\mu A$
2.1	−0.40	0.70	−0.20	0.54	−1.00	1.30	−0.90	1.42
4.5	−0.74	0.70	−0.37	0.68	−1.22	1.14	−1.13	1.30
5.5							−1.20	0.95
6.2							−1.30	0.38
6.3	−0.82	0.71	−0.46	0.69				
6.8					−1.43	0.43		
8.3	−0.96	0.72	−0.55	0.70				
8.8	−1.03	0.72	−0.66	0.70	−1.45	0.12		
10.1	−1.08, −1.54	0.72*	−0.81	0.71				
10.8	−0.95, −1.06, −1.40	0.71*	−0.99, −1.40	0.71*				
11.5	−1.06, −1.30	0.71*	−1.05, −1.28	0.70*				
12.3			−1.10, −1.23	0.70*				
13.8	−1.19	0.70	−1.15	0.69				

* Total wave height.

i = Current in μA for a depolariser concentration of 2×10^{-4} *M*.

into two, a smaller wave appearing at more negative potentials. At pH 10.8 a third wave appears at more positive potentials. Beyond approximately pH 11 the original wave disappears completely leaving two waves, until finally at pH > 13 the more positive wave disappears leaving a single wave.

1,2-Diphenyloxytriazine

This compound can exist in several tautomeric forms.

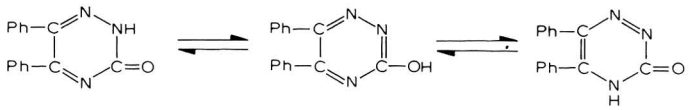

IV V VI

Evidence for structures IV and V can clearly be seen from the existence of characteristic C=O and C–OH bands in the i.r. spectrum of this compound. The compound is soluble in sodium hydroxide to form an anion[16].

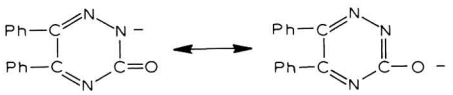

The polarographic behaviour is given in Table 1. The half-wave potential shows a dependence on pH of $dE_{\frac{1}{2}}/dpH = 50$ mV over the pH range 1–8. Wave height comparisons give $n = 2$. At low pH values the wave shape is characteristic of a reversible system. The value of the diffusion current is considerably smaller at pH 2 as compared with at higher pH values. Whether this is simply a buffer composition effect or not is not clear. The reversibility at pH 2.1 was confirmed by cyclic voltammetry at a hanging mercury drop electrode. A half-peak separation of 30 mV (Fig. 1a) is observed indicating a 2-electron process (theoretical separation 28 mV[18]). At pH 4.5 cyclic voltammetry (Fig. 1b) shows marked signs of irreversibility. In alkaline solution the reduction is completely irreversible.

Beyond pH 8 the wave splits into two, the more positive wave can be assigned to the reduction of the neutral or protonated species, while the more negative wave

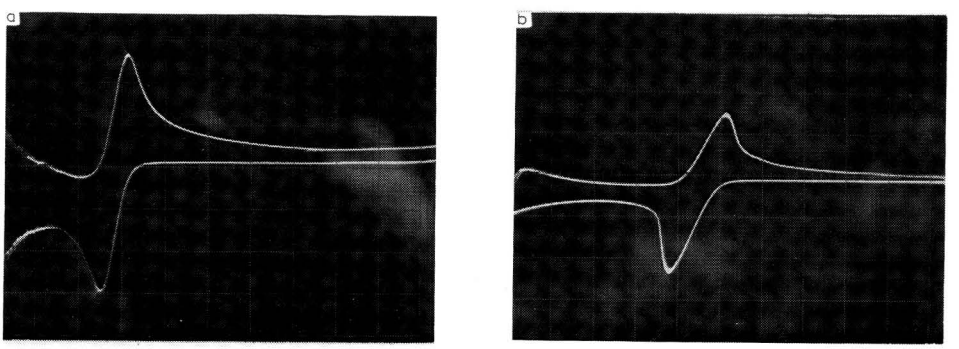

Fig. 1. Cyclic voltammograms of 2×10^{-4} *M* 1,2-diphenyloxytriazine, 50% ethanol medium, sweep rate 1 V s^{-1}. (a) pH 2.1, (b) pH 4.5.

is due to the reduction of the anionic form. Mercury reservoir height dependence studies show that the more positive wave at pH 11.5 has some kinetic character.

Polarograms of benzil monosemicarbazone and those of 1,2-diphenyloxytriazine at pH values >11 are identical, showing that the same species is in solution. Further confirmation of this is obtained from the similar u.v. spectra at pH 13.8 (Fig. 2).

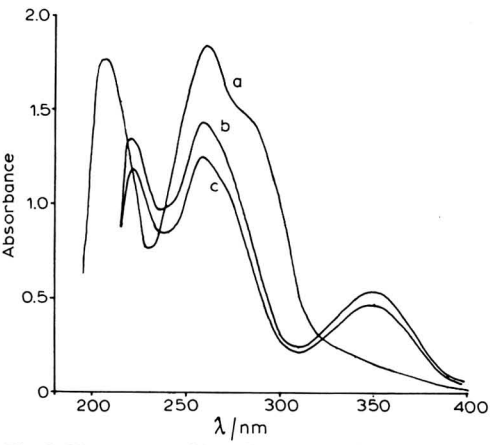

Fig. 2. U.v. spectra of benzil monosemicarbazone and 1,2-diphenyloxytriazine, 50% ethanol medium. (a) benzil monosemicarbazone pH 4.5, (b) benzil monosemicarbazone pH 13.8, (c) 1,2-diphenyloxytriazine pH 13.8.

On the basis of this evidence it is possible to explain the mixed process occurring for the monosemicarbazone from pH 8 to 13.8. Above pH 8 a wave at more negative potentials appears; this corresponds to the reduction of the anion of the cyclic compound. Although the anion will be in equilibrium with its neutral form, the reduction of the latter occurs at a potential close to that of the monosemicarbazone and consequently no separate wave is obtained. At pH 10.8 a wave at -0.95 V due to the neutral form of the cyclic compound appears, while the monosemicarbazone wave at -1.06 V is only just detectable. Above pH 11.5 the system contains only the cyclic derivative. As the cyclisation of the monosemicarbazone is an irreversible chemical process, the polarograms in alkaline solution are time dependent, as expected. Thus at pH 10.8 three waves are observed only if the polarogram is recorded immediately on introducing the depolariser. After approx. 5 min only waves at -0.95 and -1.40 V are observed, the system now being identical with that of diphenyloxytriazine at pH 10.8.

Diphenyldihydro-oxytriazine

The polarographic behaviour (Table 1) shows considerable similarity in its pH dependence to a typical semicarbazone. Wave height comparisons suggested a value for n of 3–4, the value from microcoulometry being 3.6. The non-integral value of n cannot be attributed to hydrolysis, etc., as a time dependence of the wave at pH 2.1 showed no change over a period of 3 h. The absence of an anodic peak on the cyclic voltammogram confirms irreversibility.

Benzoin semicarbazone

This compound shows the typical behaviour of a normal semicarbazone. Wave height comparisons with benzil clearly indicates $n=4$. The reduction mechanism of this compound can thus be reasonably assumed to be the same as other semicarbazones.

$$\underset{\text{Ph–CH–OH}}{\overset{\text{Ph–C=N–NH–CO–NH}_2}{|}} \xrightarrow[2H^+]{2e} \underset{\text{Ph–CH–OH}}{\overset{\text{Ph–C=NH}}{|}} \xrightarrow[2H^+]{2e} \underset{\text{Ph–CH–OH}}{\overset{\text{Ph–CH–NH}_2}{|}}$$

single wave

Electrolysis of the monosemicarbazone at a potential just on the plateau of the wave in a pH 4.5 medium gave an n value of 2.05 ± 0.10. Polarograms measured at regular intervals during the electrolysis showed the appearance of a wave at more negative potentials, which grew at the expense of the original wave. The overall height of the two waves remained the same indicating that the new wave was due to a 2-electron wave. The conventional d.c. polarogram of this compound shows no such wave thus indicating the formation initially of an electroinactive product which can slowly transform into a electroactive species.

Electrolysis at a potential of -1.30 V (pH 4.5 medium) was next performed so that the product from the first wave would also be reduced and an n value corresponding to the two processes obtained. Polarograms measured during the electrolysis showed little change in the overall height, but the reduction wave of the product of reduction of the monosemicarbazone appeared to split into two very close waves, indicating the participation of a further electroactive product.

Reduction of benzil monosemicarbazone (pH 4.5 medium) at -0.90 V using a mercury pool electrode is shown in Fig. 3. A polarogram recorded on the resulting

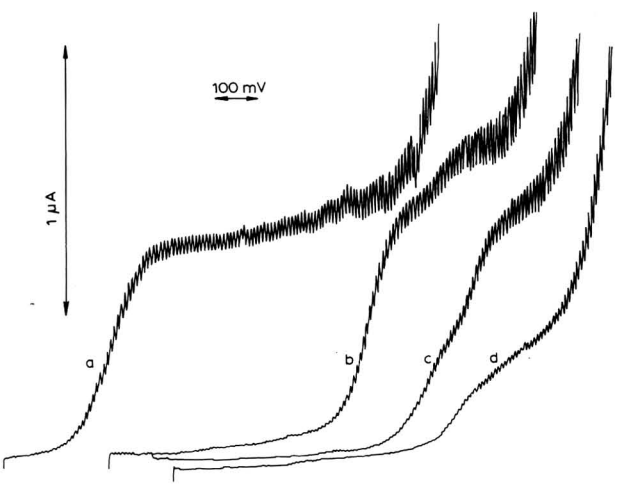

Fig. 3. Polarograms of electrolysed solutions of benzil monosemicarbazone, 2×10^{-4} M, 50% ethanol medium, pH 4.5. Electrolysed at a mercury pool electrode. Starting potential -0.50 V *vs.* SCE. (a) benzil monosemicarbazone before reduction, (b) after complete reduction at -0.90 V, (c) partial reduction of the solution from (b) at -1.20 V, (d) partial reduction of the solution from (c) at -1.40 V.

solutions shows a post wave due to the reduction product of the main wave. Electrolysis at -1.20 V shows that the first wave decreases at the expense of this post wave, the overall wave height remaining nearly constant, again indicating a 2-electron process for this further reduction step. An electroinactive intermediate must be postulated to account for the small size of the post wave on the polarogram.

The overall reduction mechanism of benzil monosemicarbazone is thus of the form:

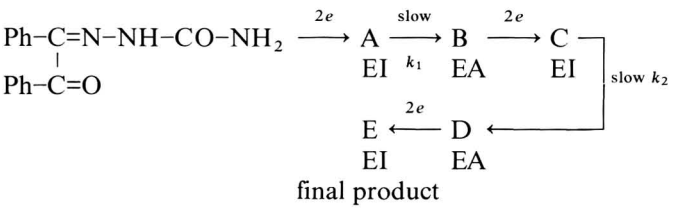

EI electroinactive species, EA electroactive species.

The first reduction step can be either the breaking of the N–N bond or reduction of Ph–C=O to Ph–CH–OH. If the latter reaction occurred then the electroactive product B would be benzoin semicarbazone. The half-wave potential for the reduction of B in the medium examined (pH 4.5, 50% ethanol) has nearly the same value as for benzoin semicarbazone in this medium. The reduction of B however is a 2-electron process while that of benzoin semicarbazone is 4-electron.

The overall mechanism can thus be reduced to one of two possibilities:

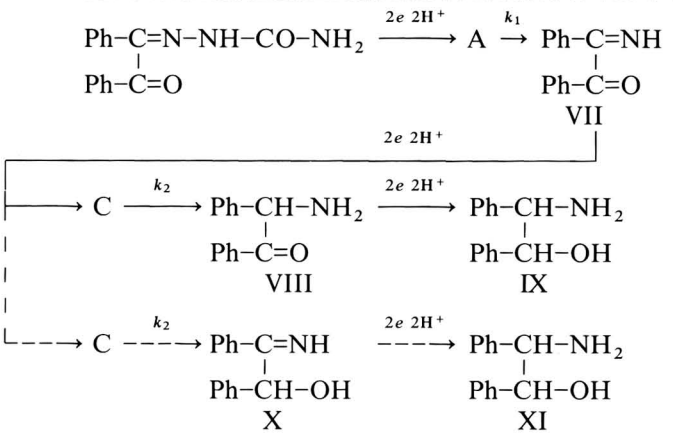

The reduction path VII→C→X→XI can be eliminated as the intermediate X is also obtained as an intermediate in the reduction of benzoin semicarbazone. The half-wave potential for the reduction of X should therefore be the same or more positive than that for benzoin semicarbazone ($E_{\frac{1}{2}} = -1.13$ V, pH 4.5). In practice the step occurs at -1.27 V (pH 4.5). The reduction scheme benzil monosemicarbazone →A→VII→C→VIII→IX would therefore appear acceptable.

The greater stability of VII over that of X is interesting and is presumably due to hydrogen bonding between the imine hydrogen and C=O.

The reduction of 1,2-diphenyloxytriazine at pH 2.1 gives rise to a final electro-

active product which is reduced at more negative potentials. This product has a half-wave potential corresponding to that of the dihydro derivative in the same medium. No post wave due to the dihydro compound is normally observed on a polarogram of 1,2-diphenyloxytriazine, thus indicating an intermediate species. The overall wave height on electrolysis increases showing that this product is reduced with an n value greater than 2. The initial product of electrolysis gives rise to a reversible couple (Fig. 4, note the anodic portion to the wave). This intermediate is of limited stability for the anodic wave reaches a maximum value after about 1 h electrolysis. If the electrolysis is stopped, this intermediate appears to revert to the original compound.

The nature of this oxidizable intermediate is far from clear. The above results, along with the evidence of reversibility from cyclic voltammetry, would suggest the

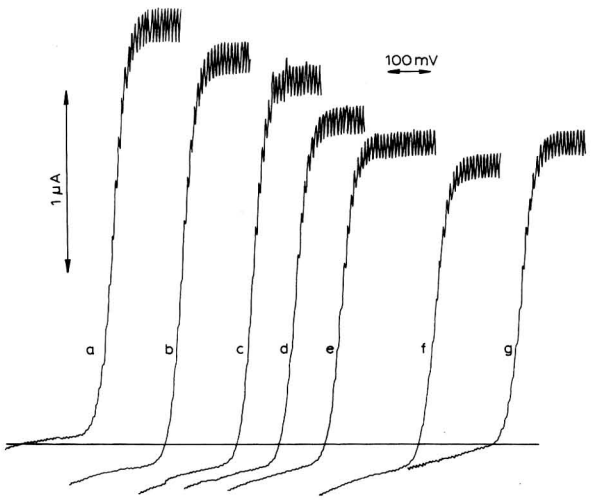

Fig. 4. Polarograms of 1,2-diphenyloxytriazine after electrolysis, 1×10^{-3} M, 50% ethanol medium, pH 2.1. Electrolysed at -1.15 V using a DME. Time of electrolysis: (a) 0, (b) 1, (c) 2, (d) 3, (e) 4, (f) 5, (g) 5 h recorded 45 min after electrolysis was stopped.

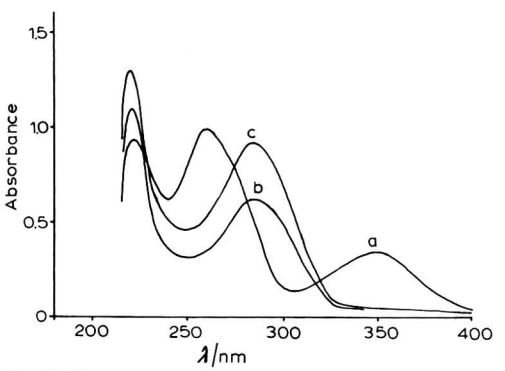

Fig. 5. U.v. spectra of 1,2-diphenyloxytriazine and diphenyldihydro-oxytriazine, 50% ethanol medium. (a) 1,2-diphenyloxytriazine, (b) reduction product of 1,2-diphenyloxytriazine, (c) diphenyldihydrooxytriazine, all at pH 13.8.

formation of a di-radical.

In alkaline medium the process is much simpler. The reduction of the anion occurs with the uptake of 2 electrons to form the dihydro derivative. The dihydro compound is electroinactive under these pH conditions, but its presence can be readily inferred from the u.v. spectrum of electrolysed solutions of the cyclic compound (Fig. 5).

Electrolysis of the dihydro compound produces no new electroactive species. The i.r. spectrum of the product isolated indicates the presence of a C=O group. The reduction path would appear to be:

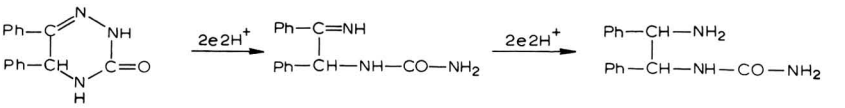

If the structure of the dihydro compound is in fact III then it is extremely difficult to postulate a 4-electron process characteristic of a semicarbazone.

The reduction scheme for benzil monosemicarbazone is summarized below:

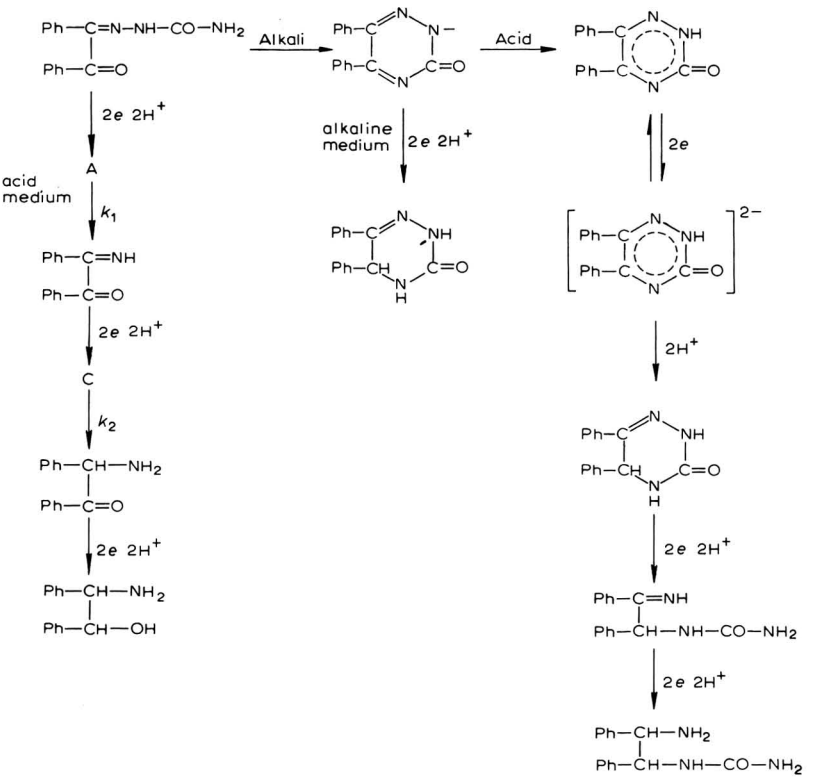

ACKNOWLEDGEMENT

The authors wish to thank Dr. P. Zuman for some helpful discussions.

SUMMARY

In acid medium benzil monosemicarbazone can be reduced in three 2-electron steps to give Ph–CH(NH_2)–CH(OH)–Ph. A normal polarogram, however, shows only a 2-electron step as the initial electroinactive product is only slowly converted to an electroactive form. A similar situation arises between the second and third steps. Above approximately pH 8, the semicarbazone cyclises to give 1,2-diphenyloxytriazine. 1,2-Diphenyloxytriazine forms an anion in alkaline medium and over the pH range 8–11 gives two polarographic waves corresponding to the reduction of the neutral and anionic forms. The 2-electron reduction of this compound gives diphenyldihydro-oxytriazine. In acid medium 1,2-diphenyloxytriazine gives a 2-electron reversible wave with the formation of an unstable intermediate. This intermediate converts slowly into diphenyldihydro-oxytriazine. A single 4-electron wave with a pH dependence typical of a semicarbazone was observed for this compound.

REFERENCES

1 H. LUND, *Acta Chem. Scand.*, 13 (1959) 249.
2 B. FLEET AND P. ZUMAN, *Collection Czech. Chem. Commun.*, 32 (1967) 2066.
3 H. E. STAPELFELDT AND S. P. PERONE, *Anal. Chem.*, 40 (1968) 815.
4 H. E. STAPELFELDT AND S. P. PERONE, *Anal. Chem.*, 41 (1969) 623.
5 A. VINCENZ-CHODKOWSKA AND Z. R. GRABOWSKI, *Electrochem. Acta*, 9 (1964) 789.
6 R. H. PHILP JR., R. L. FLURRY AND R. A. DAY JR., *J. Electrochem. Soc.*, 111 (1964) 328.
7 R. KALVODA AND G. BUDNIKOV, *Collection Czech. Chem. Commun.*, 28 (1963) 833.
8 H. BERG, *Naturwissenschaften.*, 48 (1961) 100.
9 C. A. STREULI AND W. D. COOKE, *Anal. Chem.*, 26 (1954) 963.
10 M. I. BOBROVA AND N. S. TIKHOMIROVA, *Zh. Obshch. Khim.*, 22 (1952) 2107.
11 R. PASTERNAK, *Helv. Chim. Acta*, 31 (1948) 753.
12 R. H. PHILP JR., T. LAYLOFF AND R. N. ADAMS, *J. Electrochem. Soc.*, 111 (1964) 1189.
13 W. ROGERS JR. AND S. M. KIPNES, *Anal. Chem.*, 27 (1955) 1916.
14 T. POSNER, *Chem. Ber.*, XXXIV (1901) 3973.
15 H. BILTZ, *Chem. Ber.*, XXXV (1902) 346.
16 H. BILTZ, *Ann. Chem.*, 339 (1905) 243.
17 W. I. AWAD, A. R. A. RAOUF AND A. M. KAMEL, *J. Org. Chem.*, 24 (1959) 1777.
18 L. MEITES, *Polarographic Techniques*, Interscience Publishers, New York, 1965, p. 415.

ELECTROANALYTICAL CHEMISTRY AND INTERFACIAL ELECTROCHEMISTRY
Elsevier Sequoia S.A., Lausanne – Printed in The Netherlands

SIMULTANEOUS DETERMINATION OF COPPER, CADMIUM, LEAD AND ZINC IN WATER BY ANODIC STRIPPING POLAROGRAPHY

IVAN ŠINKO
Chemical Institute "Boris Kidrič", Department of Analytical Chemistry, Ljubljana (Yugoslavia)
JAN DOLEŽAL
Department of Analytical Chemistry, Charles University, Prague (Czechoslovakia)
(Received September 15th, 1969)

INTRODUCTION

Since it is possible to infer from the chemical composition of water the geological composition of soil and utilization possibilities of water, the determination of low concentrations of some cations in natural waters is important in geochemistry and biology. The concentrations of copper, cadmium, lead and zinc ions in water are usually very low and their determination by spectrophotometric, spectrographic and polarographic methods is time-consuming since the dissolved salts must be preconcentrated, a procedure which may easily lead to erroneous results. The anodic stripping method has proved suitable for the determination of low concentrations of some cations that form amalgams with mercury. This method requires no preconcentration of ions in water because concentration takes place at the hanging mercury drop electrode (HMDE) during electrolysis, which is accomplished in a few minutes. In this way the time of analysis is shortened and the side-effects of the concentration procedure, tending to reduce the accuracy and precision of the method, avoided. Several procedures for the determination of low concentrations of cations and ions in water, are described in the literature. Kublik[1] proposes anodic stripping polarography for the determination of copper, cadmium and lead ions in drinking water. Ariel and coworkers[2,3] suggest the use of the medium exchange method for the determination of copper, cadmium and zinc ions in sea water. In addition, there are reports on methods for the direct determination of zinc ions in sea water[4] and for the determination of low concentrations of nickel and cobalt ions in natural waters[5]. Kemula and coworkers[6] use the anodic stripping method for the determination of low concentrations of bromide and iodide in water.

The literature, however, contains no report on the simultaneous determination of copper, cadmium, lead and zinc ions in natural waters. This determination has been successfully carried out in 0.1 *M* acetate buffer, pH 5.8–6.0, as supporting electrolyte.

EXPERIMENTAL

Apparatus

A LP-60 polarograph and a Radiometer Kemula electrode P-958 were used. The experiments were carried out in a 50 ml electrolysis cell using a saturated calomel

electrode. The salt bridge was filled with 1 *M* KCl solution; the ends of the salt bridge were of very small surface area and were made of sintered glass of adequate porosity. The solution was stirred with a glass stirrer at 400 rev./min. The surface area of the mercury drop electrode was 1.71 mm^2 and the rate of change of the applied e.m.f. was 0.2 V min^{-1}.

The pH values were measured with a Radiometer pH-meter PHM-4d. The purification of nitrogen was done in special columns filled with an alkaline solution of sodium 2-anthraquinone sulphonate and an acid solution of chromous sulphate.

Reagents

Standard 10^{-2} *M* solutions were prepared from analytical grade nitrates; more dilute solutions were prepared each day by diluting the 10^{-2} *M* solution. The analytical grade hydrochloric acid was purified by isopiestic[7] distillation; the analytical grade potassium chloride and sodium acetate were recrystallized twice. The 1 *M* solution of the acetate buffer, pH 5.8, was prepared as follows: 32.3 g of $CH_3COONa \cdot 3H_2O$ were dissolved in water in a 250 ml volumetric flask, 0.80 ml of 99% acetic acid was added and solution made up to volume with distilled water. The water used was distilled twice in a quartz apparatus.

RESULTS AND DISCUSSION

A. Choice of the supporting electrolyte

The determination of zinc ions in an acid solution is not feasible because the potential of the reduction of zinc ions at the HMDE is more negative than, or equal to, the potential of the reduction of hydrogen ions. A neutral or alkaline medium must therefore be used for the simultaneous determinations of copper, cadmium, lead and zinc. The experiments were carried out in a neutral medium using KCl and an acetate buffer, pH from 5 to 7. Figure 1 shows (i) the current–potential curves for these four metals in KCl and the acetate medium, and (ii) the current–potential curves for copper, cadmium and lead in HCl as supporting electrolyte. In an acetate medium the four metals yield almost identical, readily measurable anodic currents, and the differences between the half-peak potentials are large enough to permit a simultaneous recording of their oxidation peaks. Kemula and Glodowaski[8] give further data on the acetate buffer solution as supporting electrolyte. When a 0.1 *M* or 0.02 *M* KCl solution was used as supporting electrolyte in the analysis of some waters, no accurate results for the concentration of zinc ions were obtained. When this supporting electrolyte was used, the pH value tended to change, and this may have been responsible for the inaccuracy in the results (see below). The two current–potential curves in Fig. 1 show that when using 0.02 *M* KCl extremely small oxidation current peaks are obtained for lead and copper, and the oxidation current peak for copper is poorly defined. Thus an 0.1 *M* acetate buffer solution was used in these experiments as supporting electrolyte.

B. Dependence of oxidation current peaks for copper, cadmium, lead and zinc on the pH value of the solution

Figure 2 shows that for copper, cadmium, lead and zinc the oxidation current peaks are independent of the pH of the solution in the acid range up to pH 7. With

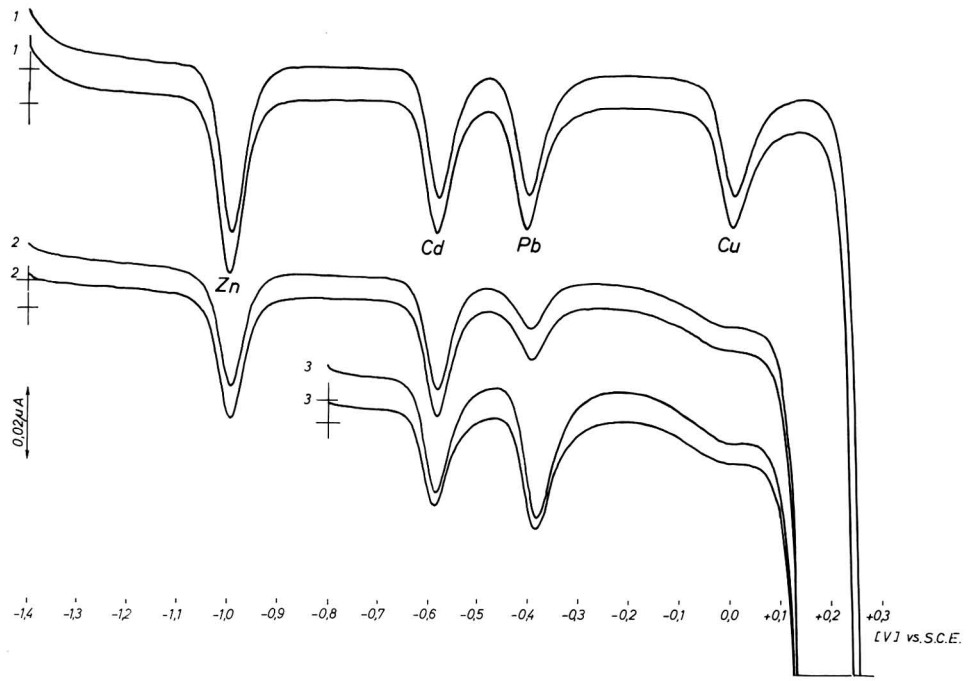

Fig. 1. Anodic curves after 3 min concentrating electrolysis. Concn. Cd^{2+}, Cu^{2+}, Pb^{2+} and Zn^{2+}, 5×10^{-7} *M*. Supporting electrolyte: (1) 0.02 *M* acetate buffer soln., pH 6.40; (2) 0.02 *M* KCl (pH of soln. 5.99); (3) 0.02 *M* HCl.

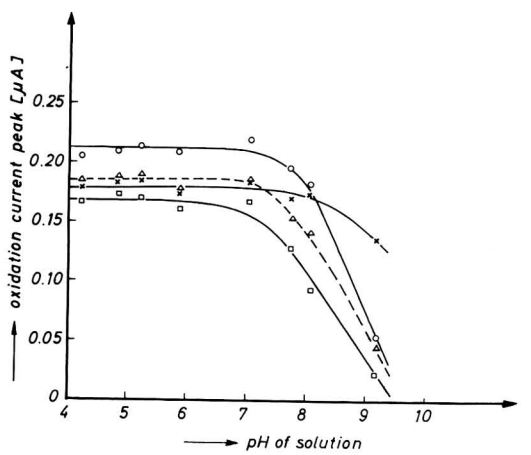

Fig. 2. Relationship between oxidation current peaks and pH of soln. Concn. Cd^{2+}, Cu^{2+}, Pb^{2+} and Zn^{2+}, 4×10^{-6} *M*; supporting electrolyte, 0.16 *M* acetate buffer soln. at different pH. (○) Zn, (×) Cd, (△) Pb, (□) Cu.

increase in pH from 7 to 10, the oxidation current peaks decrease sharply for all four metals. Figure 3 shows that besides the lowered oxidation current peaks for copper, two oxidation current peaks are observed above pH 7.8. At these higher pH values the

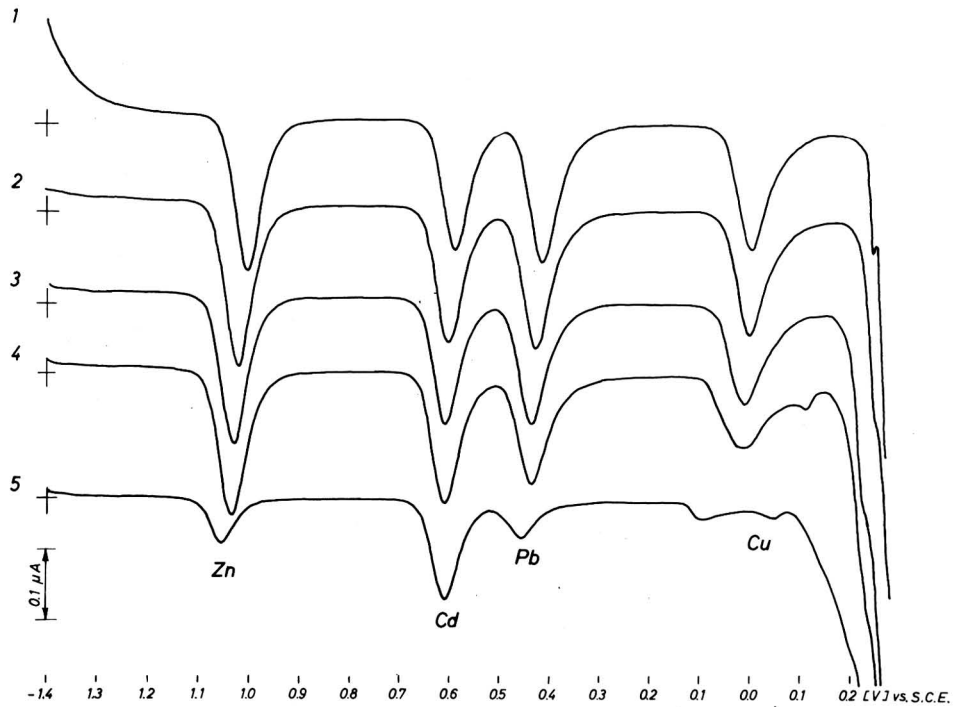

Fig. 3. Anodic curves after 3 min concentrating electrolysis at -1.4 V *vs.* SCE. Concn. of Cd^{2+}, Cu^{2+}, Pb^{2+} and Zn^{2+}, 4×10^{-6} *M*. Supporting electrolyte, 0.16 *M* acetate buffer soln. with the following pH values: (1) 5.21, (2) 7.04, (3) 7.73, (4) 8.06, (5) 9.14.

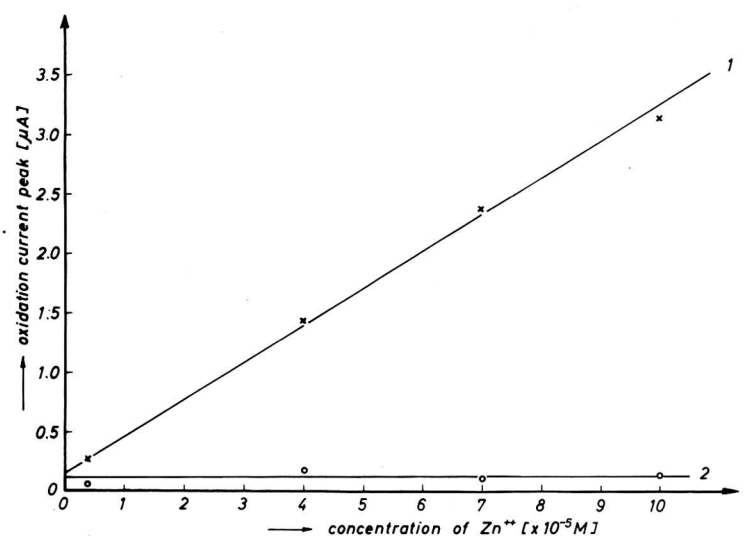

Fig. 4. Dependence of the oxidation current peaks on the concn. of Zn^{2+} at different pH of the soln. Electrolysis time, 3 min at -1.4 V *vs.* SCE; supporting electrolyte, 0.16 *M* acetate buffer soln. with the following pH values: (1) 7.80, (2) 9.15.

sum of the two oxidation current peaks is smaller than the oxidation current peak in an acid or neutral medium. A similar phenomenon was observed by Zajčko and Zaharov[9] for the oxidation current of antimony in 2 *M* KOH as supporting electrolyte, and by Sinjakova and Markova[10] for the oxidation current of lead and copper in NaOH as supporting electrolyte.

The dependence of the oxidation current peak on ion concentration is the basis of the determination of the concentration of cations in the solution. Figure 4 shows that there is a linear relationship between the oxidation current peaks and the concentration of zinc ions in a solution if the pH of the solution is below 8; at higher pH values, however, the current is independent of the concentration of zinc ions. The same is true for cadmium and lead ions. In the case of copper ions, there is a linear relationship between the oxidation current peaks and the concentration of copper ions only up to pH 7. These results show that the concentration of copper, cadmium, lead, and zinc ions in water can be accurately determined by the use of 0.1 *M* KCl or 0.02 *M* KCl as supporting electrolytes only if after the addition of the supporting electrolyte and the bubbling of nitrogen through the solution, the pH of solution is below 7. This condition, however, can be satisfied only in the analysis of distilled and some natural waters.

C. Changes in the pH of water and in the pH of the solution due to deaeration with nitrogen

Since the oxidation current peaks of copper, cadmium, lead and zinc depend on the pH of the solution, the changes in pH after the addition of the supporting electrolyte, and the effect of deaeration with nitrogen on the pH of the solution, were studied. Table 1 shows that the pH of water depends on the deaeration time. The pH values of the solutions were measured in an electrolysis cell under conditions identical with those demanded by anodic stripping polarography.

TABLE 1

EFFECT OF DEAERATION TIME ON THE pH OF WATER

Water sample	*pH of water*		
	Before deaeration with N_2	*After* 10 *min deaeration with* N_2	*After* 20 *min deaeration with* N_2
1.	7.24	8.64	8.91
2.	7.23	8.62	8.84
3.	7.22	8.59	8.79
4.	7.19	8.50	8.71
5.	7.18	8.55	8.76
distilled water	6.25	7.30	7.50

During the first 10 min of deaeration with nitrogen, the pH of the solution changes considerably; later it changes only slightly, until after more than 35 min no change in pH is observed. The increase in the pH of water during deaeration seems to be due to the removal of CO_2 from water and is responsible for the erroneous results obtained for zinc ions in water if KCl solution is used as supporting electrolyte. In

order to deal with this problem appropriate buffer solutions of pH 5–7 were used. The best results were obtained with an acetate buffer.

In the determination of low concentrations of cations in water, a possible contamination by the supporting electrolyte must be taken into consideration. Contamination can be kept to a minimum by using very pure reagents and by keeping the concentration of the supporting electrolyte as low as possible. Table 2 shows that

TABLE 2

pH OF THE WATER SOLUTION AS A FUNCTION OF CONCENTRATION AND pH OF THE ACETATE BUFFER SOLUTION, AND OF THE TIME OF DEAERATION WITH NITROGEN

pH of buffer soln.	*Concn. of acetate buffer in water soln./M*	*pH of soln.*		
		Before deaeration with N_2	*After* 10 *min deaeration with* N_2	*After* 20 *min deaeration with* N_2
5.64	0.1	5.70	5.71	5.71
5.64	0.02	5.98	6.31	6.32
6.44	0.02	6.99	8.54	8.81
5.89	0.1	5.93	5.97	5.97

at very low concentrations of the acetate buffer, the pH of the solution still changes with deaeration time and that the pH-change increases with the increasing pH of the buffer solution. Good results were obtained with 0.1 *M* acetate buffer as supporting electrolyte if the pH of the buffer solution was between 5.8 and 6.0. If a more acid buffer solution is used, the cathodic current of hydrogen ions becomes so pronounced as to interfere with the recording of the current–potential curves for zinc.

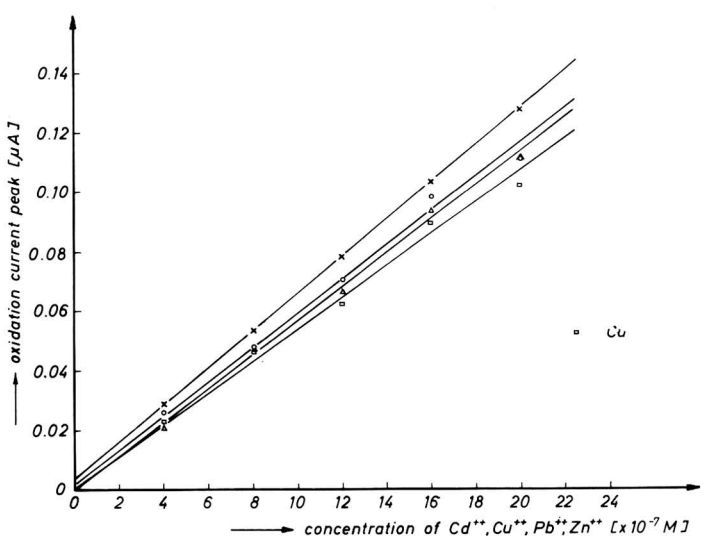

Fig. 5. Calibration curves for Cd^{2+}, Cu^{2+}, Pb^{2+} and Zn^{2+} in the concn. range 4×10^{-7}–2×10^{-6} *M*. Supporting electrolyte, 0.02 *M* acetate buffer soln., pH 6.40. Electrolysis time, 3 min at −1.4 V *vs.* SCE. (×) Zn, (○) Cd, (△) Pb, (□) Cu.

D. Procedure

20 ml of water is pipetted into the electrolysis cell and 2.0 ml of a 1 *M* acetate buffer solution, pH 5.8, is added. The oxygen dissolved in the solution is removed by bubbling nitrogen through the solution for 10–15 min and a hanging mercury drop electrode is made. The stirrer is then put into operation and the electrolysis carried out for 3–5 min at −1.4 V *vs.* SCE. During electrolysis, nitrogen is introduced into the space above the surface of the solution. After the electrolysis the stirrer is turned off, deaeration discontinued, and the solution left for one minute to become quiescent; the current potential curves are then recorded from −1.4 to +0.2 V *vs.* SCE. The concentration of copper, cadmium, lead, zinc cations in water is determined either with the aid of calibration curves or by the standard addition method. If concentrations are read from calibration curves (Fig. 5), the solutions must be thermostatted.

TABLE 3

ACCURACY OF DETERMINATION OF CADMIUM, COPPER, LEAD AND ZINC IN NATURAL WATERS

$[Cu]/\mu g\ l^{-1}$			$[Pb]/\mu g\ l^{-1}$			$[Cd]/\mu g\ l^{-1}$			$[Zn]/\mu g\ l^{-1}$		
Added	*Found*	*Deviation/%*	*Added*	*Found*	*Deviation/%*	*Added*	*Found*	*Deviation/%*	*Added*	*Found*	*Deviation/%*
1.3	1.1	−15.4	4.1	4.1	0	2.2	2.0	− 9.1	1.3	1.2	− 7.7
6.4	7.4	+15.6	8.3	7.7	− 7.2	4.5	4.4	− 2.2	2.6	2.1	−19.2
3.9	3.9	0	12.4	11.0	−11.3	6.7	7.9	+17.9	6.5	5.7	−12.3
12.7	13.5	+ 6.3	20.7	24.6	+18.8	11.2	12.0	+ 7.1	13.0	12.8	− 1.5
19.1	20.8	+ 8.9	31.0	31.0	0	16.9	17.4	+ 3.0	19.6	18.0	− 8.1

The lowest concentrations determined by the above procedure were 10^{-8} *M* for cadmium and lead ions, and 2×10^{-8} *M* for copper and zinc ions. Lower concentrations of copper and zinc ions could not be determined although well-shaped current–potential curves were obtained, because the supporting electrolyte itself was contaminated with 10^{-8} *M* of copper and zinc ions.

The accuracy of the method is satisfactory (relative error does not exceed 20%) (Table 3). The standard deviation of the measurement of oxidation current peaks is 3–6%.

SUMMARY

A procedure is described for the simultaneous determination of copper, cadmium, lead, and zinc ions in drinking and natural waters. The lowest concentrations that could be determined were 10^{-8} *M* for cadmium and lead ions, and $2 \cdot 10^{-8}$ *M* for copper and zinc ions.

In the case of copper, cadmium, lead and zinc, the pH of the acetate buffer solution (or that of the 0.1 or 0.02 *M* of KCl solution) as supporting electrolyte, if kept below 7 has no effect on the oxidation current peaks; at higher pH values, however, the current peaks become considerably smaller. Since deaeration with nitrogen tends to increase the pH, a buffer solution must be used as supporting electrolyte. For the simultaneous determination of copper, cadmium, lead and zinc ions in water, a 0.1 *M* acetate buffer solution, pH 5.8, was used as supporting electrolyte.

REFERENCES

1 Z. KUBLIK; *Acta Chim. Acad. Sci. Hung.*, 27 (1961) 79.
2 M. ARIEL AND U. EISNER, *J. Electroanal. Chem.*, 5 (1963) 362.
3 M. ARIEL, U. EISNER AND S. GOTTESFELD, *J. Electroanal. Chem.*, 7 (1964) 307.
4 G. MACCHI, *J. Electroanal. Chem.*, 9 (1965) 290.
5 E. N. VINOGRADOVA AND G. V. PROHOROVA, *Zh. Anal. Khim.*, 23 (1968) 711.
6 W. KEMULA, Z. KUBLIK AND J. TARASZEWSKA, *Chem. Anal. (Warsaw)*, 8 (1963) 171.
7 H. IRVING AND J. J. COX, *Analyst*, 83 (1958) 526.
8 W. KEMULA AND S. GLODOWSKI, *Chem. Anal. (Warsaw)*, 11 (1966) 403.
9 L. F. ZAJČKO AND M. S. ZAHAROV, *Zh. Anal. Khim.*, 22 (1967) 876.
10 S. J. SINJAKOVA AND I. V. MARKOVA, *Zavodsk. Lab.*, 27 (1961) 521.

ELECTROANALYTICAL CHEMISTRY AND INTERFACIAL ELECTROCHEMISTRY
Elsevier Sequoia S.A., Lausanne – Printed in The Netherlands

DEUTUNG DER ANOMALEN FORM DER OXAZEPAM-STROMSPANNUNGSKURVE

J. VOLKE*, H. OELSCHLÄGER UND G. T. LIM
Pharmazeutisches Institut der Johann Wolfgang Goethe-Universität, Frankfurt/Main (Deutschland)
(Eingegangen am 20. Juni 1969; revisioniert am 10. November 1969)

In unserer Mitteilung[1] über die Reduktion des Oxazepams (7-Chlor-1,3-dihydro-3-hydroxy-5-phenyl-2H-1,4-benzodiazepin-2-on, (I)) an der Hg-Tropfelektrode hatten wir auf eine Deformation des Grenzstromes der Stufe hingewiesen, die in alkalischen Puffern (pH > 7) auftritt und an ein Maximum** II. Art erinnert (s. Abb. 1).

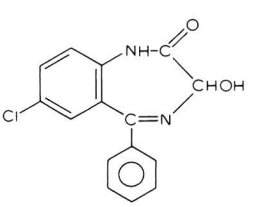

Oxazepam (I)

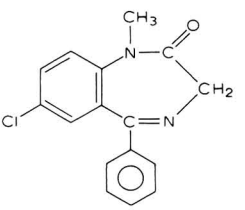

Diazepam

Diese Verzerrung des Grenzstromes war stark vom Potential abhängig und konnte nicht, wie sonst bei Maxima II. Art möglich, durch Verminderung der Leitsalzkonzentration beseitigt werden, sondern nur durch eine grössere Zugabe von Gelatine. Eine solche Anomalie haben wir bei den von uns bis jetzt polarographisch untersuchten 1,4-Benzodiazepinen[2-4] nicht festgestellt. Lediglich beim Diazepam[3] (7-Chlor-1,3-dihydro-1-methyl-5-phenyl-2H-1,4-benzodiazepin-2-on) traten in Britton–Robinson-Puffern (pH > 6.7) Maxima I. Art auf, die nach Zugabe von wenig Gelatine verschwanden. Zur Deutung des anomalen Verlaufs der Stromspannungskurven in alkalischen Puffern haben wir zahlreiche Experimente durchgeführt, die nachfolgend geschildert und anschliessend diskutiert werden sollen.

1. ABHÄNGIGKEIT DER STUFENHÖHE DES MAXIMUMS VON DER DEPOLARISATORKONZENTRATION

Während in sauren Grundlösungen (z.B. Britton–Robinson-Puffer mit 10% Dimethylformamid (DMF), pH 2.9) auch bei grösseren Depolarisatorkonzentrationen eine Linearbeziehung zur Stufenhöhe besteht, ist diese lineare $i_l = f(c)$-Abhängig-

* Ständige Anschrift: J. Heyrovský-Institut für Polarographie, Prag.
** Ein formal ähnliches anomales Maximum wurde bei der Reduktion von Phenacylsulfoniumionen von Tang und Zuman[9] beobachtet. Dieses unterscheidet sich aber in wesentlichen Kriterien von dem von uns beschriebenen Maximum. Die experimentellen Befunde führen daher zu einer anderen Deutung der Ent-

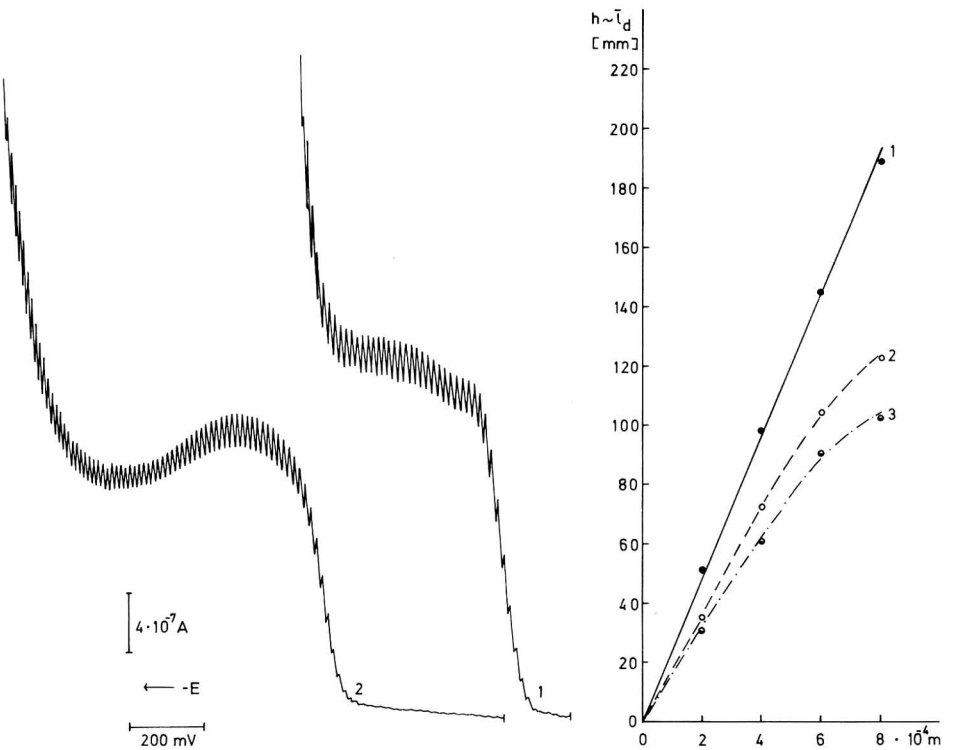

Abb. 1. pH-Einfluss auf die *i–E*-Kurve des Oxazepams. 2×10^{-4} *M* (I). (1) Britton–Robinson-Puffer mit 10% DMF, pH 2.04, ab -0.4 V; (2) Britton–Robinson-Puffer mit 10% DMF, pH 7.45, ab -0.6 V.

Abb. 2. Konzentrationsabhängigkeit der Stufenhöhe von Oxazepam. (1) pH 2.9; (2) pH 7.8, im Maximum gemessen; (3) pH 7.8, im Minimum gemessen; die Lösungen enthalten 10% Dimethylformamid; Britton–Robinson-Puffer (BR-Puffer).

keit in dem pH-Bereich, in dem das Maximum beginnt (z.B. bei pH 7.2 oder pH 7.8) nicht mehr gegeben. Die aus 10 Messungen resultierende Kurve (s. Abb. 2) ähnelt in ihrem Verlauf einer Parabel, d.h. mit steigender Depolarisatorkonzentration strebt diese Kurve einem Grenzwert zu. Dieser Kurvenverlauf ist z.B. für adsorptionsbedingte und katalytische Ströme charakteristisch, bei denen die Adsorption eine wichtige Rolle spielt. Ein weiterer Grund für diesen Kurvenverlauf könnte eine Übersättigung der Lösung sein, in der durch erst allmählich makroskopisch erkennbar werdendes Ausfallen von (I)-Kristallen eine Konzentrationsverminderung eintritt. In Übereinstimmung mit dieser Annahme beobachteten wir bei Verwendung DMF-haltiger, schwach alkalischer Puffer (pH >9) nach mehrstündigem Stehen eine Abscheidung von Oxazepam-Kristallen (DC, d.c.-Polarographie).

2. EINFLUSS DER KONZENTRATION UND ART DES LÖSUNGSVERMITTLERS

Wird bei konstanter Oxazepamkonzentration (5×10^{-4} *M*) in einem Puffer vom pH-Wert 7.2 die DMF-Konzentration erhöht, so verschwindet das beobachtete

Maximum bereits bei einer Konzentration von 20% DMF. Diese Versuche wurden bis zu einer Konzentration von 40% DMF fortgeführt. Dabei trat mit steigender DMF-Konzentration eine Erniedrigung der Stufenhöhe ein, die sich aus der erhöhten Viskosität der Lösung und den dadurch erniedrigten Diffusionskoeffizienten ergibt.

Für die Abhängigkeit der Diffusionsstromstärke von der Viskosität gilt die Beziehung $i_d \cdot \sqrt{\eta} = \text{const.}$[5]. Da wir mit dem von uns als Lösungsvermittler eingeführten DMF bei der Polarographie zahlreicher Verbindungen gute Erfahrungen gemacht haben, prüften wir am Beispiel des Oxazepams als Depolarisator die Gültigkeit vorstehender Beziehung. Die Viskositäten η der DMF-haltigen Elektrolyten wurden mit Hilfe des thermostatisierten Höppler–Kugelfall-Viskosimeters bei 20°C ermittelt. Die für die Errechnung von

$$\eta = F \cdot (s_k - s_f) \cdot K$$

[F = Fallzeit der Kugel; s_k = Dichte der Kugel (=2.3979); s_f = Dichte der Flüssigkeiten; K = Kugelkonstante (=0.05604)], erforderlichen Dichten s_f der Elektrolyten wurden nach dem Österreichischen Arzneibuch, 9. Ausgabe (1960) bei 20° pyknometrisch festgestellt.

TABELLE 1

BEZIEHUNGEN ZWISCHEN DMF-KONZENTRATION, VISKOSITÄT UND DIFFUSIONSGRENZSTROM

DMF-Gehalt des Puffers/%	*Viskosität* η/*cP*	$10^6 i_d/A$	$10^6 K = i_d \cdot \sqrt{\eta}$
0	1.0965		
5	1.2444	2.65	2.96
10	1.3814	2.55	2.99
15	1.5355	2.46	3.05
20	1.7167	2.39	3.13
25	1.8895	2.31	3.17
30	2.0472	2.20	3.15
40	2.4470	2.02	3.16

als Puffer diente ein BR-Puffer (pH 1.8) konstanter Konzentration

Im Koordinatensystem (s. Abb. 3) $i_d = f(1/\sqrt{\eta})$ sollte man bei Gültigkeit des Stoke–Einstein-Gesetzes eine Gerade erhalten. Tatsächlich ergibt sich aber bei höheren DMF-Konzentrationen eine geringfügige Abweichung vom linearen Verlauf. Wir deuten diese Abweichung durch die Annahme, dass sich bei grösseren DMF-Konzentrationen die Solvathülle des Depolarisators dergestalt ändert, dass in grösserem Umfang auch hydratisierte DMF-Moleküle zu ihrem Aufbau herangezogen werden, wodurch sich der Diffusionskoeffizient zwangsläufig verkleinert.

Ähnlich wie DMF vermindert auch Dimethylsulfoxid (DMSO) als Lösungsvermittler die Stufenhöhe und führt zu einer Unterdrückung des Maximums. Bemerkenswert ist die wesentlich kleinere Wasserstoffüberspannung in DMSO-haltigen Lösungen (Kurve 1), die zu einem anderen Verlauf der i–E-Kurven als in DMF-haltigen Lösungen führt (Kurve 2) (s. Abb. 4). Der Endanstieg wird in Kurve 1 um etwa 200 mV zu positiverem Potential verschoben.

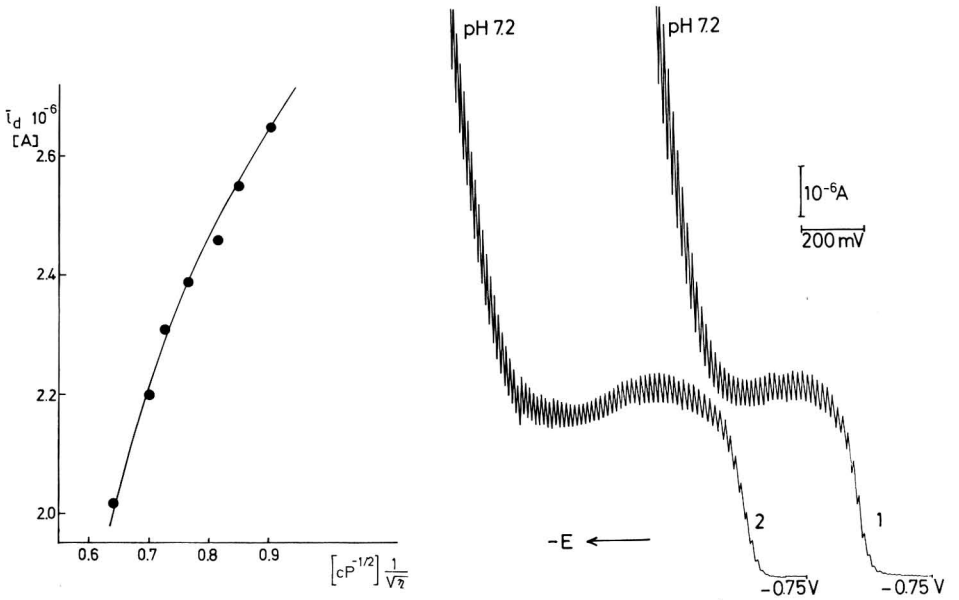

Abb. 3. Abhängigkeit des Grenzstromes von Oxazepam von dem Ausdruck $1/\sqrt{\eta}$. Die Werte wurden der Tab. 1 entnommen.

Abb. 4. Oxazepam-Stufen in Dimethylsulfoxid und Dimethylformamid. 5×10^{-4} *M* Oxazepam, *M*/15 Phosphatpuffer; (1) 10% DMSO, (2) 10% DMF.

3. ABHÄNGIGKEIT DER STUFENHÖHE VON DER BEHÄLTERHÖHE

Wir fanden weiter, dass die Stufenhöhe bei verschiedenem pH der Grundlösung und wechselnder Depolarisatorkonzentration nicht nur linear von h, sondern auch von $\sqrt{h}$ abhängig sein kann. Darüber hinaus existieren auch keine linearen Abhängigkeiten von h bzw. $\sqrt{h}$. Dieser Befund wird durch die folgenden 2 Beispiele veranschaulicht:

(1) pH 6.6 ($c = 10^{-3}$ *M*): linear abhängig von h (sowohl im Maximum als auch im Minimum)
($c = 5 \times 10^{-4}$ *M*): linear abhängig von h
($c = 2 \times 10^{-4}$ *M*): linear abhängig von $\sqrt{h}$
(2) pH 7.8 ($c = 10^{-3}$ *M*): linear abhängig von h
($c = 2 \times 10^{-4}$ *M*): weder von h noch von $\sqrt{h}$ linear abhängig; der Exponent bei m muss grösser als 1 sein.

4. ABHÄNGIGKEIT DER STUFE VON m (d.h. von h bei geregelter Tropfzeit t_1)

Durch Variation der Behälterhöhe zwischen 25 und 81 cm unter gleichen Bedingungen, aber bei konstanter Tropfzeit (Abklopfer, $t_1 = 1$ s), konnte der Einfluss von m auf den Strom festgestellt werden. Für den Strom im Maximum wurde eine lineare Abhängigkeit zwischen $\bar{i}_{max}$ und h (d.h. m) gefunden. Bei grossen Behälterhöhen entsteht auf der Stufe ein ausgesprochener "Buckel", der die Stufe deformiert.

Bei kleinen h-Werten verschwindet das Maximum und es entsteht bei dieser kurzen Tropfzeit t_1 eine normal ausgebildete, nicht verzerrte polarographische Stufe.

5. ABHÄNGIGKEIT DER STUFE VON DER TROPFZEIT

Bei konstanter Behälterhöhe (64 cm) wurde mit einem Abklopfer gearbeitet. Aus der Beziehung

$$\bar{i} = \text{const.}\ t_1^{\bar{\beta}}$$
$$\log \bar{i} = \text{const.}' + \bar{\beta} \log t_1$$

wurden die $\bar{\beta}$-Werte als Richtungstangente ermittelt:

pH 6.6	$c = 10^{-3}\ M$	$\bar{\beta}_{max} = 0.25$
(10% DMF)		$\bar{\beta}_{min} = 0.20$
	$c = 2 \times 10^{-4}\ M$	$\bar{\beta}_{max} = 0.25$
		$\bar{\beta}_{min} = 0.20$
pH 7.8	$c = 10^{-3}\ M$	$\bar{\beta}_{max} \rightarrow 0.3$
(10% DMF)		$\bar{\beta}_{min} = 0.2$
	$c = 2 \times 10^{-4}\ M$	$\bar{\beta}_{max} \rightarrow 0.3$
		$\bar{\beta}_{min} \rightarrow 0.22$

Ein Vergleich der $\bar{\beta}$-Werte im Minimum und im Maximum zeigt, dass die $\bar{\beta}$-Werte im Minimum sowohl bei kleinen als auch bei grösseren Depolarisatorkonzentrationen und verschiedenem pH-Wert = 0.2 sind, während die $\bar{\beta}$-Werte im Maximum zwischen 0.25–0.3 schwanken. Auch die β-Exponenten, die bei Registrierung von Momentanströmen an einzelnen Tropfen erhalten wurden, stimmen mit den $\bar{\beta}$-Exponenten überein. Die gefundenen Werte der Exponenten bei m und t_1 liegen also denen sehr nahe, die Dvořák[6] für ein Maximum II. Art festgestellt hat. Dieser fand, dass die Stromstärke dem Produkt $m^{\frac{2}{6}} \cdot t^{\frac{1}{6}}$ proportional ist, d.h. also in linearer Abhängigkeit von der Behälterhöhe h steht.

6. EINFLUSS DER IONENSTÄRKE

Eine Veränderung der Ionenstärke, die durch wechselnde Zugaben von Kaliumchlorid (0–0.65 M KCl) möglich ist, beeinflusst das Maximum bei pH 7.8 ($5 \times 10^{-4}\ M$) nur wenig. Mit steigender KCl-Konzentration sinkt die Höhe des Maximums um weniger als 5%, während sich der Strom im Minimum nahezu bis auf den Wert von $\bar{i}_{max}$ erhöht. Die Erhöhung ist stark von der Behälterhöhe abhängig, denn bei kleineren Behälterhöhen verschwindet sie vollkommen. Offensichtlich tritt bei negativerem Potential ein weiteres Maximum auf, das von dem hier untersuchten unabhängig ist. Es ist von der Pufferkonzentration unabhängig.

7. ABHÄNGIGKEIT VON DER TEMPERATUR

Erhöht man die Temperatur des zu prüfenden Phosphatpuffers (pH 7.8; 10% DMF) auf Werte zwischen 20–60°, so verändert sich die Form der i–E-Kurven nicht wesentlich. Der Strom im Maximum wächst mit einem Temperaturkoeffizienten von etwa 1.8% pro Grad linear an, während für den Strom im Minimum ein exponentieller Verlauf ermittelt wurde.

8. EINFLUSS DER OBERFLÄCHENAKTIVEN STOFFE

Gelatinezusätze haben nur einen geringen Einfluss auf den Verlauf der Stromspannungskurven, der Gesamtstrom wird partiell reduziert. Gleichzeitig tritt ein Ausgleich zwischen dem i_{max} und dem i_{min} ein.

Setzt man den gepufferten Lösungen bis zu 0.05 *M* Tetramethylammoniumchlorid zu, dessen Kation schwächer als K^+ adsorbiert wird, so verändert sich bei pH 7.8 das Maximum praktisch nicht. Bei grösserer Konzentration (ab 0.5 *M*) rufen diese Zusätze bei negativeren Potentialen als das Maximum ein neues Maximum II. Art hervor.

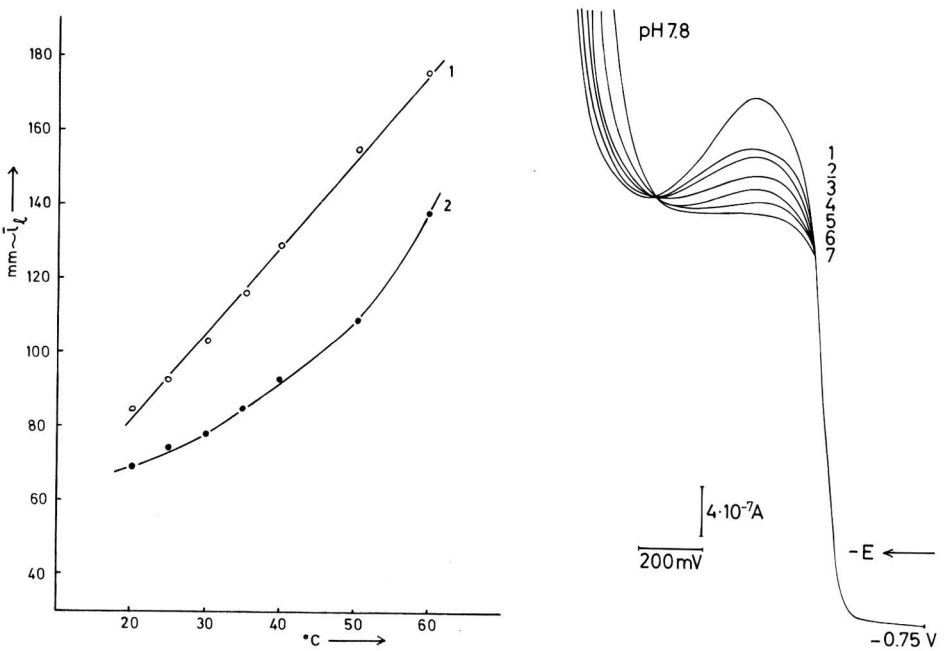

Abb. 5. Temperaturabhängigkeit der Höhe der anomalen Oxazepam-Stufe bei pH 7.8. 5×10^{-4} *M* Oxazepam, 0.1 *M* Phosphatpuffer pH 7.8. (1) Stufenhöhe im Maximum gemessen; (2) Stufenhöhe im Minimum gemessen.

Abb. 6. Einfluss von Atropin auf die Reduktionsstufe von Oxazepam bei pH 7.8. 5×10^{-4} *M* (I); 0.1 *M* Phosphatpuffer mit 10% DMF; jede Kurve ab −0.75 V; Dämpfung 6. (1) Kein Atropinsulfat, (2) 2.5×10^{-5} *M* Atropinsulfat, (3) 5×10^{-5} *M*, (4) 9.8×10^{-5} *M*, (5) 1.4×10^{-4} *M*, (6) 1.13×10^{-3} *M*, (7) 2.3×10^{-3} *M*.

Am wirksamsten liess sich das Maximum durch Zusätze von Atropinsulfat beeinflussen. Schon von einer Konzentration ab 5×10^{-5} *M* wird der Verlauf der *i*–*E*-Kurve deutlich beeinflusst. Der Strom im Maximum wird bei Konzentrationen zwischen 5×10^{-4}–10^{-3} *M* völlig unterdrückt, der Grenzstrom der auf diese Weise entstandenen normalen Stufe entspricht annähernd dem ursprünglichen Strom im Minimum.

9. MIKROSKOPISCHE UNTERSUCHUNGEN

Bei pH 6.6 und pH 7.8 (Phosphatpuffer, 10% DMF) wurden über den gesamten Potentialbereich, in dem das Maximum auftritt, die Stromverhältnisse um den Quecksilbertropfen durch Zugabe von Aktivkohle mikroskopisch untersucht. Dabei konnte keine Strömung in unmittelbarer Nähe der Elektrodenoberfläche beobachtet werden. Erst bei Beginn der Hydroxonimionenentladung der Grundlösung setzte eine lebhafte Strömung um den Tropfen ein.

10. POLAROGRAMME MIT ÜBERLAGERTER WECHSELSPANNUNG NACH BREYER

Die a.c.-Polarogramme nach Breyer (s. Abb. 7) zeigen bei pH 7–8 (10% DMF) eine scharfe konzentrationsabhängige Spitze bei etwa −1.05 V. Dieses Potential entspricht dem Halbstufenpotential der polarographischen Stufe. Ein weiteres niedriges Maximum bildet sich bei etwa −1.30 V, das dem Bereich des Absinkens des Maximums auf den *i*–*E*-Kurven bei der d.c.-Polarographie entspricht. Die Potentialdifferenz zum Maximum beträgt 60–80 mV. Besonders aufschlussreich ist der Verlauf der a.c.-Kurve mit Depolarisator (2) im Vergleich zur Kurve der Leerlösung (1). Hierbei ergibt sich, dass der Depolarisator bis zum Potential seiner Reduktion adsorbiert wird.

Auch in sauren Lösungen (pH 1.8) wird der Depolarisator adsorbiert. Von grosser Bedeutung für das Verhalten des Depolarisators und seines Reduktionsproduktes ist die Konzentration des Lösungsvermittlers DMF. Bei kleineren DMF-Konzentrationen, geprüft wurden DMF-Konzentrationen im Bereich von 1–5%,

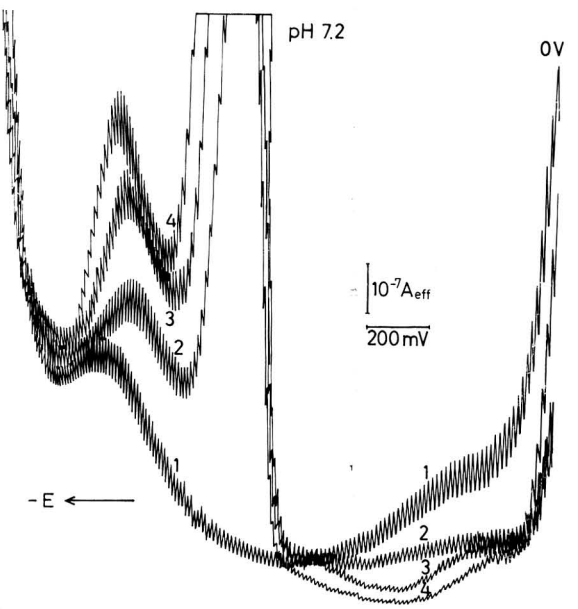

Abb. 7. Wechselstrompolarogramme von Oxazepam. 0.1 *M* Phosphatpuffer pH 7.2 mit 10% DMF; alle Kurven ab 0 V; E = 0.050 V. (1) Leerlösung, (2) 2×10^{-4} *M* Oxazepam, (3) 5×10^{-4} *M*, (4) 10^{-3} *M*.

entsteht bei -1.48 V (pH 7.2) ein Minimum auf der a.c.-Kurve, das unter der Kurve der Leerlösung liegt. Hieraus darf mit Vorbehalt geschlossen werden, dass bei diesem Potential auch das Reduktionsprodukt adsorbiert wird.

Mit Hilfe der a.c.-Polarographie konnte darüber hinaus bewiesen werden, dass im Bereich der d.c.-Anomalie DMF, DMSO und $N(CH_3)_4^+$ nur schwach, Atropinsulfat dagegen stark adsorbiert wird.

DISKUSSION

Aus den unter 1.–10. mitgeteilten experimentellen Befunden ziehen wir folgende Schlüsse: Oxazepam (I) wird in schwach alkalischen Puffern an der Elektrodenoberfläche adsorbiert und in diesem Zustand reduziert. Bei negativer werdendem Potential erfolgt entweder Desorption des Produktes oder Umorientierung desselben an der Elektrodenoberfläche (vgl. Abb. 7). Die Anomalie auf dem d.c.-Polarogramm dürfte auf die Änderung der Doppelschicht zurückzuführen sein.

Für die Richtigkeit unserer Interpretation spricht besonders stark das Verhalten von (I) in gepufferten Lösungen (pH 7.2) an der Tropfelektrode in Gegenwart oberflächenaktiver Protonendonatoren (z.B. Atropin, pK_a 10.0). Aufgrund der Stufenform bei pH 7.2 und unter Berücksichtigung der Tatsache, dass (I) bei diesem pH-Wert nicht mehr vierelektronig reduziert wird (s. Nachschrift), könnte leicht gefolgert werden, dass die Anomalie der (I)-Stufe dadurch verursacht wird, dass (I) in adsorbiertem Zustand protoniert und dann reduziert wird[7]. Da mit negativer werdenden Potentialen die Absorbierbarkeit von (I) absinkt, verringert sich der Stromumsatz an der Elektrode, d.h. der Strom sinkt mit negativer werdendem Potential ab[7]. Es resultieren *i–E*-Kurven ähnlich der anomalen (I)-Kurve, die gegenüber oberflächenaktiven Protonendonatoren (z.B. Atropin[8]) äusserst empfindlich sind. Diese H^+-Donatoren erhöhen den Grenzstrom durch Protonierung des Depolarisators. (Sie können auch gleichzeitig die Stufen durch Hemmung der Elektronenübertragung zu negativeren Potentialen verschieben!). Wir beobachteten jedoch einen gegenteiligen Einfluss des Atropins: die Stufe von (I) im Maximum sinkt mit steigender Atropin-Konzentration bis eine normale Stufe entsteht. Im Einklang mit unserer Deutung steht der unbedeutende Einfluss der Pufferkapazität auf die anomale Stufe.

Nachschrift

Reduktionsmechanismus von (*I*). Aufgrund unserer ersten[1] experimentellen Untersuchungen haben wir bereits die nachfolgende These aufgestellt, die inzwischen eindeutig bewiesen wurde. Hierüber werden wir in Kürze berichten.

in sauren Puffern:

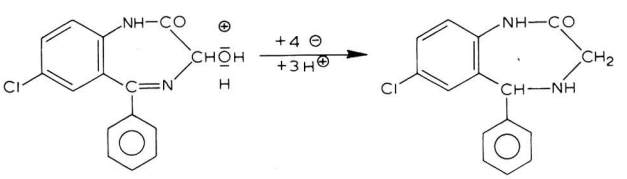

in alkalischen Puffern:

in diesen Puffern tritt keine Umlagerung zum 7-Chlor-5-phenyl-4,5-dihydro-2H-benzodiazepin-2,3-(1H)-dion ein[10]:

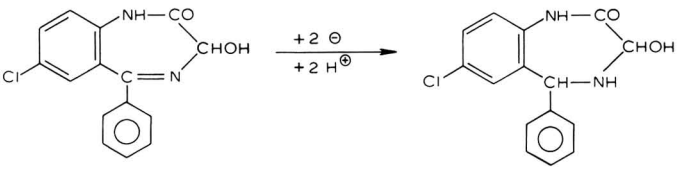

ZUSAMMENFASSUNG

Bei der Reduktion des Oxazepams (I) an der Hg-Tropfelektrode in Puffern (pH > 7) tritt eine Deformation des Grenzstromes der Stufe auf, deren Ursache geklärt werden konnte. (I) wird nämlich bis zum Potential seiner Reduktion an der Elektrodenoberfläche adsorbiert. Bei negativeren Potentialen als denen des Maximums erfolgt eine Desorption des Reduktionsproduktes oder eine Umorientierung desselben an der Elektrodenoberfläche, wodurch die Verhältnisse in der Doppelschicht geändert werden. Im gleichen Sinne wirkt sich unter bestimmten Bedingungen die Entstehung eines Maximums II. Art aus, das bei steigender (I)-Konzentration und höherer Ausflussgeschwindigkeit resultiert.

SUMMARY

An anomalous dependence of the limiting current of oxazepam (I) on potential has been observed in the current–voltage curves recorded with a dropping mercury electrode in buffers pH > 7. This is due to adsorption of (I) on the mercury electrode up to the potential of its reduction. At potentials more negative than that of the maximum current on the polarographic wave a desorption or reorientation of the reduction product occurs by which the conditions in the electrode double layer are changed. At higher concentrations of (I) and with higher outflow velocities of mercury *m* the above phenomenon becomes still more pronounced by a simultaneous formation of a maximum of the second kind.

LITERATUR

1 H. Oelschläger, J. Volke, G. T. Lim und R. Spang, *Arch. Pharm.*, 302 (1969) 946.
2 H. Oelschläger, *Arch. Pharm.*, 296 (1963) 396.
3 H. Oelschläger, J. Volke und E. Kurek, *Arch. Pharm.*, 297 (1964) 431.
4 H. Oelschläger, J. Volke, G. T. Lim und U. Frank, *Arzneimittel-Forsch.*, 16 (1966) 82.
5 J. Heyrovský und J. Kuta, *Grundlagen der Polarographie*, Akademie-Verlag, Berlin, 1965, S.91.
6 J. Dvořák, *Collection Czech. Chem. Commun.*, 19 (1954) 39.
7 J. Koryta in I. S. Longmuir (Red.), *Advances in Polarography*, Band I, Pergamon Press, London, 1966, S. 359.
8 V. Volková, *Nature*, 185 (1960) 743.
V. Volková in I. S. Longmuir (Red.), *Advances in Polarography*, Band III, Pergamon Press, London, 1960, S.840.
9 S.-Y. Tang und P. Zuman, *Collection Czech. Chem. Commun.*, 28 (1963) 1524.
10 S. C. Bell und S. J. Childress, *J. Org. Chem.*, 27 (1962) 1691.

ELECTROANALYTICAL CHEMISTRY AND INTERFACIAL ELECTROCHEMISTRY
Elsevier Sequoia S.A., Lausanne – Printed in The Netherlands

ELECTROCHIMIE DANS L'ACIDE TRIFLUOROACETIQUE

I. SYSTÈMES OXYDO-RÉDUCTEURS DE L'IODE

GÉRARD PETIT ET JACQUES BESSIÈRE
Laboratoire de Chimie Analytique de la Faculté des Sciences associé au C.N.R.S., E.S.P.C.I. Paris V° (France)
(Reçu le 10 octobre, 1969)

INTRODUCTION

L'acide trifluoroacétique constitue un milieu réactionnel intéressant par ses propriétés faiblement basiques et par son caractère d'acide fort. Son domaine acide–base est voisin de 8 unités de pK; il est situé en milieu très acide (de $H_0 = -2.5$ à $H_0 = -10.5$)[1].

Bien que sa constante diélectrique soit faible, $\varepsilon = 8.4$[2], les solutions concentrées de sel ionisé sont suffisamment conductrices pour rendre possible l'utilisation des méthodes électrochimiques d'analyse[3].

Les propriétés du solvant sont mises à profit pour l'étude des degrés d'oxydation de l'iode par voie électrochimique.

Des études antérieures[4–6] ont souligné le comportement spectrophotométrique et cinétique différent de l'iode dans l'acide acétique et dans l'acide trifluoroacétique. La coloration violette des solutions indique que l'iode n'est pas complexé par le solvant. Par ailleurs, il a été montré que l'acide trifluoroacétique constitue un milieu propice aux réactions d'halogénation des composés organiques ; la cinétique des réactions est généralement plus rapide que dans l'acide acétique[4,5].

L'étude électrochimique suivante confirme ces résultats. La réduction, puis l'oxydation de l'iode seront examinées successivement.

I. REDUCTION DE L'IODE

L'étude est réalisée en milieu basique anhydre (CF_3COONa molaire). Le rôle de l'eau et l'influence de l'acidité seront précisés. Le tracé des courbes intensité–potentiel, les études coulométriques et une étude spectrophotométrique complémentaire montrent que l'iode est directement réduit en iodure dans l'acide trifluoroacétique et que le complexe triiodure n'est thermodynamiquement pas stable dans le solvant anhydre.

Réduction de l'iode

La vague unique de réduction est bien définie. Elle est identique, à une électrode tournante à disque de platine poli ou de carbone vitreux, si l'on prend soin, dans ce dernier cas, d'effectuer le balayage des potentiels dans le sens des potentiels croissants. Si le balayage a lieu en sens inverse, la courbe de réduction présente un maximum

que l'on attribue à une adsorption de l'iode sur le carbone.

A une électrode de platine poli, le critère de Levich[7] : $i_l = f(\sqrt{N})$ (où N représente la vitesse de rotation de l'électrode) appliqué à cette vague de réduction, indique que le courant-limite observé est contrôlé uniquement par la diffusion de l'iode. Il est proportionnel à la concentration de l'iode en solution. La droite $i_l = k|I_2|$ permet donc l'étalonnage en concentration des solutions d'iode (Figs. 1 et 2).

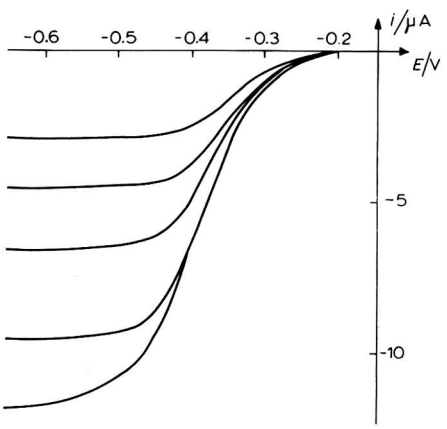

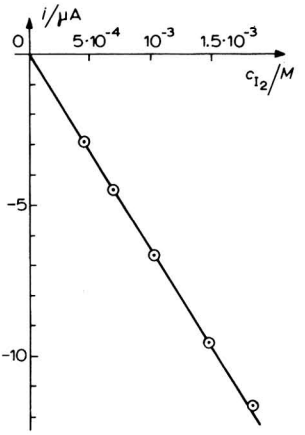

Fig. 1. Courbes de réduction de l'iode en fonction de la concentration.

Fig. 2. Variation de la hauteur du palier à -0.6 V en fonction de la concentration.

Les études coulométriques à -0.4 V, par rapport au potentiel de référence $Ag(s)|AgClO_4(s)|(C_2H_5)_4NClO_4\ 10^{-1}\ M$ confirment le fait que l'iode est directement réduit en iodure. En fin d'électrolyse, la solution est incolore et l'intégration du courant de réduction montre que deux électrons sont échangés par molécule d'iode.

Ces résultats, vague de réduction unique, échange de deux électrons par molécule d'iode lors des coulométries de réduction, ne permettent pas de savoir si le triiodure est peu stable (c'est ce que l'on observe dans l'eau), ou s'il n'existe pas. Une étude spectrophotométrique complémentaire indique que le complexe triiodure n'est pas stable en milieu anhydre. L'iode est violet dans CF_3COOH, son spectre présente un maximum d'adsorption à 510 nm. Le coefficient d'extinction moléculaire à cette longueur d'onde est égal[6] à 815 l mol^{-1} cm^{-1}. Il se comporte donc comme dans les solvants non polaires tels que le tétrachlorure de carbone.

Dans ces solvants le triiodure, lorsqu'il est stable, est brun, et adsorbe vers 290 et 350 nm. C'est le cas par exemple dans le dichloro-1,2-éthane, où le pK de dissociation du triiodure est 7.0[8]. L'acide trifluoroacétique et le dichloro-1,2-éthane ayant le même comportement vis-à-vis de l'iode, il parait logique d'admettre que si le triiodure existe dans CF_3COOH, son spectre sera très voisin de celui que l'on obtient dans l'autre solvant. Le triiodure de tétrapentylammonium dissous dans CF_3COOH conduit au spectre de l'iode. Il est donc complètement dissocié en iode et en iodure de tétrapentylammonium. Remarquons en outre, que le spectre de l'iode n'est pas modifié par l'addition d'iodure cent fois plus concentré.

Réaction électrochimique. La réaction électrochimique, compte tenu du faible pouvoir dissociant du solvant, est la suivante:

$$I_2 + 2CF_3COONa + 2e \rightleftharpoons 2NaI + 2CF_3COO^-$$

La vague de réduction de l'iode indique que la réaction électrochimique mise en jeu a une cinétique lente; le courant cathodique s'étend sur près de 300 mV avant d'atteindre sa valeur limite. L'équation théorique établie dans le cas de ce système[9] ne rend pas compte totalement de la réaction électrochimique. Ceci peut s'expliquer par le comportement électrochimique particulier des iodures. Le potentiel de demi-vague cathodique correspondant à la vague de réduction d'une solution d'iode 10^{-3} *M*, est égal à -0.36 V.

Influence de l'acidité du milieu. Le potentiel de demi-vague cathodique n'est pas influencé par l'acidité de la solution. La limitation inférieure du domaine d'électroactivité est due à la réduction du solvant en milieu basique et neutre et à celle des protons en milieu acide. Elle est déplacée vers les potentiels oxydants lorsque l'acidité du milieu augmente[3]. De ce fait, la vague de réduction de l'iode est moins bien définie en milieu neutre non tamponné qu'en milieu basique. En milieu acide, l'iode n'est plus électroactif.

Influence de l'eau. L'addition d'eau ne modifie pas la courbe de réduction de l'iode.

Oxydation des iodures

En milieu anhydre (léger excès d'anhydride trifluoroacétique) les iodures ne sont pas électroactifs, qu'ils soient introduits directement en solution ou produits par réduction électrochimique de l'iode. Ce phénomène est indépendant de la nature de l'électrolyte indifférent et de la nature de l'électrode (platine poli, platine platiné, carbone).

L'utilisation de la voltammétrie cyclique ne permet pas de mettre en évidence l'oxydation des iodures. Les iodures peuvent cependant être lentement oxydés en iode par le solvant. L'oxydation chimique des iodures par l'iode au degré d'oxydation $+I$ est quantitative.

Rôle de l'eau. En présence d'eau (10^{-2} *M*), les iodures deviennent électroactifs. La vague d'oxydation n'est pas une vague de diffusion pure, le critère de Levich se révèle négatif. Le courant-limite d'oxydation dépend de la concentration d'eau présente en solution, mais il ne lui est pas proportionnel. L'intensité du courant anodique se stabilise en fonction du temps mais reste inférieure à la valeur théorique que l'on peut calculer si l'on admet que l'iodure a le même coefficient de diffusion que l'iode (Fig. 3). Le potentiel de demi-vague apparent pour une solution d'iodure de sodium à la concentration $2 \cdot 10^{-3}$ *M*, en présence d'eau à la concentration 1 *M*, est voisin du potentiel de demi-vague cathodique apparent correspondant à la réduction de l'iode à la concentration 10^{-3} *M*.

Il est possible d'oxyder complètement par voie électrochimique l'iodure présent en solution. L'intégration du courant d'oxydation lors d'une électrolyse à potentiel contrôlé à 0 V, indique qu'un électron est échangé par iodure (sous forme Na^+I^-).

La solution, incolore au départ, prend une coloration rouge orangé au cours de l'électrolyse et vire au violet lorsque tout l'iodure est oxydé. Cette coloration rouge

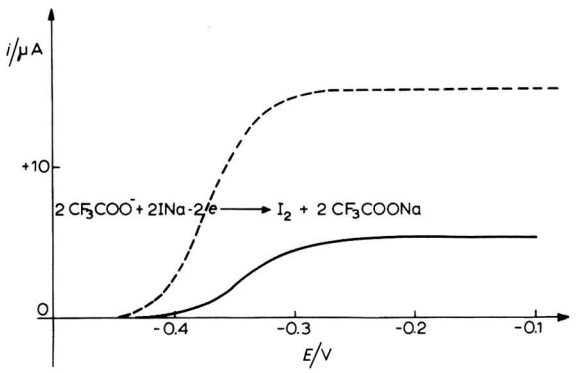

Fig. 3. Courbe d'oxydation des iodures en milieu basique ($CF_3COONa = 0.5$ *M*) et en présence d'eau (1 *M*) à une électrode de platine poli. (------) Courbe théorique, (——) courbe expérimentale. Concentration en iodure de sodium: 5.6×10^{-3} *M*.

orangé, qui n'est pas observée lors de la réduction de l'iode en milieu anhydre, laisse supposer l'existence d'une étape d'oxydation intermédiaire des iodures en présence d'eau. Ces phénomènes sont observés en milieu neutre et basique.

Mélanges iode–iodure

En milieu anhydre les solutions conservent la coloration violette de l'iode.

L'addition d'iodure à une solution d'iode ne modifie pas l'allure de la courbe de réduction. Le potentiel de demi-vague est indépendant de cette addition.

Influence de l'eau. Les courbes intensité-potentiel relatives au mélange iode–iodure de sodium ont l'aspect des courbes caractéristiques des systèmes rapides en présence d'eau à la concentration 1 *M* (Fig. 4).

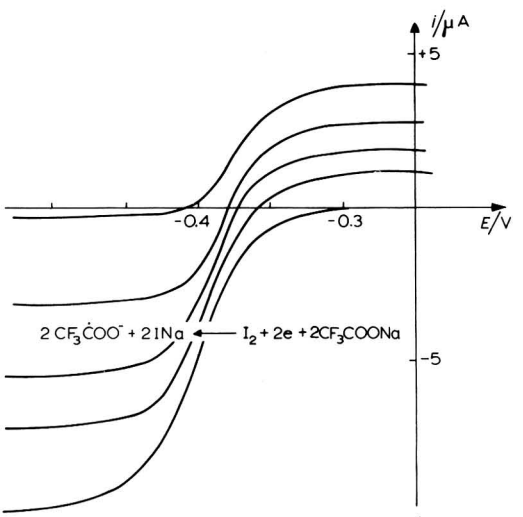

Fig. 4. Evolution des courbes intensité–potentiel de l'iode au cours de sa réduction à potentiel contrôlé (0 V). Concentration molaire en eau.

L'addition d'eau modifie la coloration de la solution du mélange d'iode et d'iodure, qui vire au rouge orangé à partir d'une concentration 10^{-1} *M*. Par contre, une solution d'iode en présence de la même concentration d'eau reste violette.

Comme le montre le Tableau 1, il faut atteindre des concentrations d'eau beaucoup plus élevées pour assister au déplacement du spectre de l'iode.

TABLE 1

INFLUENCE DE L'EAU SUR LE SPECTRE DE L'IODE DANS CF_3COOH

N_{H_2O}	λ_{max}/nm
0	510
0.31	502
0.57	495
0.64	492
0.69	482
eau pure	460

N_{H_2O} : fraction molaire en eau.
λ_{max} : longueur d'onde correspondant au maximum d'adsorption.

Cette coloration, comme nous l'avons vu précédemment, est attribuable à la formation du triiodure en milieu hydraté. L'addition d'une forte concentration d'iodure à une solution d'iode contenant 10^{-2} mol d'eau par litre, ne modifie pratiquement pas la densité optique de la solution à 510 nm ce qui indique que I_3^- est peu stable. Néanmoins, la forte absorption qui apparait vers 350 nm prouve que le triiodure se forme bien et qu'il est doué d'un coefficient d'extinction suffisant pour être décelé (Fig. 5).

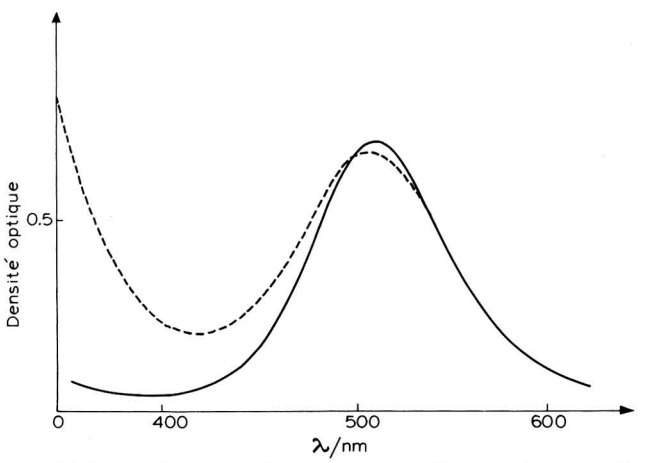

Fig. 5. Influence de l'eau sur les spectres des mélanges iode–iodure. (——) Spectre dans l'acide anhydre, (------) spectre en présence d'eau.

Discussion

Non-électroactivité des iodures. L'électroactivité des iodures est liée à la présence du complexe triiodure. Rappelons qu'un certain nombre de travaux effectués

dans l'eau concluent au fait que l'ion iodure ne serait pas électroactif, mais que seul I_3^- le serait. Ainsi Kolthoff et Jordan[10] expliquent l'absence du courant anodique pour une solution d'iodure dans l'eau, en milieu basique, par la dismutation de l'iode, le complexe I_3^- ne pouvant pas se former. Parallèlement, il est montré que toute réaction chimique rapide susceptible de consommer l'iode tend à faire disparaître l'électroactivité apparente de l'halogénure I^- [11].

Si l'on fait les mêmes hypothèses dans l'acide trifluoroacétique, l'absence de stabilité du complexe triiodure en milieu anhydre a pour conséquence directe la non-électroactivité des iodures. La présence d'eau tend à stabiliser le complexe et permet ainsi l'oxydation des iodures.

Le fait que la vague anodique ne soit pas une vague de diffusion pure laisse supposer l'intervention d'une cinétique assez lente dans le processus global d'oxydation en présence d'eau.

Le mécanisme global d'oxydation peut être représenté par le schéma suivant :

$$2I_3^- - 2e \rightarrow 3I_2$$
$$+$$
$$3I^-$$
$$\downarrow$$
$$3I_3^-$$

L'oxydation électrochimique des iodures est donc catalysée par la présence de I_3^-, dont la vitesse de formation est fonction de la concentration en eau.

Remarque. La présence de I_2 est nécessaire pour déclencher la réaction électrochimique d'oxydation. Cette condition est toujours réalisée dans l'acide trifluoroacétique puisque l'iodure est oxydé lentement par le solvant.

II. OXYDATION DE L'IODE

Dans l'acide trifluoroacétique, l'iode est oxydable en I(+I) et en I(+III). Les courbes voltampérométriques sont souvent complexes, principalement en réduction ; leur interprétation reste délicate comme dans les quelques solvants où ces études ont déjà été faites (à titre d'exemple[12-15]). Elles dépendent essentiellement de deux facteurs : d'une part, de la nature de l'électrolyte et d'autre part, de la nature de l'électrode indicatrice. Les deux étapes d'oxydation sont examinées successivement. Seul le cas se rapportant au milieu neutre non tamponné ($(C_2H_5)_4NClO_4$) sera envisagé en détails.

A. Première étape d'oxydation

Oxydation de l'iode. La courbe d'oxydation de l'iode n'est pas influencée par la nature de l'électrode. La hauteur de la première vague d'oxydation est proportionnelle à la concentration. Elle est égale à la vague de réduction de l'iode en iodure (Fig. 6a).

Le système électrochimique présente les caractéristiques d'un système lent. La vague anodique s'étend sur environ 300 mV avant d'atteindre sa hauteur limite. Le potentiel de demi-vague anodique d'une solution d'iode 1.8×10^{-3} *M* est voisin de +1 V par rapport au potentiel de référence $Ag(s)|AgClO_4(s)|(C_2H_5)_4NClO_4$ 10^{-1} *M*.

Les oxydations à potentiel contrôlé compris entre 0.6 V et 0.9 V concordent

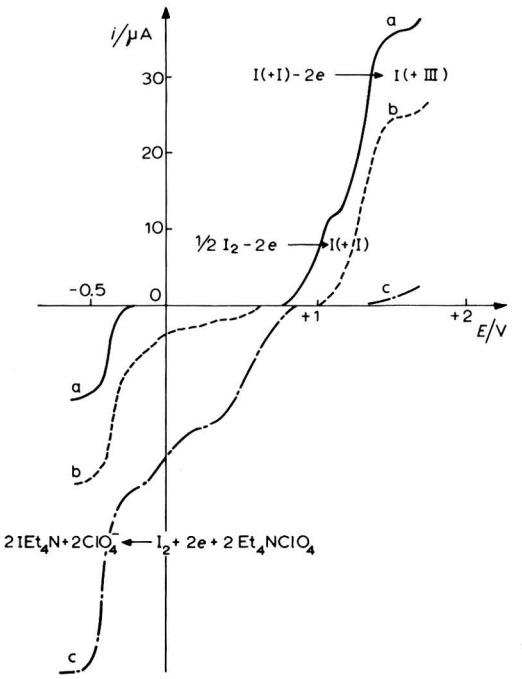

Fig. 6. Courbe intensité–potentiel en milieu neutre non-tamponné à une électrode de carbone vitreux: (a) Solution d'iode 1.85×10^{-3} *M*, (b) solution de I(+I) 3.7×10^{-3} *M*, (c) solution de I(+III) 3.7×10^{-3} *M*.

avec le tracé des courbes, deux électrons sont échangés par molécule d'iode. La réaction électrochimique est la suivante:

$$I_2 - 2e \rightarrow 2I(+I)$$

Réduction de I(+I). La courbe de réduction de I(+I) dépend de la nature de l'électrode indicatrice. A une électrode de carbone vitreux, elle se décompose en deux vagues (Fig. 6b). La première, qui correspond théoriquement à l'étape de réduction $I(+I) \rightarrow I_2$, est assez mal définie ce qui indique l'existence de phénomènes secondaires au niveau de l'électrode. La deuxième se situe dans une zône de potentiel où s'effectue la réduction de l'iode en iodure.

La vague de réduction globale de I(+I) en iodure a la hauteur théorique (que l'on peut calculer si l'on admet que les espèces ont le même coefficient de diffusion). Ce n'est pas le cas pour la première vague de réduction.

Le résultat des réductions à potentiel contrôlé successivement à 0 V et à −0.4 V, confirme le fait que la réduction de I(+I) passe par l'étape intermédiaire I_2.

Les phénomènes sont plus complexes lorsque l'électrode indicatrice est en platine poli. La courbe de réduction de I(+I) comprend encore deux vagues, mais aucune n'a la hauteur prévue.

Le titrage de I(+I) par l'iodure de sodium est quantitatif. Il peut être suivi par ampérométrie au potentiel +1.2 V (Fig. 7).

Mélanges I_2/I(+I). Comme le laissent prévoir les résultats précédents, les courbes intensité–potentiel tracées au cours de l'oxydation électrochimique de I_2

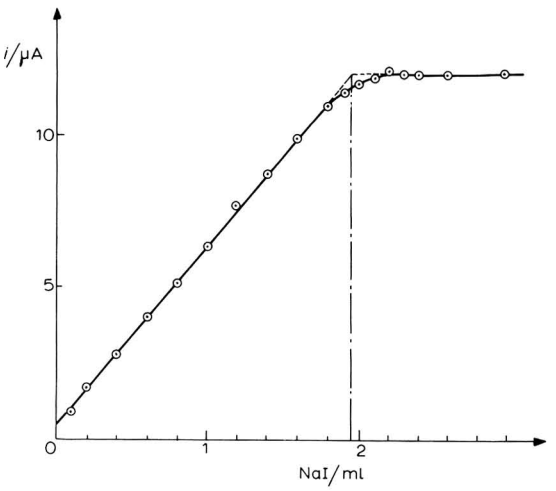

Fig. 7. Courbe de titrage ampérométrique à +1.2 V de I(+I) par NaI. $|I(+I)| = 1.84 \times 10^{-3}$ *M*; $|NaI| = 1.9 \times 10^{-2}$ *M*.

en I(+I), s'écartent des courbes théoriques. A intensité nulle, le potentiel ne suit pas la loi de Nernst.

Influence de l'acidité sur la première étape d'oxydation. En milieu acide, la courbe d'oxydation de l'iode reste la même qu'en milieu neutre. La courbe de réduction de I(+I) ne présente plus qu'une seule vague, la réduction des protons s'effectuant avant celle de l'iode.

En milieu basique, des phénomènes d'adsorption rendent plus difficile l'exploitation des courbes[16].

Discussion. Les résultats exposés confirment l'existence du degré d'oxydation +1 de l'iode dans l'acide trifluoroacétique.

En milieu perchlorate, I(+I) peut se trouver sous les formes : $IClO_4$, CF_3COOI ou CF_3I provenant de la décomposition de CF_3COOI selon la réaction :

$$CF_3COOI \rightarrow CF_3I + CO_2\,(g)$$

Le trifluoroacétate d'iode et le trifluoroiodométhane sont des composés connus[17-19].

La courbe de réduction de I(+I) est identique en milieu neutre non tamponné (perchlorate de tétraéthylammonium) et en milieu basique (trifluoroacétate de sodium). Or en milieu basique ne peuvent se former que CF_3COOI et CF_3I. Ceci laisse supposer que I(+I) se trouve sous ses deux formes, d'autant plus que I^+ a très certainement un caractère acide comme dans l'eau.

L'oxydation de l'iode en milieu neutre non tamponné doit donc faire apparaître des protons suivant la réaction :

$$I_2 + 2CF_3COOH + 2ClO_4^- - 2e \rightleftharpoons 2CF_3COOI + 2HClO_4$$

$$I_2 + 2CF_3COOH + 2ClO_4^- - 2e \rightleftharpoons 2CF_3I + 2HClO_4 + 2CO_2\,(g)$$

Il ne nous a pas été possible de déceler cette variation d'acidité car la quantité de protons qui sont libérés est peu élevée en raison de la faible solubilité de l'iode dans le solvant ($\simeq 2 \times 10^{-3}$ *M*). De plus, le domaine acide–base est trop réduit.

La courbe de réduction de I(+I) ne peut s'expliquer qu'en supposant qu'il existe simultanément sous les formes CF_3COOI et CF_3I, l'une d'elles, CF_3I par exemple, n'étant pas électroactive.

La première vague de réduction correspond alors à la réduction du trifluoroacétate d'iode en iode. A -0.4 V commence la réduction de l'iode en iodure. Ce dernier réagit chimiquement avec CF_3I pour donner I_2 à nouveau réductible jusqu'à la disparition complète du trifluoroiodométhane. Le tracé des courbes intensité–potentiel des solutions d'acide trifluoroacétique saturées par CF_3I gazeux confirme sa non électroactivité. Cependant, il réagit chimiquement sur l'iodure. Ceci est en accord avec les hypothèses précédentes.

La coexistence de I(+I) sous les formes CF_3COOI et CF_3I explique l'allure inattendue de la courbe de réduction. Par contre ICl et IBr, qui sont des complexes stables dans l'acide trifluoroacétique, ont un comportement électrochimique normal. Les deux vagues de réduction ont la même hauteur (Fig. 8). Les réductions à potentiel contrôlé montrent qu'en milieu trifluoroacétate de sodium les réactions électrochimiques sont les suivantes:

$$2ICl + 2CF_3COONa + 2e \rightarrow I_2 + 2NaCl + 2CF_3COO^-$$

$$I_2 + 2CF_3COONa + 2e \rightarrow 2NaI + 2CF_3COO^-$$

Par ailleurs ces deux composés sont titrés quantitativement par l'iodure de sodium, le titrage étant suivi par ampérométrie à un potentiel fixé à 0 V.

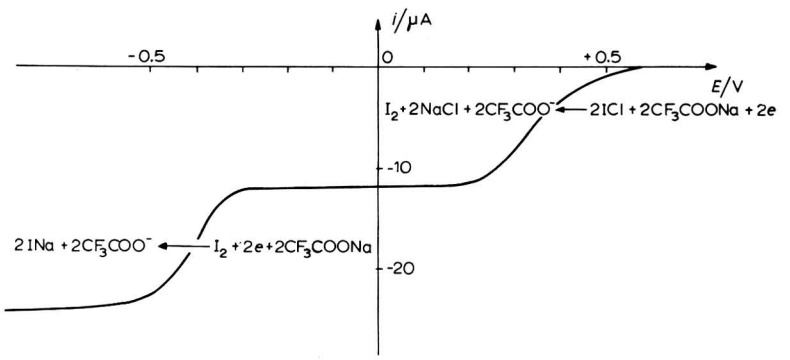

Fig. 8. Réduction de ICl 3.6×10^{-3} *M* à une électrode de platine poli en milieu basique.

B. Deuxième étape d'oxydation

L'étude de cette seconde étape d'oxydation est rendue difficile pour deux raisons: la première est due au fait que l'oxydation de I(+I) se situe dans une zône de potentiel assez proche de celle où a lieu l'oxydation du solvant. La seconde raison est relative à I(+I) qui existe sous les formes CF_3COOI et CF_3I.

Oxydation de I(+I). Quelle que soit la nature de l'électrode utilisée, la hauteur de la vague d'oxydation de I(+I) est égale au double de celle qui correspond à l'oxydation de l'iode en I(+I). Elle est de plus égale à la hauteur de la vague de réduction globale de I(+I) en iodure (Fig. 6b).

Il résulte de ces considérations que la deuxième étape d'oxydation correspond bien au passage de l'iode du degré +I au degré +III. Une oxydation effectuée à

potentiel contrôlé sur la vague d'oxydation de I(+I) confirme ces résultats. La réaction électrochimique est la suivante:

$$I(+I) - 2e \rightarrow I(+III)$$

Réduction de I(+III). La solution obtenue par électrolyse est incolore. La courbe de réduction de I(+III) est mal définie. A une électrode de carbone, la vague de réduction globale de I(+III) en iodure a la hauteur attendue, mais les vagues intermédiaires s'écartent de la courbe théorique puisque I(+I) existe sous les formes CF_3COOI et CF_3I et que CF_3I n'est pas électroactif.

Un titrage ampérométrique effectué à +1.25 V indique que I(+III) est réduit quantitativement en iode par l'iodure de sodium.

Mélanges I(+III)–I(+I). Le système est lent; le potentiel de demi-vague est mal défini et ne suit pas la loi de Nernst.

Discussion. Cette étude confirme l'existence de l'iode au degré +III dans le solvant. I^{3+} est probablement un cation très acide comme I^+.

Par analogie avec I(+I), on peut supposer que I(+III) introduit en solution sous la forme ICl_3, conduit à une courbe de réduction mieux définie puisque ICl est stable. En fait, ICl_3 est réduit lentement par le solvant selon la réaction suivante:

$$ICl_3 + 2CF_3COOH \rightarrow ICl + 2HCl + 2CO_2(g) + C_2F_6(g)$$

Néanmoins les courbes tracées rapidement après la solubilisation laissent entrevoir que le trichlorure d'iode est réduit en deux étapes, la première correspond à la réduction de ICl_3 en iode et la seconde à la réduction de l'iode en iodure (Fig. 9). Le courant cathodique à 0 V et à −0.6 V est dans le rapport $\frac{3}{4}$, ce qui est en accord avec les valeurs théoriques.

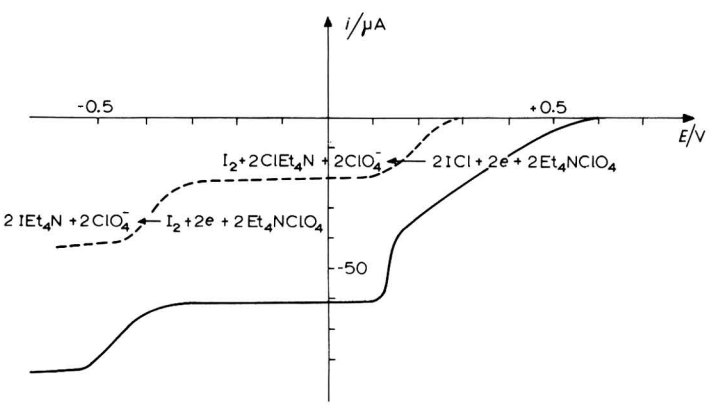

Fig. 9. Réduction de ICl_3 en milieu neutre non tamponné. (——) Courbe tracée après addition de ICl_3, (------) courbe tracée une heure après l'addition.

III. CONCLUSION

De l'étude comparative du comportement électrochimique de l'iode dans l'acide trifluoroacétique et dans l'acide acétique, peuvent être dégagées un certain nombre de remarques.

Il est possible de comparer la position des couples oxydo–réducteurs en utilisant une référence connue dans les deux solvants: le couple ferrocène/ferricinium[21,3,13].

Les systèmes $I(-I)/I_2$, $I_2/I(+I)$ et $I(+I)/I(+III)$ seront successivement envisagés.

La solubilité de l'iode est très voisine dans l'acide trifluoroacétique et dans l'acide acétique. Les coefficients de solvatation Γ_{I_2} rapportés à l'eau sont donc très proches bien que le mode de solvatation soit différent (l'iode est violet dans CF_3COOH, il est brun dans CH_3COOH).

Le complexe I_3^- n'existe pas dans l'acide trifluoroacétique alors qu'il est relativement stable dans l'acide acétique[13]. Il semble donc que les gros anions soient peu solvatés comparativement aux petits anions dans le premier solvant, alors que cette différence est beaucoup moins importante dans le second.

La comparaison de la position du couple I_2/I^- par rapport à celui du ferrocène, laisse supposer que l'acide trifluoroacétique est le solvant qui solvate le plus l'iodure.

I(+I) est mis en évidence dans les deux solvants. Dans CH_3COOH il réagit avec l'acide pour donner l'acide iodoacétique CH_2ICOOH[13]. Dans CF_3COOH il se trouve sous forme de trifluoroacétate d'iode et de trifluoroiodométhane.

L'iode au degré +3 a pu être isolé dans CF_3COOH ; il est stable. Dans l'acide acétique, I(+III) formé électrochimiquement catalyse l'oxydation du solvant comme dans l'anhydride acétique[12].

Les différences du comportement de l'acide acétique et de l'acide trifluoroacétique, comme solvants, sont principalement dues à deux facteurs. Le premier intervient au niveau des propriétés acide–base et oxydoréductrices. Il est lié aux différences d'effet inductif des groupements CH_3- et CF_3-. Le second se manifeste lors de l'étude de l'oxydation de l'iode. Il est dû à l'impossibilité dans l'acide trifluoroacétique de substituer un fluor par un iode.

PARTIE EXPÉRIMENTALE

Solvants et réactifs

L'acide trifluoroacétique est purifié et déshydraté selon une technique décrite dans le mémoire précédent[3].

Les réactifs sont les suivants: acide perchlorique, acétonitrile, dichloro-1,2-éthane, Prolabo R.P.; perchlorate de tétraéthylammonium, iodure de tétrapentylammonium, Eastman Kodak ; iodure de sodium déssèché, Billault ; chlorure d'iode, bromure d'iode, trichlorure d'iode, Touzart et Matignon ; iode bissublimé, Prolabo.

L'iode est peu soluble dans l'acide trifluoroacétique ; la cinétique de dissolution est lente. La solubilité atteinte à 25°C après une agitation de 12 h est voisine de 2×10^{-3} *M*.

La préparation du trifluoroacétate de sodium est décrite dans le mémoire précédent[3].

Le triiodure de tétrapentylammonium est préparé selon la méthode de Chattaway et Hoyle[22], non dans le méthanol mais dans l'acétonitrile où le complexe est plus stable[23].

Le trifluoroiodométhane est synthétisé par action de l'iode sur le trifluoroacétate d'argent[17]. C'est un gaz incolore à 25°C (T_{eb} sous une atmosphère -22°C).

Technique électrochimique

Des courbes intensité–potentiel sont tracées à l'aide d'un montage potentiostatique classique à trois électrodes. Les électrodes indicatrices sont des électrodes tournantes à disque de platine poli et de carbone vitreux de 1 mm de diamètre. La vitesse de rotation des électrodes est fixée à 660 tours/min.

L'électrode de référence $Ag(s)|AgClO_4(s)|(C_2H_5)_4NClO_4$ 10^{-1} M est décrite dans l'article précédent[3].

Les coulométries sont effectuées à l'aide d'un montage coulométrique Tacussel.

Spectrophotométrie

Les spectres sont enregistrés en cuve de quartz de 1 cm d'épaisseur sur un appareil Beckman DK2.

REMERCIEMENTS

Nous tenons à remercier Madame J. Badoz-Lambling, Directeur de Recherches au C.N.R.S., pour l'intérêt qu'elle a bien voulu porter à cette étude, ainsi que Monsieur G. Durand pour les fructueuses discussions que nous avons eues et Madame Bardin pour sa collaboration technique.

RÉSUMÉ

L'étude électrochimique de l'iode dans l'acide trifluoroacétique permet d'identifier les degrés d'oxydation $-I$, O, $+I$ et $+III$. L'instabilité du complexe triiodure en milieu anhydre est mise en évidence par une étude spectrophotométrique complémentaire. Le complexe triiodure est stabilisé par addition d'eau.

Le système électrochimique $I_2/I(-I)$ est lent. En milieu anhydre les iodures ne sont pas électroactifs. L'électroactivité des iodures, en présence d'eau, est liée à la présence du complexe triiodure.

Les systèmes $I_2/I(+I)$ et $I_2/I(+III)$ sont également lents. En milieu neutre non tamponné, $I(+I)$ existe sous les formes CF_3I et CF_3COOI. Le trifluoroiodométhane n'est pas électroactif. Un examen comparatif du comportement électrochimique de l'iode dans l'acide trifluoroacétique et dans l'acide acétique est proposé en conclusion.

SUMMARY

The electrochemical study of iodine in trifluoroacetic acid leads to the identification of the oxidation states: $-I$, O, $+I$ and $+III$.

The instability of the triodide complex in anhydrous media is shown by a complementary spectrophotometric study. The triodide is stabilized by addition of water.

The $I_2/I(-I)$ electrochemical system is not reversible. In anhydrous media, iodides are not electroactive. The redox behaviour of iodides in the presence of water is related to the presence of the triodide complex.

The $I_2/I(+I)$ and $I(+I)/I(+III)$ systems are also irreversible. In neutral, unbuffered media, $I(+I)$ is present in the forms: CF_3I and CF_3COOI. Trifluoro-

iodomethane is not electroactive.

In conclusion, a comparison between the redox behaviour of iodine in trifluoroacetic acid and acetic acid is suggested.

BIBLIOGRAPHIE

1 J. BESSIERE, Thèse, Paris, 1969.
2 J. H. SIMMONS ET K. E. LORENTZEN, *J. Am. Chem. Soc.*, 74 (1952) 4746.
3 G. PETIT, article à paraître.
4 H. C. BROWN ET R. A. WIRKKALA, *J. Am. Chem. Soc.*, 88 (1966) 1447, 1453.
5 L. J. ANDREWS ET R. M. KEEFER, *J. Am. Chem. Soc.*, 79 (1957) 1412, 5169.
6 R. E. BUCKLES ET J. F. MILLS, *J. Am. Chem. Soc.*, 76 (1954) 6021.
7 V. G. LEVICH, *Physicochemical Hydrodynamics*, Prentice Hall Inc., Englewood Cliffs, N.J., 1962.
8 R. E. BUCKLES, J. F. YUK ET A. I. POPOV, *J. Am. Chem. Soc.*, 74 (1952) 4379.
9 G. CHARLOT, J. BADOZ-LAMBLING ET B. TREMILLON, *Les réactions électrochimiques*, Masson, Paris, 1959.
10 I. M. KOLTHOFF ET J. JORDAN, *J. Am. Chem. Soc.*, 75 (1953) 1571.
11 J. BADOZ-LAMBLING ET C. DUTRUC-ROSSET, *Anal. Chim. Acta*, 19 (1958) 43.
12 V. PLICHON, J. BADOZ-LAMBLING ET G. CHARLOT, *Bull. Soc. Chim. France*, (1964) 287.
13 G. DURAND, article à paraître.
14 I. POPOV ET D. H. GESKE, *J. Am. Chem. Soc.*, 80 (1958) 1340.
15 G. DRYHURST ET P. J. ELVING, *Anal. Chem.*, 39 (1967) 606.
16 G. PETIT, Thèse, Paris, 1969.
17 R. N. HASZELDINE, *J. Chem. Soc.*, (1951) 584.
18 R. N. HASZELDINE ET A. G. SHARPE, *J. Chem. Soc.*, (1952) 993.
19 G. H. CRAWFOAD ET J. H. SIMMONS, *J. Am. Chem. Soc.*, 77 (1955) 2605.
20 R. E. BUCKLES ET J. F. MILLS, *J. Am. Chem. Soc.*, 76 (1954) 4845.
21 H. M. KOEPP, H. WENDT ET H. STREHLOW, *Z. Elektrochem.*, 64 (1960) 483.
22 F. D. CHATTAWAY ET G. HOYLE, *J. Chem. Soc.*, (1923) 654.
23 J. DESBARRES, *Bull. Soc. Chim. France*, (1961) 502.

ELECTROANALYTICAL CHEMISTRY AND INTERFACIAL ELECTROCHEMISTRY
Elsevier Sequoia S.A., Lausanne – Printed in The Netherlands

THE EFFECT OF THE SUPPORTING ELECTROLYTE ON THE ELECTROREDUCTION OF ETHYL BROMIDE

RICCARDO GALLI AND FRANCO OLIVANI
Montecatini Edison S.p.A.,"G. Donegani" Research Institute, Novara (Italy)
(Received October 3rd, 1969; in revised form November 5th, 1969)

INTRODUCTION

Recently[1,2], the electrode behaviour of ethyl bromide (EtBr) at Pb cathodes has been examined in propylene carbonate (PC) solutions, with tetraethylammonium bromide (Et_4NBr) as supporting electrolyte.

The reaction products depend on electrode potential: EtBr proves to be electroactive only when the cathode polarization (η_c) is above 500 mV. When $500 < \eta_c < 1400$ mV, the discharge process brings about the formation of alkyl-lead compounds, mainly tetraethyllead ($PbEt_4$), according to the one-electron reaction:

$$\tfrac{1}{4}Pb + EtBr + e \longrightarrow \tfrac{1}{4}PbEt_4 + Br^- \qquad (1)$$

When $\eta_c > 1400$ mV, C_2–C_4 hydrocarbons are also produced; ethane is the most abundant of them and this has been attributed to the two-electron reduction:

$$EtBr + H^+ + 2\,e \longrightarrow C_2H_6 + Br^- \qquad (2)$$

Water is the probable source of protons: in the solution used, the content ranges from 100 to 1000 p.p.m., which corresponds to molarities of about 10^{-3}–10^{-2}.

More recently, Ulery[19] investigated the behaviour of alkyl halides in acetonitrile at Pb electrodes, obtaining results which, from a qualitative point of view, are comparable with ours.

The behaviour of organic electroactive compounds is strongly affected by the solvent system components: solvent molecules and supporting ions can adsorb at the electrode surface, in competition with the reactive species, and eventually with the reaction intermediates. From this point of view, little is known about the electroreduction of alkyl halides[2,3]. We have now extended our investigations on EtBr by examining the effect of several classes of supporting electrolytes: onium (tetraalkylammonium, trialkylsolfonium, pyridinium), ammonium-, alkali-, alkali earth-salts.

The experimental techniques were as described previously[1]. The static potential of a Pb electrode in the system PC–EtBr 0.1 *M*–Et_4NBr 0.1 *M* is $\simeq -0.71$ V (*vs.* a satd. Hg_2Br_2 electrode in PC, the reference cell used), which corresponds to -0.65 V (*vs.* SCE).

The experimental cathode polarization η_c is equal to the electrode potential with current flow, less its value in the absence of current[23], *i.e.* the static potential.

1. RESULTS

1.1. *Polarization curves*

Three potentiostatic polarization curves at Pb cathodes are shown in Fig. 1 and correspond to three different systems:

curve 1–PC alone

curve 2–PC, EtBr 1 *M*, $LiClO_4$ 1 *M*

curve 3–PC, EtBr 0.1 *M*, Et_4NBr 0.1 *M*

Curves 1 and 2 show a similar trend up to $\eta_c \rightarrow 2000$ mV: therefore, EtBr in the presence of $LiClO_4$ is not an electroactive species until this polarization is attained. When $\eta_c > 2000$ mV, curve 2 indicates a reduction process of EtBr.

The behaviour of solutions containing Et_4NBr is quite different (curve 3); it is characterized by three limiting currents ($\eta_c = 500$, 1400, 2000 mV) which correspond respectively to oxygen reduction, $PbEt_4$ formation and ethane discharge[1].

The published $E_{\frac{1}{2}}$ polarographic values of EtBr for reaction (2) are:

−2.13 V (*vs.* SCE)[20] in dimethylformamide + Et_4NBr

−1.70 V (*vs.* AgBr electrode)[21] in dimethylformamide + Et_4NBr

−2.08 V (*vs.* SCE)[22] in dioxane/water + Et_4NBr

These values agree well with the $E_{\frac{1}{2}}$ value obtained from our measurements for ethane discharge, by taking into account the liquid-junction potentials between aqueous and organic phases: −2.20 V (*vs.* SCE), which corresponds to $\eta_c \simeq 1.55$ V.

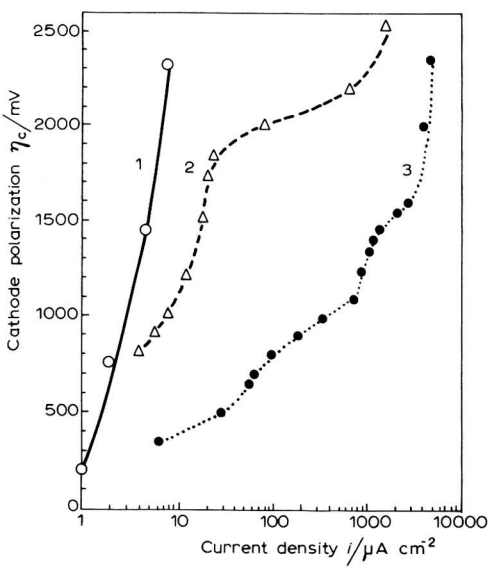

Fig. 1. Potentiostatic polarization curves at Pb cathode. (1) PC alone (○); (2) PC, EtBr 1 *M*, $LiClO_4$ 1 *M* (△); (3) PC, EtBr 0.1 *M*, Et_4NBr 0.1 *M* (●).

1.2. *Electrolysis*

In order to determine the reaction products during electrolysis of EtBr–PC solutions with various supporting electrolytes, tests have been carried out between Pb

cathodes and graphite anodes in a H-cell with diaphragm. The working electrode potential was kept within a suitable range ($1000 < \eta_c < 1400$ mV) by controlling the current accordingly.

The results obtained are summarized in Table 1: the experimental conditions and the current yields for the production of $PbEt_4$ are given for each test. The Table shows a highly specific action of onium salts: $PbEt_4$ has been obtained only in their presence and with satisfactory yields. The difference noticed on using the various onium salts may be attributed, at least partly, to slightly different experimental conditions. In the case of pyridinium ion, its discharge potential is comparable with the EtBr one: thus, in addition to $PbEt_4$, pyridine derivatives[4] have been found as products, with a lowering in output.

Surprisingly, the output of $PbEt_4$ is practically nil when using inorganic electrolytes and no decrease in weight of the cathode is noticeable. Currents are of very low density, and greatly inferior to those obtained in the presence of onium salts; in the polarization range considered, they are background currents, due to impurities and dissolved oxygen, as it is also shown by the polarization curves.

With $LiClO_4$ as supporting electrolyte (tests 11–14), the reaction products have been examined by widely varying electrode polarization (η_c up to 4000 mV) and EtBr concentration (up to 3 *M*). No attack of the cathode has ever been noticed. At high polarizations, a discharge of hydrogen and C_2–C_4 hydrocarbons takes place, and, in extreme conditions, lithium metal deposition is observed.

TABLE 1

ELECTROLYSIS OF PC–EtBr SOLUTIONS, WITH VARIOUS SUPPORTING ELECTROLYTES

Test No.	*Concn. EtBr/M*	*Electrolyte*		*Cathode polarization/mV*	*Current density/μA cm⁻²*	*Current yields/%*
1	0.1	Et_4NBr	−0.1 *M*	1400	300–500	98
2	0.1	Et_4NI	−0.1 *M*	1300–1400	600–800	71
3	1	Et_4NClO_4	−0.1 *M*	1150–1200	1260–1290	100
4	0.1	Bu_4NBr	−0.1 *M*	1200–1300	460–480	87
5	0.1	Bu_4NBF_4	−0.04 *M*	1300–1400	400–500	80
6	1	Me_2EtSBr[a]	−1 *M*	1000–1100	1380–1450	77
7	0.9	N-ethylpyridinium bromide[b]	−0.1 *M*	1000–1300	1000–1100	present
8	1	NH_4PF_6	−0.1 *M*	1000–1100	140–160	0
9	0.1	KCl	−satd.	900–1300	1–3	0
10	0.1	$CaCl_2$	−satd.	1200	2–3	0
11	0.1	$LiClO_4$	−0.1 *M*	900–1000	1–2	0
12	0.1	$LiClO_4$	−0.1 *M*	1900–2100	40–50	0
13	3	$LiClO_4$	−1 *M*	1500–2000	10–50	0
14	3	$LiClO_4$	−1 *M*	2000–4000	200–500	0

[a] Corresponding to a Me_2S + EtBr equimolar mixture.
[b] Corresponding to a pyridine + EtBr equimolar mixture.

1.3. *Solvent effect*

We examined the influence of the solvent on the specific action of onium salts for reaction (1), as it appeared from the results referred to in Table 1. For the half-

element, Pb/PC, EtBr, Et_4NBr 0.1 *M*, the relationship between cathode current density (at $\eta_c = 1000$ and 1400 mV) and EtBr concentration (up to [EtBr] = 7 *M*)* has been studied (Fig. 2, non-stirred solution). As a comparison, the values of current density at the same polarizations have been reported for EtBr alone (supporting electrolyte Bu_4NBr 0.1 *M*).

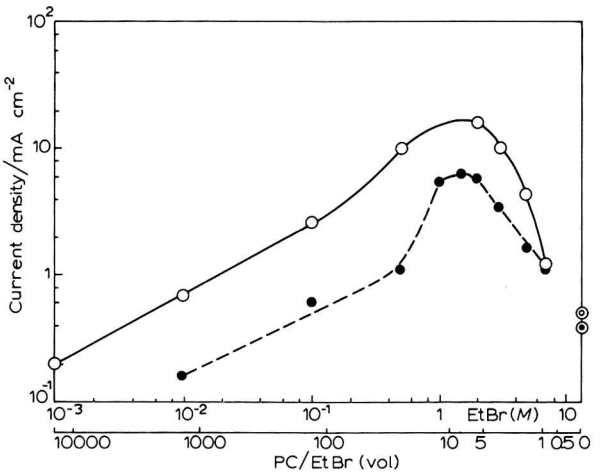

Fig. 2. Effect of EtBr concn. current density, at Pb cathode. Electrolytic soln.: PC–EtBr–Et_4NBr 0.1 *M*. η_c: (●) 1000, (○) 1400 mV. Points ◎, ⊙ refer to measurements in EtBr–Bu_4NBr 0.1 *M* soln.

Log *i vs.* log [EtBr] plots show a maximum for [EtBr] $\simeq$ 1.5 *M*; we can therefore distinguish two different behaviours:

(*a*) [EtBr] < 1.5 *M*. We have a linear relationship showing a formal reaction order dlog *i*/dlog [EtBr] $\simeq$ 0.5 up to [EtBr] $\simeq$ 0.5 *M*. Above this the current sharply increases up to a maximum.

(*b*) [EtBr] > 1.5 *M*. EtBr concentration has a negative effect on the current density.

For 1 *M* < [EtBr] < 3 *M*, the stirring influence is negligible: diffusion does not control the reaction kinetics. Outside this concentration range, current is low and more sensitive to background and parasitic processes (*e.g.*, impurities, oxygen), which are strongly affected by the stirring.

The results indicate a change in the reaction mechanism depending on the PC/EtBr ratio, and do not permit straightforward conclusions to be drawn as to the kinetics of the reaction, which need a more extensive study.

The electrolysis of EtBr alone, without cosolvent, can be carried out with onium salts R_4NX as supporting electrolyte: these salts are highly soluble in EtBr when R $\geqq$ 4 C atoms. It is not possible to electrolyse solutions of EtBr alone with inorganic electrolytes (*e.g.*, $LiClO_4$), owing to the low conductivity of the solution[5].

The most significant features observed from the tests carried out without

* At concentrations above 7 *M*, the solubility of Et_4NBr is less than 0.1 *M*.

cosolvent, in EtBr with Bu_4N^+ salts as supporting electrolytes, are:
- current density is low and stirring effect is negligible for $\eta_c > 1000$ mV.
- the reaction products are mainly $PbEt_4$ and its haloderivatives.
- surprisingly, no discharge of gaseous hydrocarbons is noticed, not even at high polarization ($\eta_c \simeq 2500$ mV) and in water-saturated solution ($\simeq 0.4\%$ weight).

1.4. *Conductivity measurements*

Specific conductivity (χ) *vs.* EtBr concentration plots for two systems PC–EtBr–onium salt (Et_4NBr and Bu_4NBr 0.1 *M*) are reported in Fig. 3: these measurements have been carried out in order to study possible modifications of the liquid structure, which could be related to the current density *vs.* EtBr concentration curves.

Curves in Fig. 3 are similar, both showing a maximum which, in the case of Et_4NBr occurs for [EtBr] $\simeq 4$ *M*, while in the case of Bu_4NBr is for [EtBr] $\simeq 7$ *M*. The slight increase in conductivity up to such massive EtBr concentrations is rather strange considering that the EtBr dielectric constant ($D = 9$) is much lower than the PC one ($D = 65$). Nevertheless, similar phenomena have already been observed—for instance, when adding toluene or ethyl ether to PC[6]—and they can be attributed, at least partly, to viscosity effects ($visc_{EtBr} = 0.004$; $visc_{PC} = 2.5$ g cm^{-1} s^{-1}).

The maximum points in the i/[EtBr] curves occur at much lower concentrations than those of χ/[EtBr] curves. This shows that the variation of the PC/EtBr ratio has a much larger influence on the double-layer structure (and consequently on the current density values) than it has on the structure of the bulk solution (and therefore on the electrolytic conductivity).

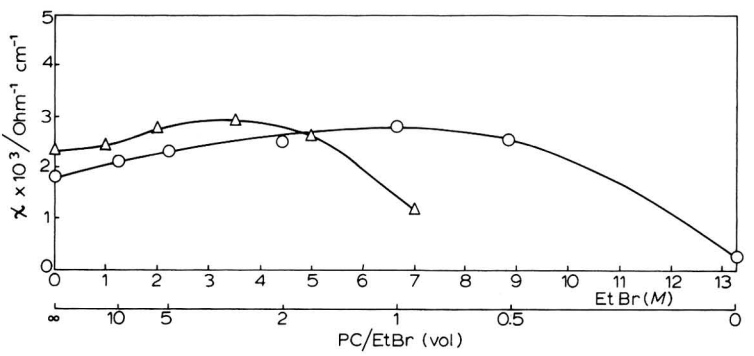

Fig. 3. Effect of EtBr concn. on conductivity of PC–EtBr–onium salt solns. (○) Bu_4NBr 0.1 *M*, (△) Et_4NBr 0.1 *M*.

1.5. *Salting-in effect*

The solubility of EtBr has been measured in various aqueous solutions (Table 2). The solubility in water is very poor (~ 6 g l^{-1}), and it is not markedly affected by inorganic electrolytes. Tetraalkylammonium ions cause a salting-in effect, which increases with the ionic size. Bu_4NBr exerts a strong influence: at high concentration, the molar ratio EtBr/Bu_4NBr in solution tends to 1.

This hydrotropic action occurs because dispersion forces become greater than the purely electrostatic forces involved[18], and suggests a strong interaction between the aliphatic chains of onium ions and EtBr.

TABLE 2

SOLUBILITY OF EtBr IN AQUEOUS SOLUTIONS

Electrolyte		*Solubility (mol EtBr/l H_2O)*
–		0.06
HCl	1 *M*	0.04
KCl	1 *M*	0.07
$BaCl_2$	1 *M*	0.04
$LiClO_4$	1 *M*	0.08
KOH	1 *M*	0.04
Me_4NBr	1 *M*	0.06
Et_4NBr	1 *M*	0.10
	>1 *M*	0.10
Bu_4NBr	0.5 *M*	0.07
	1 *M*	0.12
	1.5 *M*	0.43
	3.1 *M*	2.47

The quantitative determination of EtBr in solution was carried out by vapor phase chromatography with a Teflon column, with a stable phase of 20% $\beta\beta'$-oxydipropionitrile on Chromosorb W ($T = 50°C$; injector 100°C; helium carrier gas; pressure 0.5 atm.) and thermistor detector.

2. DISCUSSION

The data reported suggest that the EtBr discharge potentials and mechanisms, at Pb cathodes, strongly depend on the electrolyte–solvent system. Table 3 summarizes the results.

When metallic salts are present, only the process of direct reduction of EtBr to hydrocarbons is noticed with a comparative abundance of ethane.

The discharge of EtBr, in PC with onium salts, occurs in two subsequent stages corresponding to reactions (1) and (2), according to the following scheme:

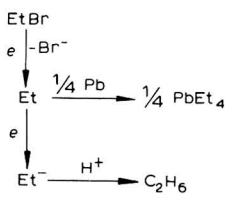

The effect of various cations on $PbEt_4$ formation according to reaction (1), occurs in the following order:

$$NEt_4^+ \simeq NBu_4^+ > EtMe_2S^+ \gg Li^+, Ca^+, K^+, NH_4^+ = 0$$

Electrochemical literature on alkyl halides does not quote anything similar and information regarding the reduction of these compounds at cathodes which may undergo alkylation is very scarce[2,3,10–13,19].

The specific action of onium salts in electrode processes both in inorganic and in organic processes is well-known in the literature[7–9]. Several studies were carried

out on their action in electro-hydrodimerizations[14,16]. In the reduction of acrylonitrile (AN), onium salts act by promoting the hydrodimerization process to adiponitrile (ADN):

$$CH_2{=}CH{-}CN + H^+ + e \longrightarrow \tfrac{1}{2}(-CH_2{-}CH_2{-}CN)_2 \quad (3)$$

instead of favouring the complete reduction to proportionitrile (PN):

$$CH_2{=}CH{-}CN + 2H^+ + 2e \longrightarrow CH_3{-}CH_2{-}CN \quad (4)$$

According to Beck[15], cations exert a specific action in the following order: NEt_4^+, $NBu_4^+ > NMe_4^+ > NEt_3H^+ > Na^+ > Li^+$. There is, therefore, a parallelism in the action exerted by onium salts on the electrochemical reduction of EtBr and AN at cathodes with high hydrogen overvoltage. As a whole, these reactions are rather dissimilar, but we can nevertheless single out some common aspects. In both cases there are two competitive processes: onium salts favour, respectively, reactions (1) and (3) instead of (2) and (4). Both (1) and (3) are formally one-electron reactions and require the absence (1) or a low concentration (3) of protons at the interface, and, *vice versa*, a

TABLE 3

SUMMARY OF THE BEHAVIOUR OF EtBr AT Pb CATHODES

Solvent	*Supporting electrolyte*	*Reaction products*	
		$PbEt_4$	*Hydrocarbons*
PC	onium salt	yes ($\eta_c > 500$ mV)	yes ($\eta_c > 1500$ mV)
PC	inorganic	no	yes ($\eta_c > 2000$ mV)
EtBr	onium salt	yes	no

high concentration of the organic reactant; on the contrary, (2) and (4) are formally two-electron reactions and require the presence of protons at the interface and a low concentration of the organic reactant. In addition, the molecular structures of EtBr and AN are rather similar: a C_2 hydrocarbon chain with a polar and electronegative group at the end. The hydrocarbon chain can promote an interaction with those of tetraalkylammonium ions, as indicated by the hydrotropic action of these ions on AN[15] and EtBr.

It has been pointed out[15] that the action of onium salts is mainly interfacial and it is due to the preferential adsorption of onium ions at the electrode. The double-layer structure and potential profile in the interphase are thus modified and, consequently, the potential at the position of the reactive molecule is modified too. The strong adsorption and the remarkable dimensions of onium ions may draw in the organic electroactive species in the double layer (thus increasing their surface concentration). In effect, Tomilov *et al.* observed an increase of AN adsorption at Hg electrodes in the presence of Et_4N^+ ions[17]. Onium ions may exert an additional effect by removing water molecules from the double layer.

3. CONCLUSIONS

Our studies on EtBr reduction at Pb cathodes confirm the strong influence of the nature of the solution on the electrode behaviour of organic compounds, already observed in other cases, as in the electro-hydrodimerization of activated olefines.

Up to $\eta_c = 1400$ mV, onium salts promote the $PbEt_4$ formation reaction (1) in spite of ethane discharge (2). This may be attributed to a twofold action, exerted by the strongly adsorbed cations:

(a) they enhance the EtBr concentration at the electrode surface;

(b) they remove water molecules, and hence protons, from the double layer.

At higher polarizations, hydrocarbon discharge takes place in the presence of PC, while in solutions of EtBr alone, no ethane has been detected.

The electrode behaviour pattern shown by the system EtBr + onium ions calls for further detailed investigation of the adsorption and interaction of the compounds involved in the electrode double layer.

ACKNOWLEDGEMENT

The authors wish to thank Prof. G. Bianchi for his valuable suggestions and his continuous interest in the work.

SUMMARY

The effect of several classes of supporting electrolytes on the electroreduction of ethyl bromide in propylene carbonate at lead cathodes has been examined. Tetraethyllead is formed only in presence of onium salts, while with inorganic salts only hydrocarbon discharge takes place. The action of onium ions and solvent molecules on the EtBr electrode behaviour pattern is discussed with reference to similar phenomena, such as the acrylonitrile electro-hydrodimerization.

REFERENCES

1 R. GALLI, *J. Electroanal. Chem.*, 22 (1969) 75.
2 R. GALLI, *Chim. Ind. Milan*, 50 (1968) 977.
3 O. R. BROWN AND J. A. HARRISON, *J. Electroanal. Chem.*, 21 (1969) 387.
4 J. VEDEL AND B. TREMILLON, *Bull. Soc. Chim. France*, (1966) 220.
5 R. GALLI AND T. MUSSINI, *Nature*, 223 (1969) 178.
6 J. E. CHILTON, W. J. CONNER, G. M. COOK AND R. W. HOLSINGER, Techn. Rep. AFAPL-TR-64-147, AD 612189, February, 1965.
7 L. GIERST, J. TONDEUR AND E. NICOLAS, *J. Electroanal. Chem.*, 10 (1965) 397.
8 S. R. MISSAN, E. I. BECKER AND L. MEITES, *J. Am. Chem. Soc.*, 83 (1961) 58.
9 R. PARSONS, *J. Electroanal. Chem.*, 21 (1969) 35.
10 E. I. du Pont de Nemours & Co., Fr. Pat. 1.450.613; Ger. Pat. 1.246.734; Brit. Pat. 949.925.
11 General Motors, US Pat. 1.567.159, 1.539.297.
12 L. G. FEOKTISTOV, A. P. TOMILOV, YU. D. SMIRNOV AND M. M. GOLDIN, *Elektrokhimiya*, 1 (1965) 767.
13 J. W. SEASE AND R. C. REED, E.C.S. New York Meeting, 1969, Electro-organic Division, Abs.No. 134, p. 328.
14 M. M. BAIZER, *J. Electrochem. Soc.*, 111 (1964) 215.
15 F. BECK, *Z. Elektrochem.*, 72 (1968) 379.
16 A. P. TOMILOV, E. V. KRYUKOVA, V. A. KLIMOV AND I. N. BRAGO, *Elektrokhimiya*, 3 (1967) 1501.

17 A. P. TOMILOV, L. A. FEDOROVA, V. A. KLIMOV AND G. A. TEDORADZE, *Elektrokhimiya*, 4 (1968) 1264.
18 G. KORTÜM, *Treatise on Electrochemistry*, Elsevier, 1965.
19 H. E. ULERY, *J. Electrochem. Soc.*, 116 (1969) 1201.
20 F. L. LAMBERT AND K. KOBAYASHI, *J. Am. Chem. Soc.*, 82 (1960) 5324.
21 J. W. SEASE, P. CHANG AND J. L. GROTH, *J. Am. Chem. Soc.*, 86 (1964) 3154.
22 M. VON STACKELBERG AND W. STRACKE, *Z. Elektrochem.*, 53 (1949) 118.
23 R. DEFAY, N. IBL, E. LEVART, G. MILAZZO, G. VALENSI AND P. VAN RYSSELBERGHE, *J. Electroanal. Chem.*, 7 (1964) 426.

Elsevier Sequoia S.A., Lausanne – Printed in The Netherlands

SHORT COMMUNICATIONS

Halide electrocatalysis in the reduction of hydrogen ions on mercury

The reduction of H^+ on Hg is accelerated by the presence of halides[1]. This effect has been interpreted as resulting from the influence of halide specific adsorption on the "outer Helmholtz" potential φ. However, Parsons[2] has recently pointed out that the observed acceleration is much larger than can be accounted for by the Frumkin correction[3]. Instead, Parsons[2] tentatively proposed another explanation, invoking the activity coefficient of the "activated complex".

In our recent work on the electrocatalysis in the reduction of indium[4], we have established the importance of the surface activity βa rather than the surface excess Γ in the study of electrocatalyzed reactions. By analogy with Parsons' plot of $\log i_x/i_o$ *vs.* the charge density Q_c attributable to adsorbed halide ions, we have plotted $\log (i_x - i_o)/i_o$ *vs.* $\log \beta a$ for the same data of Iofa *et al.*[1]. Here, i_x is the reduction current in the presence of halide X, and i_o is the current observed at the same applied potential in the absence of halides.

Data for $\log i_x/i_o$ and for Q_c were read from ref. 2 Fig. 3. Values of Q_c were converted into values for the electronic charge density Q_e on the metal, using data of Grahame and Parsons[5], Lawrence and Parsons[6] and Grahame[7] for 1 *M* KCl,

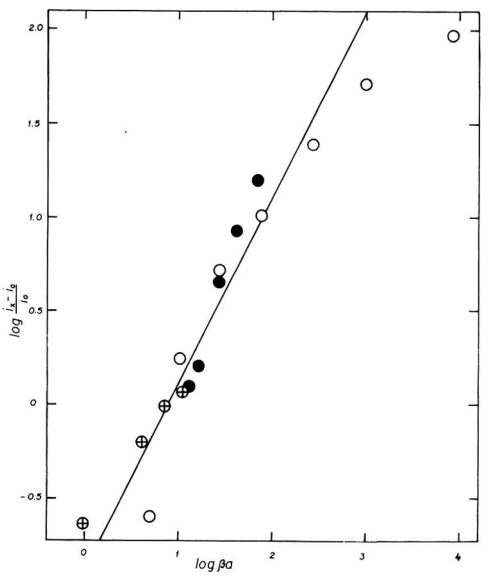

Fig. 1. Double-logarithmic plot of $(i_x - i_o)/i_o$ for the reduction of protons in the presence (i_x) or absence (i_o) of adsorbed halides, *vs.* estimated values of βa for halide adsorption. (⊕) 0.1 *M* HCl + 1 *M* KCl, (●) 0.1 *M* HCl + 1 *M* KBr, (○) 0.1 *M* HCl + 1 *M* KI. The line is drawn under unity slope. The accuracy of the points in the present Figure is rather poor since all pertinent data were unavailable in numerical form and consequently had to be read from printed journal illustrations.

1 *M* KBr and 1 *M* KI, respectively. Subsequently, the corresponding values of β were estimated from plots of Q_c *vs.* log a^2/Q_c for KCl and KBr, and taken from similarly obtained data reported by Parsons for KI[8].

The resulting graph, Fig. 1, exhibits two striking features: the points for X=Cl^-, Br^- and I^- fall essentially on the same straight line, and this straight line has unity slope. This strongly suggests that the *additional* reduction current in the presence of halides is caused by the reduction of H^+ through adsorbed X^-_{ads}, and that the rate-determining step can be written as

$$H^+ + X^-_{ads} + e^- \rightarrow \ldots \quad (1)$$

which implies the formation of a transient intermediate HX_{ads}. Of course, no direct evidence for the existence of such an intermediate can be obtained from surface tension or double layer capacitance data, when the reduction of protons from HX_{ads} is faster than the generation of HX_{ads} through reaction (1). The above description in terms of an adsorbed intermediate HX_{ads} is of course equivalent to a bridging mechanism of electron transfer.

Summarizing, we have observed that the additional, halide-connected current observed 30 years ago by Iofa *et al.*[1] can be represented by the rate law

$$k = \beta a k_0 \exp(-\alpha n F \eta / RT) \quad (2)$$

and that such a rate law indicates that a chemical rather then a physical phenomenon is involved. The fact that the curves for Cl^-, Br^- and I^- in Fig. 1 essentially coincide, within the accuracy of the data, is suggestive of a common slow mechanism, probably labilization or loss of coordinated water.

Acknowledgement

This research was supported by National Science Foundation grant GP 8575, Air Force Office of Scientific Research (OAR, USAF) grant 68-1344 and Office of Naval Research contract N00014-69-A-0220-0002. This manuscript is submitted in the understanding that the United States Government is authorized to reproduce and distribute reprints for governmental purposes.

Department of Chemistry,
Georgetown University,
Washington, D.C. 20007 (U.S.A.)

Robert de Levie
Lubomír Pospíšil

1 S. A. Iofa, B. Kabanov, E. Kuchinsky and F. Chistyakov, *Acta Physicochim. USSR*, 13 (1939) 1105.
2 R. Parsons, *J. Electroanal. Chem.*, 21 (1969) 35.
3 A. N. Frumkin, *Z. Physik. Chem.*, 164A (1933) 121.
4 L. Pospíšil and R. de Levie, *J. Electroanal. Chem.*, 25 (1970) 245.
5 D. C. Grahame and R. Parsons, *J. Am. Chem. Soc.*, 83 (1961) 1291. Numerical data kindly provided by Dr. R. Parsons through a long chain of intermediaries.
6 J. Lawrence and R. Parsons, *J. Electroanal. Chem.*, 16 (1968) 193.
7 D. C. Grahame, *J. Am. Chem. Soc.*, 80 (1958) 4201.
8 R. Parsons, *Trans. Faraday Soc.*, 55 (1959) 999 Fig. 2.

Received October 21st, 1969

Elsevier Sequoia S.A., Lausanne – Printed in The Netherlands

Hydrogen solubility in electrolytically deposited thin films of palladium

The quantity of hydrogen absorbed in electrodeposited thin films of palladium, in equilibrium with the atmospheric pressure, was determined in 0.1 *M* H_3PO_4 solution at 25°C.

Palladium films of different thicknesses were cathodically deposited on Pt supports ($\phi = 9.3$ mm). The deposition current density was 5.5 mA cm^{-2}. The Pd-black deposition was made in a 2% $PdCl_2$ solution in 1 *M* HCl solution; for bright depositions a phosphate bath[1] was used. Some bright films were obtained by using a Pt-anode during the deposition.

For the determination of the hydrogen content in Pd, the method of anodic oxidation with linear sweep voltammetry was used[2], after the potential of the Pd-film electrode had reached the zero value *vs.* NHE (normal hydrogen electrode) in the same solution. The Pd–H electrode is a hydrogen reversible electrode[3]; its potential is determined by the thermodynamic equilibrium between the quantity of superficial hydrogen and the inner dissolved quantity[4]; therefore, if a zero potential *vs.* NHE is obtained, this indicates a quantity of inner dissolved hydrogen in equilibrium with the external atmospheric pressure.

To avoid errors caused by the spontaneous desorption of the gas dissolved in Pd, hydrogen bubbling was maintained through the solution during the voltammetric measurements; the molecular hydrogen oxidation was corrected for by drawing base curves[2]. The determination of hydrogen solubility in electrodeposited Pd films was done before and after heating the film to about 700°C, for 2 min.

The experimental results are presented in Table 1.

For comparison, the hydrogen solubility in a compact, rolled, 20 μ thick foil of Pd, is also given here.

The hydrogen solubility in both a compact Pd and a Pd-black layer is of the same value, $r = 0.654 \pm 0.008$, independent of the quantity and thermal treatment of the metal. The solubility value is smaller than the value calculated ($r_{calc} = 0.690$) for our working hydrogen pressure, 0.92 atm.[5]. This difference could be caused by the systematic errors of the voltammetric method in the determination of the hydrogen content of Pd, but as all the measurements were made under the same experimental conditions, the hydrogen solubility value in compact Pd and in Pd-black layers can be taken as a reference value.

The hydrogen solubility in bright Pd-films is smaller than the reference value and particularly sensitive to heating. The variation of hydrogen solubility in bright Pd films with and without heating exceeds the voltammetric measurement error, so that these variations can be regarded as significant.

The use of a Pt-anode in the electrodeposition of bright films results in an increase in hydrogen solubility over the reference value.

The behaviour of thin, bright Pd electrodeposited films—as far as the hydrogen solubility is concerned—cannot at present be accounted for. The results seem to confirm the anomalous behaviour of bright thin films (thickness $\leqq 1$ μ) reported in a voltammetric hydrogen diffusion study[6].

Further experimental work is in progress.

TABLE 1

Film thickness[a]/μ	*Kind of deposition*	$r(=H/Pd)$ (−)	$r(=H/Pd)$ (+)
	compact	0.64	
20	rolled	0.68	
		Av. val. 0.66	—
		0.65	
1.2[b]	black	0.70	
		Av. val. 0.67	0.65
			0.65
1.8[b]	black		0.65
		Av. val. 0.64	0.65
0.5	bright	0.56	
		0.57	0.12
0.7	bright	0.57	0.13
		Av. val. 0.57	0.12
		0.47	
		0.51	0.35
1.5	bright	0.41	0.37
		Av. val. 0.46	0.36
			0.41
		0.94	0.45
1.0	bright[c]	0.87	0.42
		Av. val. 0.90	0.43
		0.74	
1.8	bright[c]	0.74	
		Av. val. 0.74	0.61

[a] Thickness determined from the quantity deposited. [b] Equivalent thickness, calcd. from the quantity deposited on the hypothesis of a compact structure. [c] With Pt anode during the film deposition. (−)(+) Without (−) and with (+) thermal treatment.

Institute for Atomic Physics,
Cluj (Rumania)

R. V. Bucur
Livia Stoicovici

1 V. V. OSTROUMOV, *Zh. Fiz. Khim.*, 31 (1957) 1812.
2 R. V. BUCUR, *J. Electroanal. Chem.*, 10 (1965) 8.
3 D. J. G. IVES AND G. J. JANZ, *Reference Electrodes*, Academic Press, New York and London, 1961.
4 R. V. BUCUR, *J. Electroanal. Chem.*, 17 (1968) 427.
5 R. V. BUCUR, *Rev. Phys. Acad. Rep. Populaire Roumaine*, 6 (1961) 583; R. V. BUCUR AND M. CRIŞAN, *J. Phys. Chem. Solids*, 28 (1967) 995.
6 R. V. BUCUR, *J. Electroanal. Chem.*, 22 (1969) 127.

Received October 1st, 1969

Elsevier Sequoia S.A., Lausanne – Printed in The Netherlands

An illustration of the problem of "*a priori* separation" of double-layer and faradaic currents

In this paper, "the *a priori* problem" is illustrated by analysis worked out for an extremely simple physical model.

Recent discussions[1-6] on the problem of *a priori* separation of the "double layer" and "faradaic" currents have offered a newer perspective on the "active" role played by the electrical double layer and cautioned that an over-simplified picture* —though desirable—can lead to serious errors. The assumption that the total current is a linear superposition of the faradaic and the non-faradaic components is still retained in the conceptual level but sufficient care has now been taken to account for the "non-equilibrium" state of the electrical double layer. The essence of such analysis shows that the "double layer capacity" is no "capacity" but is a generalised impedance whose elements exhibit an involved dependence on almost everything that is happening in the interface! The interface is "capacity-like" only to the extent that its capability to "store charges" is recognised. Thus, one could also view this as a capacity that exhibits "leakage characteristics" dependent upon various kinetic steps.

The frequency dispersion of the double layer impedance has been worked out for certain models, indicating as a corollary that an *a priori* knowledge of the double layer impedance is not possible if the detailed steps constituting the faradaic process and the parameters such as i_0, α, etc., occurring therein are not known. This is to be expected as a natural consequence since in this charge separation (whether accompanied or not by the charge transfer) phenomena, the "dielectric" (medium) has besides the solvent dipoles a large number of "free ionic carriers" in the specifically and non-specifically adsorbed states. Hence, the spectrum of relaxation times is extended and comprises those characteristic of the various processes involving these charge carriers and dipoles. The dependence on adsorption/desorption, diffusion, etc., is only an example of this manifestation. The above statement applies to polarisable and non-polarisable systems alike. If such a behaviour was not observed in most of the well-studied polarisable media, it is only because—in the frequency range studied—such steps are either absent or not important. For example, at sufficiently low concentrations or with complex adsorption–desorption kinetics involving these ions, even an ideally polarisable system should exhibit an involved frequency dispersion.

We now illustrate the problem of *a priori* separation for a simple model for the faradaic process. This is identical with that used by Laitinen and Randles[7] except that the related mass transfer aspect and a parallel charge transfer by the ions in the non-adsorbed state are neglected *here*. Again, one could identify this with the "non-collision limited faradaic process" discussed recently by Reinmuth[6]. However, the following analysis differs in certain respects from that of Reinmuth[6]. We assume here that "it is the loss or gain of an electron by ions of the reactant *which remain*

* For example: the assumption that an excess supporting electrolyte "takes care of" the electrical double layer. Usually, the role of an excess supporting electrolyte is taken as two-fold: first as a "current carrier" under non-equilibrium conditions and secondly as one determining the charge separation at the interface.

adsorbed on the electrode surface which is postulated as the source of an additional current, not the adsorption and desorption of these ions"[7]. Since no mass transfer effect in the solution is assumed in this paper, the reactive species Γ_O and Γ_R contribute to the faradaic process through

$$i_f = nFA(d((1-x)\Gamma)/dt)$$
$$\simeq i^0_{ad}(\Delta x/x_0 + \Delta x/(1-x_0) + nFE/RT)$$

in the linear approximation. The total surface excess concentration of O and R is Γ and x is the fraction that is in the form O. It is implicit in the model that $\Gamma_O + \Gamma_R = \Gamma$, a constant, for all t; x_0 is the value of x at $t=0$. i^0_{ad} is the exchange current density and $\Delta x = x - x_0$.

Writing

$$i = dq/dt + i_f \tag{2}$$

where dq/dt is the so-called "charging current", we note that

$$dq/dt = q_E(dE/dt) + q_\Gamma(d\Gamma_R/dt) \tag{3}$$

since it is assumed that Γ_R and E are the only independent variables determining the charge separation at the interface. It should be noted *that x changes due to its participation in the faradaic reaction, but in so doing, alters the ability of the interface to store the charges, i.e., the double layer impedance is itself altered.* Thus, we see here clearly the interplay of the two, *viz*, the faradaic and the double layer currents expressed through (1)–(3) (note that Reinmuth[6] does not consider the faradaic branch and the limitations imposed thereby).

Since

$$d\Delta x/dt = -i_f/nFA\Gamma, \quad \text{or} \quad d\Delta\Gamma_R/dt = i_f/nFA \tag{4}$$

(eqn. (9) of ref. 7),

$$dq/dt - q_e \cdot dE/dt = +i_f \cdot q_\Gamma/nFA \tag{5}$$

i.e. "the error" in assuming that the double layer capacity equals $(\partial q/\partial E)$ is directly proportional to the amount of faradaic current flowing at the instant! Also, note that

$$i = (\partial q/\partial E) \cdot dE/dt + \delta i_f \tag{6}$$

with

$$\delta = (1 + q_\Gamma/nFA) \tag{7}$$

Hence, the mathematics of the analysis continue to remain simple for this model even after allowing for the dependence of the double layer impedance on the faradaic process, but the parameters acquire now a different significance.

The complete solution itself is easy to obtain and we have for the generalised impedance

$$Z(p) = [pq_E + pC'/(pR'_t C' + 1)]^{-1} \tag{8}$$

where p is the transform variable,

$$q_E = (\partial q/\partial E) \tag{9}$$

$$C' = n^2 F^2 x_0(1-x_0)\delta\Gamma/RT = \delta C \tag{10}$$

and

$$R'_t = (RT/nF)\delta i^0_{ad} = R_t/\delta \tag{11}$$

The equivalent circuit emerging out of (8) is a capacity q_E parallel to an impedance comprising the resistance R'_t and a capacitance C' in series. Both R'_t and C' are frequency-independent but depend on $(\partial q/\partial\Gamma_R)$. The above expressions are different from those of Laitinen and Randles[7] only through the factor δ in C' and R'_t. It looks —at least in this case—that a simple δ-factor (refer eqn. (7)) could account for the double layer effects. Another interesting aspect that follows this analysis refers to the difficulties that may arise in the "impedance-plot procedures" that are being very successfully employed[3]. If one recognises *a priori* the possibility that $q_\Gamma \neq 0$, the correct estimates for i^0_{ad} and α will be obtained knowing q_Γ but if it was not realised *a priori* that the double layer can distort the faradaic process, only "apparent" values of the parameters are deduced. Hence, from the frequency or concentration dependence alone, it may be difficult to clinch this issue (see *Appendix*). This arises because there is no one-to-one correspondence between the various models (general or limiting) and their frequency dependence; this is all the more true when the frequency intervals used happen to be limited. It is only wishful thinking that such a model would fit most practical systems and it is conceded that the discussion of the problem presented here is only formal but, as indicated by Laitinen and Randles[7], Reinmuth[6] and Kooijman[4], there may exist certain real systems fitting this model. We mention, in passing, a subtle question that arises in these studies (and more particularly in the model treated here) *viz*, whether the specifically adsorbed oxidised and reduced species can be distinguished "operationally"[8] and "conceptually"[9]. We propose to discuss this later.

Appendix

The "*a posteriori*" admittance elements are, from (8),

$$\begin{aligned} Y'^*_{el} &= \omega^2 R'_t C'^2/(1+\omega^2 R'^2_t C'^2) \\ Y''^*_{el} &= \omega q_E + Y'^*_{el}\omega R'_t C' \end{aligned} \tag{A}$$

with R'_t, C' *defined by* (10–11).

If one "*a priori*" assumes Randles' circuit with a view to decide C_d, the "real" double layer capacity, the admittance elements would then be written as

$$\begin{aligned} Y'_{el} &= \omega^2 R_t C^2/(1+\omega^2 R_t C^2) \\ \text{and} \quad Y''_{el} &= \omega C_d + Y'_{el}\omega R_t C \end{aligned} \tag{B}$$

Let us see what the usual analysis could say of the phenomenon:

(i) The frequency variation of Y'_{el} is the same for *both* A and B. The difference lies however in interpreting the constants. A measures apparent rate constants R'_t and C', but while using B, one identifies these wrongly with the real constants R_t and C.

(ii) The Y''_{el} *vs.* Y'_{el} plot will be a straight line—according to *both* A and B, with the *same* slope (see eqns. (10) and (11)). But the intercept—according to A—is not the double layer capacity, but only a part of it, *viz*, $q_E = (\partial q/\partial E)$ and is nearly the ca-

pacity of the supporting electrolyte. But one using B will identify this with C_d and, on subsequent analysis, will find C_d nearly the same as that of the supporting electrolyte and consequently conclude erroneously that there is no reactant adsorption! It is true that R_t' and C' should show a "distorted" concentration dependence due to both q_Γ and x_0, but it is doubtful whether it is possible to use this as a criterion to distinguish A and B in practical cases.

Acknowledgement

The author thanks Dr. H. V. K. Udupa, Scientist-in-charge for his keen interest in the work and Dr. Roger Parsons for his useful comments.

Central Electrochemical Research Institute, S. K. Rangarajan
Karaikudi-3 (India)

1 P. DELAHAY, *J. Phys. Chem.*, 70 (1966) 2067, 2373; P. DELAHAY AND C. G. SUSBIELLES, *ibid.*, 70 (1966) 3150; P. DELAHAY, K. HOLUB, C. G. SUSBIELLES AND G. TESSARI, *ibid.*, 71 (1967) 779; K. HOLUB, G. TESSARI AND P. DELAHAY, *ibid.*, 71 (1967) 2612.
2 P. DELAHAY AND K. HOLUB, *J. Electroanal. Chem.*, 16 (1968) 131; K. HOLUB, *ibid.*, 17 (1968) 277; C. G. SUSBIELLES AND P. DELAHAY, *ibid.*, 17 (1968) 289.
3 B. TIMMER, M. SLUYTERS-REHBACH AND J. H. SLUYTERS, *J. Electroanal. Chem.*, 15 (1967) 343; J. H. SLUYTERS, M. SLUYTERS-REHBACH AND B. TIMMER, *ibid.*, 15 (1967) 452.
4 D. J. KOOIJMAN, *J. Electroanal. Chem.*, 19 (1968) 369.
5 W. H. REINMUTH, *Anal. Chem.*, 40 (1968) 185R.
6 W. H. REINMUTH, *J. Electroanal. Chem.*, 21 (1969) 425.
7 H. A. LAITINEN AND J. E. B. RANDLES, *Trans. Faraday Soc.*, 51 (1955) 54.
8 W. J. PLIETH AND K. J. VETTER, *Z. Elektrochem.*, 72 (1968) 673; 73 (1969) 79.
9 W. J. PLIETH AND K. J. VETTER, *Z. Physik. Chem. N.F.*, 61 (1968) 282.

Received September 26th, 1969

ANNOUNCEMENT

THE FARADAY SOCIETY

SPECIAL DISCUSSION ON

Thin Liquid Films and Boundary Layers

To be held at The University of Cambridge, Cambridge, England, 28th-30th September, 1970.

SESSION I

Equilibrium and non-equilibrium properties of thin films of surfactants and lipids.

SESSION II

Liquid layers near to solids.

SESSION III

Lubrication and transport properties of boundary layers.

Further information from:
The Secretary, The Faraday Society, 6 Gray's Inn Square, London, W.C.1., England.

ELECTROANALYTICAL CHEMISTRY AND INTERFACIAL ELECTROCHEMISTRY App.17
Elsevier Sequoia S.A., Lausanne - Printed in The Netherlands

Preliminary note

On the theory of adiabatic and non-adiabatic electrochemical reactions

R.R. DOGONADZE, A.M. KUZNETSOV and M.A. VOROTYNTSEV
Institute of Electrochemistry, Academy of Sciences, Moscow, Leninskii Prospekt 31 (U.S.S.R.)
(Received February 21st, 1970)

In calculating the probability of electrode reactions it is necessary to take into account the fact that there are many potential energy surfaces (terms) in the initial and final states, corresponding to different populations of the electron energy levels in a metal (Fig. 1). The transition probability for each two terms is determined by the matrix element L of the perturbation operator V

$$L = \Omega^{-1/2} \int \psi(\vec{r})\, V \varphi(\vec{r})\, \mathrm{d}\vec{r} \qquad (1)$$

where $\Omega^{-1/2}$, $\psi(\vec{r})$ and $\varphi(\vec{r})$ are the electron wave functions in the metal and the reactant respectively (Ω is the volume of the electrode). Because $\Omega \to \infty$, and therefore $L \to 0$, the transition between each two terms is non-adiabatic. Nevertheless the reaction as a whole can be either non-adiabatic or "adiabatic" since the spacing of terms is an order $1/\Omega$ ($\sim 1/\rho$, where ρ is the electron state density in the metal). The basic results of general calculation carried out for non-adiabatic and adiabatic electrochemical reactions are summarized below (the details will be given in another paper).

In solving the problem we took into consideration the manyfold transitions of the system from initial terms to final ones and *vice versa* while moving along the reaction coordinate★.

To calculate the transition probability for a given set of terms one must find two functions: $r(\epsilon,\epsilon')\mathrm{d}\epsilon$, which is the probability for the system moving along either of terms U_ϵ in the energy interval between $\epsilon + \mathrm{d}\epsilon$ to reach the term $U_{\epsilon'}$, and $r'(\epsilon,\epsilon')\mathrm{d}\epsilon'$, which is the probability for the system moving along either of terms $U_{\epsilon'}$, in the corresponding energy interval $\mathrm{d}\epsilon'$ to reach the term U_ϵ. It must be emphasized that these functions present the probabilities averaged over the equilibrium initial electron distribution function in the metal. The set of partial differential equations was derived and solved for the functions $r(\epsilon,\epsilon')$ and $r'(\epsilon,\epsilon')$. The results for two limit cases are listed below.

1. Non-adiabatic reactions. It was found that if the condition (2) is fulfilled, *i.e.*

$$\kappa \rho kT \equiv 2\pi L^2 \rho kT/h\nu \,|F_\epsilon - F_{\epsilon'}| \ll 1 \qquad (2)$$

★ The validity of considering the transition between terms as independent ones will be proved in a special paper.

where v is the velocity of the system movement along the terms, F_ϵ and $F_{\epsilon'}$ are the slopes of the initial and the final terms, then

$$r(\epsilon,\epsilon') \approx \delta(\epsilon-\epsilon_0)[1-\kappa\rho kT \ln\{1+\exp[\beta(\epsilon'-\epsilon_0)]\}]$$
$$r'(\epsilon,\epsilon') \approx \theta(\epsilon_0-\epsilon)\kappa\rho n(\epsilon_F-\epsilon'+\epsilon_0) \quad (3)$$

where ϵ_F is the Fermi energy, $n(x)$ is the Fermi distribution function, $\beta = 1/kT$, $\delta(x)$ and $\theta(x)$ are the Dirac delta-function and Heaviside function.

In this case at the given full energy E the system reaches the point a along the initial term U_{ϵ_0} with the probability which is almost equal to 1 (Fig. 1). The probability of transition to the final terms in the case of single passing of the system through the region of crossing the terms is small. In this case the expressions for the electric current coincide with those derived in our earlier papers (*cf.* refs. 1 and 2).

2. "Adiabatic" reactions. If the inverse condition is fulfilled ($\kappa\rho kT \gg 1$) we have

$$r(\epsilon,\epsilon') \approx \beta\exp[\beta(\epsilon-\epsilon_0)]\,\delta(1-\exp[\beta(\epsilon-\epsilon_0)]-\exp[\beta(\epsilon'-\epsilon_0')])$$
$$r'(\epsilon,\epsilon') \approx \beta(1-\exp[\beta(\epsilon-\epsilon_0)])\,\delta(1-\exp[\beta(\epsilon-\epsilon_0)]-\exp[\beta(\epsilon'-\epsilon_0')]) \quad (4)$$

In this limiting case the "trajectory" of the system in the (ϵ,ϵ') plane is described by the equation (curve b in Fig. 1):

$$1 = \exp[\beta(\epsilon-\epsilon_0)] + \exp[\beta(\epsilon'-\epsilon_0')] \quad (5)$$

For any given form of terms eqn. (5) permits one to find E^*, which is the minimum energy necessary for transition to the final state (Fig. 1). At $E_1 < E^*$ the system reaches

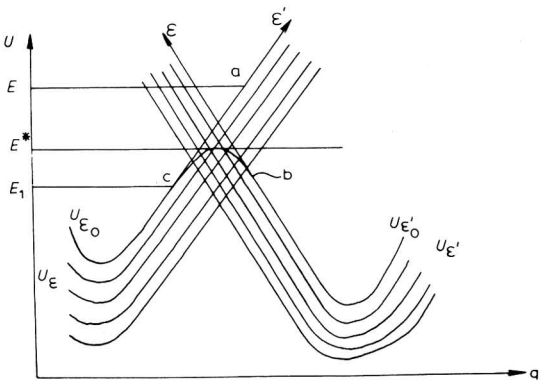

Fig. 1. Potential energy surface profiles (terms) : q is the generalized coordinate describing the state of solvent polarization and the reactant classical degrees of freedom; U_ϵ is the potential energy of the system in the initial state for arbitrary population of the electron energy levels in an electrode, a subscript ϵ designates the full energy of all electrons in an electrode; $U_{\epsilon'}$ is the potential energy for the final state; U_{ϵ_0} is the initial term for the Fermi distribution of the electron in an electrode; the full electron energy for the term $U_{\epsilon_0'}$ differs from that for the term U_{ϵ_0} by Fermi energy ($\epsilon_0-\epsilon_0' = \epsilon_F$). The curve b represents a "trajectory" of the system for the adiabatic reaction at $E > E^*$.

the point c and then moves back. At $E \geqq E^*$ the transition into the final state occurs with the probability equal to 1. In this sense such a reaction may be referred to as adiabatic though the transition from one term to another in each intersection point is non-adiabatic. In this limiting case the electric current is proportional to

$$i \sim \int_{E^*}^{\infty} \exp(-E/kT)\, dE \sim \exp(-E^*/kT) \tag{6}$$

i.e. E^* plays the role of an activation energy. The electrochemical reaction adiabaticity or non-adiabaticity criteria (2) are essentially the same as those derived from qualitative considerations[2]. It should be noted that these criteria differ in principle from those for homogeneous reactions.

REFERENCES

1 R.R. Dogonadze, A.M. Kuznetsov and V.G. Levich, *Electrochim. Acta*, 13 (1968) 1025.
2 R.R. Dogonadze and A.M. Kuznetsov, in Viniti, Itogi Nauki, *Electrohkimija 1967*, 1969.

ELECTROANALYTICAL CHEMISTRY AND INTERFACIAL ELECTROCHEMISTRY
Elsevier Sequoia S.A., Lausanne - Printed in The Netherlands

Preliminary note

Zum Diffusionswiderstand einer teilweise blockierten Elektrode bei Wechselstrom (Theorie)

J. LINDEMANN und R. LANDSBERG
Sektion Chemie der Humboldt-Universität zu Berlin, 108 Berlin, Bunsenstrasse 1 (D.D.R.)
(Eingegangen am 19. Januar, 1970)

Auf der Grundlage der früher entwickelten Vorstellung[1] von parallel geschalteten Diffusionszylindern als Modell für eine teilweise blockierte Elektrode soll im folgenden versucht werden, die Frequenzabhängigkeit des Diffusionswiderstandes einer solchen Elektrode zu berechnen. Wir fühlen uns bestärkt, diese Modellvorstellung auf das vorliegende Problem zu übertragen, da stationäre[2,3], galvanostatische und potentiostatische Versuche an mit Photoresist[2,3] hergestellten Modellelektroden die quantitative Gültigkeit der Theorie, die auf Gleichungen von Smythe beruht[4], bestätigt.★

In allen Fällen muss in den entsprechenden Gleichungen die Diffusionsschichtdicke δ durch einen Summanden S korrigiert werden, der von den Elektrodenparametern abhängt

$$S = \Sigma A_n \ \text{tgh} \ \frac{x_n \delta}{r_2} \tag{1}$$

A_n = Koeffizienten, für die Smythe[4] eine Bestimmungsgleichung angibt,
x_n = Nullstelle der Besselfunktion erster Ordnung,
δ = Diffusionsschichtdicke,
r_2 = Radius eines Diffusionszylinders.

Wir wollen uns bei der Ableitung der Gleichungen auf den ohmschen Anteil der Diffusionsimpedanz beschränken. Warburg[5] und Krüger[6] berechneten zuerst die Abhängigkeit der Diffusionsimpedanz von der Frequenz, die sehr viel später von Randles[7], Gerischer[8] und Vetter[9,10] bestätigt und erweitert wurde. Nach den genannten Autoren ergibt sich für den Diffusionswiderstand R_d

$$R_d = \frac{\sqrt{2}RT}{n^2 F^2 qc\sqrt{D\omega}} \qquad \text{(Parallelschaltung)} \tag{2}$$

★ Veröffentlichungen über galvanostatische und potentiostatische Versuchsergebnisse sind in Vorbereitung.

$$R_d = \frac{RT}{n^2 F^2 qc\sqrt{2D\omega}} \quad \text{(Reihenschaltung)} \tag{3}$$

Diese Gleichungen gelten für sehr kleine Amplituden der Spannung (< 5 mV). In Klammern sind die Arten des Ersatzschaltbildes angegeben. Es bedeuten: R = Gaskonstante, T = Temperatur, n = Anzahl der ausgetauschten Elektronen, F = Faraday-Konstante, q = geometrische Fläche, c = Konzentration des potentialbestimmenden Stoffes in der Lösung, D = Diffusionskoeffizient, ω = Frequenz der Wechselspannung.

Um diese Gleichungen anzuwenden, muss eine formale Diffusionsschichtdicke eingeführt werden. Dazu wird in erster Näherung ein linearer Konzentrationsgradient angenommen und das 1. Ficksche Gesetz als Differenzengleichung angesetzt:

$$i = nF\,q\,D\ \frac{\Delta c}{\delta} \tag{4}$$

Nach Randles[7] erhält man für die maximale Amplitude des Faradayschen Stromes I_{Max}

$$I_{Max} = n\,Fq\,\Delta c\ \frac{\sqrt{D\omega}}{2} \tag{5}$$

und damit für den effektiven Strom i_{eff}

$$i_{eff} = n\,F\,q\,\Delta c\ \frac{\sqrt{D\omega}}{2\sqrt{2}} \tag{6}$$

Setzt man Gleichung (6) in Gleichung (4) ein, so erhält man für die effektive Diffusionsschichtdicke

$$\delta = \frac{2\sqrt{2D}}{\sqrt{\omega}} \tag{7}$$

Beschränkt man sich zunächst auf die Parallelschaltung, so erhält man nach Einsetzen von Gleichung (7) in Gleichung (2) für den Diffusionswiderstand

$$R_d = \frac{RT\,\delta}{n^2 F^2 qc\ 2D} \tag{8}$$

Man hat damit eine Funktion von δ, die man mit Hilfe der Gleichung (1) korrigiert und erhält so die Beziehung für den Diffusionswiderstand einer teilweise bedeckten Elektrodenoberfläche:

$$R_d = \frac{RT\ \left[\delta + \Sigma\ A_n\ \mathrm{tgh}\ x_n\delta/r_2\right]}{n^2 F^2 qc\ 2D} \tag{9}$$

Jetzt kann man zwei Grenzfälle unterscheiden:

1. Die Diffusionsschichtdicke ist sehr gross (kleine Frequenzen), so gilt:

$$\text{tgh}\, x_n \delta / r_2 \simeq 1 \quad \text{für} \quad x_n \delta / r_2 \gg 1$$

Ersetzt man δ wieder durch Gleichung (7), so erhält man für $\delta / r_2 > 1$

$$R_d = \frac{\sqrt{2}\, RT}{n^2 F^2 qc \sqrt{D\omega}} + \frac{RT \Sigma A_n}{n^2 F^2 qc\, 2D} \tag{10}$$

2. Die Diffusionsschichtdicke ist klein (hohe Frequenzen), so gilt:

$$\text{tgh}\, x_n \delta / r_2 \simeq x_n \delta / r_2 \quad \text{für} \quad x_n \delta / r_2 \ll 1$$

In diesem Fall kann man nach Einsetzen in Gleichung (9) δ ausklammern und wieder durch Gleichung (7) ersetzen

$$R_d = \frac{\sqrt{2}\, RT\, (1 + \Sigma A_n\, x_n / r_2)}{n^2 F^2 qc \sqrt{D\omega}} \tag{11}$$

Trägt man also R_d gegen $\omega^{-1/2}$ auf, so erhält man eine Kurve, die sich aus zwei Geraden zusammensetzt. Für hohe Frequenzen erhält man eine Gerade, aus deren Anstieg der Ausdruck $\Sigma A_n x_n / r_2$ berechnet werden kann. Dieser Ausdruck kann als Funktion von r_1 / r_2 dargestellt werden und ist damit ein Mass für den Blockierungsgrad ψ

$$\psi = 1 - (r_1 / r_2)^2$$

Dies gilt für das früher angewendete Modell[2,3] unter den dafür angegebenen Voraussetzungen. Für die Darstellung der Funktion $\Sigma A_n x_n / r_2$ als Funktion von r_1 / r_2 muss auf eine spätere Arbeit verwiesen werden, in der auch die Gültigkeit dieser Funktion mit Hilfe von galvanostatischen und potentiostatischen Messungen an Modellelektroden nachgewiesen wird. Gleichung (11) ist unabhängig von der Definition von δ, wie aus der Ableitung von (11) folgt. In der $R_d / \omega^{-1/2}$ Auftragung wird (10) durch eine Gerade dargestellt, der Extrapolation erhält man einen Ordinantenabschnitt, aus dem ΣA_n berechnet werden kann. Hat man den Blockierungsgrad nach Gleichung (11) berechnet, so kann man mit ΣA_n Grösse und Anzahl der aktiven Stellen berechnen[2]. Der Wert von ΣA_n hängt allerdings von der Definition der Diffusionsschichtdicke ab, für die man noch mindestens zwei weitere Definitionsmöglichkeiten hat. Einmal kann man die maximale Amplitude des Stroms in Gleichung (4) einsetzen und erhält dann eine um den Faktor $2^{-1/2}$ kleinere Diffusionsschichtdicke. Weiterhin kann man die von Vetter[10] angegebene mittlere Eindringtiefe der Konzentrationswelle gleich der Diffusionsschichtdicke setzen und erhält eine um den Faktor 0.5 kleinere Diffusionsschichtdicke. Eine Entscheidung könnte evtl. mit Modellmessungen getroffen werden.

Für die Reihenschaltung sind alle Gleichungen mit dem Faktor 0.5 zu multiplizieren.

Vetter[11] hat das gleiche Problem bearbeitet. Er gibt eine Gleichung für hohe Frequenzen an. In dieser Gleichung ist im Unterschied zur homogenen Elektrode nur die gesamte Fläche durch den aktiven Teil der Elektrodenoberfläche ersetzt. Die Gleichung kann quantitativ nicht erfüllt sein, weil hierbei die nichtlineare Diffusion unberücksichtigt bleibt, was zu erheblichen Fehlern führt. Der von Vetter postulierte Kurvenverlauf stimmt qualitativ mit unserem überein.

Zum Schluss sei noch darauf hingewiesen, dass bei vorgelagerter chemischer Reaktion sich der gleiche Kurvenverlauf ergeben kann[12].

LITERATURVERZEICHNIS

1 R. Landsberg und R. Thiele, *Electrochim. Acta*, 11 (1966) 1243.
2 F. Scheller, S. Muller, R. Landsberg und H.J. Spitzer, *J. Electroanal. Chem.*, 19 (1968) 187.
3 F. Scheller, R. Landsberg und S. Müller, *J. Electroanal. Chem.*, 20 (1969) 357.
4 W.R. Smythe, *J. Appl. Phys.*, 24 (1953) 70.
5 E. Warburg, *Am. Phys. Chem. (Wiedermann)*, 67 (1899) 493.
6 F. Krüger, *Z. physik. Chem. (Leipzig)*, 45 (1903) 1.
7 E.B. Randles, *Discussions Faraday Soc.*, 1 (1947) 11.
8 H. Gerischer, *Z. Physik. Chem. (Leipzig)*, 198 (1951) 286.
9 K.J. Vetter, *Z. Physik. Chem. (Leipzig)*, 199 (1952) 285.
10 K.J. Vetter, *Elektrochemische Kinetik*, Springer-Verlag, Berlin-Göttingen-Heidelberg, 1961, S.180.
11 K.J. Vetter, *Z. Physik. Chem. (Leipzig)*, 199 (1952) 300.
12 H. Gerischer, *Z. Physik. Chem. (Leipzig)*, 201 (1952) 55.

Vol. 25 No. 2 JOURNAL OF ELECTROANALYTICAL CHEMISTRY APRIL 1970
AND INTERFACIAL ELECTROCHEMISTRY

CONTENTS

Continued on page 4 of cover

Continued from inside page of cover